



Deutsche Neutronenstreutagung 2008

Garching

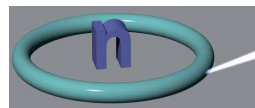
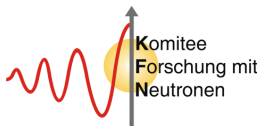
15.- 17. September 2008

Program and Abstracts



Eds.:

Ina Lommatzsch, Jürgen Neuhaus, Björn Pedersen, Winfried Petry



Impressum:

Eds.: Ina Lommatzsch, Jürgen Neuhaus, Björn Pedersen, Winfried Petry
Deutsche Neutronenstreutagung 2008
Program and Abstracts

Technische Universität München
Forschungs-Neutronenquelle Heinz Maier-Leibnitz (FRM II)
D-85747 Garching
September 2008

Program Committee: Th. Brückel, G. Krexner, W. Petry, H. Schober, H. Zabel.

© Technische Universität München
Forschungs-Neutronenquelle Heinz Maier-Leibnitz (FRM II), 2008
Alle Rechte vorbehalten
Luftbilder: Quelle: TU München
The conference is supported by:



Preamble

Every two years, the German Komitee für Forschung mit Neutronen holds the German neutron conference. Previous meetings took place at Lüneburg (1995), Kloster Seeon (1997), Potsdam (1999), Jülich (2001), Bonn (2002), Dresden (2004) and Hamburg (2006). This series of conferences is based on the long tradition of meetings of the neutron users organised by the so called "Verbundtreffen". This time we assemble together with our Austrian friends, the Fachausschuss NESY, Physik an Neutronen- und Synchrotronquellen der Österreichischen Physikalischen Gesellschaft at Garching.

The bi-annual rhythm in between the greater European and International Conferences on Neutron Scattering gives the opportunity the German neutron community to present its achievements in neutron scattering. Traditionally this event serves also as a platform for the latest achievements in neutron instrumentation and neutron sources. Certainly the new German neutron source, the Forschungsneutronenquelle Heinz Maier-Leibnitz (FRM II), will be the focus of many contributions. Of course, our excellent sources at the ILL, GKSS and HZB will compete. DN 2008 will go beyond: we will listen to the progress made on spallation sources like SNS and the 2nd target station of ISIS and – most important – we will hear about the developments related to the European Spallation Source.

DN 2008 dares to develop the conference program. For the 1st time we have three mini-symposia. These symposia focus on multiferroics, SANS & reflectometry and material sciences. They are organised by specialists in the field.

We would like to thank the German neutron facilities FRM II, GKSS, JCMS and HZB and the ILL for their longstanding tradition in financial support of the German neutron conferences. They also sponsor the Wolfram Prandl Prize.

To welcome neutron scientists to Bavaria is always a pleasure. The local organisers tried to meet the expectations by inviting to the conference dinner at the traditional Hofbräukeller in downtown Munich and organising guided tours of the Forschungsneutronenquelle Heinz Maier-Leibnitz (FRM II).

Welcome to Garching to DN 2008

The organisers

DN 2008						
Sunday	Monday		Tuesday		Wednesday	
Welcome reception (17:00-20:00)	Welcome address (9:00-9:20)		Plenary talk (9:00-9:35)		Plenary talk (9:00-9:35)	
	Mini-SYM 1A (9:20-10:40)	Soft Matter I (9:20-10:40)	Mini-SYM 2B (9:40-11:00)	Magnetism I (9:40-11:00)	Plenary talk (9:35-10:10)	
	Break (10:40-11:10)		Break (11:00-11:30)		Break (10:10-10:30)	
	Mini-SYM 1B (11:10-12:30)	Soft Matter II (11:10-12:30)	Mini-SYM 3A (11:30-12:30)	Magnetism II (11:30-12:30)	Mini-SYM 3B (10:30-12:10)	Structure and dynamics (10:30-12:10)
	Lunch (12:30-13:30)		Lunch (12:30-13:30)		Guided Tours (12:15-15:00)	
	Plenary talk (13:30-14:05)		Award ceremony (13:30-14:00)			
	Mini-SYM 2A (14:10-15:55)	Instrumentation (14:10-15:55)	BMBF (14:00-14:20)			
			Spallation sources (14:25-15:55)	Materials (14:25-16:05)		
	Break (16:00-16:30)		Break (16:00-16:30)			
	Poster I (16:30-19:00)		Poster II (16.30-19:00)			
		Dinner reception (20:00)				

Monday, 09-15-2008			
Time	HS 1	Time	HS 2
09.00-09.20	Welcome Address		
	<i>Mini-SYM 1A: Function from Frustration in Modern Multiferroics</i>		<i>Session 1: Soft Matter I</i>
09.20-09.25	Introduction	09.20-09.40	Regine Willumeit (GKSS) et al.: Study of lipid modified implant surfaces (1.1)
09.25-09.55	Alois Loidl (Universität Augsburg): Excitations in Multiferroics (9.1)	09.40-10.00	Christine Papadakis (TU München) et al.: Micellar solutions and hydrogels from temperature-responsive, amphiphilic block copolymers (1.2)
09.55-10.25	Markus Braden (Universität zu Köln) et al.: Neutron scattering studies on spiral multiferroics (9.2)	10.00-10.20	Rumen Krastev (MPI Potsdam/Golm) et al.: Formation Of Polyelectrolyte/Lipid Composite Multilayer Structures (1.3)
10.25-10.40	Sven Landsgesell (HZ Berlin) et al.: Tuning magnetic interaction in orthorhombic Neodymium-Yttrium Manganites Nd _{1-x} YxMnO ₃ (9.3)	10.20-10.40	Max Wolff (Ruhr-Universität Bochum) et al.: The solid-liquid boundary condition for flowing liquids (1.4)
10.40-11.10	Break		
	<i>Mini-SYM 1B: Function from Frustration in Modern Multiferroics</i>		<i>Session 2: Soft Matter II</i>
11.10-11.40	Ralf Feyerherm (HZ Berlin) et al.: Interplay between rare earth and manganese magnetism and its effect on ferroelectricity in or-RMnO ₃ (9.4)	11.10-11.30	Fajun Zhang (Universität Tübingen) et al.: Protein-Protein Interactions in Solution Studied by Small-Angle Scattering (2.1)
continued on next page			

Monday, 09-15-2008			
Time	HS 1	Time	HS 2
11.40-11.55	Fabiano Yokaichiya (HZ Berlin) et al.: Influence of Applied Magnetic Field in Incommensurate Magnetic Structure of ZnCr ₂ Se ₄ and ZnCr ₂ S ₄ (9.5)	11.30-11.50	Thomas Hellweg (Universität Bayreuth) et al.: Temperature Dependence Of The Dynamics In Sugar Surfactant Based Bicontinuous Microemulsions As Seen With Quasielastic Scattering Techniques (2.2)
11.55-12.10	to be announced	11.50-12.10	Tinka Spehr (TU Darmstadt; ILL) et al.: Structure and Dynamics of Reverse Micelles Under the Addition of Amphiphilic Triblock Copolymers (2.3)
12.10-12.30	Magnetism II Florian Jonietz (TU München) et al.: Spin Torque Effects in a Helical Magnet (5.4)	12.10-12.30	Tobias Unruh (FRM II) et al.: Self-diffusion in molecular liquids: medium-chain n-alkanes and coenzyme Q10 studied by QENS (2.4)
12.30-13.30	Lunch		
13.30-14.05	Plenary Talk: Christian Pfeleiderer (TU München): Exploring condensed matter with a twist (P-1)		
14.10-14.35	<i>Mini-SYM 2A: Dynamics, kinetics, complex materials in the light of SANS and reflectometry</i> Peter Lindner (ILL): Rheo-SANS with complex fluids (10.1)	14.10-14.25	<i>Session 3: Instrumentation</i> Axel Reimer Müller (TU München) et al.: TOF inelastic neutron scattering on D2, a key tool on the way to a very strong UCN source (3.1)
14.35-15.00	Claus Czeslik (TU Dortmund): Controlling protein adsorption at aqueous-solid interfaces (10.2)	14.25-14.40	Simon Mayer (Atominstitut Wien) et al.: The phase-space transformer up-scattering project: first results (3.2)
continued on next page			

Monday, 09-15-2008			
Time	HS 1	Time	HS 2
15.00-15.25	Julian Oberdisse (Université Montpellier II) et al.: Small-angle scattering from self-assembled and hierarchical structures (10.3)	14.40-14.55	Petra Kudejova (Universität zu Köln) et al.: Overview of the new PGOA and PGAI facility at the research reactor FRM II (3.3)
		14.55-15.10	Catherine Pappas (HZ Berlin) et al.: Polarimetric Neutron Spin Echo Spectroscopy (3.4)
15.25-15.55	Albrecht Wiedenmann (ILL) et al.: Stroboscopic Small Angle Neutron Scattering Investigations of Microsecond Dynamics in Magnetic Nanomaterials (10.4)	15.10-15.25	Jörg Voigt (JCNS) et al.: TOPAS, the future thermal time-of-flight spectrometer at the FRM II (3.5)
		15.25-15.40	Christian Pruner (Universität Salzburg) et al.: Light-induced gratings in polymers and polymer nanocomposites for neutron optics (3.6)
		15.40-15.55	Adrian Rühm (MPI Stuttgart) et al.: The Neutron/X-Ray Contrast and Spin-Echo Reflectometer N-REX+ at FRM II: Present Status, First Experiments and Future Perspectives (3.7)
16.00-16.30	Break		
16.30-19.00	<i>Poster I</i>		

Tuesday, 09-16-2008			
Time	HS 1	Time	HS 2
9.00-9.35	Plenary Talk: Ralf Biehl (FZ-Jülich): Interdomain dynamics in yeast alcohol dehydrogenase (P-2)		
	<i>Mini-SYM 2B: Dynamics, kinetics, complex materials in the light of SANS and reflectometry</i>		<i>Session 4: Magnetism I</i>
9.40-10.00	Isabelle Grillo (ILL) et al.: Formation and Growth of Vesicles Studied by Time Resolved Small Angle Neutron Scattering Combined with a Stopped-flow Equipment (10.5)	9.40-10.00	Katharina Theis-Bröhl (Hochschule Bremerhaven) et al.: Highly Ordered Spin-State in an Epitaxial Spin-Valve as Observed by Polarized Neutron Reflectometry (4.1)
10.00-10.20	Bert Nickel (LMU München): Combining neutron reflectivity and fluorescence microscopy to study biological interfaces (10.6)	10.00-10.20	Dieter Lott (GKSS) et al.: Chirality in Dy/Y Multilayers (4.2)
10.20-10.40	Michael Kerscher (FZ Jülich) et al.: Microemulsions Near Planar Surfaces (10.7)	10.20-10.40	Philipp Niklowitz (University of London) et al.: Crystal-lattice response to antiferromagnetic and hidden order in URu ₂ Si ₂ (4.3)
10.40-11.00	Franziska Gröhn (MPI Mainz): Small-Angle Neutron Scattering to Characterize Electrostatically Assembled Supramolecular Structures (10.8)	10.40-11.00	Arno Hiess (ILL) et al.: The static and dynamic magnetic properties of PuCoGa ₅ and NpCoGa ₅ investigated by neutron scattering experiments (4.4)
11.00-11.30	Break		
	<i>Mini-SYM 3A: Material Science</i>		<i>Session 5: Magnetism II</i>
11.30-11.50	Peter Staron (GKSS) et al.: Influence of the welding sequence on residual stresses in laser welded T-joints of aluminium alloys (11.1)	11.30-11.50	Yixi Su (JCNS) et al.: Magnetic ordering and spin fluctuations in BaFe ₂ As ₂ and Ba _{1-x} K _x Fe ₂ As ₂ (5.1)
continued on next page			

Tuesday, 09-16-2008			
Time	HS 1	Time	HS 2
11.50-12.10	Bo Zhang (DLR) et al.: Direct observation of chemical diffusion in liquid alloys using X-ray and neutron radiography (11.2)	11.50-12.10	Andreas Michels (Universität des Saarlandes) et al.: Spin structure of nanocrystalline gadolinium (5.2)
12.10-12.30	Pavel Strunz (NRI Řež) et al.: Scattering contrast dependence on thermalexpansion-coefficient difference of phases in twophase system (11.3)	12.10-12.30	Oliver Waldmann (Universität Freiburg): Inelastic Neutron Scattering on Molecular Nanomagnets (5.3)
12.30-13.30	Lunch		
13.30-14.00	<i>Award ceremony (Wolfram-Prandl-Prize for young scientists in neutron research) and lecture of the prize recipient</i>		
14.00-14.20	Dr. Beatrix Vierkorn-Rudolph (BMBF): Forschung mit Neutronen aus Sicht der Wissenschaftspolitik		
	<i>Session 6: Upcoming Spallation Sources</i>		<i>Session 7: Materials</i>
14.25-14.55	Robert Mc Greevy (ISIS): Development at ISIS - the next ten years (6.1)	14.25-14.45	German Kulin (FLNP JINR) et al.: New gravitational experiment with ultracold Neutrons (7.1)
14.55-15.25	Kenneth W. Herwig (Oak Ridge National Laboratory): Commissioning Experience, Early Results, and Status of the Spallation Neutron Source at Oak Ridge National Laboratory (6.2)	14.45-15.05	Anja Ines Pommrich (DLR) et al.: Nickel self-diffusion in Si-Ni melts (7.2)
15.25-15.55	Helmut Schober (ILL) and Ferenc Mezei (Los Alamos National Laboratory): The European Spallation Source: Perspectives (6.3)	15.05-15.25	Ralph Gilles (FRM II) et al.: Studies of ordering in anti phase nanodomain FeCo alloys with different ternary additions using neutron diffraction (7.3)
continued on next page			

Tuesday, 09-16-2008			
Time	HS 1	Time	HS 2
		15.25-15.45	Heloisa Bordallo (HZ Berlin) et al.: Natural Soil Environments: The role of cations and superparamagnetic iron oxides (7.4)
		15.45-16.05	P. Klaus Pranzas (GKSS) et al.: Characterisation of the Hydrogen Distribution in Metal Hydride Tanks Using Neutron Radiography and Tomography (7.5)
16.00-16.30	Break		
16.30-19.00	<i>Poster II</i>		
20.00	<i>Dinner at "Hofbräukeller", Innere Wiener Straße 19, 81667 München</i>		

Wednesday, 09-17-2008			
Time	HS 1	Time	HS 2
9.00-9.35	Plenary Talk: Niko Froitzheim (Universität Bonn): From intracrystalline deformation to continent collision: Neutron texture goniometry of sheared rocks from the Alps (P-3)		
9.35-10.10	Plenary Talk: Gerald Badurek (Atominstytut Wien): Quantum Physics with Neutrons (P-4)		
10.10-10.30	Break		
10.30-10.50	<i>MiniSYM 3B: Material Science</i> Thomas Hirsch (IWT Bremen) et al.: Eigenspannungen als Träger des Verzugspotenzials: Messungen und Rechnungen an Bauteilen der Wälzlager- und Getriebeindustrie (11.4)	10.30-10.50	<i>Session 8: Structure and Structural Dynamics</i> Markus Raichle (MPI Stuttgart) et al.: The phonon buckling mode in $\text{YBa}_2\text{Cu}_3\text{O}_{6+x}$ measured by inelastic neutron scattering (8.1)
10.50-11.10	Felix Beckmann (GKSS) et al.: Neutron Tomography on tyrannosaurid foot at GENRA-3 (11.5)	10.50-11.10	Michael Prager (FZ Jülich) et al.: The impact of SPHERES on rotational tunneling spectroscopy: recent examples (8.2)
11.10-11.30	Heinz-Günther Brokmeier (TU Clausthal) et al.: The robot concept at STRESS-SPEC for the characterization of semi-finished products (11.6)	11.10-11.30	Anatoliy Senyshyn (TU Darmstadt) et al.: Thermal expansion and atomic vibrations in CaWO_4 studied by neutron and synchrotron powder diffraction (8.3)
11.30-11.50	Weimin Gan (TU Clausthal) et al.: Texture homogeneity in a single pass ECAPed pure Mg (11.7)	11.30-11.50	Werner Schweika (FZ Jülich) et al.: Dumbbell rattling in thermoelectric zinc-antimony (8.4)
11.50-12.10	Steven Van Petegem (PSI) et al.: In-situ mechanical testing at the time-of-flight neutron diffractometer POLDI (11.8)	11.50-12.10	Werner F. Kuhs (Universität Göttingen) et al.: The nature of "cubic ice" established by timeresolved neutron diffraction (8.5)
12.15-15.00	<i>Guided tours of the FRM II</i>		

General Information

Location and Venue

The conference takes place in the lecture halls H1 and H2 at the Physics Department of the TU München, James Franck Straße, 85748 Garching.

The best way to reach the Garching Campus is by underground (U6), terminal stop "Garching-Forschungszentrum". Follow the signs to the "Physik Department".

Plans are to be found in the inside front and back cover.

Conference Office

The conference office is located in the foyer of the Physics Department.

Opening hours:

Sunday, Sept. 14th: 05:00 - 08:00

Monday, Sept. 15th: 08:00 - 16:30

Tuesday, Sept., 16th: 08:00 - 16:30

Wednesday, Sept. 17th: 08:30 - 12:30

Phone during the conference: (+49) (0)89 289 14965

Fax during the conference: (+49) (0)89 289 14995

The conference office has your conference bag with information ready. Please don't forget to pay the conference fee - you will get your receipt from the conference office.

Welcome Reception

A Bavarian "Brotzeit" is served in the foyer of the Physics Department on Sunday, 14th from 17:00 to 20:00.

Lunch

The conference members have the opportunity to take their lunch at the nearby "Mensa" (= canteen). Luncheon vouchers are sold by the conference office for 7,50 Euro. (Please note that it is not possible to make a cash payment at the "Mensa"!). There are signs "DN 2008" to avoid problems finding a seat.

You can also use the cafeteria, which accepts cash payment.

Posters

The required standard paper-size is A0 portrait.

Materials for fixation will be provided.

There are two poster sessions:

The posters for the Monday's session (M1 - M94) can be hung up from Sunday, 17:00 onwards and must be taken down after the session on Monday evening.

The posters for the Tuesday's session (T1 - T94) can be hung up from Tuesday, 08:00 onwards and can rest there until Wednesday, 12:00.

Talks

Please note, that time for discussion is included in the given time for your lecture.

Each lecture hall is equipped with overhead projector, laptop running Windows XP and a beamer. Please hand over your file (.pdf or .ppt) on a USB flash drive or on CD for testing in the break one session before. You should use your own personal computer only in exceptional cases.

Conference Dinner

The conference dinner takes place at the restaurant Hofbräukeller.

Address: Innere Wiener Straße 19, 81667 München

Phone: 089 - 459925-0 (in case you get lost)

Dinner starts at 20:00.

From Garching Campus the U6 will take you to the stop "Odeonsplatz", where you have to change to U4 (direction "Arabellapark") or U5 ("Neuperlach Süd") for just two stations. Leave the underground at "Max-Weber-Platz". Follow the signs "Bayerischer Landtag" and walk the "Innere Wiener Straße". About 200 m ahead there is a place called "Wiener Platz". The "Hofbräukeller" is the multi-story building in front of you.

The underground will take about 33 min, departure from Garching-Forschungszentrum at 18:52, 19:10 or 19:30. The last U4 back to Garching starts at 0:27 from Max-Weber-Platz.

Please note that the conference dinner is only available for you, if you had registered for it! This had to be done by Sept. 5th the latest. The same applies to requests for a vegetarian meal: you have to tell us this by email by Sept. 5th the latest, too.

Guided Tour of the FRM II

Please note that you have to register in advance. A valid passport or identity card (no driving licence) is required to enter the site of the FRM II. We will arrange groups of 15 people in advance. The departures will start at 12:15 on Wednesday 17.09.2008 at every 15 minutes from the registration desk. The tour will take about one hour. During the registration you will get the information of the departure of your group. Please be strictly in time at the registration desk.

Industry

There are two industrial exhibitions on DN 2008:

Astrium GmbH, Systemengineering Mechanisms develops and delivers neutron instrumentation like velocity selectors and chopper systems: <http://www.astrium.eads.net/>.

During the conference Berno Spiegelhalter and Hugo Betzold will be present.

Swiss Neutronics present optical equipment for neutron and synchrotron sources: <http://www.swissneutronics.ch/>.

During the conference Dr. Christian Schanzer will be present.

Contents

Preamble	1
General Information	11
Abstracts: Talks	23
Plenary talks	25
P-1 Exploring Condensed Matter with a Twist	26
P-2 Interdomain dynamics in yeast alcohol dehydrogenase	27
P-3 From intracrystalline deformation to continent collision: Neutron texture geometry of sheared rocks from the Alps	28
P-4 Quantum physics with neutrons	29
1 Session 1: Soft matter I	31
1.1 Study of lipid modified implant surfaces	32
1.2 Micellar solutions and hydrogels from temperature-responsive, amphiphilic block copolymers	33
1.3 Formation Of Polyelectrolyte/Lipid Composite Multilayer Structures	34
1.4 The solid-liquid boundary condition for flowing liquids	35
2 Session 2: Softmatter II	37
2.1 Protein-Protein Interactions in Solution Studied by Small-Angle Scattering	38
2.2 Temperature Dependence Of The Dynamics In Sugar Surfactant Based Bicontinuous Microemulsions As Seen With Quasielastic Scattering Techniques	39
2.3 Structure and Dynamics of Reverse Micelles Under the Addition of Amphiphilic Triblock Copolymers	40
2.4 Self-diffusion in molecular liquids: medium-chain n-alkanes and coenzyme Q10 studied by QENS	41
3 Session 3: Instrumentation	43
3.1 TOF inelastic neutron scattering on D2, a key tool on the way to a very strong UCN source	44
3.2 The phase-space transformer up-scattering project: first results	45
3.3 Overview of the new PGAA and PGAI facility at the research reactor FRM II	46
3.4 Polarimetric Neutron Spin Echo Spectroscopy	47
3.5 TOPAS, the future thermal time-of-flight spectrometer at the FRM II	48
3.6 Light-induced gratings in polymers and polymer nanocomposites for neutron optics	49
3.7 The Neutron/X-Ray Contrast and Spin-Echo Reflectometer N-REX+ at FRM II: Present Status, First Experiments and Future Perspectives	50
4 Session 4: Magnetism I	51
4.1 Highly Ordered Spin-State in an Epitaxial Spin-Valve as Observed by Polarized Neutron Reflectometry	52
4.2 Chirality in Dy/Y Multilayers	53
4.3 Crystal-lattice response to antiferromagnetic and hidden order in URu ₂ Si ₂	54

4.4	The static and dynamic magnetic properties of PuCoGa ₅ and NpCoGa ₅ investigated by neutron scattering experiments	55
5	Session 5: Magnetism II	57
5.1	Magnetic ordering and spin fluctuations in BaFe ₂ As ₂ and Ba _{1-x} K _x Fe ₂ As ₂	58
5.2	Spin structure of nanocrystalline gadolinium	59
5.3	Inelastic Neutron Scattering on Molecular Nanomagnets	60
5.4	Spin Torque Effects in a Helical Magnet	61
6	Session 6: Upcoming Spallation Sources	63
6.1	Development at ISIS - the next ten years	64
6.2	Commissioning Experience, Early Results, and Status of the Spallation Neutron Source at Oak Ridge National Laboratory	65
6.3	ESS: progress towards a neutron source of the next generation	66
7	Session 7: Materials	67
7.1	New gravitational experiment with ultracold neutrons	68
7.2	Nickel self-diffusion in Si-Ni melts	69
7.3	Studies of ordering in anti phase nanodomain FeCo alloys with different ternary additions using neutron diffraction	70
7.4	Natural Soil Environments: The role of cations and superparamagnetic iron oxides	71
7.5	Characterisation of the Hydrogen Distribution in Metal Hydride Tanks Using Neutron Radiography and Tomography	72
8	Session 8: Structure and Structural Dynamics	73
8.1	The phonon buckling mode in YBa ₂ Cu ₃ O _{6+x} measured by inelastic neutron scattering	74
8.2	The impact of SPHERES on rotational tunneling spectroscopy: recent examples	75
8.3	Thermal expansion and atomic vibrations in CaWO ₄ studied by neutron and synchrotron powder diffraction	76
8.4	Dumbbell rattling in thermoelectric zinc-antimony	77
8.5	The nature of "cubic ice" established by time-resolved neutron diffraction	78
9	Mini-SYM 1: Function from Frustration in Modern Multiferroics	79
9.1	Excitations in Multiferroics	80
9.2	Neutron scattering studies on spiral multiferroics	81
9.3	Tuning magnetic interaction in orthorhombic Neodymium-Yttrium Manganites Nd _{1-x} Y _x MnO ₃	82
9.4	Interplay between rare earth and manganese magnetism and its effect on ferroelectricity in or-RMnO ₃	83
9.5	Influence of Applied Magnetic Field in Incommensurate Magnetic Structure of ZnCr ₂ Se ₄ and ZnCr ₂ S ₄	84
10	Mini-SYM 2: Dynamics, kinetics, complex materials in the light of SANS and reflectometry	85
10.1	Rheo-SANS with complex fluids	86
10.2	Controlling protein adsorption at aqueous-solid interfaces	87
10.3	Small-angle scattering from self-assembled and hierarchical structures	88
10.4	Stroboscopic Small Angle Neutron Scattering Investigations of Microsecond Dynamics in Magnetic Nanomaterials.	89
10.5	Formation And Growth Of Vesicles Studied By Time Resolved Small Angle Neutron Scattering Combined With A Stopped-Flow Equipment	90

10.6	Combining neutron reflectivity and fluorescence microscopy to study biological interfaces	91
10.7	Microemulsions Near Planar Surfaces	92
10.8	Small-Angle Neutron Scattering to Characterize Electrostatically Assembled Supramolecular Structures	93
11	Mini-SYM 3: Materials Science and Engineering	95
11.1	Influence of the welding sequence on residual stresses in laser welded T-joints of aluminium alloys	96
11.2	Direct observation of chemical diffusion in liquid alloys using X-ray and neutron radiography	97
11.3	Scattering contrast dependence on thermal-expansion-coefficient difference of phases in two-phase system	98
11.4	Eigenspannungen als Träger des Verzugspotenzials: Messungen und Rechnungen an Bauteilen der Wälzlager- und Getriebeindustrie	99
11.5	Neutron Tomography on tyrannosaurid foot at GENRA-3	100
11.6	The robot concept at STRESS-SPEC for the characterization of semi-finished products	101
11.7	Texture homogeneity in a single pass ECAPed pure Mg	102
11.8	In-situ mechanical testing at the time-of-flight neutron diffractometer POLDI	103

Abstracts: Posters I (Monday) 105

12	Biophysics and biology	107
M-1	Calcium-binding protein dynamics : investigation of the relationship between structural thermal stability and internal motions by quasielastic neutron scattering	108
M-2	Microdomain Formation in Lipid Mixtures	109
M-3	Losartan and Angiotensin II – Tracing structural changes by SANS	110
M-4	Elastic incoherent neutron and Quasi-elastic scattering studies of aligned DMPC multilayers at different hydrations	111
M-5	Indirect radiation therapy of cancer by Gadolinium NCT - instrumentation and cell culture models	112
13	Instrumentation and methods I	113
M-6	Neutron Scattering under Controlled Gas Atmospheres - The CGA-Sample Environment	114
M-7	SPHERES: ein rundum erfreuliches Rückstreuспекrometer	115
M-8	Single domain wall in FeNi film on Si for spin flip.	116
M-9	Magic Box and fast decaying cell - two methods of SANS polarization analysis with ^3He at the V4 SANS instrument of Helmholtz Center Berlin	117
M-10	BRISP and FOCUS-2D - Two similar Large Area Position Sensitive Neutron Detector Projects at the ILL and the PSI	118
M-11	Optimization of the SKAT texture diffractometer at Dubna for texture measurements on geological samples.	119
M-12	In-situ Sample Orientation for Neutron Scattering at Dilution Temperatures	120
M-13	Das neue Flat-Cone-Diffraktometer E2	121
M-14	Status of the new small-angle scattering instrument SANS-1 at the FRM II .	122
M-15	MARIA; the new reflectometer of the JCNS dedicated to magnetism and nano science	123
M-16	Minimisation of spurious strains by using a Si bent-perfect-crystal monochromator in residual strain scanning at the surface	124
M-17	Neutron optics from Helmholtz-Zentrum Berlin (former HMI)	125

M-18 Upgrade of FLEX: Future Perspectives for a New Cold Three-Axis Spectrometer at BENSC	126
M-19 Optimization of the NEAT neutron guide using genetic algorithms.	127
M-20 Unconventional Single Crystal Diffraction Studies with hot Neutrons on HEIDI at FRM II	128
M-21 Continuous Pole Figure Measurements as standard Method to analyse ODF at the Materials Science Diffractometer STRESS-SPEC	129
M-22 Going Ultra: How we can increase the length scales studied	130
M-23 Structure Powder Diffractometer SPODI: examples of in-situ materials characterisation	131
M-24 Focusing in q-space for angular dispersive neutron powder diffraction using an adjustable inpile fan collimator	132
M-25 New Perspectives for IN12	133
M-26 J-NSE: The Jülich Neutron Spin-Echo Spectrometer at the FRM II	134
M-27 Some applications of the multi-purpose REFSANS reflectometer	135
M-28 The new polarizer at RESEDA - simulation and first experimental results	136
M-29 Polarized ^3He for neutron instrumentation	137
M-30 Development of high m supermirrors	138
M-31 Monte Carlo simulations for focusing elliptical guides	139
M-32 Recent Advances in Neutron Holography: Resolving Atomic Positions with Picometer Accuracy	140
M-33 The planned single crystal diffractometer for biological macromolecules at the FRM II	141
M-34 TOF spectrometer NEAT: new capabilities and perspectives	142
M-35 First PGAI/NT experiments at the FRM II for the Ancient Charm project	143
M-36 Statistical Chopper method to separate elastic and inelastic scattered neutrons in TOF-experiments	144
M-37 The experimental area MEPHISTO for particle physics in the new east hall	145
M-38 Thales - The next generation cold three-axis spectrometer at the Institut Laue Langevin	146
M-39 A rotating and ramped spin turner for dynamical neutron polarization	147
M-40 POWTEX – The new High-Intensity Neutron TOF Diffractometer at FRM II	148
14 Nuclear and particle physics	149
M-41 Studies of UCN production with a small deuterium test setup at the FRM2	150
M-42 Accelerating matter effect and its first observation in neutron optics	151
M-43 Neutron Capture on Ge-76: A Background in Neutrinoless Double Beta Decay Experiments	152
M-44 Study the ROT-effect nature in $^{235}\text{U}(n, \gamma, f)$ -process	153
15 Magnetism and dynamic I	155
M-45 Freezing dynamics of magnetite ferrofluids studied by time-resolved Small Angle Neutron Scattering	156
M-46 Magnetic phase transition in $\text{Fe}_{50}\text{Pt}_{50}$ -xRhx thin films	157
M-47 Search for helimagnon excitations in MnSi: an inelastic neutron scattering study	158
M-48 Determination of the magnetic ground state in $\text{Na}_8\text{Cu}_5\text{O}_{10}$ by elastic neutron scattering	159
M-49 Determination of the magnetic ground state in $\text{Na}_8\text{Cu}_5\text{O}_{10}$ by elastic neutron scattering	160
M-50 Neutron diffraction study of the $R_2\text{PdSi}_3$ ($R = \text{Tb}, \text{Ho}, \text{Er}$)	161
M-51 Magnetism in REFeAsO ($\text{RE}=\text{Nd}, \text{Pr}$) investigated using neutron diffraction	162
M-52 Inelastic Neutron Scattering on the Antiferromagnetic Half-Heusler Alloy CeBiPt	163

M-53 Neutron scattering studies on spiral multiferroics	164
M-54 Magnetic ordering in HoCrO ₃ compound	165
M-55 Superconductivity and spin fluctuations in underdoped YBa ₂ Cu ₃ O _{6+x}	166
M-56 Metamagnetic transition in the single layer Ruthenates	167
M-57 Multitude of magnetic phases in Er ₂ Ni ₂ Pb	168
M-58 The study of the nature of the Low-Temperature Inter-Ion Correlations in CeAl ₃ by means of SAPNS	169
16 Soft matter	171
M-59 Lateral structures of buried interfaces in tri-block copolymer films	172
M-60 Solvent content in thin spin-coated polymer films: a neutron reflectometry study	173
M-61 Structural investigations of polymer blend films for photovoltaic applications	174
M-62 Multilamellar Vesicles Studied by Small Angle Neutron Scattering	175
M-63 Neutron Reflectivity Measurements on Conducting Polymer Films	176
M-64 Short Chain Carbohydrate Surfactant with Ethyl Spacer as “Super Hydrogelator”	177
M-65 On the structural features of polymeric spherulites in solution: a combined wide-Q SANS and microscopy study	178
M-66 Small Angle Neutron Scattering of Polyelectrolytes in Solution	179
M-67 The highly fragile glass former Decalin	180
M-68 Molecular Dynamics and Viscoelasticity of Polymer Chains in Presence of Nano Particles	181
M-69 Structure and dynamics of (polyethylene oxide) / layered silicate nanocomposites studied by neutron scattering	182
M-70 The volume phase transition of microgels and core-shell hybrid microgels followed by Small Angle Neutron Scattering	183
M-71 Dynamical and structural properties of microemulsions for decontamination of toxic compounds	184
M-72 Anchor architecture in tBLMs	185
M-73 Dynamics of Room Temperature Ionic Liquids by QENS	186
M-74 Comparing experiment and theory to understand Pd-NHC catalytic activity in solution	187
M-75 Methyl group dynamics in glassy, polycrystalline, and liquid coenzyme Q10 studied by QENS	188
M-76 Nanostructures at interfaces: Grazing incidence small angle neutron scattering (GISANS)	189
M-77 Looking closer to the interface: Investigation of polymer dynamics with grazing incidence neutron scattering	190
M-78 Structural analysis of self-organized diblock copolymers using GISANS	191
M-79 Molecular mobility of spider dragline and silkworm silk as a function of humidity studied by neutron spectroscopy techniques	192
M-80 Investigation of micellar crystallization in salted solutions	193
M-81 Wasser-in-Öl-Mikroemulsionen - Modellsysteme zur Untersuchung der Dynamik in eingeschränkte Geometrie?	194
M-82 Dynamics of Phospholipids used as Stabilizers in Colloidal Dispersions studied by Quasielastic Neutron Scattering	195
M-83 Water Uptake in Polyelectrolyte Multi Layers with different charge densities Studied by Neutron Reflectometry	196
M-84 Buried structures in thin block copolymer films – time-of-flight neutron reflectometry	197
M-85 Self-assembly and multi-compartment micellar hydrogel formation of amphiphilic di- and triblock copolymers containing fluorophilic blocks	198

M-86	Contrast Variation In Small-Angle Neutron Scattering From Magnetic Fluids As Polydisperse Superparamagnetic Systems	199
M-87	Lubrication in model joints – a study on shear dependence	200
M-88	Anomalous changes in the mesostructure of hydrated zirconia xerogels in the vicinity of the point of zero charge	201
M-89	Ultrasound-induced changes in mesostructure of amorphous iron (III) hydroxide xerogels: a SANS study	202
M-90	Neutron Reflectometry - A unique tool to Investigate Diffusion Processes in Solids on the Nanometre Scale	203
M-91	Hydration behavior of casein micelles in thin film: GISANS study	204
M-92	Reversible activation of a polyelectrolyte brush: Responsive monolayers.	205
M-93	Mineralization in the Presence of Proteins – an Exploration with Small Angle Neutron Scattering using Contrast Variation	206
M-94	Intrinsic bulk vortex lattice dynamics revealed by time resolved small angle scattering	207

Abstracts: Posters II (Tuesday) 209

17	Instrumentation and methods II	211
T-1	Perspectives for Materials Investigations at the Structured Pulse Engineering Spectrometer (SPES) Proposed by GKSS to be Built at ILL or FRM II	212
T-2	New Larmor precession based techniques	213
T-3	Performance of the Horizontal ToF-Neutron Reflectometer REFSANS at FRM II Munich, Highlighted by Recent Experimental Results	214
T-4	First experimental test of tensorial neutron tomography	215
T-5	A wedge-shaped polarizing analyzer - ray-trace MC simulations and experimental analysis	216
T-6	New polarized time-of-flight spectrometer DNS at FRM-II	217
T-7	The innovative upgrading of the SANS instrument D11 at ILL	218
T-8	State of art of experimental analysis at the PGAA facility in FRM II	219
T-9	SALSA at ILL: flexible beam optics for a large variety of applications	220
T-10	IN16B - der Aufbau eines neues Rückstreupektrometers am ILL	221
T-11	The reflectometer Super ADAM at the ILL	222
T-12	In-situ SEOP polarized 3He for PA on a polarized reflectometer	223
T-13	POLI-HeiDi: the New Polarised Neutron Diffractometer at the Hot Source (SR9) at the FRM II – Project Status	224
T-14	Solid state lens for neutron focusing	225
T-15	A novel analyzer design for the wide angle spin-echo spectrometer WASP	226
T-16	MIRA - New options	227
T-17	The new neutron guide system for the time-of-flight diffractometers at the beamline 7 of the pulsed neutron source IBR-2M Dubna	228
T-18	A quantitative study of neutron scattering related publications of all ENSA members from 2004 to 2006	229
18	Magnetism and dynamic II	231
T-19	Magnetism and Superconductivity in Cd-doped CeCoIn5	232
T-20	Twisted magnetization state in an antiferromagnetically coupled Fe/Si multilayer as probed by specular and off-specular polarized neutron scattering	233
T-21	Reversal Mechanism and Suppression of Training in Exchange Coupled System	234
T-22	Homogeneity and inhomogeneity in Dilute Magnetic Semiconductors	235
T-23	Magnetic Excitations in Rare-Earth Superlattices studied with Three-Axis Spectroscopy	236

T-24	Do antiferromagnetism and superconductivity coexist in 2% and 10% Ge doped CeCu_2Si_2 ?	237
T-25	Nature of magnetic correlations at the martensitic transformation in Ni-Mn-based Heusler systems studied by neutron polarization analysis	238
T-26	Study of the Self-Ordering of Cobalt Nanoparticles by PNR and Polarized SANS and GISANS	239
T-27	Neutron scattering study of $\text{Ce}_2\text{Pd}_{(1-x)}\text{Co}_x\text{Si}_3$ ($x = 0.0, 0.8, 1.0$)	240
T-28	Magnetic Excitations of a Distorted Kagome Antiferromagnet	241
T-29	Spin dynamics in superconducting CeCu_2Si_2	242
T-30	Magnetic ordering in MnSe studied using polarized neutrons	243
T-31	Magnetic excitations in R_2PdSi_3 studied by inelastic neutron scattering	244
T-32	Diffuse scattering from polarizing supermirrors	245
T-33	PNR reflectometry on Fe/ CoO films	246
T-34	Dynamical Properties of Ferromagnetic Shape Memory Alloys	247
T-35	PtMn-Behaviour in exchange biased CoFe/PtMn systems-studied using Neutron Scattering	248
T-36	Dimensionality crossover upon magnetic saturation in the itinerant ferromagnets Fe, Ni and Co	249
T-37	Determination of the Magnetic Structure of MnNCN	250
19	Materials Science and Engineering	251
T-38	Investigations Of Lattice Spacing On In718 Via Neutron Larmor Diffraction	252
T-39	Effect of residual stresses on in-service performance of friction stir welded joints	253
T-40	In-situ Strain Measurements in Composite Castings using Neutron Diffraction	254
T-41	In-situ SANS investigation of strained conductive polymer-carbon composites	255
T-42	Phase Transition Kinetics in Austenitic Ductile Iron (ADI)	256
T-43	Vortex Structure in NbTi/Nb multilayers	257
T-44	In situ temperature and stress-dependent measurements of Ni50.14Ti49.86 shape memory alloy.	258
T-45	Texture gradient in a bone-like extrusion profile of Mg-Ze10 alloy	259
T-46	Structure aspects of stabilization of ferrofluids by small-angle neutron scattering	260
T-47	In-situ high-temperature characterization of intermetallic precipitates in a new nickel-based superalloy	261
T-48	Probing polymer interfaces using time-of-flight grazing incidence small-angle neutron scattering	262
T-49	Water storage in novel undeformable hydrogel thin films as probed with in-situ neutron reflectivity	263
T-50	Microstructural Stability of Co-Re alloys at 1000°C measured by in-situ SANS	264
T-51	Neutron Diffraction Measurement of a AZ31B Magnesium Alloy Sheet Biaxially Deformed at Warm Temperatures	265
T-52	Effect of compressive and tensile residual stresses on constraint in fracture of welded components	266
T-53	SANS investigation of irradiation-induced phase separation in binary Fe-Cr alloys	267
T-54	Neutron diffraction study of texture evolution of ECAPed magnesium alloys	268
T-55	Bridging the gap between synchrotrons and neutrons in non destructive testing at the surface	269
T-56	Neutron Diffraction Measurement Of AZ31B Magnesium Alloy Sheet Biaxially Deformed At Warm Temperatures	270
T-57	Formation and stabilisation of miniemulsions based on the phase inversion concentration (PIC) method	271

T-58	Observation of the precipitation behaviour of Fe-25wt%Co-15wt%Mo by in-situ SANS and 3DAP	272
T-59	Measurement by neutron diffraction of all six components of X-ray elastic factors	273
20	Structure research	275
T-60	GISANS study of layered TiO ₂ :polymer films for photovoltaic applications .	276
T-61	Complex Metals and alloys: Neutrons for determining transition metal ordering	277
T-62	Investigation of crystal and magnetic structure of multiferroic GaFeO ₃ doped with manganese	278
T-63	Magnetic Structure of the Inverse Perovskite (Ce ₃ N)In	279
T-64	Silkworm silk under tensile stress as a function of humidity investigated by neutron spectroscopy	280
T-65	Exploring Li-Na-bearing Minerals as Prototypes for Li-ionic Conductors . .	281
T-66	Magnetische Struktur der inkommensurablen Spin-Ketten-Verbindung Ca ₂ Y ₂ Cu ₅ O ₁₀	282
T-67	GISAXS- and GISANS-Measurements on Ni- and Gd-Nanowires	283
T-68	Characterization of core-shell nanoparticles by neutron scattering	284
T-69	Unraveling the magnetic structure of CeCu ₂ (Si _{0.55} Ge _{0.45}) ₂ by using the complementarity of neutron and x-ray scattering	285
T-70	Magnetic structure of GdCu ₆	286
T-71	Texture evolution of the Mg/Al composite processed by the accumulative roll bonding (ARB)	287
T-72	Neutron Powder Investigation of Structure and Diffusion in variously doped Mayenites	288
T-73	The Solvation of Nanocarbons in Ammonia and Organic Solvents	289
T-74	Al ₄ (Cr,Fe): Single Crystal Growth by the Czochralski Method and Structural Investigation with Neutrons at FRM II	290
T-75	Martensitic Transformation of Ni-Mn-X Magnetic Shape Memory Alloys upon Cooling Under Magnetic Field	291
T-76	Columnar magnetic structure coupled with orthorhombic distortion in SrFe ₂ As ₂ ; one of the parent compounds of new FeAs superconductors . .	292
T-77	SANS Investigation of Martensite Nuclei in Potassium	293
T-78	Magnetic structure and orbital ordering in KCrF ₃	294
T-79	Structural Behaviour of Co ₂ SiO ₄ below Room Temperature	295
T-80	Deswelling kinetics of micellar solutions and hydrogels from temperature-sensitive amphiphilic block copolymers	296
T-81	Pyroxenes from Mars: Neutron powder investigation up to 900°C	297
T-82	Structural evolution of CoFeB/MgO multilayers upon annealing	298
21	Dynamics	299
T-83	Proton dynamics in solid HF	300
T-84	Dynamics in hydrous silicates studied by high temperature high pressure quasielastic neutron scattering	301
T-85	Structure-Property Relationships in the Crystals of the Smallest Amino Acid: An Inelastic Neutron Scattering Study of the Glycine Polymorphs as a Function of Temperature and Pressure	302
T-86	Water -clay interaction. Quasielastic neutron scattering study	303
T-87	Measurement of the phonon dispersion relation in YVO ₄	304
T-88	Benzene confinement in single-walled carbon nanotubes: inelastic and quasielastic neutron scattering	305
T-89	Behavior of molecular hydrogen in the confinement.	306

T-90	Molecular Hydrogen – A New Spectroscopic Property in the Attosecond Timescale Revealed with Neutron and Electron Compton Scattering	307
T-91	Renormalization of the longitudinal bond-stretching phonon branch in $\text{La}_{1.95}\text{Sr}_{0.05}\text{CuO}_4$ probed by inelastic neutron scattering technique	308
T-92	Dynamics of Argon in reduced dimensionality	309
T-93	Attosecond dynamics of protons in crystals: Momentum distribution and “anomalous” neutron scattering intensity	310
T-94	In-situ characterisation of the amorphisation of zeolites through average mean-square-displacements.	311
Index		313

Abstracts: Talks

Plenary talks

P-1 Exploring Condensed Matter with a Twist

Christian Pfleiderer¹

¹Technische Universität München, Physik Department E21, D-85747 Garching

Systems lacking inversion symmetry, such as selected three-dimensional compounds, multilayers and surfaces support Dzyaloshinsky-Moriya (DM) spin-orbit interactions. Instead of a spin-alignment, these interactions favor perpendicular spin orientation.

In recent years DM interactions attract great interest, because they may stabilize twisted and/or canted magnetic structures with a unique chirality. The inherent coupling between various properties provided by DM interactions is relevant for a variety of applications including, for instance, multiferroic and spintronic devices. On a more fundamental level DM interactions may stabilize novel magnetic states, that share certain similarities with liquid crystals and particle-like spin textures like skyrmions, merons and hedgehogs. Neutron scattering, in particular polarized neutron scattering techniques, provide a unique tool to identify the precise nature of these twisted magnetic structures and their dynamic properties.

A basic introduction will be given to DM interactions and the rich physics they may produce. Our interest in this field has been inspired by the magnetic field and pressure dependence of the magnetic properties of MnSi and related compounds. Under hydrostatic pressure of 15kbar a non-Fermi liquid state emerges in MnSi, where partial magnetic order reminiscent of liquid crystals is observed in a small pocket. At ambient pressure MnSi displays helical order, where we recently succeeded to identify the formation of a skyrmion lattice, i.e., a lattice of magnetic vortex lines. The skyrmion lattice in MnSi exhibits spin torque effects at remarkably low current densities, i.e., small electric currents generate a motion of the skyrmions. This underscores the importance of chiral magnets as show-cases, in which fundamental research readily connects with issues relevant to applications.

in collaboration with: S. Mühlbauer, F. Jonietz, M. Janoschek, A. Neubauer, S. Legl, R. Ritz, C. Franz, W. Münzer, S. Dunsiger, P. Nikolwits, T. Keller, R. Georgii, W. Häußler, P. Böni, U. Rößler, A.N. Bogdanov, B. Binz, R. Duine and A. Rosch

P-2 Interdomain dynamics in yeast alcohol dehydrogenase

Ralf Biehl¹, Bernd Hoffmann², Peter Fallus³, Michael Monkenbusch¹, Rudolf Merkel², Dieter Richter¹

¹Institut für Festkörperforschung

²Institut für Bio- und Nanosysteme

³Institut Laue-Langevin

The dynamics of proteins is a keystone to the understanding of their function as nanomachines or their mode of operation during the conversion to vitally important substances or while metabolizing toxic by-products of other production processes. To understand these processes we need information on length scales comparable to the size of the protein and its subdomains, which determine their functionality.

Neutron spin echo spectroscopy (NSE) is a versatile tool to determine the dynamics of macromolecules on nanometer scale and a timescale reaching from a few ps up to several 100 ns. The protein can be studied in a D₂O buffer solution similar to the physiological conditions. We show that aside of the observation of translational and rotational diffusion, NSE directly observes the correlated domain dynamics on its proper length and time scales.

We examine here the protein yeast alcohol dehydrogenase (ADH) responsible for the interconversion between alcohol and ketones under the utilization of the cofactor Nicotinamide Adenine Dinucleotide. ADH is a compact tetramer build up from 2 dimeric subunits.

The main characteristics of the protein dynamics can be described as the translational diffusion at low q and additional rotational diffusion at higher q , compatible with a rigid body model. Additionally it is possible to identify internal domain dynamics between the binding and the catalytic domain of ADH, which can be related to the dynamics of the conversion process in the active center in the cleft between both domains by a normal mode analysis.

P-3 From intracrystalline deformation to continent collision: Neutron texture goniometry of sheared rocks from the Alps

Nikolaus Froitzheim¹, Jan Pleuger²

¹Steinmann-Institut, Universität Bonn

²Departement Erdwissenschaften, ETH Zürich

Tectonic deformation in deep levels of the Earth's crust is accommodated by shear zones in which the rocks are transformed to mylonite through ductile deformation processes, including dislocation glide, dislocation creep, dynamic recrystallisation, grain boundary sliding, and diffusion creep, depending on the temperature and strain rate. These processes lead to reorientation of mineral grains and to crystallographic preferred orientation (texture). The texture yields information about (1) the active gliding system and hence the temperature during deformation, (2) the type of strain, e.g. extension versus flattening, (3) the kinematic path (e.g., simple shear versus pure shear, and the shear sense of simple shear). Additional and complementary information can be gained from the analysis of grain shape fabrics. Taken together, these methods allow extracting a maximum of tectonic information from deformed rocks. The application of these methods has allowed tectonic studies in the Alps to reach a new level of understanding.

Neutron texture goniometry, because of the high penetration capability, allows true volume measurement and therefore statistic measurements even in coarse-grained material. Three examples are presented which show the potential of neutron studies in the Alps: Quartz textures from a shear zone in the Southern Alps which formed at elevated temperatures during the intrusion of a granitoid pluton before the Alpine orogeny; omphacite textures in eclogites which yield evidence on processes at great depth in a subduction channel; and finally, quartz textures formed in a complex, polyphase history of shearing during continent collision.

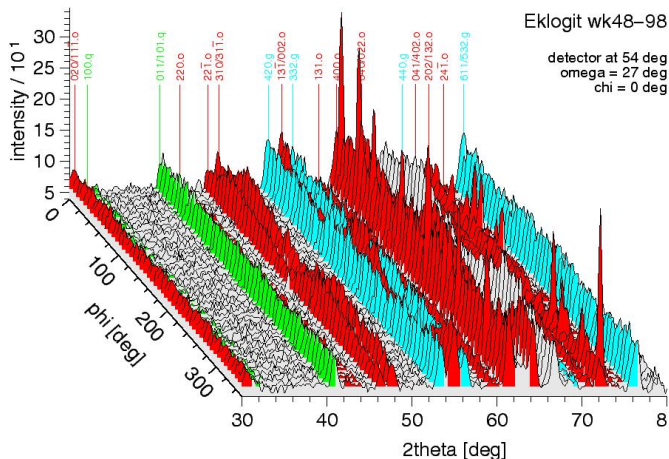


Figure 0.1: Stack of diffractograms measured at the neutron texture goniometer SV7-b at Forschungszentrum Jülich. The sample is eclogite from the Eastern Alps. Different colours indicate reflections from different mineral phases: red: omphacite, blue: garnet, green: quartz. Rotating the sample by 360 degrees (angle phi) results in rhythmic changes of reflection intensity for omphacite but not for garnet and quartz; that is, omphacite shows a preferred orientation whereas garnet and quartz are randomly oriented.

P-4 Quantum physics with neutrons

Gerald Badurek¹

¹Atominstytut der Österreichischen Universitäten Stadionallee 2, 1020 Wien, Österreich

Since its first successful realization in 1974 neutron interferometry has proven to be an almost ideal tool to experimentally verify fundamental concepts of quantum mechanics. Besides of a brief description of perfect crystal neutron interferometry and a short review of our hitherto performed quantum physics experiments, we report on recent and still ongoing neutron interferometric (ILL Grenoble) and polarimetric (ATI Vienna) experiments to demonstrate the so-called “quantum contextuality” between commuting observables. Entanglement between the spin and path degrees of freedom of single particles, generating Bell-like quantum states, is the key to such kind of measurements. So far we could verify a violation of a Bell-like inequality both by neutron interferometry and by neutron spin polarimetry. Aiming at the preparation of a single-particle triple entangled, so-called Greenberger-Horne-Zeilinger (GHZ)-like states, we consider the neutron’s energy degree of freedom as an ideal candidate. Complementing a series of experiments with entangled photons, in a recently performed neutron interferometric experiment, where two independent rf-fields were coupled to a neutron in an entangled state, we have found a value $M_{QM} = 2.555 \pm 0.005$ for triple entanglement between spin, path and energy degrees of freedom of individual neutrons, which is distinctly different from the quantity $M_{HV} \approx 2$ expected classically under the assumption of hidden variables. Due to their close relation with these topics, we report additionally on recent experiments for polarimetric and interferometric tomographic wave-packet reconstruction of Bell-states as well as of the measurement of topological quantum phases.

1 Session 1: Soft matter I

1.1 Study of lipid modified implant surfaces

Regine Willumeit¹, Frank Feyerabend¹, Sebastian Linser¹, Dieter Lott¹, Jean-Francois Moulin¹, Martin Haese-Seiller¹, Reinhard Kampmann¹, Andreas Schreyer¹, Vasyli Haramus¹

¹GKSS

Metal implants are widely used in bone repair or substitution. For a better acceptance of the implant, coating of the implant surface is one of the main interests in current research. A promising but so far not thoroughly investigated approach is the covering of the metal surface by phospholipids lipids (e.g. POPE) leading to an increase in chondroitin sulphate production by 30% for Human Articular Chondrocytes (HAC) and the osteogenic differentiation of Human Mesenchymal Stem Cells with bone nodule formation (1). The reason for this improvement however remains unclear and one can speculate that the physico-chemical properties and structure of the lipid layer(s) influence protein and cell attachment.

Neutron reflectivity is a powerful tool to study the coating structure. Data of the metallic substrate (Ti6Al7Nb), substrate with lipid coating, after incubation in water (0.5, 1.5 and 2 h) and growth medium were collected at REFSANS (FRM-II) and NeRo (GKSS). Modelling of NR data has shown that the substrate consists of a metal (112 nm) and an oxide layer (5 nm). The initial lipid coating consists of 45 POPE bilayers exhibiting a repeat distance of 5.2 nm. Incubation in water leads to decreasing of roughness of the lipid coating by 45 % and to the appearance of a sharp interference maximum at $q = 0.12 \text{ \AA}^{-1}$. Further incubation of the lipid coated implant material in growth medium shows the interaction with proteins and the reorganisation of the lipid layers.

R. Willumeit, M. Schossig, H. Clemens and F. Feyerabend: In-vitro Interactions of Human Chondrocytes and Mesenchymal Stem Cells, and of Mouse Macrophages with Phospholipid-Covered Metallic Implant Materials. *European Cells & Materials Journal* 13 (2007) 11-25.

1.2 Micellar solutions and hydrogels from temperature-responsive, amphiphilic block copolymers

Christine Papadakis¹, Abhinav Jain¹, Amit Kulkarni¹, Kordelia Troll¹, Weinan Wang¹, Achille M. Bivigou Koumba², Melissa Sharp³, Peter Busch⁴, Vitaly Pipich⁴, André Laschewsky², Peter Müller-Buschbaum¹

¹Physikdepartment E13, TU München

²Institut für Chemie, Universität Potsdam

³GKSS, Geesthacht

⁴JCNS-FRM II, Garching

Thermo-sensitive block copolymers consisting of a poly(N-isopropyl acrylamide) (PNIPAM), block and hydrophobic polystyrene (PS) end blocks, form spontaneously core-shell micelles in aqueous solution, which are swollen below the lower critical solution temperature (LCST) and collapsed above. At higher concentrations, physically cross-linked hydrogels are formed, which are of interest for a number of applications, e.g. in microfluidics. We have studied the temperature-dependent conformational changes of the micellar shell as a function of polymer architecture and the polymer concentration [1].

Using fluorescence correlation spectroscopy (FCS), dynamic light scattering (DLS), small-angle X-ray scattering (SAXS) and small-angle neutron scattering (SANS) with contrast matching by means of D₂O/H₂O mixtures, we have investigated a PS-*b*-PNIPAM diblock copolymer and a dPS-*b*-PNIPAM-*b*-dPS triblock copolymer, the latter having fully deuterated PS end blocks. The polymers were synthesized using RAFT. SANS was carried out at SANS-2, GKSS Geesthacht, and at KWS-2 at FRM II.

Using FCS, the critical micelle concentration in aqueous solution was found at 10-6 mol/l for both polymers. Above, it forms star-like core-shell micelles with a responsive shell. Using turbidimetry, the LCST was localized at 31°C. Moreover, the hysteresis upon cooling was found to depend on how deep in the two-phase region the solution has been heated. DLS and SAXS revealed the collapse of the micelles at the LCST as well as their clustering at higher temperatures. The hysteresis upon cooling is thus attributed to the dissolution of the clusters prior to swelling of the micellar shell.

The triblock copolymer forms flower-like core-shell micelles with a responsive shell. SANS revealed an invariant core radius and a significant decrease of the thickness of the responsive shell upon heating from 20 to 40°C (Fig. 1). The combination of single-molecule and scattering methods is thus ideal to gain detailed insight into the structural changes on a broad range of concentrations and length scales.

K. Troll, A. Kulkarni, W. Wang, C. Darko, A.M. Bivigou Koumba, A. Laschewsky, P. Müller-Buschbaum, C.M. Papadakis, *Colloid Polym. Sci.* 286, 1079 (2008).

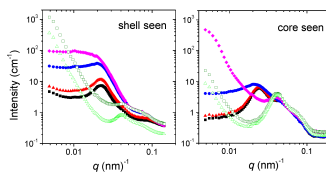


Figure 1.1: SANS curves from a 17 wt.-% solution of dPS-*b*-PNIPAM-*b*-dPS in D₂O (left) and in a 20:80 D₂O/H₂O mixture (right) at different temperatures. Filled squares: 20°C, filled triangles: 25°C, filled circles: 31°C, filled diamonds: 32°C, open squares: 33°C, open triangles: 40°C.

1.3 Formation Of Polyelectrolyte/Lipid Composite Multilayer Structures

Rumen Krastev¹, Jianghai Chen¹, Marta Kolasinska¹, Thomas Gutberlet²

¹Max-Planck Institute of Colloids and Interfaces

²Forschungszentrum Jülich

Hybrid systems between biological and artificial materials (e.g. polymers or polyelectrolytes) are sought, since they allow one to combine the functionality of natural molecules with a potential for tailoring the thickness and the shape of coatings. Lipids self-assembling in well ordered (bi)layers can be used to compartmentalise polyelectrolyte (PE) multilayers (PEM) structures thus allowing complex well-ordered layer structures to be obtained. PEM adsorbed on solid support were introduced as highly versatile surface coatings. Their formation is based on the layer-by-layer (LbL) deposition technique, which exploits the fact that PE adsorb onto surfaces of opposite charge and that the surface charge density is reversed by this process. Because of its versatility the technique has been extensively used to produce variety of materials with potential applications in biosensors, microelectronics, and optics.

The neutron reflectometry was extensively used in the present study to monitor in situ the formation of complex lipid/PEM or lipid/metal nano particles composite materials deposit on solid support. Comparison with other physical methods like QCM, AFM, UV-spectrometry allowed for detailed picture of the build-up process to be obtained.

We demonstrate formation of mixed structures which consist of PEM with incorporated lipid layers. Formation of DMPC layer with thickness of 5 nm is possible onto PEM. Homogeneous lipid layers are formed only at temperatures above the temperature of the main phase transition when the lipid is in fluid state. Fine tuning of the preparation procedure allowed formation of (charge) asymmetric lipid layers. PE layers were deposited also onto these lipid layers building-up PEM/lipid bilayer/PEM charge gradient sandwich like structures. Lipid vesicles were used as carriers of metal particles. Well ordered 2D compartments in the PEM filled with particles were prepared.

1.4 The solid-liquid boundary condition for flowing liquids

Max Wolff¹, Philipp Gutfreund¹, Marco Walz², Nicole Voss², Stefan Gerth², Andreas Magerl², Hartmut Zabel¹

¹Lehrstuhl für Festkörperphysik

²Lehrstuhl für Kristallographie

The solid-liquid interface introduces anisotropy to a fluid and represents a singularity that may result in distinct properties as compared to the volume. For example, in a static liquid this fact is manifested by tuneable absorption for molecules at functionalised interfaces. For flowing liquids, the discontinuity at the interface is quantified by a phenomenological number called slip length. To understand the microscopic origin of slip the knowledge on static samples has to be complemented by measurements under shear. Neutron scattering under grazing incident beam geometry will certainly play a major role in this context. In this presentation the possibilities offered by surface sensitive scattering techniques are evaluated.

In the first, part slip in simple liquids will be related to the structure at the solid-liquid interface. For hexadecane the amount of slip measured by complementary techniques can not be explained by a depleted layer (two-fluid model).

In the second part, the focus will be on complex liquids. For a micellar system, information over a large range of length scales is extracted from data collected under grazing incident beam geometry. The anisotropy introduced by the interface forces a rearrangement of the micellar structure. We show that micelles prefer to grow epitaxially at an interface which is attractively terminated for the micelles corona. Information on the relevant lateral correlation lengths can be extracted from diffuse scattering. Micelles crystallizing at different nucleation sites start orienting but lose long-range correlation with increasing overlap of the crystallites. This structural information is related to changes in the viscosity. For in-situ measurements under shear load, we have combined the technique of neutron reflectivity with rheology. We show that shear aligns the crystallites but decreases the long-range correlation. After stopping the shear a slower relaxation of the crystalline structure is found close to the attractive interface. This effect relates well to the molecular dynamics that were found to be faster in the vicinity of a repulsive interface.

2 Session 2: Softmatter II

2.1 Protein-Protein Interactions in Solution Studied by Small-Angle Scattering

Fajun Zhang¹, M. W. A. Skoda², R. M. J. Jacobs³, L. Ianeselli¹, R. A. Martin⁴, S. Weggler⁵, A. Hildebrandt⁵, O. Kohlbacher⁶, C. M. Martin⁷, S. Prevost⁸, F. Schreiber¹

¹Institut für Angewandte Physik, Universität Tübingen, Tübingen, Germany

²ISIS, Rutherford Appleton Laboratory, Chilton, Didcot, UK

³Chemistry Research Laboratory, University of Oxford, Oxford, UK

⁴School of Physical Science, University of Kent, Canterbury, UK

⁵Zentrum für Bioinformatik Saar, Saarbrücken, Germany

⁶Zentrum für Bioinformatik Tübingen, Tübingen, Germany

⁷SRS, Daresbury, Warrington, Cheshire, UK

⁸Helmholtz Center Berlin, Berlin, Germany

Recent progresses in the study of protein-protein interactions in solution have significantly improved the understanding of complicated biological processes [1-4]. For example, George and Wilson proposed a relation between protein crystallization behavior and the osmotic second virial coefficient, which provides a way to optimize the condition for protein crystallization [3]. The balance of a short-ranged attraction with a long-ranged Coulombic repulsion could result in the equilibrium cluster formation in protein solution, which may enhance the crystal formation [4]. Using the model globular protein bovine serum albumin (BSA) and ovalbumin, we have studied the effective protein-protein interactions in solution as a function of protein concentration, ionic strength and the chemical nature of added salts, by small angle X-ray and neutron scattering. It was found that DLVO theory is suitable at both low protein and ionic strength [5]. Novel phase behavior was observed when multivalent counterions were added in protein solutions [6]. Negatively charged globular proteins in solution undergo a condensation upon adding trivalent counterions between two critical concentrations C^* and C^{**} , $C^* < C^{**}$. This reentrant condensation behavior above C^{**} is caused by short-ranged electrostatic interactions between multivalent cations and acidic residues. SAS measurements indicate a short-ranged attraction between counterion-bound proteins near C^* and C^{**} . Monte Carlo simulations (under these strong electrostatic coupling conditions) support an effective inversion of charge on surface side chains through binding of the multivalent counterions.

[1] R. Piazza, *Curr. Opin. Colloid Interface Sci.* 5, 38 (2000) and 8, 515 (2004).

[2] A. Tardieu, A. Le Verge, M. Malfois, F. Bonneté, S. Finet, M. Riès-Kautt, L. Belloni, *J. Cryst. Growth* 196, 193 (1999). F. Bonneté, S. Finet, A. Tardieu, *J. Cryst. Growth* 196, 403 (1999).

[3] A. George, W. Wilson, *Acta Cryst.* D50, 361 (1994).

[4] A. Stradner, H. Sedgwick, F. Cardinaux, W. C. K. Poon, S. U. Egelhaaf, P. Schurtenberger, *Nature* 432, 492 (2004).

[5] F. Zhang, M.W.A. Skoda, R.M.J. Jacobs, R.A. Martin, C.M. Martin, F. Schreiber, *J. Phys. Chem. B*, 111, 251 (2007)

[6] F. Zhang, M.W.A. Skoda, R.M.J. Jacobs, S. Zorn, R.A. Martin, C.M. Martin, G. F. Clark, S. Weggler, A. Hildebrandt, O. Kohlbacher, F. Schreiber, submitted

2.2 Temperature Dependence Of The Dynamics In Sugar Surfactant Based Bicontinuous Microemulsions As Seen With Quasielastic Scattering Techniques

Thomas Hellweg¹, Stefan Wellert², Matthias Karg³, Andre Richardt⁴, Olaf Holderer⁵

¹Physikalische Chemie I, Universitätsstr. 30 95444 Bayreuth, Germany

²Hahn-Meitner Institut, Glienicker Str. 100, 14109 Berlin, Germany

³TU Berlin, Stranski Lab., Str. d. 17.Juni 124, 10623 Berlin, Germany

⁴WIS Munster, Humboldtstraße, 29633 Munster, Germany

⁵Jülich Centre for Neutron Science (JCNS)Sub-Office at the FRM II Lichtenbergstr. 1, 85747 Garching, Germany

Neutron spin-echo (NSE) spectroscopy and dynamic light scattering (DLS) are excellent tools to study dynamic processes like diffusive translational motions and undulations of the surfactant membrane in microemulsions [1]. The low q -range observed by DLS reveals information about diffusive dynamics, while NSE spectroscopy detects the bending undulations of the surfactant membrane on local length scales, much smaller than typical structural lengths in microemulsions. At present, all published NSE measurements of the dynamics of bicontinuous microemulsions study the bending elasticity and changes of the elastic constants as a function of the microemulsion composition [2].

In present work, a quaternary microemulsion system water / rapeseed methyl ester / sugar surfactant / pentanol is studied. Microemulsions, especially from the bicontinuous region are investigated in order to design environmentally compatible and low irritant decontamination media for the removal of toxic industrial compounds and chemical warfare agents. An important feature of such sugar surfactant based systems is the, compared to surfactants of the alkyl oligo ethyleneoxide group, low influence of the temperature on the phase behavior.

The theoretical approach of Zilman and Granek (ZG) [3] allows the determination of the bending elasticity from the measured normalized intermediate scattering function $S(q,t)/S(q)$, which we measured at different temperatures. Here, for the first time, we analyze and discuss the temperature dependence of the dynamics of the interfacial film in bicontinuous microemulsions within the framework of ZG.

[1] T. Hellweg and D. Langevin; Physical Review E, 1998, 57, 6825-6833

[2] M. Mihailescu et.al. ; Journal of Chemical Physics, 2001, 115, 9563-9577

[3] A.G. Zilman and R. Granek; Chemich

2.3 Structure and Dynamics of Reverse Micelles Under the Addition of Amphiphilic Triblock Copolymers

Tinka Spehr¹, Bernd Stühn², Bernhard Frick³

¹TU Darmstadt and Institut Laue-Langevin, Grenoble

²TU Darmstadt

³Institut Laue-Langevin

We investigate the static structure and the dynamical behaviour of a d-water/AOT/toluene-d8 droplet microemulsion under the addition of the amphiphilic triblock copolymer poly(ethyleneoxide-styrene-ethyleneoxide) (PEO-PS-PEO). We chose a molar ratio water to AOT of $w=8$ where the pure microemulsion consists of reverse water swollen AOT micelles with a water core radius of about 12 Å that are dispersed in toluene. Addition of the polymer leads to the formation of a transient network. By means of Small Angle Neutron Scattering (SANS) we characterize the static structure of the pure microemulsion and the polymer-induced ordering. The combination of Dynamic Light Scattering (DLS) and Neutron Spin Echo (NSE) allows to investigate the dynamics on a large range of timescales. We discuss the effect of polymer addition on droplet diffusion and droplet shell fluctuations.

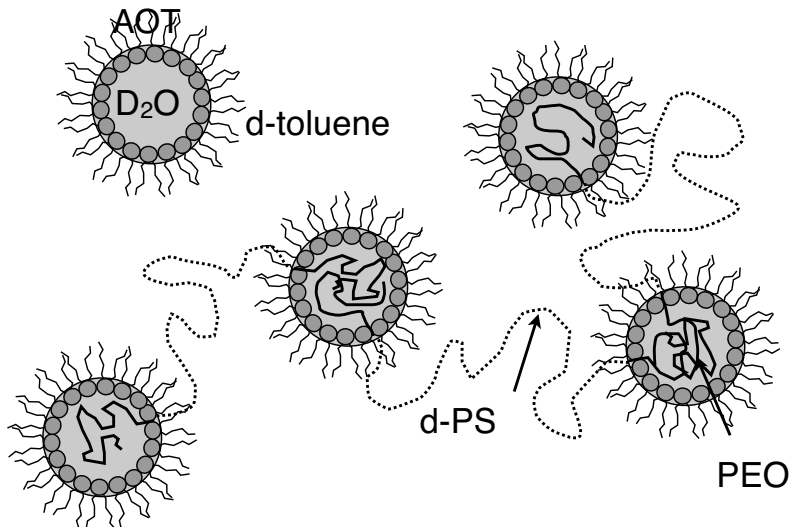


Figure 2.1: Schematic sketch of the transient network formed of water swollen reverse micelles and an amphiphilic triblock copolymer.

2.4 Self-diffusion in molecular liquids: medium-chain n-alkanes and coenzyme Q10 studied by QENS

Christoph Smuda¹, Sebastian Busch¹, Gerd Gemmecker², Tobias Unruh¹

¹Technische Universität München, Forschungsneutronenquelle Heinz Maier-Leibitz (FRM II), D-85747 Garching

²Bayerisches NMR-Zentrum, Chemie-Department, Technische Universität München

A systematic time-of-flight quasielastic neutron scattering (TOF-QENS) study on diffusion of n-alkanes in a melt is presented for the first time. As another example of a medium-chain molecule, coenzyme Q10 is investigated in the same way. The data were evaluated both in the frequency and in the time domain. TOF-QENS data can be satisfactorily described by different models, and it turned out that the determined apparent diffusion coefficients are largely independent of the model used for the description of the local motions [1]. The derived diffusion coefficients are compared with values measured by pulsed-field gradient nuclear magnetic resonance (PFG-NMR) [2]. With increasing chain length, an increasing difference between the TOF-QENS diffusion coefficient and the PFG-NMR diffusion coefficient is observed [1].

Molecular dynamics (MD) simulations of the n-alkane C32H66 were performed providing an insight into the dynamics on a pico- to nanosecond time scale. The extracted mean square displacements (msd) of the atoms as well as the center of mass motion of the molecules deviate significantly from a linear behavior as it is predicted by Fick's law. This deviation was experimentally confirmed by resolution-resolved TOF-QENS measurements [3] which are presented and discussed in comparison to the results of MD simulations.

[1] C. Smuda, S. Busch, G. Gemmecker, and T. Unruh, *J. Chem. Phys.*, in print

[2] E. von Meerwall, S. Beckman, J. Jang, and W. L. Mattice, *J. Chem. Phys.* 108, 4299 (1998)

[3] T. Unruh, C. Smuda, S. Busch, J. Neuhaus, and W. Petry, *Phys. Rev. Lett.*, submitted

3 Session 3: Instrumentation

3.1 TOF inelastic neutron scattering on D₂, a key tool on the way to a very strong UCN source

Axel Reimer Müller¹, Erwin Gutmiedl¹, Rainer Stöpler¹, Stephan Paul¹, Andreas Frei¹, Markus Urban¹, Helmut Schober², Tobias Unruh³

¹Technische Universität München, Physik Department E18, D-85747 Garching

²Institut Laue Langevin

³Technische Universität München, Forschungsneutronenquelle Heinz Maier-Leibitz (FRM II), D-85747 Garching

The development of strong next generation UCN sources to deal with fundamental research questions like the neutron EDM or its lifetime is on the way at various neutron centers like PSI, ILL and FRM2. The achievable UCN density is a function of the UCN down scattering cross section, the incident neutron flux and spectrum and the losses from the converter material itself. The method of inelastic time of flight neutron scattering provides now a technique to study from the measured dynamic structure factor $S(q, \omega)$ of a possible converter material the production probability on the neutron energy loss side as well as the UCN losses on the neutron gain side. The data for deuterium as function of different freezing methods, temperature treatments and ortho/para concentrations measured at the TOFTOF spectrometer at the FRM2 and the IN4 at the ILL are shown. The drastic influence on the UCN source design are presented.

At the end a method to get an absolute comparison between different present (He, D₂, H₂) or future (O₂, CD₄N₁₅) UCN converter materials on their UCN efficiency using the inelastic neutron scattering function $S(q, \omega)$ is shown.

Besides our interest to build a strong UCN source it turned out that it is also an interesting substrate in turns of solid state physics with the new key tool to tune the spin concentration between 66 % and 98 %.

Support from the Deutsche Forschungsgemeinschaft, The cluster of excellence “Universe” and the MLL Maier Leibnitz Laboratory

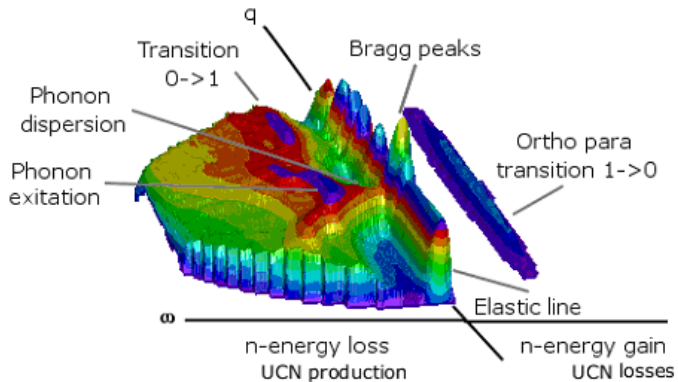


Figure 3.1: The figure shows the dynamic structure factor of solid deuterium measured at 4 K and an ortho/para spin concentration of 66 %.

3.2 The phase-space transformer up-scattering project: first results

Simon Mayer¹, Helmut Rauch¹, Geza Zsigmond², Peter Allenspach², Peter Geltenbort³, Philipp Schmidt-Wellenburg³

¹ATI

²PSI

³ILL

Neutrons from a moderating system have a certain phase space density corresponding to the moderator temperature. According to the Liouville Theorem, the phase-space density cannot be changed within a conservative system, but by using advanced cooling methods. Nevertheless it is possible to change the shape and position of the phase-space element using conservative forces. Based on the original idea of Schelten and Alefeld[1], a new kind of phase-space transformation (PST) has been proposed: to change the position of the phase-space element in order to produce a well defined neutron beam by coherent up-scattering of a UCN gas. It has been shown that this principle could yield to factors of one hundred and more compared to “classical” beam generation[2]. The Atominstytut and the Paul Scherrer Institut have joined to design and construct a proof of principle-experiment. The aims of this experiment are to exploit the feasibility as well as the experimental limitations and to validate preceding MC-simulations[3]. Employing a sophisticated mechanical system, Stage-2 Potassium intercalated HOPG crystals ($d = 8.74 \text{ \AA}$) are moved with velocities up to 250 m/s. First results of the experiment, which took place in April and May 2008 at the ILL, will be presented.

[1] J. Schelten, B. Alefeld, Backscattering spectrometer with adapted Q-resolution at the pulsed neutron source, in: R. Scherm, H.H. Stiller (Eds.), Proceedings of the Workshop on Neutron Scattering Instrumentation for SNQ, Report July-1954, 1984.

[2] H. Rauch, E. Jericha, Intensive neutron beams from a dense UCN gas, in: Proceedings of the ICANS-XVI, vol. II, FSZ-Jülich, 2003, p. 857-864.

[3] S. Mayer, G. Zsigmond, P. Allenspach, Monte-Carlo simulation of phase space transformation of ultra-cold neutrons, Nucl. Instr. and Meth. A 586 (2008) 110-115



Figure 3.2: Fig. 1: The phase-space transformer installed at the UCN source PF2 (ILL, Grenoble).

3.3 Overview of the new PGAA and PGAI facility at the research reactor FRM II

Petra Kudejova¹, Lea Canella², Ralf Schulze¹, Jan Jolie¹, Andreas Türler², Nigel Warr¹

¹Institut für Kernphysik, Univ. zu Köln

²Institut für Radiochemie, Technische Universität München

At the new research reactor FRM II in Garching the beam guide with the highest cold neutron flux is dedicated to the Prompt Gamma-Ray Activation Analysis (PGAA) and related neutron capture experiments. Using the (n,gamma) reaction, we measure non-destructively the elemental composition of diverse samples usually of mg-g weight. This year, we have measured already few interesting samples from diverse fields: magnetic nano-particles for medicine, new single-crystal intermetallic compounds, impurities in silicon wafers, air filters for ecology or meteorites [1]. We also successfully finished first gamma-gamma coincidence measurement on ⁷⁷Ge [2]. Now the system has been changed for the position sensitive analysis of valuable archaeological objects in frame of the EU Ancient Charm project [3]. Our part of the project, called PGAI-maging combined with Neutron Tomography (PGAI/NT) is to make a 3D map of the elemental composition of the archaeological objects. Our goal is to reach 1mm³ precision [3].

We have designed a partially ballistic form of the neutron guide with the aim to concentrate the cold neutrons at the target position of the PGAA experiment. With this elliptical tapering and a removable neutron guide end of 1.1m length, we can choose between two positions for the measurement: For bigger samples one is situated about 35cm behind the neutron guide exit window with a neutron flux up to 7.3×10^9 n/cm²s and with an useful beam dimensions of 14mm x 38mm (width x height). For small samples the beam is focused to a spot of about 4mm x 10mm at a 9cm distance. The flux measured about 10.5cm far from the exit window reached 1.7×10^{10} n/cm²s. The PGAA neutron spectrum has a mean wavelength of 6.7Å [4], the thermal neutron flux equivalent corresponds to 6.3×10^{10} n/cm²s. We are not aware of any higher cold neutron flux worldwide at this time.

[1] L. Canella, P. Kudejova, R. Schulze, N. Warr, A. Türler, J. Jolie: State of art of experimental analysis at the PGAA facility in FRM II, poster presentation at this conference

[2] G. Meierhofer: Prompt Gamma Rays in ⁷⁷Ge after Neutron Capture on ⁷⁶Ge, presentation at this conference

[3] R. Schulze, P. Kudejova, L. Canella, J. Jolie, A. Türler, Z. Kis, L. Szentmiklosi, T. Belgys: First PGAI/NT experiments at the FRM II for the Ancient Charm project, poster presentation at this conference

[4] P. Kudejova, G. Meierhofer, K. Zeitelhack, J. Jolie, R. Schulze, A. Türler, T. Materna, The new PGAA and PGAI facility at the research reactor FRM II in Garching near Munich, JRNC in press

3.4 Polarimetric Neutron Spin Echo Spectroscopy

Catherine Pappas¹, Eddy Lelièvre-Berna², Phillip Bentley³, Bela Farago², Peter Falus², Evgeny Moskvina⁴, Sergey V. Grigoriev⁵

¹HZ Berlin

²ILL

³HZ Berlin and ILL

⁴PNPI and HZ Berlin

⁵PNPI

Neutron Spin Echo spectroscopy (NSE) uses polarized neutrons and in turn polarization analysis is an intrinsic feature of NSE [1]. However, the multifaceted dynamics of antiferromagnets and hellimagnets ask for more than the classical Neutron Spin Echo set-up (NSE). In these systems the magnetic interaction vector is complex and the neutron beam polarization is not necessarily flipped upon scattering but can rotate at any angle around or towards a specific direction. The only way to access the components of the scattered polarization that are transverse to the incoming polarization is to implement a zero-field area around the sample position. Here we present the feasibility test and first results of the Polarimetric NSE, a powerful technique which combines a variant of the Intensity Modulated NSE (IMNSE) [2] and the Cryopad [3]. The Cryopad is a zero-field polarimeter based on Meissner shields and μ -metal screens able to do the most generalized polarization analysis experiments measuring all theoretically possible pair-correlation functions at any point of the reciprocal space. On the other side, IMNSE is a powerful variant of NSE that disconnects completely the sample area from the precession area at the price of some intensity losses due to the addition of polarizer and analyzer devices.

This new technique was successfully developed on the wide angle NSE spectrometer SPAN at the HMI [4] and then implemented on IN15 [5] at the ILL, where new results on the magnetic relaxation in MnSi, a reference hellimagnet were obtained.

[1] F. Mezei (ed.), Neutron Spin Echo, Lecture Notes in Physics Series, Vol. 128 (Springer, Heidelberg, 1980) and in "Neutron spin echo spectroscopy", Lecture Notes in Physics Series, Vol. 601, ed.: F. Mezei, C. Pappas, Th. Gutberlet (Springer, Heidelberg, 2003)

[2] B. Farago, F. Mezei, Physica B 136 (1986) 627.

[3] F. Tasset, Physica B 157 (1989) 627 and E. Lelièvre-Berna, P.J. Brown, F. Tasset, K. Kakurai, M. Takeda, L.-P. Regnault, Physica B 397 (2007) 120-124

[4] C.Pappas, G. Kali, T. Krist, P. Böni and F. Mezei, Physica B 283 (2000) 365-371

[5] P. Schleger, G. Ehlers, A. Kollmar, B. Alefeld, J. F. Barthelemy, H. Casalta, B. Farago, P. Giraud, C. Hayes, C. Lartigue, F. Mezei and D. Richter, Physica B, 266 (1999) 49

3.5 TOPAS, the future thermal time-of-flight spectrometer at the FRM II

Jörg Voigt¹, Michael Prager², Klaus Bussmann³, Hans Kämmerling³, Achim Heynen³, Thomas Brückel³

¹JCNS, Forschungszentrum Jülich

²Forschungszentrum Jülich

³Forschungszentrum Jülich

We present the design of the new thermal time-of-flight TOF spectrometer with polarizations analysis, TOPAS. The design is optimized for a high intensity instrument with a large solid angle coverage to enable fast surveys of the scattering function $S(Q, \omega)$ with large momentum and energy transfer.

The instrument features a rather compact design with a sample to detector distance of 2.5 m, allowing a solid angle coverage of 3 sr. and repetition rates as high as 900 Hz. Position sensitive detectors in combination with the TOF analysis give access to $S(Q, \omega)$ in four dimensional momentum and energy transfer space. Monochromatization is achieved by a system of Fermi choppers, resulting in an overall relative elastic resolution of about 4 %. A high intensity at the sample position is provided by an elliptically focusing neutron guide, transferring thermal neutrons over 50 m from the reactor to the spectrometer. We show that such a long neutron guide is necessary to effectively focus thermal neutrons.

3.6 Light-induced gratings in polymers and polymer nanocomposites for neutron optics

Christian Pruner¹, Martin Fally², Romano Rupp², Irena Drevensek-Olenik³, Mostafa Ellabban⁴, Yasuo Tomita⁵, P. Klaus Pranzas⁶, Jürgen Vollbrandt⁶, Helmut Eckerlebe⁶, Roland P. May⁷, Augustinus Asenbaum¹

¹Fachbereich Materialforschung und Physik, Universität Salzburg, Österreich

²Nichtlineare Physik der kondensierten Materie, Universität Wien, Österreich

³Fakultät für Mathematik und Physik, Universität Ljubljana und J. Stefan Institut, Slowenien

⁴Nichtlineare Physik der kondensierten Materie, Universität Wien, Österreich und Abteilung Physik, Universität Tanta, Ägypten

⁵Universität für Elektro-kommunikation, Tokyo, Japan

⁶GKSS Forschungszentrum Geesthacht, Deutschland

⁷Institut Laue-Langevin, Grenoble, Frankreich

We report the applicability of optically structured polymers, polymer-dispersed liquid crystals and polymer-dispersed nanoparticles as powerful elements for neutron optics. Furthermore, neutron diffraction is shown to serve as a tool for following the temporal evolution of the polymerization process. Diffraction experiments of cold neutrons from transmission gratings made of either a 3 mm thick polymethylmethacrylate, a 30 micron thick holographic polymer-dispersed liquid crystal (H-PDLC) or polymer-dispersed SiO₂ nanoparticles are presented. The gratings were recorded by means of a standard holographic two-wave mixing setup. Diffraction measurements were carried out at a small angle neutron scattering beamline at the Geesthacht neutron facility or at the Institut Laue-Langevin. For characterizing the gratings with neutrons we monitored the angular dependencies of the diffraction efficiency at various wavelengths (Fig. 1).

We show that by employing holographically produced gratings in PMMA arranged in triple Laue geometry allow the successful setup of an interferometer for cold and ultracold neutrons. Using this device we measured the coherence function of a cold neutron beam by means of interferometry [1]. The result for H-PDLC was unexpected and amazing: the light-induced refractive-index modulation for neutrons is nearly 2 orders of magnitude larger than in the best photo-neutron-refractive materials probed up to now [2]. First experiments on gratings made of holographic polymer-dispersed nanoparticles revealed their high potential and versatility for use as neutron optical elements. Future perspectives for use of these novel neutron optical devices are illustrated.

[1] C. Pruner, M. Fally, R. A. Rupp, R. P. May, and J. Vollbrandt, Nucl. In-strum. Meth. A 560, 598 (2006)

[2] M. Fally, I. Drevensek-Olenik, M. A. Ellabban, K. P. Pranzas, J. Vollbrandt, Phys. Rev. Lett. 97, 167803 (2006)

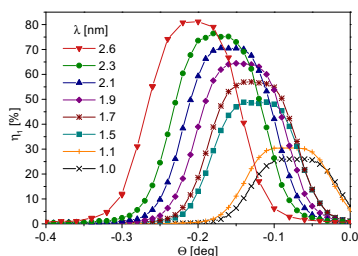


Figure 3.3: Figure 1: Rocking curves of PMMA for various wavelengths with diffraction efficiencies of up to 82%

3.7 The Neutron/X-Ray Contrast and Spin-Echo Reflectometer N-REX+ at FRM II: Present Status, First Experiments and Future Perspectives

Adrian Rühm¹, Max Nülle¹, Felix Maye¹, Marton Major¹, Janos Major¹, Helmut Dosch¹

¹MPI für Metallforschung, Stuttgart

The neutron/X-ray-contrast reflectometer N-REX+ [1] at the neutron guide NL-1 of FRM II offers unique research possibilities for the study of surfaces, buried interfaces, thin layers, and complex multilayers on the nanoscale, both within and perpendicular to the surface plane. One special feature of the instrument is the in-situ combination of X-ray and neutron reflectometry, which is especially interesting for the study of complex multicomponent systems or of irreversible time-dependent processes. Another novel feature is the SERGIS (spin-echo resolved grazing incidence scattering [2,3]) technique, which enables the structural characterization of samples on lateral length scales ranging from the nanometer up into the micron range. The big advantage of SERGIS compared to standard techniques for this purpose is that it requires no collimation in the direction of interest, so that the very high q -resolution is not penalized by the typical intensity loss. Besides these novel developments, N-REX+ provides standard polarized neutron reflectometry (PNR) and grazing incidence scattering (GISANS, GIND) with wide-angle spin analysis. The instrument also allows to study free liquid surfaces, thanks to the possibility to tilt the incident neutron beam. The orientation of the sample surface is arbitrary (e.g. horizontal or vertical).

The instrument N-REX+ is now available for external users. Based on first experiments conducted at N-REX+, we will present the current status of the instrument as well as plans for future developments.

[1] A. Rühm, U. Wildgruber, J. Franke, J. Major, and H. Dosch, "n/X materials science reflectometer at FRM-II in Garching", In: "Neutron Reflectometry, A Probe for Materials Surfaces", Proceedings of a Technical Meeting organized by the International Atomic Energy Agency and held in Vienna, 16-20 August 2004, Vienna, Austria, 2006, p. 161-175.

[2] G. P. Felcher, S. G. E. te Velthuis, J. Major, H. Dosch, C. Anderson, K. Habicht, T. Keller, in: I. S. Anderson, B. Guerd (Eds.), *Advances in Neutron Scattering Instrumentation*, Proceedings of SPIE, Vol. 4785, SPIE Optical Engineering Press, Bellingham, WA, USA, 2002, p. 164.

[3] J. Major, H. Dosch, G. P. Felcher, K. Habicht, T. Keller, S. G. E. te Velthuis, A. Vorobiev, M. Wahl, *Physica B* 336, 8 (2003).



Figure 3.4: N-REX+ - The neutron / X-ray contrast reflectometer with spin-echo option

4 Session 4: Magnetism I

4.1 Highly Ordered Spin-State in an Epitaxial Spin-Valve as Observed by Polarized Neutron Reflectometry

Katharina Theis-Bröhl¹, Frank A. Brüssing², Maximilian Wolff², Boris P. Toperverg², Hartmut Zabel²

¹University of Applied Science, 27568 Bremerhaven

²Ruhr-University Bochum, D-44780 Bochum, Germany

The combination of different magnetic elements within one magnetic stack is at the heart of today's spintronic applications. Our aim is the understanding of interactions between different magnetic elements in a stack of magnetic layers.

In order to study such interactions we have grown by molecular beam epitaxy several periods of Fe and Co on MgO (001) separated by Cr layers which form an epitaxial spin-valve superlattice. We adjusted the film thicknesses of the Fe and the Co layers so that the magnetic moments in the both magnetic layers are comparable and cancel out in the case of an antiparallel spin state. In order to achieve a proper spin-valve behavior we have chosen a Cr spacer thickness which provides a weak antiferro-magnetic coupling. The quality of the layering and the epitaxial relationship were verified via x-ray methods.

For investigating the arrangement of the magnetic moments in the different magnetic layers we performed polarized neutron reflectometry studies in the as-grown state and with an applied magnetic field. Ferromagnetic and antiferro-magnetic alignment between neighboring Co and Fe layers can be recognized in the specular data in Fig. 1(a) and (b) via intensity variations on the nuclear [Co/Cr/Fe/Cr] superlattice peaks which are different for odd and even orders. Interestingly, additional half-order peaks appear in the as grown state in Fig 1(c) indicating a new magnetic state. In this state an antiferromagnetic alignment between complete neighboring [Co/Cr/Fe/Cr] unit cells occurs suggesting a highly-ordered demagnetized state induced by dipolar interaction during growth. Applying a magnetic field destroys this state which also can not be recovered during field reversal.

We acknowledge funding by the Deutsche Forschungsgemeinschaft via SFB 491, by BMBF (O3ZA6BC1) and by ILL.

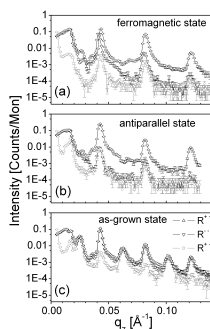


Figure 4.1: PNR data showing the peak evolution in an [Fe/Cr/Co/Cr]₈ multilayer in parallel (a), antiparallel (b) alignment of neighbouring Fe and Co moments and in the as-grown state (c).

4.2 Chirality in Dy/Y Multilayers

Dieter Lott¹, Sergey V. Grigoriev², Yuri O. Chetverikov², Andreas Schreyer¹

¹GKSS

²PNPI, Gatchina

Chirality plays a crucial role in a wide variety of disciplines from biology to chemistry and physics. However, in the field of magnetism it did not attract a lot of attention until recently, when it was demonstrated for the first time that a single layer of manganese on tungsten orders of a specific chirality [1]. It was interpreted being caused by the Dzyaloshinskii-Moriya (DM) interaction which arises from spin-orbit interactions of electrons due to the breaking of the inversion symmetry at the interface. Here, we present studies using polarized neutron scattering on Dy/Y multilayer structures demonstrating that the magnetic system possess a coherent spin helix with a preferable chirality induced by the magnetic field [2]. The average chirality, being proportional to the difference in the left- and right-handed helix population numbers, is measured as a polarization-dependent asymmetric part of the magnetic neutron scattering. The magnetic field applied in the plane of the sample upon cooling below TN is able to repopulate the otherwise equal population numbers for the left- and right-handed helices. The experimental results strongly indicate that chirality observed here for the first time in a multilayer system is a more general phenomenon and may play an important role in future spintronic devices.

[1] M. Bode, M. Heide, K. von Bergmann, P. Ferriani, S. Heinze, G. Bihlmayer, A. Kubetzka, O. Pietzsch, S. Blugel, and R. Wiesendanger, *Nature (London)* 447, 190 (2007).

[2] S.V. Grigoriev, Yu. O. Chetverikov, D. Lott, and A. Schreyer, *Phys. Rev. Lett.* 100, 197203 (2008).

4.3 Crystal-lattice response to antiferromagnetic and hidden order in URu₂Si₂

Philipp Niklowitz¹, Christian Pfleiderer², Thomas Keller³, John Mydosh⁴

¹Department of Physics, Royal Holloway, University of London; Physik Department, TU München

²Physik Department, TU München

³MPI für Festkörperforschung; ZWE FRMII, TU München

⁴2. Physikalisches Institut, Universität zu Köln

Following the border of antiferromagnetism to zero temperature often turned out to be a promising route to unconventional metallic and superconducting phases. Even the simple d-electron system NiS₂ revealed an extended non-Fermi-liquid regime dominated by spin-fluctuations above the quantum phase transition.[1] In the latter case, measurements of the electrical resistivity measurements were done in the framework of the clean and highly controlled technique of pressure tuning. The range of further quantitative experimental probes, which can be realised in a high-pressure environment is limited. However, advances have recently been made in neutron scattering, where elliptically shaped neutron guides can now increase the beam intensity sent to mm size sample for high pressure studies.[2] Neutron scattering also allows highly accurate measurements of the thermal expansion via the Larmor diffraction technique, which proved extremely useful in studying the high-pressure phase diagram of the itinerant helimagnet MnSi.[3] We now combined Larmor diffraction with conventional diffraction measurements to investigate the pressure-temperature phase diagram of URu₂Si₂ up to 20 kbar. URu₂Si₂ offers a further spectacular example for the presence of unconventional phases in the vicinity of antiferromagnetism. In this compound, antiferromagnetism (AF) is replaced below approximately 5 kbar by the mysterious “hidden order” (HO) and unconventional superconductivity. Our measurements allow the simultaneous observation of magnetic order and changes in the a- and c-axis lattice constants across the phase transitions. The results contain clear indications of a first-order transition and strong differences between the AF phase and the HO phase in the coupling to the lattice, questioning simple models of coupled order parameters.

[1] P. G. Niklowitz et al.; Phys. Rev. B 77, 115135 (2008)

[2] S. Mühlbauer, P. G. Niklowitz, et al.; Nucl. Inst & Methods in Phys. Res. A 586, 77 (2008)

[3] C. Pfleiderer, P. Böni, T. Keller, U. K. Rößler, and A. Rosch; Science 316, 1871 (2007)

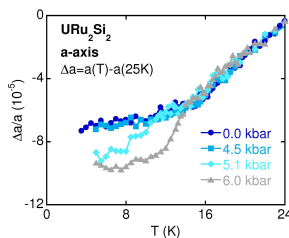


Figure 4.2: Pressure evolution of the relative change of the a-axis lattice constant of URu₂Si₂ with temperature.

4.4 The static and dynamic magnetic properties of PuCoGa₅ and NpCoGa₅ investigated by neutron scattering experiments

Arno Hiess¹, Anne Stunault¹, Nicola Magnani², Eric Colineau², Jean Rebizant², Franck Wastin², Roberto Caciuffo², Gerry Lander²

¹Institut Laue Langevin

²ITU, Europ. Commission

The discovery of superconductivity in the actinide intermetallics PuCoGa₅ at the surprisingly high temperature $T_{sc} = 18$ K [1] stimulated considerable research into the interplay of magnetism and superconductivity in the AnTGa₅ series with An = (U, Np, Pu), X = (Co, Rh). We present neutron scattering results on single crystals, which shed light on the static and dynamic magnetic properties of the superconductor PuCoGa₅ and its isostructural but antiferromagnetic (TN = 47 K) homologue NpCoGa₅ [2]. Our findings are put in context with the experimental results obtained for the isostructural cerium-based superconductors. Implications for superconducting properties of PuCoGa₅ are discussed.

By polarized neutron diffraction the orbital and spin components of the microscopic magnetization in the paramagnetic state of both compounds have been established [3]. The microscopic magnetization of NpCoGa₅ is consistent with localized Np magnetic moments. In the case of PuCoGa₅ the microscopic magnetization is substantially different from that anticipated from a conventional Pu³⁺ ion. Fitting the form factor shows that the orbital moment dominates the magnetisation. The microscopic magnetisation is small and temperature-independent (see figure).

The magnetization dynamics of NpCoGa₅ in the antiferromagnetically ordered state investigated by three-axis spectroscopy using unpolarised [4] and polarised thermal neutrons establishes a gapped magnetic response in the energy range of about 5 to 10 meV. It is dispersive and strongest at the antiferromagnetic zone center. Magnetic fluctuations persist at this position in the paramagnetic state, although weaker in intensity. This supports the possibility that magnetic fluctuations could also be present in the paramagnetic superconductor PuCoGa₅.

[1] J. L. Sarrao et al.; Nature 420, 297 (2002)

[2] N. Metoki et al.; Phys. Rev. B 72, 014460 (2005)

[3] A. Hiess et al.; Phys. Rev. Lett. 100 (2008) 076403

[4] N. Magnani et al.; Phys. Rev. B 76 (2007) 100404R

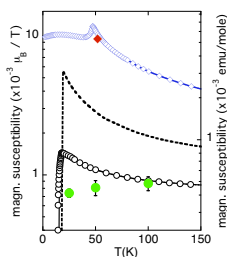


Figure 4.3: Magnetic susceptibility ($1 \text{ emu/mole} = 1.79 \mu\text{B} / \text{T}$) of NpCoGa₅ and PuCoGa₅ as a function of temperature with $B \parallel a$. Blue diamonds: NpCoGa₅ [2]; red closed diamond: NpCoGa₅ deduced from the neutron form factor (this work); dashed line: PuCoGa₅ as previously published [1]; open black circles: measured at ITU on the sample single crystal as used for the neutron experiments; green closed circles: deduced from the neutron form factor (this work).

5 Session 5: Magnetism II

5.1 Magnetic ordering and spin fluctuations in BaFe₂As₂ and Ba_{1-x}K_xFe₂As₂

Y. Su¹, M. Rotter², M. Tegel², D. Johrendt², R. Mittal¹, T. Chatterji³, A. Senyshyn⁴, Th. Brückel¹

¹JCNS, Forschungszentrum Jülich, Outstation at FRM II, Garching

²Department Chemie und Biochemie, LMU, München

³JCNS, Forschungszentrum Jülich, Outstation at ILL, Grenoble

⁴Technische Universität Darmstadt

Recent discoveries of superconductivity in iron pnictides such as LaFeAsO_{1-x}F_x [1] and Ba_{1-x}K_xFe₂As₂ [2] have heralded a new era on the pursuits of high-T_c superconductors. The nature of magnetic ground state in the parent compound and possible spin fluctuations in the superconducting phase are at the center of present investigations. The appearance of antiferromagnetic (AF) ordering of small iron magnetic moments (≈ 0.35 Bohr magneton) below 140 K in LaFeAsO [3] and the absence of such ordering in NdFeAsO [4] have cast doubts on the possible role of AF spin fluctuations in mediating superconductivity. Here we report on the neutron scattering investigations of magnetic ordering and spin fluctuations in the second family of iron pnictides high-T_c superconductors, BaFe₂As₂ and Ba_{1-x}K_xFe₂As₂ compounds. A similar AF ordering to that in LaFeAsO has been confirmed in BaFe₂As₂ via neutron polarization analysis carried out at DNS, FRM II [5]. This technique is able to separate magnetic scattering from nuclear and spin incoherent scattering, therefore, allows us to obtain the pure magnetic structure factor S(Q). The missing magnetic moments in Fe ions due to possible magnetic frustrations were not observed both above and below the Neel temperature. This result could clearly rule out many frustration-based scenarios in explaining the smallness of iron magnetic moments. Spin fluctuations in both parent and superconducting compounds have also been investigated via inelastic neutron scattering at several time-of-flight spectrometers. The implications of our observations to possible AF and ferromagnetic spin fluctuations will be discussed.

[1] H. Takahashi, et al., Nature 453, 376 (2008)

[2] M. Rotter, M. Tegel, D. Johrendt, arXiv:0805.4630 (2008)

[3] C. de la Cruz, et al., Nature 453, 899 (2008)

[4] Y. Qiu, et al., arXiv:0806.2195 (2008)

[5] Y. Su, M. Rotter, M. Tegel, D. Johrendt, R. Mittal, et al., submitted (2008)

5.2 Spin structure of nanocrystalline gadolinium

Andreas Michels¹, Frank Döbrich¹, Mihdi Elmas¹, Adrian Ferdinand¹, Jürgen Markmann¹, Rainer Birringer¹, Melissa Sharp², Helmut Eckerlebe², Joachim Kohlbrecher³

¹Universität des Saarlandes

²GKSS Research Center

³Paul Scherrer Institute

We report on magnetic-field dependent small-angle neutron scattering (SANS) experiments on nanocrystalline inert-gas condensed bulk Gd, which was synthesized using the low-capturing isotope ^{160}Gd . The angular dependency of the scattering cross section is in very good agreement with recent theoretical predictions. Rather unexpected for this type of material, we observe a “clover-leaf”-shaped anisotropy in the SANS signal (see figure), the origin of which is attributed to the existence of longitudinal magnetization fluctuations associated with atomic site disorder and modified coupling inside the defect cores of grain boundaries.

A. Michels et al., *Europhys. Lett.* 81, 66003 (2008).

A. Michels and J. Weissmüller, *Rep. Prog. Phys.* 71, 066501 (2008).

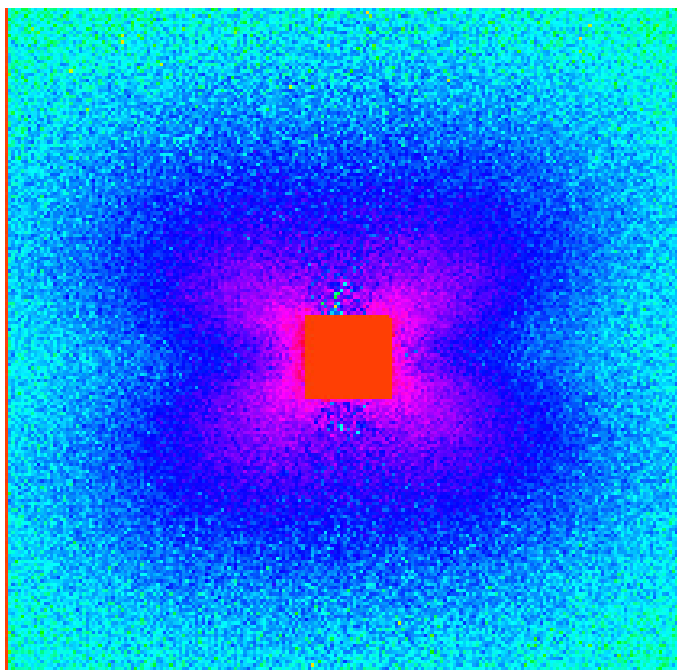


Figure 5.1: Magnetic SANS intensity of nanocrystalline ^{160}Gd (grain size: 21 nm) at 78 K and 600 mT.

5.3 Inelastic Neutron Scattering on Molecular Nanomagnets

Oliver Waldmann¹

¹Physikalisches Institut

Molecular nanomagnets establish a new class of magnetic materials providing a fascinating view on the magnetism of small, mesoscopic objects. These molecules typically consist of tens of magnetic metal ions, which are linked by organic ligands, such as to form well defined geometrical structures. They thus represent magnetic nanoclusters with ideal properties: they don't exhibit any form or shape dispersion and are virtually decoupled magnetically from each other. This allows for the unique opportunity to study the physics of single molecules from experiments on bulk samples.

A particularly important aspect is that of the spin dynamics in these nanosized magnetic molecules. Inelastic neutron scattering is a very powerful tool in this regard. The quantum rotation of the Néel vector and the discrete spin-wave excitation in finite antiferromagnetic spin cluster can be studied, as well as the tunneling of the Néel vector in antiferromagnetic molecular rings. As yet another example, time-resolved inelastic neutron scattering allows one to follow the slow magnetic relaxation in the single-molecule magnet Mn12-ac in the time domain with spectroscopic resolution. The selected examples from our own work shall illustrate the power of inelastic neutron scattering in the field of molecular magnetism.

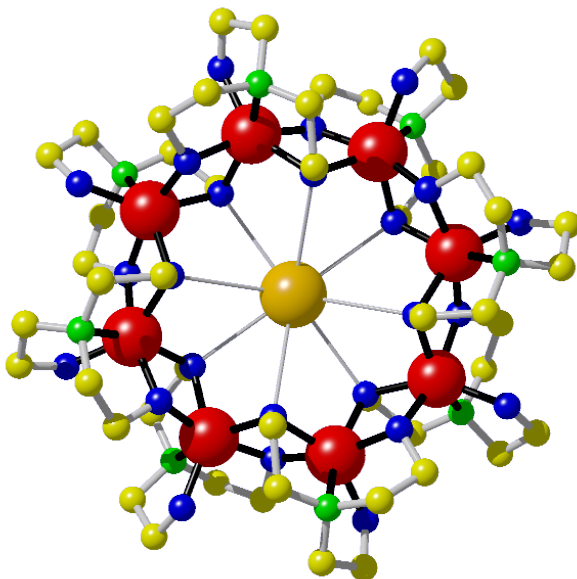


Figure 5.2: Molecular structure of the CsFe8 antiferromagnetic wheel, which consists of a ring of eight antiferromagnetically coupled spin-5/2 Fe(III) ions (red balls).

5.4 Spin Torque Effects in a Helical Magnet

Florian Jonietz¹, Sebastian Mühlbauer², Christian Pfleiderer¹, Rembert Duine³, Benedikt Binz⁴, Achim Rosch⁴, Andreas Neubauer⁵, Robert Ritz⁵, Stefan Legl⁵, Wolfgang Münzer⁵, Robert Georgii², Peter Böni⁵

¹Physik Department E21, Technische Universität München

²Forschungsneutronenquelle Heinz Maier-Leibnitz FRM II; Physik Department E21, Technische Universität München

³Institute for Theoretical Physics, Utrecht University

⁴ITP, University of Cologne

⁵Physik-Department E21, Technische Universität München

NOTE: This talk is scheduled in the Mini-Symposium 1B on Monday

In recent years a large number of experimental studies explore so-called spin torque interactions in soft ferromagnets as a new route to novel spintronics devices. In these systems the spin torque is due to changes of the orientation of the spin-polarization of the conduction electrons in non-colinear spin structures, notably Bloch domain walls. A major constraint of these studies is the need for very large current densities, which cause uncontrolled heating and magnetic stray fields. The large current densities reflect sensitively the extrinsic nature of magnetic pinning in soft ferromagnets. We report AC susceptibility and neutron scattering measurements in the A-phase of MnSi, a two-dimensional skyrmion lattice [1], as a function of electric DC currents. The non-colinear spin structure is here intrinsic and due to Dzyaloshinsky-Moriya interactions, resulting in a pinning that is vanishingly small. We find distinct features that suggest spin torque effects at current densities that are 5 to 6 orders of magnitude smaller than those observed in soft ferromagnets. This identifies helical magnets as a new route to exploiting spin torque effects in novel spintronic applications.

[1] S. Mühlbauer, B. Binz, F. Jonietz, C. Pfleiderer, A. Rosch, R. Georgii, P. Böni, in review (2008).

6 Session 6: Upcoming Spallation Sources

6.1 Development at ISIS - the next ten years

Robert McGreevy¹

¹ISIS

At the time of writing this abstract ISIS Target Station 2 is due to produce first neutrons within the following ten days. By the end of 2008 the first 7 instruments will be in commissioning/first user operation. Funding has already been earmarked for the next two phases of ISIS instrument development, up to 2016. This presentation will give a status report on ISIS, including both the current instrument projects and the possible future developments.



Figure 6.1: ISIS Target Station 1 (left) and Target Station 2 (right)

6.2 Commissioning Experience, Early Results, and Status of the Spallation Neutron Source at Oak Ridge National Laboratory

Ken Herwig¹

¹Oak Ridge National Laboratory

The Spallation Neutron Source (SNS) located at Oak Ridge National Laboratory became operational with the first protons striking the mercury target and producing neutrons a little over two years ago in April 2006. Neutron scattering instrument commissioning began the next month with a few days of 5 kW of proton beam power producing neutrons resulting in the initial inelastic spectra collected. Since these early days, the number of operational instruments has doubled from three to six and the accelerator has achieved routinely high reliability operation at nearly 500 kW of proton beam power. Four additional beam lines are scheduled to open their beam shutters and count neutrons for the first time before the end of 2008. In addition, full user access to the initial instruments began in December 2007 and the neutron facilities at ORNL have just completed the third round of proposal submissions to both SNS and the High Flux Isotope Reactor. This talk will relate some of the challenges that were overcome during commissioning of the initial instruments, illustrate the capabilities of the currently operational instruments with several science results, summarize the status of the accelerator/target complex, and conclude with a look forward towards new instrument capabilities and enhanced accelerator/target performance.



Figure 6.2: Aerial view of the Spallation Neutron Source at Oak Ridge National Laboratory

6.3 ESS: progress towards a neutron source of the next generation

Ferenc Mezei¹

¹Neutron Spectroscopy

After many years of preparation, all conditions are gradually coming together for the timely realization of the European Spallation Source (ESS). This applies to technical, economic and science-policy aspects. By its concept and level of performance ESS represents the next generation beyond the recently completed most advanced facilities, SNS and J-PARC. While these facilities will offer new opportunities compared to the current world leader ILL in some applications, ESS will inaugurate in the same comparison a jump in instrument performance by at least an order of magnitude in all neutron scattering work. The technology of long pulses pioneered by ESS is less demanding than the one used by its predecessors SNS and J-PARC, and will allow us to achieve higher performance at lower costs and exceptionally low technical risks compared to these facilities. At the same time, while all other approaches to neutron sources, including reactors and short pulse spallation sources, achieved by now their probable limits of reasonable technical feasibility, ESS with its 5 MW power will still be far from these limits, possibly by as much as an order of magnitude. On the financial side, the realization of ESS requires the emergence of new actors in the European neutron science scene, to help to provide the extra resources needed to build ESS in parallel to the best use of the capabilities of the existing neutron sources, in order to maintain and rejuvenate the continent's world leading community in neutron research. The priority of strengthening the research infrastructures in the European science policy, also expressed by the European Strategic Forum on Research Infrastructures (ESFR!), offers a set of favourable conditions for the realization of such a most ambitious research facility.

7 Session 7: Materials

7.1 New gravitational experiment with ultracold neutrons

German Kulin¹, Alexander Frank¹, Dmytro Kustov¹, Alexander Strepetov², Vadim Nosov², Peter Geltenbort³, Michael Jetschel³

¹FLNP JINR

²RRC Kurchatov Institute

³ILL

The results of a new neutron gravitation experiment are reported. The change in the energy of a neutron falling to a known height in the Earth's gravitational field is compensated by an energy quantum $h\nu$ transferred to the neutron as a result of the phase modulation of the neutron wave. A phase diffraction grating moving across the direction of the propagation of the neutron wave is used as a modulator. The experiment has been carried out with ultracold neutrons Interference filters, neutron analogues of Fabry-Perot interferometers, are used for the spectrometry of ultracold neutrons. The force acting on the neutron in the Earth's gravitational field has been measured with an accuracy of about 0.2%.

1. L.Koester//Phys. Rev. D. 1976. V. 14. P. 907.

2. V.F.Sears//Phys. Rev. D. 1982. V. 25. P. 2023.

3. R.Collela, A.W.Overhauser, S.A.Werner//Phys. Rev. Lett. 1975. V. 34. P. 1472.

4. A.I.Frank, V.G.Nosov//Phys. Lett. A. 1994. V. 188. P. 120.

5. A.I.Frank, S.N.Balashov, I.V.Bondarenko et al.//Phys. Lett. A. 2003. V. 311. P. 6.

6. A.I.Frank, P.Geltenbort, G.V.Kulin, D.V.Kustov, V.G.Nosov, A.N.Strepetov //JETP Lett. 2005. V. 81 P. 427

7. A.I.Frank, P.Geltenbort, M. Jentschel, G.V.Kulin, D.V.Kustov, V.G.Nosov, A.N.Strepetov //JETP Lett. 2007. V. 86 P. 255

7.2 Nickel self-diffusion in Si-Ni melts

Anja Ines Pommrich¹, Andreas Meyer¹, Dirk Holland-Moritz¹, Tobias Unruh²

¹Materialphysik im Weltraum

²Forschungsneutronenquelle Heinz Maier-Leibnitz

The purification of Silicon for solar cell applications is done by directional solidification. This process is limited by diffusion of mass at the liquid/solid phase boundary. For an understanding of this process the knowledge of the temperature and concentration dependence of the diffusion coefficients is a necessary prerequisite. Diffusion experiments on liquid Silicon are difficult due to the high chemical reactivity of Silicon at high process temperatures. In addition, diffusion experiments with tracer or long capillary methods are altered by buoyancy driven convection. Therefore, diffusion data in these system are rare.

For elements with an incoherent scattering cross section (σ_{inc}) the self-diffusion coefficient can be determined by means of quasi-elastic neutron scattering (QNS) on absolute scale. The combination with electromagnetic levitation enables container-free processing. This allows us to study the temperature dependence of the self-diffusion coefficient in a range of several 100 K above and below the liquidus temperature at around 1600 K. One of the main metal impurities in Silicon is Nickel. We study Si-rich alloys with 5 to 20 atm-% Nickel, which is besides a good incoherent scatterer ($\sigma_{inc} = 5.2$ barn).

Over the entire temperature range the results exhibit an Arrhenius-like temperature dependence of the nickel self-diffusion D_{Ni} . In liquid Si-Ni D_{Ni} is about a factor of 5 faster as compared to the self-diffusion in pure liquid Ni. D_{Ni} is fairly independent of the Ni concentration in the Si-Ni alloy. Viscosity data of pure liquid Silicon, rescaled with the Stokes-Einstein relation, lie on comparable time scales. This indicates that the impurity diffusion of Nickel in liquid Silicon is independent from the impurity concentration in the melt. With this the Silicon purification by directional solidification will not be slowed down by a decreasing diffusion coefficient with increasing Ni concentration at the liquid/solid interface.

7.3 Studies of ordering in anti phase nanodomain FeCo alloys with different ternary additions using neutron diffraction

Ralph Gilles¹, Michael Hofmann¹, Yan Gao², Frank Johnson², Luana Iorio², Markus Hoelzel³

¹FRM II ZWE

²GE Global Research

³TU Darmstadt, FRM II ZWE

FeCo alloys are industrially important engineering materials due to their very high saturation magnetization and Curie temperature. These alloys play an important role in applications requiring soft magnetic materials, such as electrical generators, motors and transformers. For many industrial applications, the challenge involves increasing the tensile strength and ductility of FeCo alloys while maintaining magnetic performance. Methods used to meet this challenge include alloy design (eg. addition of certain ternary metals such as Ni, V, Nb, Ta, Cr, Mo etc.), annealing, and advanced deformation processing. However, modern applications require even better mechanical and magnetic performance.

The effects of alloying FeCo with Pt, Pd, Mn, Ir, and Re have been investigated as part of this work. In the composition range of about 30%-70% Co, FeCo alloys undergo a continuous order-disorder phase transformation at a maximum temperature of 730°C at the equiatomic composition. The effect of temperature and composition on the ordering phenomena in six alloys (Fe70Co30, Fe67Co30Pt3, Fe67Co30Pd3, Fe67Co30Mn3, Fe67Co30Ir3, and Fe67Co30Mn3; atomic %) has been compared using neutron diffraction.

7.4 Natural Soil Environments: The role of cations and superparamagnetic iron oxides

Heloisa Bordallo¹, Laurence Aldridge², G. Jock Churchman³, Will P. Gates⁴, Mark Telling⁵, Klaus Kiefer⁶, Peter Fouquet⁷, Tilo Seydel⁷, Simon Kimber⁶

¹Helmholtz-Zentrum Berlin für Materialien und Energie, SF6

²Senior Fellow IMES, ANSTO and School of Civil and Environmental Engineering, University of New South Wales

³School of Earth and Environmental Sciences, University of Adelaide

⁴SmecTech Research Consulting and Dept Civil Engineering, Monash University

⁵ISIS Facility

⁶Helmholtz-Zentrum Berlin für Materialien und Energie, SF2

⁷Institut Laue Langevin

Even in a barren and hot desert clays can contain significant fractions of water that are normally unavailable to plants. Why does this happen? It is supposed that the cations act as gatekeepers regulating the reversible adsorption of water. That is indeed the case for the clay mineral montmorillonite that contains certain cations in the interlayer space. However, in the clay halloysite no cations are present, and when halloysite is dried water cannot be readmitted to the interlayer space.

In this study we show that by using incoherent inelastic neutron scattering, it was possible to discriminate the dynamics of surface water from interlayer water. The analysis of the elastic fixed window scans in the temperature range 5-300 K revealed an extension of water dynamics in montmorillonite to lower temperatures than in halloysite. These differences suggested mechanisms that cations in the interlayer regions facilitate water mobility allowing interlayer water to be readmitted to montmorillonite.

Finally our neutron spin echo and SQUID results have given evidence for the existence of paramagnetic fluctuations in halloysite and montmorillonite. Currently, understanding of the spatial heterogeneity of magnetic properties in natural soil environments is limited. Thus our results open a new multi-disciplinary perspective for emerging applications of neutron scattering in soil magnetism and in environmental, geological, and soil sciences.

7.5 Characterisation of the Hydrogen Distribution in Metal Hydride Tanks Using Neutron Radiography and Tomography

P. Klaus Pranzas¹, Heinz-Werner Schmitz¹, Oliver Metz¹, Felix Beckmann¹, Martin Dornheim¹, Rüdiger Bormann¹, Andreas Schreyer¹

¹GKSS Forschungszentrum

Hydrogen is one of the favoured energy carriers for the future. A reliable storage solution has to be found, especially for mobile applications. One very promising option is the chemical storage in metal hydrides. The aim of this study is the in situ characterisation of hydrogen absorption and desorption in metal hydrides in order to visualise the hydrogenation and powder compaction of the material inside the tank. The results of these investigations are necessary for the optimisation of tank design and construction of metal hydride hydrogen storage tanks.

The neutron radiography and tomography instrument GENRA-3 at the Geesthacht Neutron Facility (GeNF, <http://genf.gkss.de>) at GKSS serves as an instrument for non-destructive testing and damage analysis of materials and technical structures by static and dynamic imaging. As a first step to an in situ study, metal hydride tanks filled with different amounts of hydrogen were measured with neutron radiography using the direct gadolinium method to record the image. Different metal hydrides and tank geometries were tested. During the absorption process the hydrogen distribution was found to be homogeneous over the whole tank. The swelling of the metal hydride material due to the hydrogen absorption could also be verified. For Neutron Computerized Tomography (NCT) a 2-dimensional neutron detector and a high precision sample manipulator are available. In situ studies are planned using two metal hydride tanks in order to control the hydrogen flow from one tank to the other.

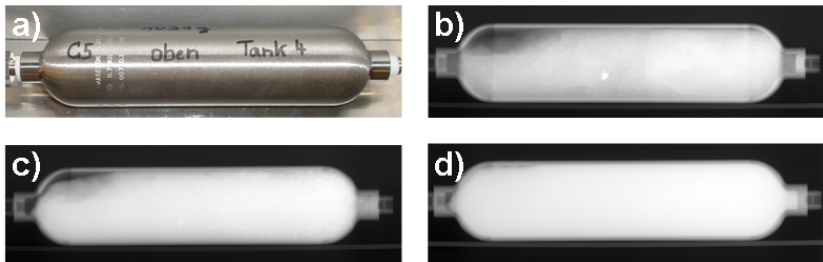


Figure 7.1: a) Photo of a hydrogen tank filled with the room temperature metal hydride "C5". b) - d) Neutron radiography images of this tank filled with different amounts of hydrogen: b) empty, c) 9 litres hydrogen, d) 90 litres hydrogen

8 Session 8: Structure and Structural Dynamics

8.1 The phonon buckling mode in $\text{YBa}_2\text{Cu}_3\text{O}_{6+x}$ measured by inelastic neutron scattering

Markus Raichle¹, Dmitry Reznik², Bernhard Keimer¹

¹MPI-FKF

²Forschungszentrum Karlsruhe

Cuk et al. [1] and Devereaux et al. [2] relate the anti-nodal kink in ARPES measurements with the B_{1g} phonon buckling mode. Therefore they claim that this particular phonon mode may be necessary for a complete explanation of the mechanism for the building of Cooper-pairs in high temperature superconductors. However, this assumption is highly controversial as this kink has also been related to the magnetic resonance mode by Kaminski et al. [3] and Kim et al. [4]. Until now inelastic neutron scattering measurements on this phonon mode on $\text{YBa}_2\text{Cu}_3\text{O}_{6+x}$ by Reznik et al. [5] has only been done on twinned samples and with rather high spectrometer resolution for $x=1.0$. Here we present high resolution neutron measurements on the buckling mode on YBCO for $x=0.6$ and $x=1.0$. These measurements performed at Puma and 1T1 at Saclay have been made on fully detwinned samples. Thus we could show that this phonon mode performs an anisotropic superconductivity-induced transfer of spectral weight with a neighboring phonon mode (see picture). Hence these measurements enrich the experimental evidence for superconductivity induced phonon effects in high temperature superconductors.

[1] Phys. Rev. Lett. 93, 117003 (2004)

[2] Phys. Rev. Lett. 93, 117004 (2004)

[3] Phys. Rev. Lett. 86, 1070 (2001)

[4] Phys. Rev. Lett. 91, 167002 (2003)

[5] Phys. Rev. Lett. 75, 2396 (1995)

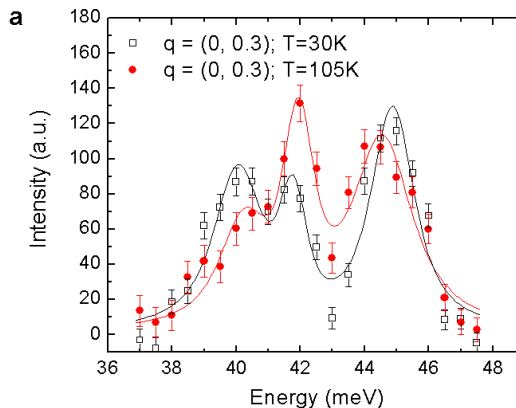


Figure 8.1: Superconductivity-induced spectral-weight transfer. Comparison of spectra at $q = (0, 0.3)$ above and below the superconducting transition temperature, demonstrating a transfer of spectral weight from buckling to apical-oxygen modes. The effect is absent at $q = (0.3, 0)$, so that the spectrum below T_c exhibits a pronounced anisotropy in the a - b plane. The lines are the results of least-squares fits of the data to Voigt functions. A linear background has been subtracted for clarity.

8.2 The impact of SPHERES on rotational tunneling spectroscopy: recent examples

Michael Prager¹, Oliver Kirstein², Gerald Schneider³, Joachim Wutke³

¹IFF

²ANSTO, Au

³JCNS

The backscattering spectrometer SPHERES is characterized by a very high energy resolution of actually 0.69 μ eV at energy transfer up to \approx 30 μ eV. This combination allows to observe fine structure of tunneling transitions. In case of methyl fluoride the predicted [1,2] direct methyl-methyl coupling could be confirmed (Fig.). Coupling to phonons depends on the symmetry of the rotor levels involved [3]. The situation is more complex for ammonium ions than for methyl groups. This will be demonstrated for the case of ammoniumhexchloropalladate.

1) O. Kirstein and M. Prager, J. Chem. Phys. 120,5199(2007)

2) O. Kirstein et al, J. Chem. Phys. 127,094504(2007)

3) A. Würger, Z. Phys. B76,65(1989)

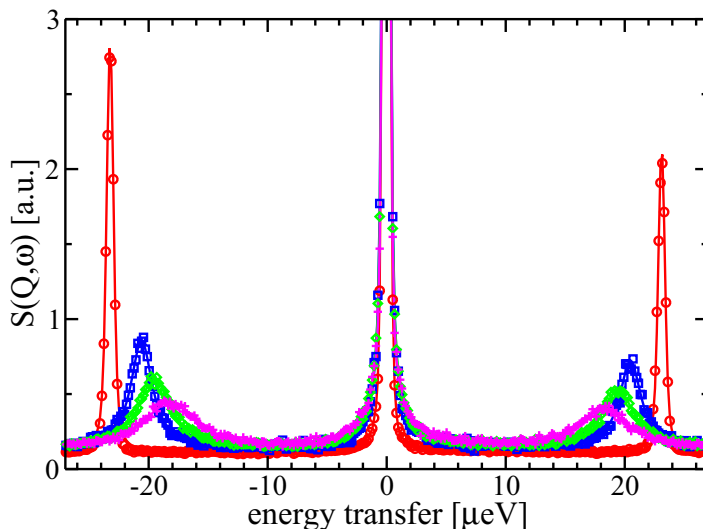


Figure 8.2: Rotational tunneling of methyl groups in methyl fluoride at temperatures $T=4,24,26$ and 28K. A finite linewidth at $T=4$ K reveals direct coupling. Coupling to phonons explains the evolution with temperature.

8.3 Thermal expansion and atomic vibrations in CaWO₄ studied by neutron and synchrotron powder diffraction

Anatoliy Senyshyn¹, Leonid Vasylechko², Richard Mole³, Markus Hoelzel¹, Thomas C. Hansen⁴, Vitalii Mikhailik⁵, Hans Kraus⁵, Hartmut Fueß¹

¹Strukturforschung, Materialwissenschaft, TU Darmstadt

²Semiconductor Electronics Department, Lviv Polytechnic National University, Ukraine

³Forschungszentrumquelle Heinz Maier-Leibnitz (FRM II)

⁴Institute Laue-von Langevin

⁵Physics Department, Oxford University

Alkaline-earth tungsten and molybdenum oxides with scheelite structure are applied as phosphors, laser hosts and scintillators. A new field for the application of these materials has emerged a few years ago when a new generation of cryogenic detectors, offering the capability of discrimination between electron and nuclear recoils has been implemented in some particle physics experiments. The increasing interest in using CaWO₄ for rare events searches initiated research in the fundamental physical characteristics of this material over a wide temperature range.

A high structural stability for both WO₄ and MoO₄ tetrahedra has been observed for CaWO₄ and CaMoO₄ by theoretical studies [1,2] along with a pronounced anharmonicity of thermal expansion in both a- and c- directions of the tetragonal cell. To extend the knowledge about materials with scheelite structure as well as about the correlations between anisotropy of thermal expansion, structural parameters of CaWO₄ and thermal vibrations a number of structural studies of calcium tungstate has been performed.

These investigations were carried out by both elastic/inelastic neutron scattering and high-resolution synchrotron powder diffraction techniques. Low temperature (5 - 295 K) neutron diffraction studies were performed at instrument D2B (Institute Laue-Langevin, Grenoble, France), whereas structural studies at high temperatures (300 - 1773 K) have been performed at instrument SPODI (research reactor FRM-II, Technical University of Munich, Garching n. Munich, Germany). Additionally, high-resolution powder diffraction experiments were carried out at the beamline B2 of HASYLAB/DESY over the temperature range 12 - 295 K. The data were collected during cooling and heating of the samples in small temperature increments, using the image plate detector OBI. In-situ inelastic neutron scattering experiments were performed at triple-axis spectrometer PUMA.

Agreement of experimental data collected using various techniques to results of theoretical simulations will be shown. Origin of the anisotropy of the thermal expansion as well as its relation to bond lengths, bond angles, anisotropic displacement parameters and anharmonic vibrations will be discussed in brief.

[1] Senyshyn A., Kraus H., Mikhailik V.B., Yakovyna V., Phys. Rev. B, 2004, 70, 214306.

[2] Senyshyn A., Kraus H., Mikhailik V.B., Vasylechko L., Knapp M., Phys. Rev. B, 2006, 73, 014104.

8.4 Dumbbell rattling in thermoelectric zinc-antimony

Werner Schweika¹, Raphael Hermann¹, Michael Prager¹, Jörg Perßon¹, Veerle Keppens²

¹IFF, Forschungszentrum Jülich

²Univ. Tennessee, Knoxville, USA

A significant reduction in energy consumption through the recovery of waste heat could be achieved by efficient materials for thermoelectric power generation. Efficient thermoelectric materials require "electron crystal, phonon glass" behavior, combining both good electric and poor thermal conductivity [1]. Dynamic disorder of "rattling" heavy atoms has been shown to impede the thermal transport in filled cage structures such as skutterudites and clathrates [2,3].

We report [4] inelastic neutron scattering and heat capacity measurements that identify a new type of dynamical disorder in Zn_4Sb_3 , namely localized dumbbell vibrations. The anharmonicity of this soft vibration is in quantitative agreement with the low thermal conductivity. Soft localized phonon modes appear to be a universal feature of good thermoelectric materials not restricted to cage-like structures.

[1] V. Keppens, D. Mandrus, B. C. Sales, B. C. Chakoumakos, P. Dai, R. Coldea, M. B. Maple, D. A. Gajewski, E. J. Freeman, and S. Bennington, *Nature* **395**, 876-878 (1998).

[2] R. Hermann, R. Jin, W. Schweika, F. Grandjean, D. Mandrus, B.C. Sales, & G.J. Long, *Phys. Rev. Lett.* **90**, 135505 (2003).

[3] R. P. Hermann, W. Schweika, O. Leupold, R. Ruffer, G. S. Nolas, F. Grandjean, and G. J. Long, *Phys. Rev. B* **72**, 174301 (2005).

[4] W. Schweika, R. P. Hermann, M. Prager, J. Perßon, V. Keppens, *Phys. Rev. Lett.* **99**, 125501 (2007).

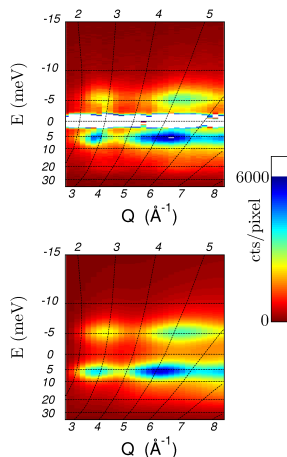


Figure 8.3: Neutron inelastic scattering by polycrystalline Zn_4Sb_3 at 300 K obtained in time-of-flight measurements (top) compared to model refinements (bottom) for weakly coupled Sb-dumbbell vibrations along the dumbbell axis. The dynamic response is dominated by the soft dumbbell modes with a Lorentzian broadening due to short phonon life times,

8.5 The nature of “cubic ice” established by time-resolved neutron diffraction

Werner F. Kuhs¹, Thomas C. Hansen², Michael M. Koza²

¹GZG Kristallographie Uni Göttingen

²Institut Laue Langevin Grenoble

Ice Ic, often called “cubic ice” can be formed in various ways from the gas phase, from liquid water and from other solid forms of water ice; its diffraction pattern is clearly not strictly cubic and shows a considerable variability depending on its origin – one may even call it “the chameleon of icy worlds”. The nature of this variability gave rise to many speculations based on usually rather weak experimental evidence. Moreover, ice Ic shows a complex annealing behaviour with changes of its diffraction pattern on a timescale of minutes to hours upon warming [1]. An earlier suggestion [2] ascribed the deviation from a clean cubic structure to deformation stacking faults combined with particle size broadening effects. This has been corroborated in recent time-resolved experiments on D20 at ILL. Data of excellent quality were obtained permitting to check a specifically developed general stacking fault model [3] used to refine structural parameters for the one-dimensional stacking disorder and anisotropic particle size broadening [4]. For the first time a satisfactory description of “cubic ice” was achieved in this way. The time-dependent changes can now be quantified and will help to better understand a number of important phenomena, like the complex self-preservation behaviour of gas hydrates [1] or the “supersaturation puzzle” in the higher atmosphere [5], which may find its explanation in the variable T-dependent defectiveness of cubic ice, now believed to exist in the higher atmosphere in cirrus clouds and contrails [6].

[1] WF Kuhs, G Genov, DK Staykova and T Hansen 2004 Phys.Chem.Chem.Phys. 6, 4917.

[2] WF Kuhs, DV Bliss, JL Finney 1987 J.Physique C1 48, 631.

[3] TC Hansen, MM Koza and WF Kuhs 2008 J.Phys.Cond.Matt. 20, 285104.

[4] TC Hansen, MM Koza, P Lindner and WF Kuhs 2008, J.Phys.Cond.Matt. 20, 285105.

[5] T Peter, C Marcolli, P Spichtinger, T Corti, MB Baker and T Koop 2006 Science 314, 1399.

[6] BJ Murray, DA Knopf and AK Bertram 2005 Nature 434, 202.

9 Mini-SYM 1: Function from Frustration in Modern Multiferroics

9.1 Excitations in Multiferroics

Alois Loidl¹, Andrei Pimenov², A. A. Mukhin³

¹Center for Electronic Correlations and Magnetism

²Experimentelle Physik 4, Universität Würzburg

³General Physics Institute, Russian Academy of Sciences

Magnetodielectric materials are characterized by a strong coupling of magnetic and dielectric properties and, in rare cases, simultaneously show both ferromagnetic and ferroelectric order. Magnons are the characteristic excitations of magnets, while soft phonons as inferred by the Lyddane-Sachs-Teller relation condense at canonical ferroelectric phase transitions. It seems clear that this scenario can not be valid in multiferroics and it has been proposed theoretically that as a consequence of the strong magnetodielectric coupling fundamentally new excitations should exist [1, 2] but whose existence could not be proven experimentally in the past. Recently Pimenov et al. [3] reported the observation of electromagnons in GdMnO₃ and TbMnO₃ by infrared and millimeter-wave spectroscopy. Electromagnons are spin waves which can be excited by an ac electric field and these excitations appear in the incommensurate magnetic structure of the manganese spins. As this structure can be suppressed by external magnetic fields the electromagnons can be wiped out by moderate fields, thereby inducing considerable changes in the index of refraction.

In this presentation we will summarize our observations of electromagnons in GdMnO₃, TbMnO₃ and in a series of concentrations of Eu(1-x)Y(x)MnO₃, a compound which shows strong magnetodielectric effects for Y concentrations $0.2 < x < 0.5$ [4]. The electromagnetic excitations are studied by FIR and mm-wave spectroscopy as function of temperature and external magnetic field. For GdMnO₃ we document the strong coupling of phonons and electromagnons [5]. Our results are compared with recent neutron scattering results [6] in TbMnO₃.

In addition we present a complete analysis of the temperature dependence of all phonon modes in TbMnO₃ and document that strong spin phonon coupling is active in this compound.

[1] G. A. Smolenski, I. E. Chupis, *Sov. Phys. Usp.* 25 (1982) 475 [2] H. Katsura, A. V. Balatsky, N. Nagaosa, *Phys. Rev. Lett.* 98 (2007) 027203 [3] A. Pimenov et al., *Nature Physics* 2 (2006) 97 [4] J. Hemberger et al., *Phys. Rev. B* 75, (2007) 035118 [5] A. Pimenov et al., *Phys. Rev. B* 74 (2006) 1004403 [6] D. Senff et al., *Phys. Rev. Lett.* 98 (2007) 137206

9.2 Neutron scattering studies on spiral multiferroics

Markus Braden¹, Daniel Senff¹, Thomas Finger¹, Max Baum¹, Alexander C. Komarek¹, Nadir Aliouane², Dimitri Argyriou², Arno Hiess³, Karin Schmalzl⁴, Paul Steffens³, Peter Link⁵, Klaudia Hradil⁵, Petra Becker⁶, Ladislav Bohatý⁶, Louis-Pierre Regnault³

¹II. Physikalisches Institut

²HMI

³ILL

⁴ILL & FZ Juelich

⁵FRM-II

⁶Inst. f. Kristallographie, Koeln

The non-collinear order in spiral or cycloidal magnets can cause a ferroelectric polarization through the inverse Dzyaloshinski-Moriya interaction implying a multiferroic phase. This magnetoelastic coupling may give rise to a hybridized phonon-magnon excitation, called electromagnon. We discuss elastic and inelastic neutron scattering studies on three different multiferroic compounds : TbMnO₃, MnWO₄ and NaFeSi₂O₆. In the three materials the ferroelectric polarization is well explained by the Dzyaloshinski-Moriya interaction and their complex magnetic order. By unpolarized and polarized neutron scattering studies the frequencies and polarization patterns of the magnetic excitations are determined. Strong evidence for an electromagnon excitation is obtained for TbMnO₃ when combining the neutron scattering results with optical spectroscopy data.

[1] D. Senff, P. Link, K. Hradil, A. Hiess, L. P. Regnault, Y. Sidis, N. Aliouane, D. N. Argyriou, and M. Braden, *Phys. Rev. Lett.* 98, 137206 (2007).

[2] D. Senff, N. Aliouane, D. N. Argyriou, A. Hiess, L. P. Regnault, P. Link, K. Hradil, Y. Sidis, and M. Braden; review to appear in *Journal of Physics Cond. Matter*.

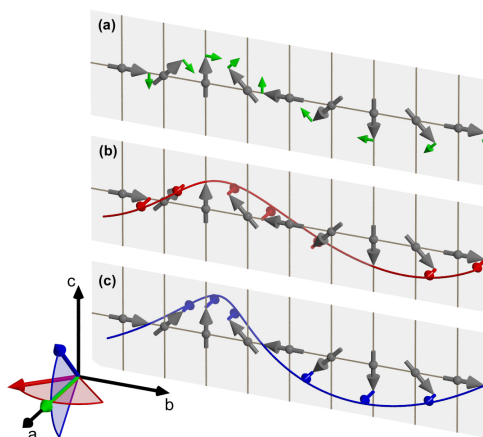


Figure 9.1: Polarization patterns of three magnetic excitations at the incommensurate zone center in the cycloidal phase of TbMnO₃. The upper mode is the phason of the incommensurate phase, and the lowest one possesses the symmetry of the electromagnon excitation.

9.3 Tuning magnetic interaction in orthorhombic Neodymium-Yttrium Manganites $\text{Nd}_{1-x}\text{Y}_x\text{MnO}_3$

Sven Landsgesell¹, Dimitri Argyriou¹

¹Hahn Meitner Institut

By lowering the Mn-O-Mn bond angle in LnMnO_3 with $\text{Ln}=\text{La}-\text{Ho}$ the Neel-temperature decreases and at $\text{Ln}=\text{Tb}$ the A-type antiferromagnet transforms to an incommensurate (IC) spin-spiral phase for $\text{Ln}=\text{Gd}, \text{Tb}, \text{Dy}$. The spin-spiral breaks both inversion and time reversal symmetry leading to a strong coupling between magnetism and ferroelectric polarization [1]. We investigate the evolution of the crystal and magnetic structure from the A-type phase to the IC spin spiral phase by systematically replacing neodymium by yttrium in NdMnO_3 resulting to a decrease of the tolerance factors to values similar to that for multiferroic TbMnO_3 . One advantage of this approach is that the tolerance factor can be tuned and that neodymium and yttrium are not high neutron absorbing elements in sharp contrast to other rare earths like Gd, Dy and Eu. Single crystal and powder samples of compositions of $x=0.0$ to 0.6 have been prepared, neutron and x-ray diffraction patterns were measured as well as the magnetic and dielectric properties. It can be shown that by decreasing the tolerance factor that way, similar effects can be seen as with varying the ionic size of the rare earth ions. For example we found that between $0.4 < x < 0.6$ the IC component co-exists with the A-type antiferromagnetic phase and with $x=0.6$ the system is only incommensurate. Samples displaying an IC phase undergo a transition from a long wavelength spin density wave to a spin spiral exhibiting ferroelectric polarization with $\text{P} \parallel \text{c}$.

T. Kimura et al., Phys. Rev. B 67, 180401(R) (2003)

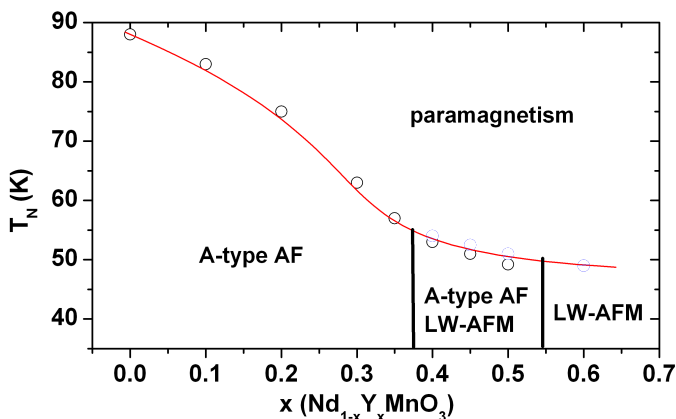


Figure 9.2: Phase diagram of $\text{Nd}_{1-x}\text{Y}_x\text{MnO}_3$ from $x=0.0$ to $x=0.6$ and T_N showing the transitions from A-type antiferromagnet (AF) to purely long-wavelength AF (LW-AFM).

9.4 Interplay between rare earth and manganese magnetism and its effect on ferroelectricity in or -RMnO₃

Ralf Feyerherm¹

¹Helmholtz-Zentrum Berlin

Exceptionally strong magneto-electric coupling effects observed in the perovskite manganites RMnO₃ (R = Tb, Dy) [1,2] have been the starting point of recent broad interest in multiferroic materials [3]. In this new class of multiferroics, ferroelectricity is induced by complex magnetic ordering and often related to magnetic frustration.

While the basic multiferroic properties appear to be governed by the Mn magnetism, several peculiarities point to an intricate role of the rare earth R in these materials. In DyMnO₃, e.g., the magnetic ordering of Dy below 6.5 K causes a strong anomaly of the electric polarization [4]. In the series Eu_{1-x}Y_xMnO₃ with non-magnetic rare earths, a spontaneous electric polarization $P \parallel a$ is observed [5], while for R = Tb and Dy $P \parallel c$. In the latter compounds, however, a polarization flop to $P \parallel a$ occurs on application of an external magnetic field [1].

We present combined neutron and x-ray resonant scattering investigations of the interplay between the rare earth and manganese magnetism in RMnO₃ (R = Tb, Dy) and its effect on the multiferroic properties. Our central findings are an enhancement of the electric polarization by an induced ordering of Dy spins at temperatures above 6.5 K in DyMnO₃ [6] and an unexpected harmonic coupling of the Tb and Mn propagation vectors in the ground state of TbMnO₃ [7]. New results on GdMnO₃ and the series Nd_{1-x}Y_xMnO₃ will be discussed briefly.

(In collaboration with N. Aliouane, D. Argyriou, E. Dudzik, S. Landsgesell, M. Mostovoy, O. Prokhenko and others)

[1] T. Kimura et al., Nature 426 (2003) 55.

[2] N. Hur et al., Phys. Rev. Lett. 93 (2004) 107207.

[3] S.-W. Cheong & M. Mostovoy, Nature Materials 6 (2007) 13.

[4] T. Goto et al., Phys. Rev. Lett. 92 (2004) 257201.

[5] J. Hemberger et al., Phys. Rev. B 75 (2007) 035118.

[6] O. Prokhenko et al., Phys. Rev. Lett. 98, 057206 (2007).

[7] O. Prokhenko et al., Phys. Rev. Lett. 99, 177206 (2007).

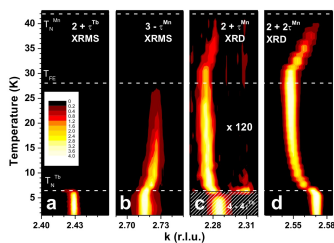


Figure 9.3: Temperature dependence of characteristic magnetic and lattice distortion reflections in the form of a color intensity plot measured in TbMnO₃ using x-ray resonant magnetic scattering (XRMS) and non-resonant x-ray diffraction (XRD). These data are interpreted in Ref. [7] as pointing to a harmonic coupling of the Tb and Mn propagation vectors below 6 K.

9.5 Influence of Applied Magnetic Field in Incommensurate Magnetic Structure of ZnCr_2Se_4 and ZnCr_2S_4

Fabiano Yokaichiya¹, Heloisa Nunes Bordalo¹, Dimitri Argyriou¹, Alexander Krimmel², Alois Loidl², Vladimir Tsurkan²

¹Helmholtz-Zentrum Berlin

²University of Augsburg

Chalcogenide chromium spinels have shown a coupling between ferroelectricity and magnetism. The aim of this work is to observe the influence of an applied magnetic field (5T) in the incommensurate magnetic structure of the spinels ZnCr_2Se_4 and ZnCr_2S_4 . The incommensurate magnetic structures through the Néel transition in these systems, at 0 and 5 T, have been studied by high-resolution powder neutron diffraction at E9 at HZB. Below T_N ($T_N \approx 21\text{K}$ for ZnCr_2Se_4 and $T_N \approx 18\text{K}$ for ZnCr_2S_4) at 0 T, for both cases, the magnetic structure is described as ferromagnetic layers in the ab-plane stacked in a spiral arrangement along the c-axis with a propagation vector $k = (0, 0, \approx 0.46)$ for ZnCr_2Se_4 and $k = (0, 0, \approx 0.79)$ for ZnCr_2S_4 . In ZnCr_2Se_4 and ZnCr_2S_4 the magnetic phase transition is of first order. For ZnCr_2S_4 , another magnetic transition (T_{N2}) is observed at 8K, with an incommensurate ($k_1 = (0, 0, \approx 0.79)$) and two commensurate ($k_2 = (0.5, 0.5, 0)$ and $k_3 = (1.0, 0.5, 0)$) magnetic structures. However, at 5T, for ZnCr_2Se_4 it is observed a shift in T_N ($\approx 22\text{K}$) to $T_N' (\approx 8\text{K})$ and a suppression of the incommensurate helical magnetic structure in the range $T_N' < T < T_N$. In the case of ZnCr_2S_4 , it is observed a negative thermal expansion in the lattice parameter in the temperature range: $T_{N2} < T < T_N$, and a suppression of the commensurate magnetic structures below T_{N2} . In this work we present results of Rietveld analysis on the magnetic structure through the magnetic transitions at 0 and 5 T.

10 Mini-SYM 2: Dynamics, kinetics, complex materials in the light of SANS and reflectometry

10.1 Rheo-SANS with complex fluids

Peter Lindner¹

¹ILL

SANS investigations of soft matter systems under non-equilibrium conditions, such as shear flow, reveal significant information on the interplay between microscopic structure and macroscopic material properties. The contribution will focus on some recent results and give an outlook on the equipment available at ILL.

10.2 Controlling protein adsorption at aqueous-solid interfaces

Claus Czeslik¹

¹TU Dortmund, Physikalische Chemie I

The spontaneous adsorption of protein molecules at aqueous-solid interfaces plays a key role in a series of biotechnical and biomedical applications. For example, when using contact lenses or medical implants, the first biological response is usually the adsorption of proteins which then determine the subsequent biological compatibility of the foreign material. Furthermore, adsorbed proteins are involved these days in the application of medical solid-phase immunoassays and protein biochips.

Here, we will discuss recent experimental findings that allow for a control of the spontaneous adsorption of protein molecules at aqueous-solid interfaces and for an evaluation of the underlying driving forces. Experimental parameters include the temperature, polyelectrolyte surface coatings, and cosolvents. Neutron reflectometry and total internal reflection fluorescence (TIRF) spectroscopy are the main experimental techniques applied. As a major result, it has been found that a polyelectrolyte brush made of poly-(acrylic acid) has unique protein binding properties: Regardless of the sign of the protein net charge, protein molecules penetrate this brush at low ionic strength, whereas almost complete protein resistance of the polyelectrolyte brush can be induced by adding salt to the protein solution. Furthermore, protein molecules appear to be highly mobile inside this brush. In the case of a silica surface, proteins are likely to be adsorbed via hydrophobic interactions, as can be inferred from static and time-resolved studies as a function of temperature. Finally, the effects of the non-charged cosolvents, glycerol and urea, on the degree of protein adsorption at a silica surface have been determined and will be discussed.

10.3 Small-angle scattering from self-assembled and hierarchical structures

Julian Oberdisse¹, Jean-Francois Berret²

¹Université Montpellier II/CNRS

²Université Paris-Diderot/CNRS

Small Angle Neutron Scattering is a powerful tool for the study of structures in soft condensed matter. Advances in colloid and polymer chemistry have opened access to increasingly complex nanostructures, constructed by combinations of basic building blocks, like block copolymers, micelles, and colloids. In this talk, several examples for the determination of complex nanostructures by small angle scattering will be discussed.

In the past years, we have studied the structure of finite-sized complexes ($R \approx 13$ nm) made of double-hydrophilic copolymers and micelles by SANS, DLS, and cryo-TEM. A structural model has been proposed and it has been shown by direct numerical simulations that this model was compatible with all data sets. In a second time, we have attempted to construct such complexes replacing the micelles by inorganic nanoparticles. The observed SANS data look very similar, but aggregates are usually anisotropic, which would introduce additional parameters in a direct simulation. Using a Reverse Monte Carlo approach, as used successfully for the description of nanoparticle aggregates in polymer melts, the intensity curves could be described reasonably well. To finish, we will present a recent development of Reverse Monte Carlo, termed Russian Doll RMC, applicable to very big systems.

J.F. Berret et al, J Phys Chem B 2003, 107, 8111 J. Oberdisse, Soft Matter 2006, 2, 29-36

J. Oberdisse et al, Soft Matter 2007, 3, 476-485

10.4 Stroboscopic Small Angle Neutron Scattering Investigations of Microsecond Dynamics in Magnetic Nanomaterials.

Albrecht Wiedenmann¹, Roland Gähler¹, Roland P. May¹, Ulrich Keiderling², Klaus Habicht², M. Russina², S. Prévost³, M. Klokkenburg⁴, B. Ern ⁴, J. Kohlbrecher⁵

¹Institut Laue Langevin, F-38042 Grenoble Cedex, France

²Helmholz Zentrum Berlin, Structure Research, D-14109 Berlin, Germany

³Technical University Berlin D-10623 Berlin, Germany

⁴Utrecht University, NL-3584 CH Utrecht, The Netherlands

⁵Laboratory for Neutron Scattering, ETH Zurich & PSI, CH-5232 Villigen PSI, Switzerland

Time-resolved Small Angle Neutron Scattering (SANS) techniques have recently been developed which allow ordering and relaxation processes of magnetic moments in nanoparticles to be monitored. In stroboscopic experiments, time-frame data acquisition has been synchronized with a periodic external magnetic field. Slow relaxation of magnetic particle moments onto equilibrium has been studied in periods of the order of 30 s after switch off of a static field. By applying a sine-wave modulated magnetic field at frequencies above 50 Hz, the time-resolved SANS response to a forced oscillation could be analyzed. When a continuous neutron flux was used in conventional SANS, the shortest accessible time range was limited to about 3 ms resulting from the wavelength spread. A breakthrough of time resolution into the micro-second range was achieved with the pulsed frame overlap TISANE technique, which allows us to exploit a dynamical range similar to that of X-ray photon-correlation spectroscopy.

Here we present a combination of these stroboscopic neutron techniques on surfactant stabilized ferrofluids with nearly monodisperse Cobalt and Fe₃O₄ nanoparticles. Results are compared to a solid CuCo alloy with superparamagnetic nanosized Cobalt-precipitates. The SANS scattering response was measured stroboscopically in an oscillating applied magnetic field at frequencies up to 2800 Hz. As long as the magnetic moments followed the applied field, the 2D scattering patterns alternated between fully isotropic and strongly anisotropic.

The analysis of time-dependent SANS data as a function of frequency, field and temperature allowed us i) to proof the validity of the Langevin statistics describing the particle moment orientation, ii) to extract the effect of field-induced interparticle correlations, iii) to monitor the slowing down of the dynamics of moment rotation with decreasing temperature and iv) to decide between the possible relaxation mechanisms (N el and Brownian).

10.5 Formation And Growth Of Vesicles Studied By Time Resolved Small Angle Neutron Scattering Combined With A Stopped-Flow Equipment

Isabelle Grillo¹, Efim Kats¹

¹Institut Laue Langevin

Scattering experiments provide powerful method to explore colloidal structures from the scale of a few Angströms to thousands of Angströms. Time resolved using SLS, DLS and SAXS techniques have been developed since few years. Time resolved (TR) measurements are now also possible by Small Angle Neutron Scattering. The new generation of SANS diffractometers like D22 at the ILL (Institut Laue Langevin, Grenoble) with very high flux at the sample position (up to 10^8 neutrons/s/cm²) and a large dynamic q-range covered in only one setting allows very short acquisition times, of the order of a few hundreds of ms with a reasonable signal over background ratio.

A stopped-flow apparatus has been adapted to fulfil geometry of scattering experiments on D22. The interest of this equipment is to control the mixing of several solutions within a short time window (10-90 ms) and to control precisely the delay between the time of mixing and the beginning of observation.

Vesicles, which are single bilayer shells showed a growing interest during the last decades. Used as model for biologic membranes, they found also applications as micro-reactor or for drug encapsulation and delivery. The challenge in formulation is to find stable vesicles with well-defined sizes.

Two surfactant systems forming spontaneously vesicles will be presented. In the first one, the formation and growth of the vesicles is induced by the addition of salt in micellar solution of the anionic surfactant AOT. The TR-SANS experiment has shown that the vesicle radii and the growth rate depend on the salt concentration. In the second system, nano-sized vesicles are obtained by mixing non-ionic and cationic surfactants. Their size can be tuned by varying the molar ratio between the surfactants.

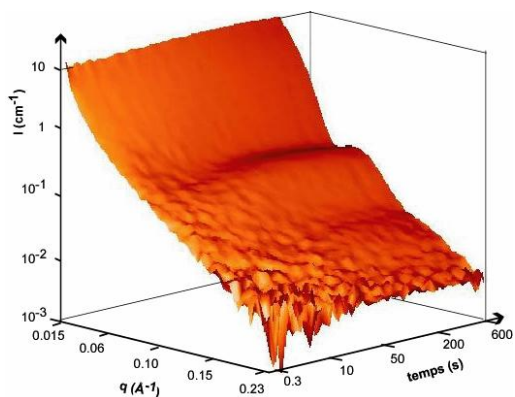


Figure 10.1: Formation of nanosized vesicles as revealed by time resolved small angle scattering experiment.

10.6 Combining neutron reflectivity and fluorescence microscopy to study biological interfaces

Bert Nickel¹

¹Ludwig-Maximilians Universität München, Department für Physik

We have studied structural and dynamical properties of membrane associated proteins by a combination of optical fluorescence microscopy and neutron reflectometry on the same samples. Examples include Annexin 2, a Ca binding protein. We show that the simultaneous information from both techniques allows one to follow protein absorption to solid supported membranes in terms of structure and self-diffusion of the lipids. Special sample cells which provide access for neutrons and an optical microscope have been developed for the REFSANS instrument and are available for users.

10.7 Microemulsions Near Planar Surfaces

Michael Kerscher¹, Henrich Frielinghaus², Dieter Richter¹

¹IFF

²JCNS

The domain structure of microemulsions is certainly influenced by a planar wall with preferential interactions for one domain. The ordering near the wall is locally elevated, while the bulk state is reached far from the surface. Lamellar and bicontinuous microemulsions are exposed to a well defined hydrophilic silicon surface. Using reflectometry and grazing incidence small angle neutron scattering (GISANS) the alternating domain sequence and the lateral order is recorded.

The studied microemulsion consists of water, decane and a non-ionic surfactant of the CiEj type. By varying the surfactant concentration and choosing the right temperature bicontinuous and lamellar phases are rendered. While the lamellar phase is studied in the film contrast (only surfactant protonated), the bicontinuous microemulsion is prepared in the bulk contrast. The latter sample will be studied by GISANS, where we intend to vary the overall scattering length density in order to vary the penetration depth of the evanescent wave, while the bulk contrast remains dominating. In this way the lateral order is resolved as a function of the depth, and the local ordering near the surface can be resolved. These measurements are the first of their kind.

The reflectometer measurements aim mainly at the structure in the normal direction since the lateral structure is only resolved at large length scales. The classical model of Caillé [1] describes the membrane correlations of the lamellar phase. In this way the membrane bending rigidity and the osmotic pressure are obtained.

The collected information will be used to improve the microemulsion behavior near surfaces in the static state and under flow. By using amphiphilic polymers as additives the response of the system to the surface and the flow will be tailored.

[1] K.D. Goetting, M. Monkenbusch, Europhys. Lett. 43, 135 (1998)

10.8 Small-Angle Neutron Scattering to Characterize Electrostatically Assembled Supramolecular Structures

Franziska Gröhn¹

¹Max Planck Institute for Polymer Research

Supramolecular assemblies obtained by self-organization of small building units are of high interest due to the potential for easily designing complex nanostructures with tailored physical, chemical and biological properties. Inspiration originates from natural supramolecular assemblies with a variety of architectures and functions from cell membranes to DNA-histone complexes. The main advantage of association via non-covalent interactions over a molecular synthetic design is the capability for rearrangements, leading to "self-healing" or "switchable" systems. In this contribution we present the formation of supramolecular structures by "electrostatic self-assembly" of macroions such as polyelectrolyte dendrimers and multivalent organic counterions such as naphthalene dicarboxylic acid and sulfonate dyes. This concept may open a field of versatile functional structures. Crucial tool to establish a new self-assembly concept of course is the careful characterization of the resulting nanoassemblies. This can be performed by a combination of scattering methods, in particular using small angle neutron scattering. Data are predominantly analyzed by Fourier Transformation of the scattering curve into the pair distance distribution function $P(r)$.

F. GRÖHN, K. Klein, S. Brand, "Facile route to supramolecular structures: self-assembly of dendrimers and naphthalene dicarboxylic acids", Chem. Eur. J. 2008, accepted

I. Willerich, F. GRÖHN, "Switchable nanoassemblies by electrostatic self-assembly", 2008, submitted.

F. GRÖHN, "Supramolecular structures by electrostatic self-assembly", Macromol. Chem. Phys. 2008, invited contribution, submitted.

C. Schmuck, T. Rehm, K. Klein, F. GRÖHN, "Formation of vesicular structures through the self-assembly of a flexible bis-zwitterion in dimethyl sulfoxide", Angew. Chem. Int. Eng. Ed. 2007, 46, 1693.

11 Mini-SYM 3: Materials Science and Engineering

11.1 Influence of the welding sequence on residual stresses in laser welded T-joints of aluminium alloys

Peter Staron¹, Funda S. Bayraktar¹, Winulf Machold¹, Stefan Riekehr¹, Mustafa Kocak¹, Andreas Schreyer¹

¹GKSS Forschungszentrum

Replacing riveted by laser beam welded (LBW) joints of aluminium alloys is a current topic in the aircraft industry because of the weight and cost saving potential. The start (run-in) and end (run-out) locations of short welds are critical locations with respect to crack initiation and growth due to high stress concentration. Recent measurements indicated that longitudinal tensile stresses are lower at the run-in locations than at the run-out locations. Therefore, in the present study, the LBW joint of 2 mm thick AA6013-T6 clips to 4.5 mm thick AA6156-T6 base plates – resembling a skin-clip joint of an airframe – using a 3.3 kW Nd:YAG Laser source are investigated. Particularly, the effect of different welding sequences on the residual stress state was studied. One welding sequence was made straight from one end of the clip to the other, a second with two starting points in the centre, and a third with starting points at the clip ends. Experimental determination of residual stresses was done using neutron and high-energy X-ray diffraction. The results show that the stress distribution around the weld depends strongly on the welding sequence. The residual stress results will be discussed with respect to fatigue properties.

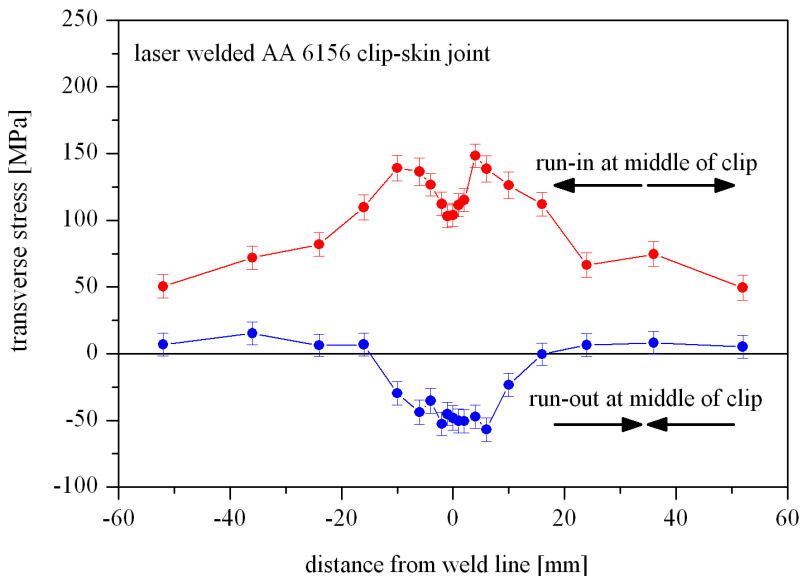


Figure 11.1: Transverse residual stresses for two different welding sequences.

11.2 Direct observation of chemical diffusion in liquid alloys using X-ray and neutron radiography

Axel Griesche¹, Bo Zhang¹, Andreas Meyer²

¹Institut für Materialphysik im Weltraum, DLR Köln

²nstitut für Materialphysik im Weltraum, DLR Köln

The description of nucleation and crystal growth in liquid alloys requires the knowledge of chemical (inter-) diffusion coefficients and their relation to self diffusion and thermodynamic driving forces. However, the measurement of chemical diffusion by capillary techniques is hampered by bouyancy-driven convective flow, especially during melting and solidification of the diffusion couple. Therefore, diffusion (concentration) profiles obtained ex situ on the solidified samples are severely altered and reliable data can not be obtained. As a consequence, accurate diffusion coefficients in liquid alloys are rare and limited in most cases to results from experiments under microgravity conditions in space, and our understanding of nucleation and growth is not far evolved. We use X-ray and neutron radiography for an in situ observation of the entire process: melting, diffusion annealing and solidifying of the liquid alloy. By that we obtain evolving concentration profiles as a function of time. Hence, artefacts due to convective flow can be identified and taken into account in the further data analysis.

Challenges, limitations and perspectives of this new method are discussed.

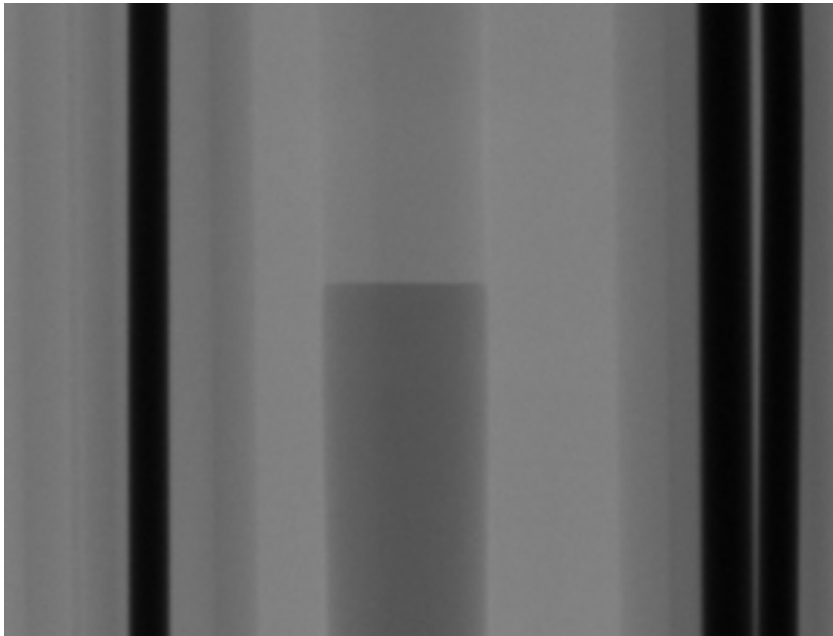


Figure 11.2: Monitoring interdiffusion of a AlCu diffusion couple by X-ray radiography. The different Cu content in the alloy results in an X-ray radiography contrast. In this context neutron radiography extends the accessible alloy systems to diffusion couples where the large X-ray absorption prevents measurements, like steels and nickel based alloys.

11.3 Scattering contrast dependence on thermal-expansion-coefficient difference of phases in two-phase system

Pavel Strunz¹, Ralph Gilles², Debashis Mukherji³, Michael Hofmann², Dominique del Genovese³, Joachim Roesler³, Markus Hoelzel², Vadim Davydov⁴

¹Research Centre Rez

²TU München

³TU Braunschweig

⁴Nuclear Physics Institute Rez

In the recent in-situ small-angle neutron scattering (SANS) experiment on Ni-Fe-base superalloy DT706, a rather surprising increase of the measured scattering curve amplitude (without observing any shape change) was detected during cooling at temperatures below 800°C. It is envisaged that an explanation for this observed increase in the SANS intensity could lie in the difference in the thermal expansion coefficients of the matrix and the precipitate. At these low temperature (below 800°C) diffusional processes in Ni-alloys are rather slow and changes in precipitate morphology and composition should be negligible.

The theoretical expressions describing the dependence of SANS contrast on temperature in the abovementioned region were derived. The theory considers difference in thermal expansion coefficients of the two primary phases in Ni-base superalloys (γ matrix and ordered γ' precipitates). It is demonstrated, that this difference is the determining factor for the temperature dependence of the contrast in the case where the sum of scattering lengths in the matrix and in the precipitate are not very different. The simulations show that the value of scattering contrast is firmly connected with the particular shape of the temperature dependence. This fact can be used for the determination of the scattering contrast without the knowledge of the compositions of the individual phases.

The presented hypothesis on SANS contrast was proven by performing experiment on DT706. The evolution of lattice parameters of both the matrix and the precipitate phases, necessary for determining the evolution of unit cell volumes with temperature, was obtained from the in-situ wide angle neutron diffraction experiment (FRM-II - SPOD), Stressspec). Then, the theoretical scattering contrast dependence was successfully fitted to the measured SANS integral intensity. The direct output of this fit is the scattering contrast at RT and its temperature dependence.

11.4 Eigenspannungen als Träger des Verzugspotenzials: Messungen und Rechnungen an Bauteilen der Wälzlager- und Getriebeindustrie

Jeremy Epp¹, Thomas Hirsch¹, Tobias Poeste², Rainer Schneider²

¹Institut für Werkstofftechnik, Bremen

²Helmholtz-Zentrum, Berlin

An Einsatz- und Wälzlagerstählen werden in einem Sonderforschungsbereich der DFG (SFB 570 Distortion Engineering) umfangreiche Untersuchungen zur Messung und Bewertung des durch alle Fertigungsschritte erzeugten Verzugs vorgenommen. Eine gegebenenfalls in einzelnen Fertigungsschritten mögliche Kompensation des Verzugs ist nur möglich, wenn die relevanten Werkstoffeigenschaften nach jedem Fertigungsschritt bekannt sind und auch modelliert werden können. Träger des Verzugspotenzials sind beispielsweise auch die in den einzelnen Fertigungsschritten durch Umformung, Bearbeitung und Wärmebehandlung erzeugten oder ausgelösten Eigenspannungen.

Da die Modellierung der Verzüge Eigenspannungstensoren an jedem Ort der Bauteile liefert, sind experimentelle Kenntnisse dieser Tensoren zur Verfeinerung der Rechnungen unabdingbar. Zur Eigenspannungsbestimmung vorzugsweise im gesamten Querschnitt von Bauteilen wie Wälzlagering, Wellen und Zahnräder reicht damit eine einzelne Messmethode nicht aus. Daher wurden und werden umfangreiche Messungen mit Neutronenstrahlen zur Detektion des Eigenspannungszustandes im Kern der Bauteile in Ergänzung zu röntgenographischen Messungen und Berechnungen durchgeführt.

Die Ergebnisse von bearbeiteten, geglühten und blindgehärteten Zuständen eines Wälzlagerstahls 100Cr6 und eines Einsatzstahls 20MnCr5 werden vorgestellt. Die Resultate werden mit FEM - Rechnungen verglichen.

11.5 Neutron Tomography on tyrannosaurid foot at GENRA-3

Felix Beckmann¹, Tjard Kusche², J. Vollbrandt¹, P.K. Pranzas¹, H.-W. Schmitz¹, A. Schreyer¹

¹GKSS-Research Center Geesthacht

²GeoStudio, Heidmoor

The recently developed setup for Neutron Computerized Tomography (NCT) at the neutron radiography facility GENRA-3 at the research reactor Geesthacht FRG-1 was used to study the 3-dim. bony structure of tyrannosaurid left foot specimen. NCT is used as preanalysing method to find organic remains that could be destroyed through the required following preparation. Furthermore, it became possible to combine Neutron and Synchrotron Radiation CT techniques. The different tomographic stations operated by the GKSS, the advantage and disadvantage for biological and materials science applications will be described.

F. Beckmann, J. Vollbrandt, T. Donath, H.W. Schmitz, A. Schreyer, "Neutron and synchrotron radiation tomography: New tools for materials science at the GKSS-Research Center", Nuclear Instruments and Methods in Physics Research A 542 (2005) 279-282.

11.6 The robot concept at STRESS-SPEC for the characterization of semi-finished products

Heinz-Günter Brokmeier¹, Ulf Garbe², Michael Hofmann³, Christian Randau¹, Peter Spalthoff⁴, William Tekouo⁵, Wolfgang Vogl⁵, Rainer Schneider⁶, Andreas Schreyer⁴

¹IWW-TU Clausthal

²Bragg Institute, ANSTO

³Forschungsgneutronenquelle Heinz Maier-Leibnitz (FRM-II), TU München

⁴GKSS-Forschungszentrum

⁵IWB-TU München

⁶HMI-Berlin

The materials science diffractometer STRESS-SPEC located at Forschungsgneutronenquelle Heinz Maier-Leibnitz (FRM-II) in Garching/Germany is a dedicated instrument for residual strain, texture and microstrain analysis. Comparably low gauge volumes of $1 \times 1 \times 1 \text{ mm}^3$ for gradient investigations in many types of materials can be investigated. Routine operation of STRESS-SPEC starts in mid 2005. Previous texture investigations on laser beam welded and friction welded materials as well as on a bonelike extrudate have shown that positioning of the gauge volume and the free space in our Eulerian cradle to rotate and tilt compact samples is restricted. On the other hand, all these samples have texture and strain gradients on a small length scale so that a mapping to investigate these gradients is necessary. For texture measurements a large freedom in tilt of 90° and in rotation for any tilt position of 360° is needed. As an example the measurement of the texture gradient in a dissimilar friction welded Al7020/Steel 316L express the need of a high positioning of the central axis during the pole figure measurement. Thus, a robot system will be installed at STRESS-SPEC supported by the BMBF. The specification of the robot is a load capacity of 50 kg, a positioning length of 50cm in all directions a positioning accuracy between 5/100 and 1/100 in x-,y-,z-direction. Of course the robot has a great freedom in omega ($0^\circ - 90^\circ$), in phi (sample rotation $0^\circ - 360^\circ$) and chi (sample tilt $0^\circ - 90^\circ$). A second application of the robot system is the usage as an automatic sample changer, as already shown for conventional X-ray. This is of great importance for a fast and also cheap routine investigation of large sets of standard samples on industrial level.

11.7 Texture homogeneity in a single pass ECAPed pure Mg

Weimin Gan¹, Heinz-Günter Brokmeier¹

¹TU-Clausthal

Quadratic extruded pure Mg billet was 50 % deformed by equal channel angular pressing (ECAP) using a die angle of 90° at 350°C. Textures of small bulk samples cut from different regions of the ECAPed billet were analyzed by neutron radiation. A texture gradient was attributed to the inhomogeneous distribution of the effective stress and strain, and also the inevitable existence of friction. By the texture evolution deeper inside in the complex flow filed was obtained. These textures were characterized by the combination of shear deformation, inhomogeneous flow (grain rotation) and quadratic extrusion (friction). In the die region all three components overload each other, while incoming and outgoing channel show less shear. Comparing with previous work pure extrusion or rolling texture results after 8 passes of ECAP deformation, that no shear was visible. Due to the strong texture gradient, the deformation region was investigated with higher resolution of 1mm² in cross section by high energy synchrotron radiation. Shearing and extrusion components with respect to the extrusion direction depend on the distance from the top of the ECAPed billet. The transformation point of the extrusion component to shearing component was localized, which indicated the main deformation mode in local regions.

11.8 In-situ mechanical testing at the time-of-flight neutron diffractometer POLDI

Steven Van Petegem¹, Ludovic Thilly², Helena Van Swygenhoven¹

¹Paul Scherrer Institut

²University of Poitiers

The neutron diffractometer POLDI for residual stress measurements at the continuous spallation source SINQ (Paul Scherrer Institut) is a novel type of time-of-flight neutron diffractometer with multiple frame overlap, a method, which allows tuning to high intensity and high resolution simultaneously.

Recently POLDI has been extended with a tensile machine which allows investigating the development of intra- and intergranular stresses during mechanical loading or the influence on the mechanical properties of elastic, plastic and thermal misfit stresses between different phases in composite materials.

In this talk we present results recently obtained from in situ tensile tests at POLDI on Copper-based high strength nanofilamentary wires reinforced by Niobium nanofilaments[1,2]. The evolution of elastic strains and peak profiles versus applied stress evidences a co-deformation behavior with different elastic-plastic regimes: the Cu matrix exhibit size effect in the finest channels while the Nb nanofilaments remain elastic up to the macroscopic failure, with a strong load transfer from the Cu matrix onto the Nb filaments. The measured yield stress in the finest Cu channels is in agreement with calculations based on a single dislocation regime.

[1] V. Vidal, L. Thilly, S. Van Petegem, U. Stuhr, F. Lecouturier, P.-O. Renault, H. Van Swygenhoven, Applied Physics Letters 88, 191906 (2006)

[2] V. Vidal, L. Thilly, S. Van Petegem, U. Stuhr, F. Lecouturier, P.-O. Renault, H. Van Swygenhoven, Materials Research Society Symposium Proceedings 977, 0977-FF07-07-EE07-07 (2007)

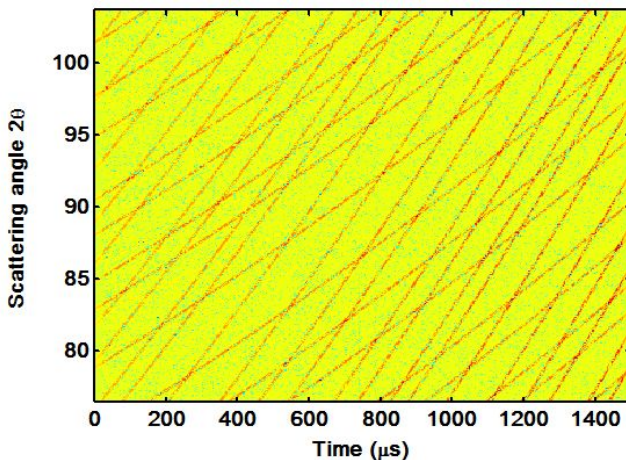


Figure 11.3: A typical POLDI spectrum showing intensity versus arrival time and scattering angle.

Abstracts: Posters I (Monday)

Biophysics: M1 - M5

Instrumentation and methods I: M6 - M40

Nuclear and particle physics: M41 - M44

Magnetism I: M45 - M58

Soft Matter : M59 -M94

12 Biophysics and biology

M-1 Calcium-binding protein dynamics : investigation of the relationship between structural thermal stability and internal motions by quasielastic neutron scattering

Marie-Sousai Appavou¹, Wolfgang Doster²

¹IFF-Jülich Center for Neutron Science

²TUM-Physik Department E13

It is "widely" assumed [1,2] that enhanced thermal stability of proteins is associated with a decrease in structural flexibility. In particular thermo-stable proteins are thought to be less flexible than their mesophilic analogues. The experimental evidence however is inconclusive: While some thermo-stable enzymes like malate dehydrogenase [2,3] show the expected reduction in structural fluctuations, α -amylase [1] displays the opposite effect: the thermo-stable form exhibits larger motional amplitudes. The evidence presented by neutron scattering data so far, is restricted to the analysis of the elastic spectrum, where slight differences in the temperature dependence of the corresponding displacements or in the quasi-elastic amplitudes are detected. No detailed spectral analysis at high resolution using back-scattering has been performed. In the spectral window of a time-of-flight spectrometer (resolution 100 μ eV) only motions on a pico-second time-scale are recorded and changes in line-width cannot be discriminated easily from amplitude variations. It is important to study several related proteins to document whether the proposed dogma of stability by global rigidity holds not just in a single case. Therefore we investigated the quasi-elastic spectra of two Ca-binding proteins α -amylase and α -lactalbumin on a nano-second time scale using neutron back-scattering spectroscopy. With both proteins calcium binding results in a large increase in the thermal denaturation temperature: The stabilization leads to an upshift in the denaturation temperature by 40° C [2,4]. Although the apo-form (Ca-free) of α -lactalbumin is much less stable than the holo-form (Ca-bound) there are only minor differences in their native structures. α -lactalbumin thus exhibits two similar structural states with potentially very different flexibility. Moreover the calcium ion cross-links two structural domains, which may suppress inter-domain motions. A 250 ps molecular dynamics simulation of α -lactalbumin with and without calcium was performed by Iyer and Qasba [5]. The analysis of the mean square displacements suggests that the calcium-bound α -lactalbumin exhibits more fluctuations than the apo-protein. Our back-scattering data reveal a clear depression of molecular dynamics with both proteins in the Ca-bound form relative to the holo-enzymes.

[1] J. Fitter and J. Herberle *Biophys.J.* 79, 1629-1636, (2000).

[2] J. Fitter et al, *Biochemistry*, 40, p 10723 -10731, (2001).

[3] M. Tehei et al. *J.Biol.Chem.* 280, p 40974 - 40979, (2005).

[4] Hendrix T et al, *Biophysical Chemistry*, 84, p27-34 ,(2000).

[5] L.K Iyer and P.K.Qasba , *Prot. Eng.*, 12, pp 129-139,(1999).

[6] W. Doster and M. Settles, *BBA* 1749, p.173, (2005),

[7] W. Doster, *Physica ,B* 385-386 part II, p 831-834, (2006).

M-2 Microdomain Formation in Lipid Mixtures

Karsten Vogtt¹, Christoph Jeworrek²

¹Helmholtz-Zentrum Berlin

²TU Dortmund

Microdomains in lipid bilayers, or so called rafts, attracted much interest in the last years, for they are assumed to play essential roles in biological processes like cell signalling and trafficking. Since rafts are formed by lateral phase separation within the membranes, small angle neutron scattering in combination with solvent matching offers a unique approach to study this phenomena: By deuterating one compound of the lipid mixture and using a mixture of water and deuterium oxide as solvent, it is possible to match the scattering length density of the solvent with the average scattering length density of the formed liposomes.

Thus, in the case of a homogenous lipid distribution in the bilayers, no variation of scattering length density is present. But upon microdomain formation, i.e. lateral changes in lipid composition, the scattering length density will vary, allowing detection by small angle neutron scattering.

The poster will present recent results obtained on the temperature dependent phase behaviour of a ternary mixture of dioleoylphosphatidylcholine, cholesterol and deuterated dipalmitoylphosphatidylcholine.

M-3 Losartan and Angiotensin II – Tracing structural changes by SANS

Julia Preu¹, Thomas Gutberlet², Thomas Heimburg¹

¹Membrane Biophysics Group, Niels Bohr Institute, University of Copenhagen, 2100 Copenhagen, Denmark

²Jülich Centre for Neutron Science, 85747 Garching, Germany

In a healthy individual, the renin-angiotensin system helps to maintain blood pressure at normal levels. Part of this system is the peptide hormone Angiotensin II (Ang II), a potent vasoconstrictor that aids in the blood pressure regulation, as well as in body fluid balance maintenance. Ang II derives from the precursor angiotensinogen, through enzymatic reaction catalyzed by renin and the angiotensin converting enzyme (ACE). On the heart, acting in both endocrine and paracrine fashions Ang II regulates contractility, remodelling, growth, apoptosis, and reduces cell coupling and conduction velocity in cardiac muscles. In patho-physiological states of hypertension and congestive heart failure or in cases of excessive levels of angiotensin II (Ang II) β -blockers may enable relief. Another potent drug is Losartan, an Ang II antagonist. Apart from binding to different protein receptors Ang II is interacting with the cell membrane, the same effect was shown for losartan. We are interested in the influence of Ang II and Losartan on the structural arrangement of pure lipid bilayers as model membrane systems. Studies by differential scanning calorimetry (DSC) have shown strong effects due to electrostatic interactions between model membrane systems and Losartan. At high concentrations of Losartan the zwitterionic lipid dimyristoyl phosphatidylcholine (DMPC) behaves like the charged dimyristoyl phosphatidylglycerol (DMPG), whereas the thermodynamic interaction with Ang II is much weaker. In our presentation we show first results using small angle neutron scattering (SANS) on the structural interactions of Ang II and Losartan with lipid bilayers.

M-4 Elastic incoherent neutron and Quasi-elastic scattering studies of aligned DMPC multilayers at different hydrations

Marcus Trapp¹, Thomas Gutberlet², Fanni Juranyi³, Moeva Tehei⁴, Judith Peeters⁵

¹Institut de Biologie Structurale, 38042 Grenoble Cedex 9, France

²Jülich Centre for Neutron Science, 85747 Garching, Germany

³LNS, ETHZ & Paul Scherrer Institut, 5232 Villigen, Switzerland

⁴AINSE, University of Wollongong, NSW 2522, Australia

⁵Universite Joseph Fourier, 38042 Grenoble Cedex 9, France

Lipid model membranes such as 1,2-Dimyristoyl-sn-Glycero-3-Phosphocholine (DMPC) serve as role models for their more complex counterparts in biological systems. Inelastic neutron scattering (INS) [1], quasi elastic neutron scattering (QENS) [2,3] and neutron spin echo spectroscopy (NSE) [4] have been employed to study local as well as collective dynamics of these membranes. Most of these studies lack a systematic investigation of the behavior of the model membranes in dependence on their hydration.

We have performed elastic incoherent neutron scattering (EINS) measurements at the high momentum transfer backscattering spectrometer IN13 at ILL, Grenoble and QENS measurements at the TOFTOF time-of-flight spectrometer at FRMII in Munich. These experiments were done with samples of chain deuterated DMPC-d54 at two different states of hydration (repeating distance $d=62,5\text{\AA}$ for 100 % r.h. and $d=54,9\text{\AA}$ for 99,7% r.h., respectively).

The data reveal the influence hydration has on the mobility of the system clearly and expand earlier neutron backscattering investigations [5].

Results of the two measurements and an outlook for further measurements at MIRA (Munich) and at IN12 (Grenoble) will be presented.

[1] M.C. Rheinstädter et al., Phys Rev. Lett., 93, 108107, 2004

[2] W. Pfeiffer et al., Europhys Lett., 8, 201, 1989

[3] S. König et al., J.Phys.II France, 2, 1589-1615, 1992

[4] M.C. Rheinstädter et al., Phys. Rev. Lett. 97, 048103, 2006

[5] M.C. Rheinstädter et al., Phys. Rev. E, 71, 061908, 2005

M-5 Indirect radiation therapy of cancer by Gadolinium NCT - instrumentation and cell culture models

Thomas Nawroth¹, Tanja Peters¹, Natalie Glube¹, Peter Langguth¹, Bruno Pairet², Heinz Decker², Heinz Schmidberger³, Christoph Alexiou⁴, Bernhard Lauss⁵, Michael Jentschel⁶, Roland P. May⁷

¹Institut für Pharmazie

²Inst. für Molekulare Biophysik

³Radioonkologie Klinik Mainz

⁴HNO Klinik, Erlangen

⁵ILL-PN3, Grenoble; PSI

⁶ILL-PN3, Grenoble

⁷ILL-D22, Grenoble

Indirect radiation therapy IRT inactivates cancer cells by secondary radiation products evolving from incorporated target material upon specific absorption of a therapy beam. The power of the method depends on the absorption cross section, the physiological acceptable concentration of the target material and the intracellular location after incorporation. We have developed heavy metal chelate entrapped nanoparticles for radiation therapy with neutron-capture, synchrotron-, and gamma-photons.

Nanoparticles are suitable for tumor-local deposition and uptake of absorption material at high concentration level, >10 mM in tissue. As nanoparticles systems we use a combination of liposomes and metal complexes, solid lipid particles for hydrophobic drugs, and Ferrofluids for magnetic manipulation.

Biocompatible target materials with Gadolinium, Erbium, Boron, Lutetium and cis-Platinum were entrapped, and tested with cell cultures as tumor models. Animal test are planned (rat, rabbit).

Target liposomes entrapping Gd-, Er-, Lu-DTPA, Boron-compounds, cis-Platinum and a cis-Pt-lipid were characterized by time resolved neutron small angle scattering (TR-SANS), ASAXS, XAFS, DLS and electron microscopy. Optimal particles of 100nm size, avoiding the embolic risk limit of 500 nm, were optimised for maximal beam absorption.

For the cell culture tests we have developed an irradiation setup and protocol for a late apoptosis test. In the setup a multiple collection of submerge cells is irradiated. The protocol provides the proliferation rate, which is the equivalent of tumor growth and inactivation. The study is done in parallel with synchrotron radiation, neutrons (Gd-NCT, Gadolinium neutron capture therapy) and gamma photons from a clinics accelerator (E-PT, enhanced photon therapy). Neutron therapy tests with F98 cells showed a relevant inactivation with a Gadolinium-Erbium mixture, which produces free radicals by a double absorption (fig.).

Nawroth T, Rusp M, May RP. Magnetic liposomes and entrapping. *Physica B* 2004; E635-638. Specific WEB-site: www.mpsd.de/irt/

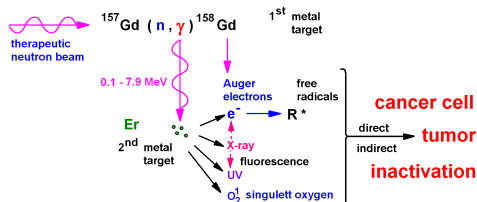


Figure 12.1: Neutron capture and subsequent conversion reactions by an incorporated Gd-Er target produce cell inactivating radiation products by double absorption.

13 Instrumentation and methods I

M-6 Neutron Scattering under Controlled Gas Atmospheres - The CGA-Sample Environment

Dirk Wallacher¹, Astrid Brandt¹

¹Helmholtz-Zentrum Berlin

In 2006 the Hahn-Meitner-Institute Berlin started establishing a laboratory acronymed DEGAS to set-up a modular sample environment, dedicated to the increasing requests on neutron scattering investigations combined with gas adsorption measurements. The applications for the so developed CGA-sample environment are manifold. One main topic is the characterization of new tailored or functionalized mesoscopic materials by in-situ contrast matching methods, where the local distribution of pore condensed vapors can be monitored along the adsorption process, e.g. by SANS, which gives direct information of the length scales accessibility and the connectivity of the void volumes in nano-structured host materials [1-3]. Other important tasks for Gas adsorption set-ups are investigations on host materials for gas storage, where typically gases like Hydrogen and Methane at pressures up to 10 kbars are in the focus of the neutron scattering experiments performed at temperatures ranging from 2 K to 1300 K [4-7].

Up till now more than 10 different modular constructed experimental set-ups for the above mentioned experimental requests have been realized in the Berlin Neutron Scattering Center (BENS) at the Hahn-Meitner Institute, and will be expanded in the "Helmholtz Centre Berlin for Materials and Energy" in the future. A detailed overview on the existing set-ups will be given on the poster.

[1] E. Hoinkis and B. Rühl-Kuhn, *Langmuir* 21, 7366 (2005)

[2] M. Thommes et al., *Langmuir* 22, 756 (2006)

[3] Sel, O.; Brandt, A.; Wallacher, D.; Thommes, M.; Smarsly, B., *Langmuir*, 23, 4724 (2007) [4] K.A. Lokshin et al., *Phys. Rev. Lett* 93, 125503 (2004)

[5] M. Felderhof et al., *Phys. Chem. Chem. Phys.* 9, 2643 (2007)

[6] A. Züttel et al., *Scripta Materialia* 56, 823 (2007)

[7] D. Wallacher, M. Rheinstaedter, T. Hansen, K. Knorr, *J. Low Temp. Phys.* 138, 1013 (2005)

M-7 SPHERES: ein rundum erfreuliches Rückstreu-spektrometer

Joachim Wuttke¹, Gerald Johannes Schneider¹, Luis Carlos Pardo Soto¹, Michael Prager¹, Dieter Richter¹

¹FZ Jülich

Nach einjährigem Probebetrieb hat sich SPHERES unter den drei führenden Rückstreu-spektrometern etabliert. Auflösung und dynamischer Bereich sind exzellent; der Fluss ist so hoch, dass Temperatur-Scans nicht mehr auf elastische Streuung beschränkt werden müssen. Das Signal-zu-Untergrund-Verhältnis von 350:1 werden wir in naher Zukunft deutlich steigern; die Neuauslegung des Phasenraumtransformations-Choppers ermöglicht weitere Optimierungen.

M-8 Single domain wall in FeNi film on Si for spin flip.

Wicher Kraan¹, Theo Rekveldt¹

¹Fac.Applied Sciences Section R3/NPM2

A permalloy film on Si is divided over its thickness into 2 opposite domains by passing a DC "wall current" of 20 A through the film. The position of the resulting domain wall is adjusted inside the film thickness by an in-plane magnetic field. To investigate the flipping properties we perform 3D-analysis of the polarisation vector of the transmitted beam ($\lambda=0.2$ nm) around loops at 10-1000 Hz with this field, with the film positioned under 3-15 deg to the beam.

At all frequencies the domain wall annihilates before reaching either surface. At 7 deg, with restricted amplitude of this field (0.3 A/cm), the net precession of the polarisation vector after the film can be varied between $-\pi$ and $+\pi$ without hysteresis, with a depolarisation 0.85. The response of the domain wall is quick enough to follow the required $1/t$ time dependence of the applied field when the film is used as $\pm\pi$ -flipper at a pulsed source operated at 20 to 50 Hz. The geometry allows that a beam of cross section 20x10 mm² can be intercepted and flipped. This demonstrates that the film can be used for such a flipper.

The annihilation of the domain wall and the depolarisation are attributed to disturbing magnetic/ non-magnetic nuclei on both surfaces. Eliminating their influence requires much stronger wall current fields, only possible using thicker films.

M-9 Magic Box and fast decaying cell - two methods of SANS polarization analysis with ^3He at the V4 SANS instrument of Helmholtz Center Berlin

U. Keiderling¹, A. Wiedenmann², A. Rupp¹, J. Klenke³, W. Heil⁴, D. Jullien², A.K. Petoukhov², E. Lelievre-Berna², K.H. Andersen²

¹Helmholtz Center Berlin, Glienicker Str. 100, D-14109 Berlin, Germany

²Institut Laue-Langevin, 6, rue Jules Horowitz, B.P. 156, F-38042 Grenoble Cedex 9, France

³FRM II, Technische Universität München, Lichtenbergstr. 1, D-85747 Garching, Germany

⁴Institut für Physik, Johannes-Gutenberg-Universität, D-55099 Mainz, Germany

The V4 instrument has recently been equipped with two different setups for polarization analysis of SANS data by means of ^3He neutron spin filter cells. The first setup is a "Magic Box" [1] purchased from ILL, consisting of a spin filter cell in a constant magnetic field inside a μ -metal shielding. It is equipped with an integrated flipper coil to flip the ^3He gas. This device is optimized to preserve the ^3He polarization for a maximum time (measured relaxation time to $1/e$ of the original nuclear polarization ≈ 180 h). However, due to its size it has to be placed in the detector vessel, relatively far away from the sample. This leads to a cut-off of the large scattering angles, i.e. the large values of the scattering vector Q .

In the second setup, a ^3He spin filter cell is placed directly in the homogeneous field B of the sample magnet, very close to the sample. This layout retains nearly the full Q range of the instrument. The cell only reveals a relaxation time to $1/e$ of the original nuclear polarization of approximately 5.5 h. A full polarization analysis is possible even without an additional flipper, by making use of the continuous change of the filter transmissions $T(+)$ and $T(-)$ for neutrons polarized parallel $I(+)$ and anti-parallel $I(-)$ to B during the decay of the ^3He polarization.

In the experiment, a concentrated Co-ferrofluid sample "MFT3N" was measured with both setups. The setups and the procedures of extracting the flip and non-flip components from the data are described in detail, and the results of both methods are compared. The two-dimensional flip patterns obtained represent the purely magnetic scattering contribution, featuring the typical $(\sin \theta * \cos \theta)^2$ behavior expected for super-paramagnetic systems, where θ is the azimuthal angle between B and the scattering vector Q [2].

[1] A.K.Petoukhov, V.Guillard, K.H.Andersen, E.Bourgeat-Lami, R.Chung, H.Humblot, D.Jullien, E.Lelievre-Berna, T.Soldner, F.Tasset and M.Thomas, Nuclear Instruments and Methods in Physics Research A 560 (2006) 480-484

[2] A.Wiedenmann, Physica B 356 (2005) 246-253

M-10 BRISP and FOCUS-2D - Two similar Large Area Position Sensitive Neutron Detector Projects at the ILL and the PSI

Thomas Gahl¹, Rolf Hempelmann², Fanni Jurßnyi¹, Joel Mesot¹, Wolf-Christian Pilgrim³, Thierry Straessle¹

¹Paul Scherrer Institut, Villigen

²Physical Chemistry, Saarland University, Saarbrücken

³Physical Chemistry, Philipps University, Marburg

Mid- to Large-Area-2D-Neutron-detectors with moderate position resolutions are playing an important role in neutron scattering instrumentation. They are the first choice especially on scattering applications with relative large sample-to-detector distances. A common approach for this kind of detectors is to compose them as an array of single PSD-detector tubes with Resistive Charge Division Readout along the tubes especially with high (local) count rates and/or high efficiencies with thermal neutrons.

Exploiting these technology two similar detectors had been built in the last years for the Brillouin-Spectrometer BRISP at the Institute Laue Langevin (ILL) in Grenoble, France [2], and for the Time-of-flight spectrometer FOCUS at the SINQ (Paul Scherrer Institute – PSI) in Villigen, Switzerland [3].

In this contribution we present the two detector projects by comparing their performances and common properties but also pointing out different design approaches in vacuum tightening and custom made detector electronics [1] with main focus on the circuit technology and the form factor of the analogue front end and AD-conversion electronics.

The financing of both detector projects by the BMBF (Germany) under several grants up to 2007 is gratefully acknowledged.

[1] P. van Esch, T. Gahl, B. Guerard, “Design Criteria for Electronics for Resistive Charge Division in Thermal Neutron Detection”, Nucl. Instr. Meth. A 526/3 (2004) 493

[2] D. Aisa, E. Babucci, F. Barocchi, A. Cunsolo, F. D’Anca, F. Formisano, T. Gahl, E. Guarini, S. Jahn, A. Laloni, H. Mutka, A. Orecchini, C. Petrillo, F. Sacchetti, J.-B. Suck, G. Venturi, “The development of the BRISP spectrometer at the Institut Laue-Langevin”, Nucl. Instr. Meth. A 544/3 (2005) 620

[3] F. Jurßnyi, L. Holitzner, N. Schlumpf, U. Greuter, T. Gahl, S. Janssen, J. Mesot, R. Hempelmann, “The 2D small angle detector project at the FOCUS time-of-flight spectrometer at SINQ”, Journal of Neutron Research Vol.14 No.4 (2006) 333



Figure 13.1: Front end amplifier systems for Resistive Charge Division Readout in neutron detection:
1 Ch. Ampli-DAQ CvcResRd 3.2 (PSI)

M-11 Optimization of the SKAT texture diffractometer at Dubna for texture measurements on geological samples.

Klaus Ullemeyer¹, Jan H. Behrmann²

¹Institut für Geowissenschaften

²IFM-GEOMAR Kiel

Due to high resolution, the SKAT texture diffractometer at Dubna has advantages for texture measurements on geological samples (Ullemeyer et al. 1998). Currently, the range of lattice spacings d is restricted to about 5 Angstroms. This may hamper texture analysis of polyphase rocks because of peak overlaps. Since Bragg reflections of many minerals are located beyond this limit, this restriction may be overcome by increasing the accessible d -range. Improving the resolution is another way to increase the number of non-overlapped reflections for the texture analysis. Both these options will be considered for the current upgrading of the SKAT.

Construction of a second detector system with $2\theta = 65^\circ$ will expand accessible d -range to about 6.5 Angstroms. As a disadvantage, resolution deteriorates by about 30%. A further detector system placed at $2\theta = 135^\circ$ will increase resolution significantly, however, the range of accessible lattice spacings decreases to about 3.8 Angstroms. This disadvantage may be overcome by doubling the time window for TOF analysis, i.e., by cutting out every second neutron pulse. Intensity loss as a consequence thereof will be compensated by the installation of a highly efficient neutron guide. The detector systems are intended for an alternative use to preserve the advantage of similar scattering geometry for all detectors. The detector-collimator units will be compatible and can be exchanged quickly between the systems.

To sum up, the modernized SKAT will offer the possibility of far-reaching adaptation of the experimental conditions to the composition of the samples to be investigated. The optimum balance between resolution, required d -range and other constraints may be found, leading to improved texture determinations of polyphase rocks. Keeping the present detector system preserves also the optimum geometrical conditions for the installation of uniaxial sample environments.

Ullemeyer, K., Spalhoff, P., Heinitz, J., Isakov, N.N., Nikitin, A.N., Weber, K. (1998). The SKAT texture diffractometer at the pulsed reactor IBR-2 at Dubna: experimental layout and first measurements.- Nucl. Instr. Meth. Phys. Res. A412, 80-88.

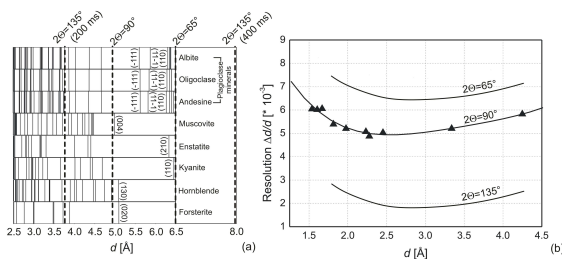


Figure 13.2: (a) Accessible d -ranges depending on the scattering angle, illustrated by line patterns of some minerals. For $2\theta = 65^\circ$ the number of accessible Bragg reflections increases at the expense of resolution. For $2\theta = 135^\circ$ and suppressing every second neutron pulse (400 ms), no additional reflections are accessible but the resolution improves such that more reflections with small lattice spacings become accessible. Using all pulses (200 ms), d is limited to 3.8 Angstroms. (b) Particular resolution functions.

M-12 In-situ Sample Orientation for Neutron Scattering at Dilution Temperatures

Klaus Kiefer¹, Bastian Klemke¹

¹BENSC-Probenumgebung, Helmholtz-Zentrum Berlin für Materialien und Energie

Fine-tuning of the sample orientation for neutron scattering experiments can become difficult at low temperatures and high magnetic fields. The problem arises specially when the magnet or cryostat in use can not be mounted on a cradle. This is the case for the high field magnets for fields up to 15T that are available at the Berlin Neutron Scattering Center (BENSC) at the Helmholtz Institute Berlin for Materials and Energy (formerly Hahn-Meitner Institute). To solve this problem an in-situ orientation of the sample sitting at the end of the sample stick is needed. This problem has been approached by the use of piezo driven goniometers [1]. These goniometers are equipped with resistive encoders so that the exact position of the sample can be monitored. An even more challenging problem is the use of the piezo driven goniometers in a dilution stick. The goniometers provide the great advantage of having a precise control over the orientation of the sample.

[1] attocube systems (www.attocube.com)

M-13 Das neue Flat-Cone-Diffraktometer E2

Jens-Uwe Hoffmann¹, Jörg Ihringer², Frank Schreiber²

¹Helmholtz-Zentrum Berlin (Abt. SF2)

²Universität Tübingen

Das neue Flat-Cone Diffraktometer E2 am Forschungsreaktor BER II des Helmholtz-Zentrum Berlin (HZB) hat einen Betrieb mit vier 30cm x 30cm Flächendetektoren aufgenommen. Es kann in zwei Positionen der Detektorbank ein 2θ von 80° und einer vertikal ist der Öffnungswinkel von 10° abgedeckt werden. Die Pixelgröße beträgt 0.1° . Der Detektor lässt sich in der Flat-Cone-Geometrie auf 20° anheben, so dass ein großer Bereich im reziproken Raum aufgenommen werden kann. Mit einer Minimierung des Neutronenuntergrundes und den großen Detektoren ist es für die Untersuchung von diffusen Streuerverteilungen optimiert.

Es wird erstmals am HZB das internationale NeXus Format zur Speicherung und Weitergabe der Daten verwendet. Damit verbunden ist auch die Entwicklung von neuer Software zur Analyse der Daten.

Der Umbau erfolgt mit der finanziellen Unterstützung des BMBF in Zusammenarbeit von der Universität Tübingen und dem Helmholtz-Zentrum Berlin.

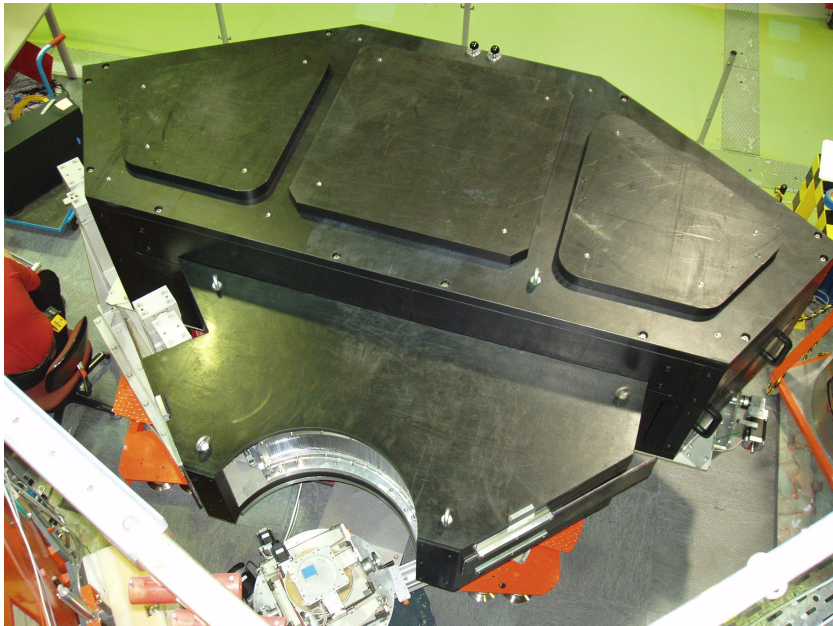


Figure 13.3: Ansicht auf das Flat-Cone-Diffraktometer E2 von oben.

M-14 Status of the new small-angle scattering instrument SANS-1 at the FRM II

Ralph Gilles¹, Andreas Ostermann¹, Werner Hornauer¹, Bernhard Krimmer¹, P. Klaus Pranzas², Andreas Schreyer², Winfried Petry¹

¹FRM II ZWE

²GKSS

A new small-angle scattering instrument SANS-1 will be installed on beam line NL 4a at the Heinz Maier-Leibnitz Forschungsneutronenquelle (FRM II). It is a joint venture of the TU München and the Geesthacht Neutron Facility (GENF). SANS-1 is optimised in a way to be one of the most intense and versatile small-angle scattering instruments. Using the program McStas the dimensions and the features of the different optical components were investigated and compared for the final selection. A vertical S-shaped neutron guide, a tower with two possible selectors, one for medium resolution at high intensity and one for high resolution and two optimised transmission polarizers are the main advantages in comparison to traditional instruments at other facilities. An additional feature will be the integration of a second detector in the detector vessel. This detector is positioned on a movable carriage and can be positioned similar as the first detector in the detector vessel. The translation sideways of the first 1m² detector allows to measure a wide angle range simultaneously with the second detector.

At the moment the collimation set up will be installed including two transmission polarizers, the slit system and the electronic for controlling the optics. Thirteen movable tables allow to combine different configurations of the collimation. The horizontal arrangement of all optical components make it possible to implement a chopper system later. A laser system is foreseen to check the positions of the different selected components of the optics.

1.) Gilles R., Ostermann A., Petry W., J. Appl. Cryst. (2007), 40, s428.

2.) Gilles R., Ostermann, A., Schanzer, C., Krimmer, B. & Petry, W. (2006). Physica B, 385-386, 1174.

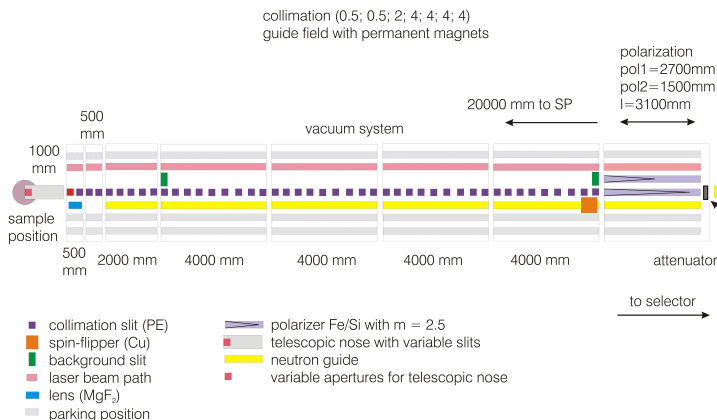


Figure 13.4: Figure 1: Schematic concept of the collimation system including a variety of optical components.

M-15 MARIA; the new reflectometer of the JCNS dedicated to magnetism and nano science

Stefan Mattauch¹, Ulrich Rücker¹, Denis Korolkov¹, Alexander Ioffe¹, Thomas Brückel¹

¹IFF

At the outstation of the Jülich Centre for Neutron Science (JCNS) at FRM II, a new reflectometer MARIA (Magnetism Reflectometer with high Incident Angle) is being built.

It is designed for investigations of thin magnetic layered structures down to the mono layer scale (optimised for layer thicknesses between 3-300 Å) with optional lateral structures of nm to μm size. Consequently the instrument is optimised for small sample sizes up to 1x1cm² and has polarisation analysis as standard. Beside the reflectometer mode with vertically focused beam and good resolution in the horizontal scattering plane, MARIA will be able to measure in the GISANS (Grazing Incidence Small Angle Neutron Scattering) mode with additional resolution in the vertical direction. The latter mode allows one to resolve lateral structures down to the nm scale. In this way MARIA is a strongly improved and extended successor of the former HADAS reflectometer at the research reactor DIDO in Jülich.

Unique features of MARIA include (i) vertical focussing with an elliptic guide from 170 mm down to 10 mm at the sample position, (ii) reflectometer and GISANS mode, (iii) polarization analysis over a large 2d position sensitive detector as standard, (iv) adjustable wavelength spread from 10 to 1 % by a combination of velocity selector and chopper, (v) flexible sample table using a Hexapod for magnetic field and low temperature sample environment and (vi) in-situ sample preparation facilities.

According to our simulations with the VITESS suite in combination with specialized programs, we expect a high polarised flux of $\approx 7 \cdot 10^7$ n/(s*cm²) at 3mrad collimation. We will therefore be able to attack challenging problems in systems such as ultrathin magnetic layers down to the monolayer regime, laterally patterned thin films, molecular magnets deposited on a substrate, remagnetization kinematics down to 10 μs time windows etc.

In this contribution we will report on the design features, the simulated performance and the scientific case of this unique instrument.

M-16 Minimisation of spurious strains by using a Si bent-perfect-crystal monochromator in residual strain scanning at the surface

Joana Rebelo Kornmeier¹, Jens Gibmeier², Michael Hofmann³

¹Hahn-Meitner-Institute, Glienicke Strasse 100, D-14109 Berlin Wannsee

²Institut für Werkstoffkunde I, Univ. Karlsruhe (TH)

³FRM-II, TU München, Lichtenbergstr. 1,85747 Garching

In order to tap the full optimisation potential for technical parts the residual stress distribution in the near surface region is of major interest for engineering work. The knowledge of the stress distribution is a necessary prerequisite to exactly tailor near surface layers of highly loaded technical components.

The most frequently applied tools for residual stress and strain analysis are the diffraction methods. Neutron radiation, provides information up to depths of several millimetres non-destructively. However, when scanning a sample surface, aberration peak shifts causing spurious strains arise due the fact that the gauge volume defined by the primary and secondary apertures is partially out of the sample.

In this study it will be demonstrated that, by optimising the horizontal bending radius of a Si (400) monochromator, the spurious surface strains can be reduced when compared to the values obtained with traditional mosaic monochromators, even when the gauge volume is mainly out of the sample surface. The spurious strain values after optimisation are in the order of 100 microstrain, which is usually tolerable for reliable residual strain analyses in most technological materials. The experiments were carried out at the STRESS-SPEC instrument at the research reactor FRM II, Munich, using a stress free steel sample of a fine grained construction steel, S690QL.

M-17 Neutron optics from Helmholtz-Zentrum Berlin (former HMI)

Thomas Krist¹, Anke Teichert¹, Jan Hoffmann¹, Roland Bartmann¹

¹Helmholtz-Zentrum Berlin

In the last years a variety of new neutron optical devices have been developed at our institute.

We show results of solid state polarising benders, solid state collimators with absorbing and with reflecting walls and a solid state radial bender for the polarisation analysis of neutrons over an angular range of 3.8 deg. A solid state device which has no classical analogue is a solid state polarising bender used in transmission together with a collimator where the polarised neutrons are not deflected from their original direction.

Two-dimensional polarisation analysers for an angular range of 5 degrees in both directions are presented.

Recent results for a polarizing cavity for wavelengths above 0.25nm are shown. In all polarizing devices polarisations around 95% were realised. Finally results from a focusing solid state lens with a gain factor of 5 will be shown.

The work was partly supported by the EU initiative NMI3 under contract no. RII3-CT-203-505925.

M-18 Upgrade of FLEX: Future Perspectives for a New Cold Three-Axis Spectrometer at BENS

Klaus Habicht¹, Markos Skoulatos¹, Leo Cussen¹

¹Helmholtz-Zentrum Berlin

After more than 15 years of successful operation providing high-standard user service with extreme sample environment, the cold neutron three-axis spectrometer V2/FLEX at BENS, Berlin will undergo a major upgrade in the near future. The core goals for the FLEX upgrade can be stated as increasing available neutron flux at the sample position while keeping low background and thus a good signal-to-background ratio, extending performance to shorter incident wavelengths and improving polarized neutron capabilities. Most important in this respect is to design a primary spectrometer which is flexible enough to adopt for different experimental resolution requirements. This flexibility is required since the instrument configuration to be chosen depends crucially on details of the particular physical problem under investigation. In other words there is no universal and generally accepted quality factor for three-axis spectrometer performance while we see an increasing number of instruments for elastic neutron scattering participating in round-robin campaigns. Perspectives to define standard TAS samples will be discussed.

An essential part of the envisaged upgrade project will be the complete renewal of the neutron guide system. Increasing the phase space volume will be realized by replacing the ⁵⁸Ni coatings by state-of-the-art $m=3$ supermirror coatings and using a double-focussing monochromator with increased mosaicity. This will only be possible by moving the instrument to a guide end position. Analysis of the user demands at FLEX shows that there is need to extend the available flux towards the thermal neutron region. The future design of the neutron guide will push the energy transfer range from currently 8 meV beyond 20 meV.

It is expected that at continuous neutron sources more weight will be on polarized neutron work in the future. FLEX currently offers two major options for polarized neutron work, the standard XYZ-polarization analysis option and the neutron resonance spin-echo option. Both instrument options will greatly benefit from increasing polarized neutron flux by advanced neutron optics in the primary beam path. We will report on results of recent simulation work using both, the VITESS and McStas Monte Carlo simulation packages. Further perspectives for a new secondary spectrometer option will also be discussed.



Figure 13.5: The Cold Three-Axis Spectrometer V2/FLEX at BENS, Berlin

M-19 Optimization of the NEAT neutron guide using genetic algorithms.

Zunbeltz Izaola¹, Margarita Russina¹

¹Helmholtz Zentrum Berlin

The majority of the instruments of the cold neutron source in the Helmholtz Zentrum Berlin will be upgraded in the next years following the change of the cold source. The cold neutron and direct geometry time of flight spectrometer NEAT[1] is part of this upgrade plan.

The guide will use the full height and width allowed by the extraction system and Nickel coated guides will be replaced with supermirrors. In this contribution the concept of the new system and the details of the calculations are discussed. The results show expected intensity gain by factor of 5. The Monte Carlo simulations has been carried out using the program Vitess[2] complemented by the genetic algorithms approach[3] to find a configuration with a maximum integrated intensity transmission.

[1] First QINS results from the TOF-spectrometer NEAT. R.E. Lechner, R. Melzer, J. Fitter. *Physica B* 226 (1996) 86-91

[2] Monte Carlo simulations of neutron scattering instruments by VITESS: Virtual instrumentation tool for ESS. G. Zsigmond, K. Lieutenant, F. Mezei, *Neutron news* 13 (2002) 11-14

[3] Instrument Design and Optimisation Using Genetic Algorithms. R. Hoelzel, P. M. Bentley, P. Fouquet, *Rev. Sci. Inst.* 77 (2006), 105107

M-20 Unconventional Single Crystal Diffraction Studies with hot Neutrons on HEiDi at FRM II

Martin Meven¹

¹FRM II

The instrument HEiDi at the neutron source Heinz Maier-Leibnitz (FRM II) uses hot neutrons for single crystal diffraction analysis of structural and magnetic properties of samples for which other methods are not applicable.

The hot topic of multiferroic compounds like REMnO₃ (RE=Dy, Gd) whose highly absorbing and heavy rare earth elements make it normally extremely difficult to get accurate structural and magnetic diffraction data is a good example for the unique capabilities of this instrument using both large penetration depth and large q range [1].

This contribution will give an overview of the instrument (like the gain factor from the hot source, see figure and [2]) and its applications in different fields of solid state physics, chemistry and crystallography concerning structural details (highly accurate atomic positions and anisotropic mean square displacements, phase transitions, local disorder, magnetism, etc.).

[1] Magnetic Structure of GdMnO₃. A. Möchel; J. Voigt; M. Meven, J.-W. Kim; and T. Brückel; Verhandlungen der Deutschen Physikalischen Gesellschaft, R. 6, Bd. 43, MA 29.2 (2008).

[2] HEiDi: Single Crystal Diffractometer at the Hot Source of the FRM II; Meven M., Hutanu, V.; Heger, G.; Neutron News 18, 19-21 (2007).

M-21 Continuous Pole Figure Measurements as standard Method to analyse ODF at the Materials Science Diffractometer STRESS-SPEC

Christian Randau¹, Ulf Garbe², H.-G. Brokmeier¹

¹IWW TU-C

²Bragg Institute ANSTO

The Materials Science Diffractometer STRESS-SPEC at the FRM II, is designed to be applied for phase specific texture analysis with neutron radiation by diffraction methods.

One of the mainly used techniques to determine pole figures with neutron radiation is based on a measurement with a single detector and a mesh of discrete chi and phi positions. The standard step size of this measuring method is $5^\circ \times 5^\circ$ in chi and phi. One disadvantage of this method is the discretisation of phi and chi. The positioning time for reaching discrete phi and chi rotations reduces the useable effective measuring time. In addition for small pole figure windows the discretisation results in a small grain statistic. This is a problem especially for sharp textured samples. The discretisation can be abolished in the chi direction with an area detector allowing the detection of a bigger chi angle range. Whereas, area detectors are already used in neutron texture experiments the phi rotation has still discrete values. This discretisation can be abolished with continuous phi rotation. The combination of an area detector and the continuous phi rotation allows reducing the measuring time up to 35% and guaranteed a better grain statistic. In addition the pole figures can be determined with another grid resolution after the measurement. In this feature, however, the statistic is reduced. In this contribution we will present new results describing advantages of continuous pole figure measurements at STRESS-SPEC.

M-22 Going Ultra: How we can increase the length scales studied

Melissa Sharp¹, P. Klaus Pranzas¹

¹Institut für Werkstoffforschung

Small-angle neutron scattering has proved a popular technique over the years to investigate a variety of problems in soft matter and materials science. The length-scales probed by this technique (from a few nanometres up to a couple of hundred of nanometres) is ideal for many systems. Systems studied using this technique include nanoparticles, emulsions, micelles, alloys, as well as many other problems within polymer and materials science. However, there are a number of problems where the length-scale of interest is larger. In order to study such systems it is possible to combine small-angle neutron scattering (SANS) with ultra-small-angle neutron scattering (USANS). This allows the study of materials on the length-scale of a few nanometres up to more than 20 micron. At the Geesthacht Neutron Facility (GeNF) USANS measurements can be carried out using a double crystal diffractometer (DCD). The instrument and data reduction allows for both the de-smearing of the data as well as the removal of multiple scattering effects. In addition it is possible to calibrate the data to be on an absolute scale. It is thus possible to combine the data from this instrument with that of the SANS-2 instrument at GeNF to achieve a combined scattering curve with a good overlap from the two instruments.

One example where SANS and USANS have been combined is in the study of metal hydrides, which may be used in hydrogen storage applications. The microstructure of the metal hydrides as hydrogen is absorbed and desorbed was studied in this way. Another example is the study of block copolymers, which are widely used in industrial applications. While SANS was able to show the structure formed by such copolymers on the nanometre scale, USANS allowed for the investigation of the long-range ordered structure on the micrometre scale.

M-23 Structure Powder Diffractometer SPODI: examples of in-situ materials characterisation

Markus Hölzel¹, Anatoliy Senyshyn¹, Norbert Jünke², Hans Boysen³, Wolfgang Schmahl³, Helmut Ehrenberg⁴, Hartmut Fieß¹

¹TU Darmstadt

²Universität Göttingen

³LMU München

⁴IFW Dresden

The powder diffractometer SPODI (FRM II) offers high resolution diffraction under various environmental conditions. In this contribution examples of experiments, the status of the in-situ investigation methods and instrumental upgrades are presented. The experimental examples demonstrate specific applications of SPODI to investigate structural parameters of technologically important materials and their relation to the materials properties.

The instrument is equipped with position-sensitive 3 He detectors of 300 mm active height covering an angular range of 160°. The two-dimensional data are treated by a sophisticated data evaluation procedure to obtain diffraction patterns with excellent profile shape. The sample environment includes a cryostat, a furnace, a tensile rig, an apparatus for gas loading and a device for charging/discharging of Li-batteries.

The tensile rig was applied to study stress-induced lattice deformations, texture evolution and phase transformations in Ni-Ti shape memory alloys and superelastic alloys. The texture development of shape memory alloys at different strain levels could be related to corresponding twinning/detwinning processes.

Measurements on hydrogen storage materials, such as sodium alanates with different doping elements, as well as metal organic frameworks have been performed for structure refinement and phase analysis. Recently, an apparatus for deuterium loading has been set into operation which can be used in combination with the closed-cycle refrigerator to follow structural changes as function of temperature and deuterium pressure. Studies on the lithium battery material Li_xCoPO_4 ($0 < x < 1$)

revealed the structural changes as a function of the Li-content. The data analysis allowed to refine phase compositions, Li occupation numbers and magnetic moments. First experiments on a lithium battery in operation were carried out recently.

M-24 Focusing in q-space for angular dispersive neutron powder diffraction using an adjustable inpile fan collimator

Norbert Stüßer¹, Alexandra Buchsteiner¹

¹Helmholtz-Zentrum Berlin

To fulfil the needs of a high quality data set for crystal structure refinement a powder diffractometer should maximize intensity and simultaneously adapt the resolution to the requirements determined by the angular dependent reflection density. In addition a well defined profile shape is highly desirable.

At BENSCH the medium resolution powder diffractometer E6 has been equipped with an adjustable fan collimator in the inpile position. This fan collimator allows the setting of the lamella openings at both ends independently. In combination with a horizontally curved monochromator the fan controls the resolution width of reflections. Focusing in q is, however, achieved in a limited angular range. For the collection of a diffraction pattern by a detector with limited detection angle in a larger angular range the focusing has to be adjusted continuously to the detector position. In this focusing mode the signal to noise ratio becomes maximized. This mode allows also the illumination of large monochromators which focus the neutrons to the sample and set up the appropriate correlation between the ray direction and the wavelength.

Here we present the performance of such a type of powder diffractometer and compare it with a standard powder machine mainly using Soller collimators. This is demonstrated by a refinement at powder specimen of PbSO_4 . Monte Carlo simulation data are in very good agreement with the experimental observations and allow further optimization and upgrades of the instrument.

M-25 New Perspectives for IN12

Wolfgang Schmidt¹, Karin Schmalz¹

¹Forschungszentrum Jülich, JCNS@ILL

The IN12 spectrometer is operated as a CRG-instrument by Forschungszentrum Jülich within the JCNS framework in collaboration with CEA Grenoble at the Institute Laue Langevin in Grenoble. As a three-axis spectrometer for cold neutrons it is dedicated for high-resolution studies of low-energy excitations.

In the near future new features and changes will be realized at IN12 that concern both the primary and secondary spectrometer:

First, IN12 is currently being upgraded with a multi-analyser option. IN12 will then be equipped with a 2-dimensional position sensitive detector and an array of fifteen analysers which can be rotated and positioned individually in order to map the scattered beam on a user-chosen path in Q - ω -space. We refer to this set-up as IN12-UFO (Universal Focusing Option). This new set-up will show an innovative flexibility that has not been realized so far elsewhere.

Second, within the ILL Millenium program concerning the re-organisation, re-siting and new constructions of various instruments also the spectrometer IN12 will be moved to a new position in the neutron guide hall of ILL. This implies the construction of a completely new guide of 90m length that is solely used by IN12. Therefore IN12 will then be placed at an end position on a modern guide that can now be optimized for the best achievable flux and energy resolution on IN12 without restrictions to other instruments. This scenario provides a unique chance to upgrade the primary spectrometer of IN12 to the possible technical limits concerning flexibility, wavelength range and flux.

In this presentation we will show the progress in the implementation of IN12-UFO and also preliminary results for possible solutions and options in the guide geometry, polarization and focussing techniques for the planned new position of IN12 in the ILL guide hall.

M-26 J-NSE: The Jülich Neutron Spin-Echo Spectrometer at the FRM II

Olaf Holderer¹, Nikolas Arend¹, Nicolas R. de Souza¹, Michael Monkenbusch¹, Dieter Richter¹

¹JCNS

Neutron spin echo (NSE) spectroscopy is due to its high energy resolution a well-suited method for studying slow dynamics, such as the dynamics of soft matter systems (glasses, polymers and complex liquids), or paramagnetic properties of e.g. spin glasses.

After the relocation from the FRJ-2 to the new FRM II reactor, the Jülich Neutron Spin-Echo Spectrometer J-NSE recommenced operation in 2007 and is accessible for external users since.

The spectrometer is positioned at the end of a neutron guide, giving access to a broad band of incident wavelengths between 4.5 and 19 Å. This, together with new correction elements in the two main precession coils, results in a significant increase in dynamic range.

The high incident flux of polarized neutrons provided by the neutron guide system leads to a gain in intensity compared to the setup in Jülich of a factor of ≈ 15 for the same wavelength of 8 Å as in Jülich.

A paramagnetic setup has been installed which allows separating magnetic and nuclear scattering in paramagnetic experiments.

We will present the new characteristics of the instrument and first experiments in different fields of physics carried out at J-NSE spectrometer.

M-27 Some applications of the multi-purpose REFSANS reflectometer

Jean-Francois Moulin¹, Reinhard Kampmann¹, Martin Haese-Seiller¹

¹GKSS-Forschungszentrum

Grazing Incidence Scattering techniques are well known to provide access to structural information relative to thin films and interfaces. By probing into different direction of the reciprocal space one gets knowledge of both the in-plane and the out of plane correlations in the sample under investigation. One of the main advantages of these techniques are the fact that they provide a signal averaged over a broad area rather than a very local one as obtained from microscopies, thus insuring that the main features of a sample are discovered and their relative importance properly evaluated.

When using neutrons as a probe (GISANS), one gains the opportunity to play with isotopic contrast variations to reveal features normally inaccessible to X-rays. Moreover the depth of penetration of the neutrons being very large, one can easily probe buried layers or work in solutions.

The instrument REFSANS based at the FRM2 neutron source in Garching (Munich) is a multipurpose reflectometer which offers the opportunity to measure both in GISANS and conventional reflectometry configurations. This instrument operates in time of flight mode (TOF), thereby enabling to record large ranges of the q space using a single angle of incidence. This mode of operation is extremely useful to characterize complex samples for which the composition and surface structure are not well known a priori.

We will here present some recent results obtained during the characterization of various systems (ranging from polymeric systems to metallic nanostructures) using TOF GISANS and TOF reflectometry, these examples will show the potentials of these methods and of the REFSANS instrument in particular.

M-28 The new polarizer at RESEDA - simulation and first experimental results

Wolfgang Häussler¹, Andreas Ostermann¹, Mathias Sandhofer², Peter Böni²

¹FRM II, Technische Universität Muenchen

²E21, Technische Universität Muenchen

RESEDA is a Resonance Spin Echo spectrometer at the FRM II using cold neutrons. The Resonance Spin Echo technique relies on the use of a polarized neutron beam. In order to reach sufficiently high polarization in the neutron wavelength range 5-8 Å, a new polarizing cavity has been installed at the end of the neutron guide NL5 of RESEDA.

We present simulation results of the expected polarization at the sample position of RESEDA taking into account the peculiarities of the neutron optical elements from the cold neutron source to the instrument, and show first experimental results.

M-29 Polarized ^3He for neutron instrumentation

Sergey Masalovich¹

¹FRM II

Polarized nuclei of helium-3 possess very high spin-dependent neutron absorption efficiency over a wide range of neutron energy. Neutron spin filters (NSF) based on a dense hyperpolarized ^3He gas may compete in polarization efficiency with such common devices as magnetized single crystals, supermirrors or soler guides. Although these latter methods are rather simple in operation, their applications are strongly limited by acceptable neutron energy and scattering angle range. By contrast, the broadband neutron spin filter can be sized and shaped in such a way that it will meet just about all practical needs.

M-30 Development of high m supermirrors

Roxana Valicu¹, Robert Iannucci¹, Gunther Borchert¹

¹FRM II

Supermirrors are important components of neutron guides used for performing neutron scattering experiments far from the reactor core to the instruments, where the background is low enough to permit measurements of even weak signals.

We will present the methods used at our facility to produce large area, high quality supermirrors, the trials that we have made to increase the performances of such supermirrors and the results confirmed by neutron reflectivity measurements.

Using the Hayter and Mook algorithm we have simulated sequences with increasing number of Ni and Ti layers and using the parameters from the simulations we have achieved a neutron reflectivity of around 84% for an m value equal to 3.

The next step in improving our facility was to develop the reactive sputtering process (by using Nitrogen as sputter gas together with Argon) in order to achieve the deposition and the stability of more layers and therefore of higher m-values.

X-ray and neutron reflectivity measurements as well as X-ray diffraction and profilometry for the stress analysis were performed in order to determine the optimized parameters for the sputtering of Ni. As a consequence we have produced supermirrors with higher m values that could not be achieved without the reactive sputtering of Ni. Neutron reflectivity measurements for the produced supermirrors show promising results.

M-31 Monte Carlo simulations for focusing elliptical guides

Roxana Valicu¹, Peter Böni²

¹FRM II

²E21

The aim of the Monte Carlo simulations using the McStas program was to improve the focusing of the neutron beam existing at PGAA (FRM II) by prolongation of the existing elliptic guide that is presently coated with supermirrors $m = 3$. First we have added an additional guide with an initial length of 75 mm and supermirror coatings with $m = 4, 5$ and 6. The gain (calculated by dividing the intensity in the focal point after adding the guide by the intensity at the focal point with the initial guide) obtained for these coatings indicated that a coating with $m = 5$ would be appropriate for the next simulation. The next step was to vary the length of the additional guide for $m = 5$ and therefore choosing the appropriate length for the maximal gain. With the m -value and the length of the guide fixed, we have introduced an aperture at a position 10 mm before the focal point and have varied the radius of this aperture in order to obtain a focused beam. We have observed a dramatic decrease in the size of the beam in the focal point after introducing this aperture. The simulation results, the gains obtained, their variation with the length of the guide and with λ as well as the evolution of the beam size will be presented.

M-32 Recent Advances in Neutron Holography: Resolving Atomic Positions with Picometer Accuracy

Manfred Prem¹, **Laszlo Cser**², **Gerhard Krexner**¹, **Marton Markó**², **Ivan Sharkov**³, **Gyula Török**²

¹Faculty of Physics, University of Vienna, Boltzmanngasse 5, A-1090 Wien

²Research Institute for Solid State Physics and Optics, H1525 Budapest P.O.Box 49, Hungary

³St. Petersburg State University, Institute of Physics, Chair of Optics and Spectroscopy, Ulyanovskaja str.1, 198904 St.Petersburg, Russia

Neutron holography constitutes a novel technique to obtain structural information on an atomic scale [1]. It is based on the recording of the interference of neutron waves coherently scattered by atomic nuclei with an appropriate reference wave. The method can be implemented by using appropriate holographic probe nuclei which can either, due to their strong incoherent scattering, serve as internal neutron sources or, due to their high absorption cross section, serve as internal neutron detectors. Several successful experiments [2,3,4] applying both of these approaches have been performed over the last years and have confirmed the underlying physical concepts. More recently, it could be demonstrated that the method is capable to determine the atomic positions within several neighbor shells around holographic probe nuclei with a precision approaching one picometer thus allowing for the quantitative determination of lattice distortions [5]. It is expected that use of the technique can be considerably extended due to the availability of a significant number of elements/isotopes which appear well suited to serve as holographic probes. A particular promise lies in the investigation of substances containing hydrogen. We discuss the current status of neutron holography, its present technical limitations, and perspectives of possible applications.

[1] Atomic-Resolution Neutron Holography, L.Cser, G.Krexner, and Gy.Török, Europhysics Letters 54 (2001) 747

[2] Atomic structure holography using thermal neutrons, B. Sur, R.B. Rogge, R.P. Hammond, V.N.P. Anghel, J. Katsaras, Nature 414 (2001) 525

[3] Holographic Imaging of Atoms Using Thermal Neutrons, L. Cser, Gy. Török, G. Krexner, I. Sharkov, and B. Faragó, Phys.Rev.Lett.89 (2002) 175504

[4] Neutron holographic study of palladium hydride, L. Cser, Gy. Török, G. Krexner, M.Prem, and I. Sharkov, Appl.Phys.Lett. 85 (2004) 1149

[5] Direct Observation of Local Distortion of a Crystal Lattice with Picometer Accuracy Using Atomic Resolution Neutron Holography, L. Cser, G. Krexner, M. Markó, I. Sharkov, Gy. Török, Phys.Rev.Lett. 97 (2006) 255501

M-33 The planned single crystal diffractometer for biological macromolecules at the FRM II

Andreas Ostermann¹, Michael Monkenbusch², Dieter Richter², Winfried Petry¹

¹Forschungsneutronenquelle Heinz Maier-Leibnitz

²Forschungszentrum Jülich

The Forschungszentrum Juelich (JCNS) in collaboration with the Forschungsneutronenquelle Heinz Maier-Leibnitz (FRM II) and will construct and build a monochromatic single crystal diffractometer dedicated to the structure determination of biological macromolecules. The diffractometer will be installed at the FRM II at the cold guide NL1 in 32.5m distance from the cold source. Using monochromatic neutrons diffractometer will be able to operate in the wavelength range of 2.4 Å to about 4 Å. At the first stage a flat highly oriented pyrolytic graphite monochromator will be used. Higher order wavelength contaminations will be blocked by a neutron velocity selector. To cover a large solid angle the detector of the diffractometer consists of a neutron imaging plate in a cylindrical geometry. A Li/ZnS scintillator CCD camera is foreseen for crystal adjustment and additional detection abilities. The main advantage of this instrument is the possibility to adapt the wavelength to the size of the unit cell of the sample crystal while operating with a monochromatic beam that keeps the background level low.

M-34 TOF spectrometer NEAT: new capabilities and perspectives

Margarita Russina¹, Zunbeltz Izaola¹, Nikolaous Tsapatsaris¹, Ferenc Mezei²

¹Helmholtz Zentrum Berlin

²Los Alamos National Laboratory

The time-of-flight (TOF) spectrometer NEAT at HMI started operation in 1995 and it was best suited to study of a wide variety of phenomena on the time scale between atomic and macroscopic. At that time it was one of the cold neutron 2 -3 chopper spectrometers in the world with the highest data collection rates in a wide range of resolution. Results of experiments by a broad external and in-house user community have been published in more than 100 papers, incl. high impact journals. The subjects cover many subjects, e.g. magnetism, material transport phenomena, glassy behavior, rotational and translational diffusion, surface binding, protein dynamics etc.

In the last years TOF neutron spectroscopy engaged in a fast evolution worldwide. New developments (including both enhanced source power and advanced instrument concepts) promise tremendous progress of performance both at pulsed and continuous neutron sources. To maintain the competitive edge of NEAT we have undertaken a number of developments. On the long run the up-grade of the whole instrument using new, state-of-the-art components (such as supermirror guides and position sensitive detectors) is the solution of choice and a gain potential in data collection rate of a factor exceeding 40 has been identified. On the short run, by the systematic use of broader chopper slits with trapezoidal pulse shapes – when the resolution requirements permit – we could enhance the beam intensity on the sample by over a factor of 2 compared with the usual approach of just slowing down the choppers to gain intensity by relaxing the resolution. Another focus of the improvements was to extend the sample environment capabilities to less readily available conditions at TOF spectrometers. In situ irradiation of the sample with laser light, high magnetic fields up to 5 T and high hydrostatic pressures (soon up to 10 kbar also for the study of inflammable matter like hydrogen) have been implemented and made available for users. A selection of examples of experiments making use of these new opportunities as well the details of the upgrade project will be presented.

M-35 First PGAI/NT experiments at the FRM II for the Ancient Charm project

Ralf Schulze¹, Petra Kudejova¹, Lea Canella², Jan Jolie¹, Andreas Türler², Zoltan Kis³, Laszlo Szentmiklosi³, Tamas Belgya³

¹Institut für Kernphysik, Univ. zu Köln

²Institut für Radiochemie, Technische Universität München

³Institute of Isotopes, Hungarian Academy of Sciences

Using neutrons for analysis of small archaeological or other valuable objects has many advantages compared to chemical methods: the analysis is non-invasive, neutrons can penetrate the entire volume and the objects can be measured without any chemical preparation. According to the neutron technique used, information about the sample structure, elemental and phase composition or about the fabrication technique can be achieved. The three years long joint EU project called Ancient Charm combines these techniques and aims to develop 3D imaging of the complex objects - a position sensitive upgrade of the well-established techniques [1]. Among these are listed: Prompt Gamma-Ray Activation Analysis (PGAA) combined with Neutron Tomography (NT), Time of Flight Neutron Diffraction (TOF-ND) and Neutron Resonance Capture Analysis (NRCA).

The Cologne group with the PGAA instrument at the new research reactor FRM II is involved in the task of 3D imaging of chemical composition of the archaeological objects, so called PGAI imaging combined with Neutron Tomography (PGAI/NT). The first tests with the PGAI set-up were performed at the running PGAA station at the Budapest Research Reactor [2]. Since the intensity of the neutron flux there is very low (5×10^7 n/cm²s thermal neutron flux equivalent), only 2D maps of the objects could be visualised.

We will continue in the task at FRM II and make first true 3D maps of the elemental distribution in the objects, since the neutron flux can be up to 1000 times higher here than at Budapest and the PGAI measurements involving scanning the sample point by point can be finished in real time scale [3]. Our aim is to reach 1mm³ precision. The first test measurements at FRM II have started in June 2008 and we will report about the results and cold neutron beam characteristics. Starting September 2008, six valuable museum objects from Rome, Milan and Budapest will arrive for the final PGAI/NT analysis.

[1] G.Gorini for the Ancient Charm collaboration, Ancient Charm: A research project for neutron-based investigation of cultural-heritage objects, *Il Nuovo Cimento*, 30 C, N.1, (2007) 47

[2] T. Belgya, Z. Kis, L. Szentmiklós, Zs. Kasztovszky, P. Kudejova, R. Schulze, T. Materna, G. Festa, P.A. Caroppi, the Ancient Charm Collaboration; First elemental imaging experiments on a combined PGAI and NT setup at the Budapest research reactor, *MTAA12 proceedings*, (2008), JRNC in press

[3] P. Kudejova, G. Meierhofer, K. Zeitelhack, J. Jolie, R. Schulze, A. Türler, T. Materna, The new PGAA and PGAI facility at the research reactor FRM II in Garching near Munich, JRNC in press

M-36 Statistical Chopper method to separate elastic and inelastic scattered neutrons in TOF-experiments

Julius Schneider¹, Wolfgang Schmahl¹

¹Department of Earth- and Environmental Sciences

A method to make use of the white reactor spectrum, producing a linear TOF-scan in reciprocal space, with a simple TOF-separation of elastic and inelastic scattered neutrons has been proposed by P. Pellionisz [1]. It combines a classical single slit chopper TOF-system with a second, pseudostatistical chopper in front of the sample. The latter produces two qualitatively distinct TOF-regions at detector level: A time pattern of purely inelastic scattered neutrons (shade) and a complementary time pattern of elastic and inelastic scattered neutrons (light). A continuous or random phase shift between both choppers allows to scan the entire TOF-domain.

The system is realized by sorting the scattered neutrons into two separate multi-channel analysers by a timewise stretched digital image of the open-close sequence (light/shadow) of the statistical chopper. They contain the TOF-diagrams of the purely inelastic and the elastic plus inelastic scattered events. No calculation of any cross-correlation is needed, as this is done automatically by the phase shift between the choppers. A simple difference calculation between these two TOF-diagrams then yields the required TOF-diagram of elastic scattered events.

The duty cycle (1%) of the first, conventional single slit chopper is reduced by the duty cycle of the pseudo-statistical chopper of 50% only. An extension of the method, replacing the first chopper by a pseudo-statistical chopper also (duty cycle 20%), was proposed by P. Pellionisz later [2]. Energy and Q-space resolution and TOF-focussing considerations were performed by J. Schneider [3], who also realized a test version of this system at the FRM-I reactor.

A combination of this method with a linear position sensitive detector (banana) would allow the concurrent measurement of two-dimensional sections in reciprocal space and the on-line monitoring of the integral inelastic, integral inelastic plus elastic and the elastic scattered intensity distributions simultaneously.

Recently at FRM-II developed high speed disc choppers or modern spin-flip techniques in combination with high flux reactors and various sample environments should make this proposed instrument interesting for the analysis of real crystals in many fields of material science.

Energy and Q-space resolution calculations of such a system as a possible add-on machine to the planned POWTEX diffractometer will be presented.

[1] Pellionisz P., Nucl. Instr. Meth. 92 (1971) 125

[2] Pellionisz P., Atomkernenergie 17 (1971) 277

[3] Schneider J., PhD-thesis, Technical University of Munich 1975

M-37 The experimental area MEPHISTO for particle physics in the new east hall

Jens Klenke¹, Hartmut Abele², Hans-Friedrich Wirth³

¹Technische Universität München, ZWE FRM II, Lichtenbergstraße 1, 85748 Garching

²Technische Universität München, Physik-Department E18, James-Franck Straße, 85748 Garching

³Technische Universität München, James-Franck Straße, 85748 Garching

Many studies of the properties of particles, their fundamental interactions and their symmetries are performed at lowest energies, by using cold neutrons. As these checks address important open questions of particle physics and cosmology, they need to be done as precisely as possible.

The MEPHISTO instrument at the FRM II is an experimental area for nuclear particle physics with cold neutrons (MEasuring facility for particle PHysics with cold neuTrons). Scientific teams build up instruments at the experimental area using MEPHISTO as an intense neutron source with a white neutron spectra. MEPHISTO is located at the end of NL1 in the neutron guide hall. The actual space for experiments in this experimental area is limited by other instruments. Therefore during the next year the MEPHISTO experimental area intend to move from the neutron guide hall into the newly erected "Osthalle" (s.c. east hall). MEPHISTO will be one of the first instruments in this hall. The demand of space for new experiments with cold neutrons leads to this solution. The authors present the actual results of monte-carlo simulations of the expected high flux and spectrum of different layouts of the guide.

The actual planned experimental area will use beam tube SR4b and a curved ($r=4000\text{m}$) neutron guide from the experimental hall into the east hall (length 56 m). The simulations show that the thermal neutron flux is in the range of $2 \text{ E}10 \text{ n/s cm}^2$ at a mean wavelength = 0.4 nm with a beam size of $6 \times 10 \text{ cm}^2$. The coating is expected to be greater than $m=2$.

M-38 Thales - The next generation cold three-axis spectrometer at the Institut Laue Langevin

Martin Boehm¹, Arno Hiess¹, Jiri Kulda¹, Stephane Roux¹

¹ILL

ThALES – Three Axis Low Energy Spectroscopy – is foreseen to replace the cold three-axis spectrometer (TAS) IN14 at the Institut Laue Langevin (ILL) Grenoble in the coming years [1,2]. Advances in neutron optics during the last decades allow enhancing considerably the performances of cold neutron TAS, permitting challenging investigations at low energy transfers such as study of the magnetization dynamics in strongly correlated electron systems, low-dimensional or frustrated magnets.

The scientific case of ThALES emphasizes four major features: (i) an overall increase of data collection rate by at least an order of magnitude maintaining ILL's leading role in cold TAS (ii) an efficient and easy-to-use neutron polarization analysis option, (iii) an extension of the incident neutron range to higher energies bridging the gap with thermal instruments, and (iv) use high-field cryomagnets under optimal conditions.

As an example representing typical future applications of ThALES we want to present the magnetic excitation spectra of the copper borate $\text{Cu}_3\text{B}_2\text{O}_6$ obtained on small single crystals with the present IN14 in combination with the multiplexed analyser-detector system FlatCone [3]. $\text{Cu}_3\text{B}_2\text{O}_6$ is considered as magnetic two-dimensional system without long range order [4], where distorted CuO_4 units presumably organise in magnetic clusters of $n=1,2$ and 4 units.

[1] Boehm M., Roux S., Hiess A., Kulda J., ThALES - towards the next generation cold neutron three-axis spectrometer. *J. of Magn. and Magn. Mat.* 310 (2007), e965-e967.

[2] Boehm M., Roux S., Hiess A., Kulda J., I. Saroun, ThALES – Three Axis Low Energy Spectroscopy at the Institut Laue Langevin. *Meas. Sci. Technol.* 19 (2008), 034024.

[3] M. Kempa, B. Janousova, J. Saroun, P. Flores, M. Boehm, F. Demmel, J. Kulda, The FlatCone multianalyzer setup for ILL's three-axis spectrometers. *Physica B* 385-86 (2006), p. 1080.

[4] [1] G.A. Petrakovskii et al., *Phys. Sol. State* 41 (1999), p.610.

M-39 A rotating and ramped spin turner for dynamical neutron polarization

Hartmut Lemmel¹, Gerald Badurek¹, Erwin Jericha¹

¹Atominstytut der Österreichischen Universitäten

The concept of dynamical neutron polarization should allow for a nearly loss-free polarization of thermal and in particular cold neutron beams. This method is based on a slight energy change of the incoming neutrons and a subsequent spin rotation in a magnetic precession field which takes differently for neutrons with opposite spin orientation. A key component in the technical realization is a final spin turner which stops Larmor rotation of the neutron spins at the position of complete polarization. We carried out a first experimental test with a prototype of such a spin turner and were able to demonstrate the operational capability of this neutron optical component in principle. We discuss the technical requirements for realization, present the experimental set-up and first experimental results which are characteristic of the functionality of the spin turner and support the practicability of our concept.

G. Badurek, C. Hartl, E. Jericha, Nucl. Instr. Meth. A 586 (2008) 95

M-40 POWTEX – The new High-Intensity Neutron TOF Diffractometer at FRM II

Andreas Houben¹, Werner Schweika², Jens Walter³, Harald Conrad², Helmut Klein³, Bernd Leiss³, Paul Müller¹, Heidrun Sowa³, Bent T. Hansen³, Thomas Brückel², Richard Dronskowski¹

¹Lehrstuhl für Festkörper- und Quantenchemie, Institut für Anorganische Chemie, RWTH Aachen University, D-52056 Aachen

²Institut für Festkörperforschung, Streumethoden, Forschungszentrum Jülich, D-52428 Jülich

³Geowissenschaftliches Zentrum der Universität Göttingen, D-37077 Göttingen

In order to provide the German and international chemistry, geo- and materials science communities with one of the most powerful tools for rapid neutron-data acquisition, the novel time-of-flight diffractometer POWTEX will be installed at the SR5 beam line at the new FRM II reactor in Munich. The construction of POWTEX, engineered and built by RWTH Aachen University, Forschungszentrum Jülich and Göttingen University, has recently been granted by the BMBF. Once finished, POWTEX will be part of the JCNS instrumentation pool and will thus profit from the well-established working conditions.

POWTEX is a shortcut for POWder and TEXture because POWTEX will fulfill the needs of the solid-state chemistry as well as the geo- and also part of the materials science communities. We expect to outperform comparable monochromator instruments by one order of magnitude in intensity ($> 3 \times 10^7$ neutrons/cm²s) for samples of less than a cubic centimeter. This extraordinary performance will be achieved by combining several new concepts. These are, namely, the ballistic beam compressor with horizontal and vertical focusing super-mirrors, the four-unit disk-chopper system, including the pulse double chopper, the use of position-sensitive detectors to access the full Debye-Scherrer cones by a huge solid angle (5.2 steradian) and, not to forget, the multiple measurements of all reflections using the time-of-flight strategy.

The high neutron current at the sample position will allow us, for example, to in-situ investigate chemical reactions and to characterize phase transitions as a function of temperature, pressure, magnetic fields (or other sample environments) in comparatively short measurement times. Geo- and materials sciences applications for this instrument are mainly related to texture measurements on natural samples and, additionally, to measurements during in-situ deformation and recrystallization/annealing experiments with special sample environments. The second geoscientific focus lies on parametric and kinetic powder-diffraction measurements. Besides the above-mentioned collaborators, POWTEX is supported by 16 institutes (22 groups) at different German universities and by the Technical University of Munich.

While POWTEX is under construction at the very moment, we expect to conduct the first measurements in the year 2012.

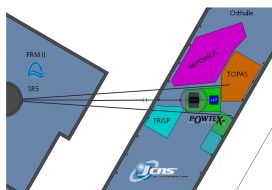


Figure 13.6: POWTEX will be installed at the SR5 beam line at the FRM II reactor in Munich. On the right, you can see the new JCNS east-building with the green area reserved for POWTEX.

14 Nuclear and particle physics

M-41 Studies of UCN production with a small deuterium test setup at the FRM2

Axel Reimer Müller¹, Erwin Gutmiedl¹, Stephan Paul¹, Andreas Frei¹, Rainer Stöpler¹, Christian Hesse¹, Hans-Friedrich Wirth¹, Daniele Tortorella¹, Leonardo Tassini², Denis Rich^{†3}

¹Technische Universität München, Physik Department E18, D-85747 Garching

²Walther Meißner Institut, Bayerische Akademie der Wissenschaften

³Technische Universität München, Forschungsneutronenquelle Heinz Maier-Leibitz (FRM II)

Solid deuterium is a favorite converter material for the production of ultra cold neutrons (UCN) in the next generation of UCN sources. In order to characterize the properties of solid deuterium and learn different freezing procedures (liquid->solid, gas->solid) the cubeD2 experiment was built. The main components of the setup and the optical results from different deuterium freezing will be shown. The influence of this freezing, temperature treatment and sample thickness on the UCN output was studied at the cold neutron beam Mephisto at the FRM2. After the experimental proof on the UCN nature of the detected events some data from the systematic parameter studies towards high UCN count rate are shown. Finally the new concept of the planned strong UCN source miniD2 for the FRM2 is extracted.

Support from the Deutsche Forschungsgemeinschaft, The cluster of excellence “Universe” and the MLL Maier Leibnitz Laboratory

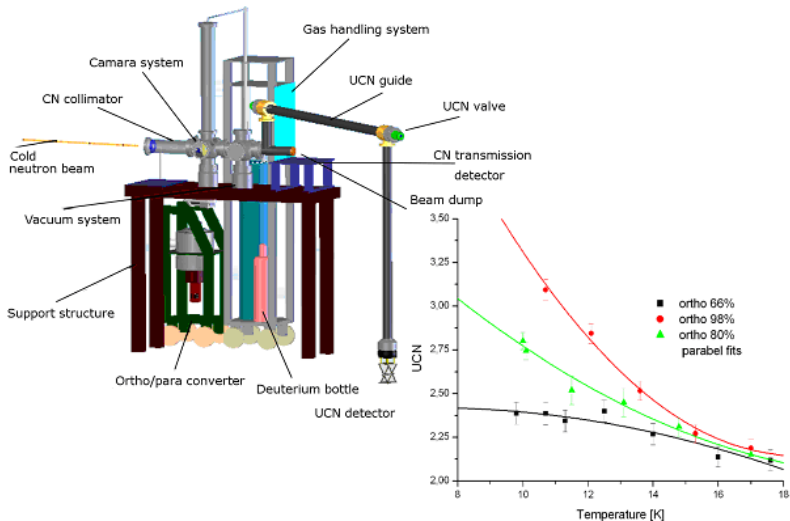


Figure 14.1: Schematic view of the cubeD2 deuterium based UCN test source as well as an example plot of the UCN count rate as function of ortho/para spin concentration of the deuterium and the converter temperature.

M-42 Accelerating matter effect and its first observation in neutron optics

Dmytro Kustov¹, Alexander Frank¹, German Kulin¹, Peter Geltenbort², Michael Jentschel², Vadim Nosov³, Alexander Strepetov³

¹JINR

²ILL

³RRC

Results of experimental observation of neutron energy change when it passes through a refractive sample moving with acceleration are reported. The experiment was done with ultra-cold neutrons and the value of transmitted energy was $(2 \div 6) \cdot 10^{-10}$ eV. Results testify that the effect is really exists and correspond to theoretical predictions with accuracy better than 10%. Similar effect was predicted earlier for the shift of electromagnetic wave frequency when light passes through a dielectric slab moving with acceleration. Seemingly, the effect is of very general nature, but until present it was only observed in neutron optics.

1. K.Tanaka. Phys.Rev.A, 25 (1982) 385. 2. F.V. Kowalski. Phys. Lett.A, 182 (1993) 335. 3. V.G.Nosov, A.I.Frank. Phys. of Atomic Nuclei, 61 (1998) 613. 4. A.I. Frank, P.Geltenbort, G.V.Kulin, D.V. Kustov, V.G. Nosov and A. N. Strepetov. JETP Letters, 84 (2006) 363.

M-43 Neutron Capture on Ge-76: A Background in Neutrinoless Double Beta Decay Experiments

Georg Meierhofer¹, Lea Canella², Peter Grabmayr¹, Josef Jochum¹, Jan Jolie³, Petra Kudejova³, Nigel Warr³

¹PIT Univ. Tübingen

²TU München

³IKP Univ. zu Köln

The Majorana nature of the neutrino can be proved by the observation of the neutrinoless double beta decay. From the measured half-life the effective neutrino mass can be derived, if theory provides precise nuclear matrix elements. The half-lives for these decays are very long (for Ge-76: $> 10^{25}$ y), so reducing the background is the major task for double beta experiments. Therefore, these experiments are performed underground to reduce the flux of cosmic rays.

The GERDA (GERmanium Detector Array) experiment at the Gran Sasso Laboratory (LNGS) in Italy searches for the neutrinoless double beta decay in Ge-76. The isotope Ge-76 is an ideal candidate as it can be source and detector at the same time. A main contribution to the background arises from the prompt gamma cascades after neutron capture by Ge-76. and the following beta-decay of Ge-77. As the prompt gamma decay scheme is poorly known, measurements with isotopically enriched Germanium samples are carried out at the PGAA facility at the FRM II. With the known prompt gamma spectrum it is possible to improve the background reduction of the GERDA experiment. The capture spectra obtained with PGAA and the measured capture cross section of Ge-76 will be discussed.

This work is supported by a grant from BMBF.

M-44 Study the ROT-effect nature in $^{235}\text{U}(n, \gamma, f)$ -process

Gevorg Danilyan¹, Vadim Novitsky¹, Anatoly Zhokhov¹, Viacheslav Krakhotin¹, Kuznetsov Valery¹, Shatalov Pavel¹, Jens Klenke², Hartmut Abele³, Hans-Friedrich Wirth³, Thomas Wilpert⁴, Pappas Catherine⁵, Ferenc Mezei⁶

¹Institute for Theoretical and Experimental Physics (ITEP), 117218 Moscow

²Technische Universität München, ZWE FRM II, Lichtenbergstraße 1, 85748 Garching

³Technische Universität München, Physik-Department E18, James-Franck Straße, 85748 Garching

⁴Helmholtz Zentrum Berlin, Glienicker Straße 100, 14109 Berlin

⁵Helmholtz Zentrum Berlin, Glienicker Straße 100, 14109 Berlin

⁶Helmholtz Zentrum Berlin, Glienicker Straße 100, 14109 Berlin

Recently the small shifting of the angular distribution (AD) of light charged particles (LCP) relative to the fission axis in ternary fission of ^{235}U nuclei induced by cold polarized neutrons have been observed. The sign of the shifting depends on the direction of neutron beam polarization. Authors explained this effect as a result of the fissile nuclei rotation around the nuclear spin and called it the "ROT-effect". It's well known that the fission process is also accompanied by the emission of prompt gamma-quanta. The shifting of the AD of prompt fission γ -rays is also observed.

The authors present preliminary results also obtained to study of the energy and angular distributions of trigger gammas using a set-up with 8 NaI(Tl) gamma-detectors with energy resolution about 8% for γ -rays 660 keV (^{137}Cs γ source).

15 Magnetism and dynamic I

M-45 Freezing dynamics of magnetite ferrofluids studied by time-resolved Small Angle Neutron Scattering

Sylvain Prevost¹, Albrecht Wiedenmann², Mark Klokkenburg³, Ben Ern ³, Uwe Keiderling¹, Dirk Wallacher¹, Michael Meissner¹, Joachim Kohlbrecher⁴

¹HZB

²ILL / LSS

³Utrecht University

⁴PSI

The dynamics of particles' ordering in magnetite-based ferrofluids has been studied by time-resolved stroboscopic SANS between 300 K and 100 K. The sample consists on nearly monodisperse Fe₃O₄ nanoparticles with a core of radius $R_c=10$ nm dispersed in decalin and stabilised by a surfactant layer of about 2 nm [1,2]. Field-induced hexagonal ordering has been found to coexist with dipolar chains [2,3]. The SANS scattering response was measured stroboscopically in an oscillating applied magnetic field up to amplitudes of $B=40$ mT and frequencies between 50 Hz and 300 Hz, superimposed to a static field up to 20 mT.

As long as the magnetic moments followed the applied field, the 2D scattering patterns alternates between fully isotropic and strongly anisotropic [4]. Oscillating behaviour with decreasing amplitudes is clearly observed down to $T_f=212$ K. At a given scattering vector Q , intensities for different orientations between Q and B are perfectly described in terms of the Langevin statistic.

The SANS intensities for Fe₃O₄ ferrofluids are highly sensitive to the interparticle structure factor due to the specific ratio of nuclear and magnetic scattering length densities. Intensities parallel and perpendicular to B are oscillating in phase, which unambiguously implies a field dependent variation of the structure factor corresponding to the variation of the effective dipolar coupling between the particle moments. With decreasing temperature, the amount of freely rotating particle moments decreases continuously and vanishes at the temperature T_f . Below T_f , particles remains frozen in more or less random orientations, leading to a time independent scattering contribution. At 100 K the system is fully static and shows no difference to the data obtained in a static magnetic field.

[1] M. Klokkenburg, B. H. Ern , J.D. Meeldijk, A. Wiedenmann, A.V. Pethukov, R.P.A. Dul-lens, A.P.Philipse, PRL 97, 185702 (2006)

[2] Klokkenburg, M., Ern , B. H., Wiedenmann, A., Pethukov, A.V., Philipse, A.P, PRE 75, 051408 (2007)

[3] A. Wiedenmann, A. Hoell, M. Kammel, P. Boesecke Phys Rev. E 68 (2003) 031203, 1-10

[4] A.Wiedenmann, U. Keiderling, K. Habicht, M.Russina, R. G hler, PRL 9, 057202 (2006)

M-46 Magnetic phase transition in Fe₅₀Pt₅₀-xRh_x thin films

Jochen Fenske¹, Dieter Lott¹, Prakash Mani², Gary J. Mankey², Frank Klose³, Wolfgang Schmidt⁴, Karin Schmalzl⁴, Elena Tatakowskaya⁵, Andreas Schreyer¹

¹GKSS Research Centre

²MINT Center, The University of Alabama

³ANSTO, Bragg Institute

⁴Jülich Centre for Neutron Science

⁵Institute for Magnetism, National Academy of Science

For a few years perpendicular recording media are used to overcome the restrictions of the longitudinal recording media due to the superparamagnetic limit. In order to further increase the storage density, the search for new materials with higher magnetic anisotropies is still ongoing. Here, FePt is a very promising candidate due to its extremely high magnetic anisotropy which enables one to increase the storage density and its capacity to more than 1 Tbit/in² [1]. However, the high anisotropy is also associated with restrictive requirements concerning i.e. the very high write field. To lower it to a feasible field range magnetic underlayers are used [2].

Possible candidates for such an underlayer for FePt systems are L10 structured Fe₅₀Pt₅₀-xRh_x alloys due to their perfect lattice match. Magnetization measurements of the bulk samples for x=10 refer to an antiferromagnetic (AF)/ferromagnetic (FM) phase transition when heated [3]. Additional magnetostriction measurements indicate that the phase transition could also be induced by applying a magnetic field [4]. In comparison with conventional underlayers it allows in principle not only to strongly reduce the write field but also to stabilize the magnetization state of the recording media by switching between the FM and AF state, respectively.

However, considering material costs and fabrication time, thin films are important for its application. In this work thin films of the L10 structured Fe₅₀Pt₅₀-xRh_x alloys are investigated for the first time by unpolarized and polarized neutron diffraction and refined by structure calculations. A detailed picture of the magnetic configuration and its dependence on temperature and magnetic field could be developed showing significant differences to the bulk properties.

[1] S.N. Piramanayagam, J. Appl. Phys. 102, 011301 (2007)

[2] J.-U. Thiele, S. Maat, E. E. Fullerton, Appl. Phys. Lett., 82 2859 (2003)

[3] Takizawa, K; Ono, T; Miyajima, H, J. Magn. Magn. Mater., 226: 572 Part 1 Sp. Iss. SI MAY 2001

[4] P.A. Algarabel, et. al, J. Appl. Phys. 79 (8), 1996

M-47 Search for helimagnon excitations in MnSi: an inelastic neutron scattering study

Marc Janoschek¹, Florian Bernlochner¹, Sarah Dunsinger¹, Bertrand Roessli², Peter Link³, Christian Pfleiderer¹, Peter Böni¹

¹Technische Universität München, Physik Department E21

²Paul Scherrer Institut

³Forschungsneutronenquelle Heinz Mayer-Leibnitz (FRM II)

The lack of inversion symmetry allows the presence of the antisymmetric Dzyaloshinskii-Moriya interaction (DMI) in MnSi. In zero field, the DMI leads to a long-period ferromagnetic spiral with a period of approximately 180 Å along the [111] direction below $T_c \approx 29.5$ K.

Recent theories by the groups of Belitz et al. [1,2] and Maleyev [3] predict a rich, novel spectrum of Goldstone modes for sufficiently small wave vectors near the helical propagation vector in the helical phase below T_c . These excitations, also referred to as helimagnons, are predicted to have a characteristic anisotropic dispersion relation with respect to the propagation direction of the magnetic helix.

We have performed extensive inelastic neutron scattering experiments by means of triple-axis spectroscopy in the helical phase in order to explore the nature of these novel excitations.

[1] D. Belitz, T. R. Kirkpatrick Phys. Rev. B 72, 180402(R) (2005)

[2] D. Belitz, T. R. Kirkpatrick and A. Rosch Phys. Rev. B 73 054431 (2006)

[3] S. V. Maleyev, Phys. Rev. B 73, 174402 (2006).

M-48 Determination of the magnetic ground state in Na₈Cu₅O₁₀ by elastic neutron scattering

Markus Raichle¹, Manfred Reehuis², Bernhard Keimer¹

¹MPI-FKF

²HMI

The magnetic structures of low-dimensional materials are of particular interest. One finds for example multiferroic behavior in 1D (undoped) edge-sharing helicoidal magnetic systems due to the anisotropic Dzyaloshinskii-Moriya interaction [1]. Up to now two different systems with doped edge-sharing spin chains have been investigated (La, Y, Sr, Ca)₁₄Cu₂₄O₄₁ [2] and Ca₂Y₂Cu₅O₁₀ [3]. However, the magnetic structure of these materials is strongly influenced by lattice incommensurabilities and substitutional disorder.

Recently a new doped edge-sharing 1D spin chain compound Na₈Cu₅O₁₀ has been synthesized at MPI for Solid State Research. This compound has a commensurate lattice structure and no substitutional disorder due to doping. In particular, it has commensurate charge order. Therefore it is an ideal compound in order to investigate the magnetic structure of doped edge sharing 1D spin chains. Due to a refinement of our (magnetic) elastic neutron scattering data of that compound (see figure), we could show that its magnetic ground state is a charge density wave with a commensurate propagation vector along the chains and an incommensurate perpendicular to the chains. We explain this incommensurability due to inter-chain interactions between different spin chains in that compound [4].

[1] Phys. Rev. Lett. 98, 057601 (2007)

[2] Physics Reports 428, 169 (2006)

[3] Phys. Rev. B 71, 104413 (2005)

[4] M. Raichle et al., accepted in Phys. Rev. Lett.

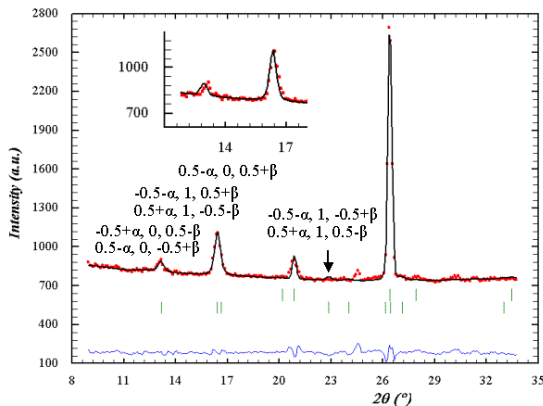


Figure 15.1: The red points mark the measured data for $T = 1.4\text{K}$. The black line shows the Rietveld refinement with which the magnetic model was determined. The green bars indicate the Bragg reflections. The bars in the first line represent the nuclear Bragg reflections and the bars in the second line represent the magnetic Bragg reflections.

M-49 Determination of the magnetic ground state in Na₈Cu₅O₁₀ by elastic neutron scattering

Markus Raichle¹, Manfred Reehuis², Bernhard Keimer¹

¹MPI-FKF

²HMI

The magnetic structures of low-dimensional materials are of particular interest. One finds for example multiferroic behavior in 1D (undoped) edge-sharing helicoidal magnetic systems due to the anisotropic Dzyaloshinskii-Moriya interaction [1]. Up to now two different systems with doped edge-sharing spin chains have been investigated (La, Y, Sr, Ca)₁₄Cu₂₄O₄₁ [2] and Ca₂Y₂Cu₅O₁₀ [3]. However, the magnetic structure of these materials is strongly influenced by lattice incommensurabilities and substitutional disorder.

Recently a new doped edge-sharing 1D spin chain compound Na₈Cu₅O₁₀ has been synthesized at MPI for Solid State Research. This compound has a commensurate lattice structure and no substitutional disorder due to doping. In particular, it has commensurate charge order. Therefore it is an ideal compound in order to investigate the magnetic structure of doped edge sharing 1D spin chains. Due to a refinement of our (magnetic) elastic neutron scattering data of that compound (see figure), we could show that its magnetic ground state is a charge density wave with a commensurate propagation vector along the chains and an incommensurate perpendicular to the chains. We explain this incommensurability due to inter-chain interactions between different spin chains in that compound [4].

[1] Phys. Rev. Lett. 98, 057601 (2007)

[2] Physics Reports 428, 169 (2006)

[3] Phys. Rev. B 71, 104413 (2005)

[4] M. Raichle et al., accepted in Phys. Rev. Lett.

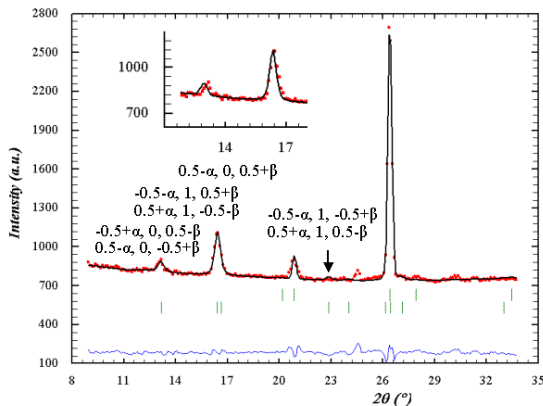


Figure 15.2: The red points mark the measured data for $T = 1.4\text{K}$. The black line shows the Rietveld refinement with which the magnetic model was determined. The green bars indicate the Bragg reflections. The bars in the first line represent the nuclear Bragg reflections and the bars in the second line represent the magnetic Bragg reflections.

M-50 Neutron diffraction study of the $R_2\text{PdSi}_3$ ($R = \text{Tb, Ho, Er}$)

Matthias Frontzek¹, Fei Tang², Astrid Schneidewind³, Peter Link³, Jean-Michel Mignot⁴, Jens-Uwe Hoffmann⁵, Michael Loewenhaupt¹

¹TU Dresden, Institut für Festkörperphysik,

²Max Planck Institute for the Physics of Complex Systems, D-01187 Dresden, Germany

³Forschungsneutronenquelle H.-M. Leibnitz, TU München,

⁴Laboratoire Léon Brillouin, CE-Saclay, F-91191,

⁵Helmholtz-Zentrum Berlin für Materialien und Energie GmbH

Rich magnetic phenomena can be found in the series of hexagonal $R_2\text{PdSi}_3$ ($R =$ heavy rare earth) resulting from the interplay between $RKKY$ interaction, crystal-electric field and geometric frustration [1]. Furthermore, the observation of crystallographic superstructure reflections indicates a non- statistically distribution of the Pd and Si ions. With the means of magnetic neutron scattering the zero field magnetic structures of $R_2\text{PdSi}_3$ ($R = \text{Tb, Ho, Er}$) have been investigated. The magnetic structures exhibit very large magnetic unit cells. In zero field reflections of higher order of the propagation vector are observed indicating squared up magnetic structures [2].

Depending on the rare earth crystal field level scheme, the ordered moment direction varies from a basal plane orientation (Tb) to be along the \mathbf{c} -direction (Er).

Applying external magnetic fields, the magnetic structure is strongly influenced by the crystalline superstructure.

We will present recent neutron diffraction results on $R_2\text{PdSi}_3$ single crystals at low temperatures and elevated magnetic fields. The comparative discussion of the different rare earth compounds elucidates the underlying mechanisms.

[1] M. Frontzek, A. Kreyssig, M. Dörr, M. Rotter, G. Behr, W. Löser, I. Mazilu, and M. Loewenhaupt, *J. Magn. Magn. Mat.* **301** (2006) 398

[2] M. Frontzek, A. Kreyssig, M. Dörr, A. Schneidewind, J.-U. Hoffman, and M. Loewenhaupt, *J. Phys.: Condens. Matter* **19** (2007) 145276

M-51 Magnetism in REFeAsO (RE=Nd,Pr) investigated using neutron diffraction

Dimitri Argyriou¹, Simon Kimber¹, Fabiano Yokaichiya¹, Günter Behr², Brend Büchner², Paul Canfield³

¹Helmholtz-Zentrum Berlin für Materialien und Energie

²IFW Dresden

³Ames National Laboratory

The discovery of superconductivity in FeAs superconductors [1] has attracted intense interest in the last few months. These materials are layered materials with superconductivity in the FeAs layers, separated by RE-O layers (RE= rare earth) in the case of REFeAsO [1] or divalent cations in the case of MFe₂As₂ (M=Ba,Sr) [2]. We shall present recent neutron diffraction measurements for the RE=Pr and Nd materials that describe the development of RE and Fe magnetism as a function of temperature and Fluorine doping.

1. Kamihara et al. Iron-based layered superconductor La[O_{1-x}F_x]FeAs (x=0.05-0.12) with T_c=26 K. J Am Chem Soc (2008) vol. 130 pp. 3296

2. Rotter et al. Spin density wave anomaly at 140 K in the ternary iron arsenide BaFe₂As₂. arXiv (2008) vol. cond-mat.supr-con

M-52 Inelastic Neutron Scattering on the Antiferromagnetic Half-Heusler Alloy CeBiPt

Gernot Goll¹, Oliver Stockert², Tobias Unruh³, Peter Link³, K. Shigetoh⁴, T. Takabatake⁴

¹Physikalisches Institut, Universität Karlsruhe, 76128 Karlsruhe

²Max-Planck-Institut CPfS, 01187 Dresden

³ZWE FRM-II, Technische Universität München, 85747 Garching

⁴Hiroshima University, Higashi-Hiroshima, Japan

CeBiPt is a semimetal with a rather low charge carrier concentration $n = 7.7 \times 10^{17} \text{ cm}^{-3}$ (Ref. 1). Below $T_N = 1.1 \text{ K}$ antiferromagnetic order occurs as evidenced by sharp maxima in the thermodynamic properties [2]. Neutron diffraction experiments have revealed an AF-type I structure with a propagation vector $\tau=(1 \ 0 \ 0)$ and moments also along $[1 \ 0 \ 0]$ (Ref. 3). The ordered moment $\mu = 0.6\mu_B$ is much lower than the effective moment determined from the Curie-Weiss behavior of the susceptibility at higher T. Crystal-electric field (CEF) splitting of the Ce^{3+} level might be one origin of a lowered ordered moment. We performed inelastic neutron scattering experiments on TOFTOF at the FRM-II with energy of the incident neutrons $E_i = 2.7, 5.7,$ and 16.9 meV and on PANDA with $E_i=5.6 \text{ meV}$ at $2.8 < T < 50 \text{ K}$. We found one strong CEF excitation at $\hbar\omega = 9.5 \text{ meV}$ at $T = 4.5 \text{ K}$ in line with previous measurements on SV29 at FRJ-2 with fixed $E_i = 30 \text{ meV}$ [4]. This excitation has been identified with the transition between a Γ_7 doublet and a Γ_8 quartet state. As seen in Fig. 1 a further magnetic excitation appears at about 2.5 meV while the excitations around 7 and 13 meV are probably caused by phonons as deduced from the q dependence of the spectra. The occurrence of a low-lying CEF excitation raises questions about the possible mechanism for the CEF symmetry breaking in CeBiPt and the role of disorder for the electronic and magnetic properties of this half-Heusler compound.

[1] G. Goll et al., Europhys. Lett. 57, 233 (2002).

[2] T. Pietrus et al., Physica B 281 & 282, 745 (2000).

[3] J. Wosnitza et al., New J. of Phys. 8, 174 (2006).

[4] G. Goll et al., J. Magn. Magn. Mat. 310, 1773 (2007).

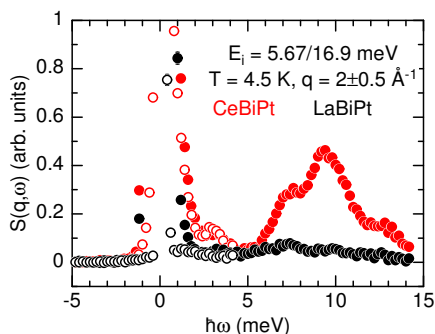


Figure 15.3: Fig. 1: Inelastic neutron scattering spectra $S(q,\omega)$ vs. $\hbar\omega$ measured at $T = 4.5 \text{ K}$ with $E_i = 5.7$ and 16.9 meV at $q = 20 \text{ nm}^{-1}$. LaBiPt has been measured as a non-magnetic reference.

M-53 Neutron scattering studies on spiral multiferroics

Markus Braden¹, Daniel Senff¹, Thomas Finger¹, Max Baum¹, Alexander C. Komarek¹, Nadir Aliouane², Dimitri Argyriou², Arno Hiess³, Karin Schmalzl⁴, Paul Steffens³, Peter Link⁵, Klaudia Hradil⁵, Petra Becker⁶, Ladislav Bohatý⁶, Louis-Pierre Regnault³

¹II. Physikalisches Institut

²HMI

³ILL

⁴ILL & FZ Jülich

⁵FRM-II

⁶Inst. f. Kristallographie, Köln

The non-collinear order in spiral or cycloidal magnets can cause a ferroelectric polarization through the inverse Dzyaloshinski-Moriya interaction implying a multiferroic phase. This magnetoelastic coupling may give rise to a hybridized phonon-magnon excitation, called electromagnon. We discuss elastic and inelastic neutron scattering studies on three different multiferroic compounds : TbMnO₃, MnWO₄ and NaFeSi₂O₆. In the three materials the ferroelectric polarization is well explained by the Dzyaloshinski-Moriya interaction and their complex magnetic order. By unpolarized and polarized neutron scattering studies the frequencies and polarization patterns of the magnetic excitations are determined. Strong evidence for an electromagnon excitation is obtained for TbMnO₃ when combining the neutron scattering results with optical spectroscopy data.

[1] D. Senff, P. Link, K. Hradil, A. Hiess, L. P. Regnault, Y. Sidis, N. Aliouane, D. N. Argyriou, and M. Braden, *Phys. Rev. Lett.* 98, 137206 (2007).

[2] D. Senff, N. Aliouane, D. N. Argyriou, A. Hiess, L. P. Regnault, P. Link, K. Hradil, Y. Sidis, and M. Braden; review to appear in *Journal of Physics Cond. Matter*.

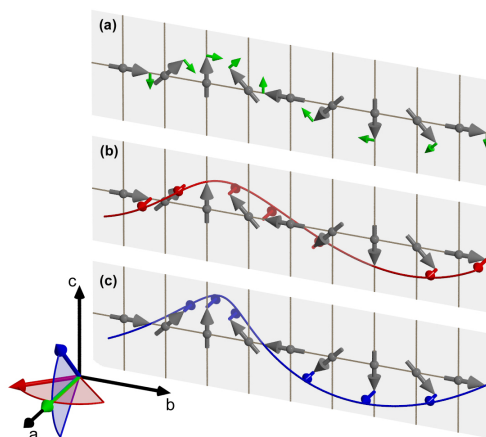


Figure 15.4: Polarization patterns of three magnetic excitations at the incommensurate zone center in the cycloidal phase of TbMnO₃. The upper mode is the phason of the incommensurate phase, and the lowest one possesses the symmetry of the electromagnon excitation.

M-54 Magnetic ordering in HoCrO3 compound

Naveen Kumar Chogondahalli M.¹, Yinguo Xiao¹, Yixi Su², Perþon Jörg¹, Anatoliy Senyshyn³, Thomas Brückel⁴

¹Institut für Festkörperforschung

²Jülich Centre for Neutron Science

³Forschungsneutronenquelle Heinz Maier-Leibnitz (FRM II)

⁴Institut für Festkörperforschung/Jülich Centre for Neutron Science

Similar to many well investigated multiferroic ReMnO3 (Re = Tb, Dy, Ho, etc.) systems [1,2], a strong coupling between magnetic ions of Ho³⁺ and Cr³⁺ in a newly synthesized HoCrO3 compound may also lead to complex magnetic ordering and possible multiferroicity. The magnetic, thermal and neutron powder diffraction (NPD) studies on HoCrO3 compound are presented. The results show that the HoCrO3 crystallizes in orthorhombic structure with the space group Pbnm in the temperature range 4 to 300 K. Both the magnetization and heat capacity measurements clearly indicate the onset of magnetic ordering at TN=137 K [3,4]. The temperature dependence of magnetic structure is investigated by using the powder neutron diffraction method and the detailed magnetic structure of HoCrO3 compound is clarified. Below the Neel temperature TN (137 K), the Cr³⁺ orders firstly with the antiferromagnetic type. With the further decrease of temperature, the canted antiferromagnetic ordering of Ho³⁺ is observed at about 50 K accompanied with the appearance of several new magnetic reflections. There is an indication of the presence of magnetic diffuse scattering at low temperatures. The implication to the existence of possible magnetic frustrations will be discussed.

1. Goto et.al.,Ferroelectricity and Giant Magnetocapacitance in Perovskite Rare-Earth Manganites, PRL 92(25)2004
2. Aliouane N et.al., Field-induced linear magnetoelastic coupling in multiferroic TbMnO3, Phys. Rev. B 73 020102(R)(2006)
3. E. F. Bertaut et.al.,J. Appl. Phys. 37 (1966)1038.
4. Hirohisa Satoh et.al., Journal of Alloys and Compounds 259 (1997) 176-182.

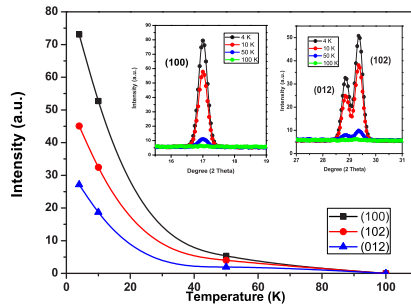


Figure 15.5: Temperature dependence on the intensity of magnetic peaks (100), (102) and (012).

M-55 Superconductivity and spin fluctuations in underdoped $\text{YBa}_2\text{Cu}_3\text{O}_{6+x}$

Chris Stock¹

¹ISIS Facility

The cuprate superconductors have continued to attract much interest due to the delicate interplay between antiferromagnetism and superconductivity. The hole doped cuprates are Mott insulators which become superconducting when a critical hole concentration is reached. We have investigated the spin response in heavily underdoped $\text{YBa}_2\text{Cu}_3\text{O}_{6+x}$ (YBCO_{6+x}) over a broad energy range extending over the entire band of fluctuations. Surprisingly, the spin fluctuations are strongly affected by superconductivity over the entire dynamic range. We will present a study of the low-energy spin fluctuations both as a function of temperature and applied magnetic fields. We will show that the low-energy spectrum is characterized by a central peak at the elastic line and a broad inelastic feature peaked at around 2 meV. The response of both of these features to superconductivity is discussed by investigating the response to both temperature and applied magnetic field.

M-56 Metamagnetic transition in the single layer Ruthenates

Paul Steffens¹, Yvan Sidis², Peter Link³, Satoru Nakatsuji⁴, Markus Braden⁵

¹ILL, Grenoble

²LLB, Saclay

³FRM2, Garching

⁴ISSP, Tokyo

⁵II. Physik. Institut, Uni Köln

By inelastic neutron scattering, we have studied the magnetic excitations in $\text{Ca}_{2-x}\text{Sr}_x\text{RuO}_4$. Our results show that in these materials there is a complex interplay of ferromagnetic and incommensurate antiferromagnetic correlations. These are seen as a paramagnon-like excitation that persists over a wide range of temperature and Sr-concentration and as incommensurate antiferromagnetic fluctuations in the range of lower temperature at low Sr-concentration.

In $\text{Ca}_{1.8}\text{Sr}_{0.2}\text{RuO}_4$, a metamagnetic transition is observed, at which the magnetization as function of field jumps by $\sim 0.5\mu_B$. By observing the change of magnetic excitations we obtain a detailed characterization of the metamagnetic transition in terms of competing magnetic instabilities. In particular, we have observed that at high magnetic field a new mode appears, which strongly resembles a magnon in a conventional ferromagnet, showing that the magnetic field does not only act to polarize spins but also induces a ferromagnetic interaction.

O. Friedt et al., Phys. Rev. Lett. 93, 147404 (2004) M. Kriener et al., Phys. Rev. Lett. 95, 267403 (2005) P. Steffens et al., Phys. Rev. Lett. 99, 217402 (2007)

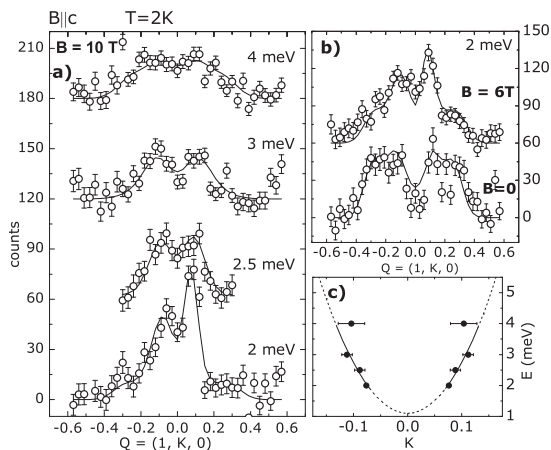


Figure 15.6: The magnetic excitations in $\text{Ca}_{1.8}\text{Sr}_{0.2}\text{RuO}_4$. Part (a) is the magnon scattering at high magnetic field, whose dispersion is summarized in part (c) of the figure. Part (b) shows the same scan at a lower and at zero magnetic field, where the incommensurate antiferromagnetic response dominates.

M-57 Multitude of magnetic phases in Er₂Ni₂Pb

Karel Prokes¹, John Mydosh²

¹Helmholtz-Zentrum Berlin

²II. Physikalisches Institut, Universität zu Köln

We have studied the magnetic structures of Er₂Ni₂Pb using powder neutron diffraction technique in zero field. Previous bulk measurements suggested three distinct magnetic phase transitions [1,2]. Our neutron diffraction experiments, which were made in the range 1.5–5 K, showed that magnetic Bragg reflections in Er₂Ni₂Pb can be indexed by several propagation vectors that coexist over an extensive temperature range. Rather than a homogeneous magnetic structure that is simultaneously described by all the existing propagation vectors several spatially separated structures appear to exist in Er₂Ni₂Pb. The appearance/disappearance of representative reflections at $T_N = 3.5$ K, $T_{m1} = 3.0$ K, $T_{m2} = 2.3$ K and $T_{m3} = 1.8$ K, denote magnetic phase transitions. The only magnetic state that is determined by a single propagation vector exists just below T_N . In all other magnetic states more than one propagation vector are stable. Except for the state at the lowest temperature, which is commensurate all other propagation vectors incommensurate with the crystal structure. It seems, however, that Er moments are oriented always along the b axis.

1 A.D. Chinchure, E. Muñoz-Sandoval, J.A. Mydosh, Phys.Rev. B 66, 020409(R) (2002)

2 A.D. Chinchure, E. Muñoz-Sandoval, J.A. Mydosh, Phys.Rev. B 64, 020404(R) (2001)

M-58 The Study of the nature of The Low-Temperature Inter-Ion Correlations in CeAl₃ by means of SAPNS

Gennady Kopitsa¹, Sergey Grigoriev¹, Nikolay Tiden², Vladimir Lazukov², Pavel Alekseev², Helmut Eckerlebe³

¹Petersburg Nuclear Physics Institute, Gatchina, Russia

²Russian Research Centre "Kurchatov Institute", Moscow, Russia

³3GKSS Research Centre, Geesthacht, Germany

Although CeAl₃ was the first material established to be a heavy-fermion compound, the origin of the low temperature ground state is still the subject of discussion. A wide variety of ground states and models have been proposed for CeAl₃: anisotropic Kondo effect, frustrated short range order, antiferromagnetic order or exciton-polaron model. The recent measurements performed at the time-of-flight (TOF) spectrometer have shown oscillations in the q-dependence of quasielastic magnetic scattering intensity at $T = T_K$ [1]. These results could be interpreted as showing the presence of dynamical magnetic inter-ion correlations.

Small-angle polarized neutron scattering (SAPNS) measurements were performed on polycrystal CeAl₃ at temperature range $8 < T < 60$ K and magnetic fields $0 < H < 213$ mT. During the course of the SAPNS experiment the reduction of the incoherent paramagnetic scattering from the non-correlated system of Ce-spins (which occur at $T = 60$ K) was observed both with the decrease of T and the increase of H . These results give the evidence of the transformation of magnetic component and are in agreement with data of [1]. Moreover, at $T < 15$ K the magnetic scattering was found in the range $q < 7.5 \cdot 10^{-2} \text{ \AA}^{-1}$. It has been found that the q-dependence of the scattering cross-section $d\Sigma_m(q)/d\Omega$ is well described by $d\Sigma_m(q)/d\Omega = A/(q^2 + \kappa^2)^{3/2}$. A such behavior of $d\Sigma_m(q)/d\Omega$ corresponds to the scattering from ferromagnetic or spin-glass like correlations.

[1] N.N. Tiden, P.A. Alekseev, V.N. Lazukov et al., Solid State Communications 141 (2007), 474.

16 Soft matter

M-59 Lateral structures of buried interfaces in tri-block copolymer films

Peter Müller-Buschbaum¹, Leander Schulz², Ezzeldin Metwalli¹, Jean-Francois Moulin³, Robert Cubitt⁴

¹Physikdepartment E13

²Universite de Fribourg

³Institut für Werkstoffforschung

⁴Institut Laue-Langevin

The lateral structure of an A-B-A type tri-block copolymer at the buried substrate interface is studied. With grazing incidence small angle neutron scattering (GISANS) high interface sensitivity is reached [1]. The powder-like oriented lamellar structure in the bulk becomes oriented along the surface normal in the vicinity of the substrate [2]. A modification of the short-ranged interface potential of the substrate introduces a stretching of the lateral spacing of this lamellar structure up to 8.3 % as compared to the bulk. The decay of the stretching towards the volume structure is probed with depth profiling. It extends at least up to a distance of 51 nm from the solid surface [3].

[1] P.Müller-Buschbaum, J.S.Gutmann, R.Cubitt, M.Stamm: Probing the in-plane composition of thin polymer films with grazing-incidence small angle scattering and atomic force microscopy; *Colloid.Polym.Sci.* 277, 1193 (1999)

[2] P.Müller-Buschbaum, E.Maurer, E.Bauer, R.Cubitt: Surface versus confinement induced morphology transition in triblock copolymer films: A GISANS investigation; *Langmuir* 22, 9295 (2006)

[3] P.Müller-Buschbaum, L.Schulz, E.Metwalli, J.-F.Moulin, R.Cubitt: Lateral structures of buried interfaces in A-B-A-type block polymer films; *Langmuir*, submitted

M-60 Solvent content in thin spin-coated polymer films: a neutron reflectometry study

Jan Perlich¹, Volker Körstgens¹, Ezzeldin Metwalli¹, Leander Schulz², Robert Georgii³, Peter Müller-Buschbaum¹

¹Physik-Department LS E13

²Université Fribourg, Département de Physique

³Forschungsneutronenquelle Heinz Maier-Leibnitz

The detection of remaining solvent in thin polymer films is of importance due to its effect on chain mobility and film homogeneity. It is essential for swelling experiments to define the initial state with respect to the amount of solvent included inside the film directly after preparation. Moreover, it gives an estimate on possible aging effects caused by the reduction of the solvent content, which typically yield an increased brittleness. The investigation focuses on a well controlled model system, which consists of protonated polystyrene (PS) with different molecular weights, spin-coated out of protonated or deuterated solvent onto silicon wafer substrates. Directly after spin-coating the thin PS films were investigated with neutron reflectometry (NR) at the MIRA instrument of the research neutron source FRM-II. A narrow q_z range around the critical edge was probed with high resolution. Due to the high sensitivity of the position of the critical edge on the ratio of protonated PS and deuterated solvent, the exact position of the critical edge enables to determine the solvent content.

Two different key parameters which influence the solvent content are addressed: the molecular weight of PS and the film thickness. In addition, annealing of the as-prepared films is discussed.

We acknowledge financial support by project MU 1487/4-2.

[1] D.W. Schubert, *Polymer Bulletin*, 38:177, 1997.

[2] L.L. Spangler, M. Torkelson, and J. S. Royal, *Polym. Eng. Sci.*, 30:644-653, 1990.

[3] J. Perlich, V. Körstgens, E. Metwalli, L. Schulz, R. Georgii, P. Müller-Buschbaum, to be published

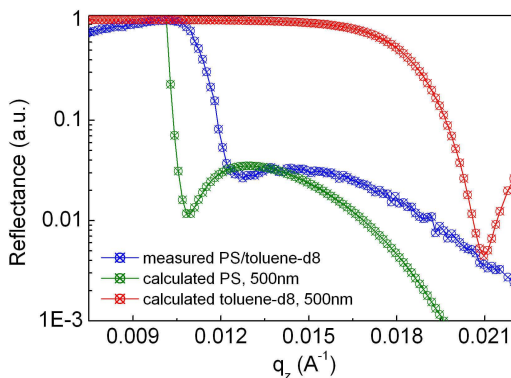


Figure 16.1: Calculated neutron reflectivity data for a single PS film on top of bulk Si. Calculated for a film SLD of protonated PS (dry film) and deuterated toluene. Since the measured data is a mixture of both, the measured reflectivity lies within the calculated limits.

M-61 Structural investigations of polymer blend films for photovoltaic applications

Matthias Ruderer¹, Robert Meier¹, Ezzeldin Metwalli¹, Jean-Francois Moulin², Peter Müller-Buschbaum¹

¹Technische Universität München, Physik-Department E13, D-85747 Garching, Germany

²Institut für Werkstofforschung, GKSS-Forschungszentrum Geesthacht GmbH, Germany

In recent years investigations on materials and systems for organic photovoltaics have attracted increasing interest.¹ The main approaches were realized by either a layered or a blended system. Due to high exciton binding energies in organic materials a two component system is required to reach reasonable charge separation and therefore a sufficient performance. To achieve such a two component system in a most simple way mixing of two photoactive polymers and preparing a thin film via spin coating seems most attractive. However, the blending ratio of the components is the crucial parameter concerning the inner film structure and thus the efficiency of a resulting device. Consequently it's necessary to investigate the inner film structure to achieve a better understanding of the principles in organic photovoltaic devices.

The semiconducting nature of photoactive polymers is due to a conjugated molecule structure, though this chemical structure results in a liability for degradation due to oxidation and high energy radiation. Thus neutrons seem to be the solution as a chemical non destructive probe for structural investigations of photoactive polymer films.

We performed the very first chemical and structural non destructive measurements of the inner film structure of polymer blends via GISANS.³ Therefore the semiconducting polymers poly(9-vinylcarbazole) (PVK) and poly((1-methoxy)-4-(2-ethylhexyloxy)-p-phenylenevinylene) (MEH-PPV) were dissolved in toluene and spin coated on Si-substrates. The contrast for neutrons was enhanced by using protonated and deuterated solvents. Due to using a time of flight (TOF) setup both the surface and the whole film could be probed separately in one measuring step. Additional, the topography was pictured by optical and atomic force microscopy. UV/Vis spectroscopy completes the investigations of the polymer blend films for photovoltaic applications.

(1) J. K. Lee et al., J. Am. Chem. Soc., 130, 3619 (2008).

(2) M. Ruderer et al., to be published.

(3) P. Müller-Buschbaum et al., Langmuir, 22, 9295 (2006).

M-62 Multilamellar Vesicles Studied by Small Angle Neutron Scattering

Henrich Frielinghaus¹

¹Jülich Centre for Neutron Science

A model to describe the small angle scattering of multilamellar vesicles is developed. At largest length scales the Guinier behavior describes the whole vesicle. A first power law is connected with the compactness of the vesicle. With many shells the vesicle appears compact and a Porod behavior is predicted, while with a few shells the 2-dimensional structure of the shells is supposedly observed. All intermediate exponents between 4 and 2 are in principle possible, and thus allow for a determination of the shell number by scattering methods. At smaller length scales a correlation peak is connected to the regular distance of the shells. Finally, the 2-dimensional structure of the individual shells will be observed.

In addition fluctuations of the shell centers were considered. This influences the correlation peak sharpness and position, and the first power law describing the compactness. With large displacements of the shell centers the structure appears more open, and the dominating shell distance increases.

So far, not too many experimental examples spanning all length scales are known. So only specific experimental results are collected and connected to the scattering model.

M-63 Neutron Reflectivity Measurements on Conducting Polymer Films

Robert Meier¹, Matthias Ruderer¹, Jan Perlich¹, Gunar Kaune¹, Robert Georgii², Peter Müller-Buschbaum¹

¹TU München, Physik-Department LS E13

²FRM2, Munich

Due to their photoactive properties conducting polymers show bright prospects for application in organic solar cells or organic light emitting diodes and therefore have been in focus of world-wide soft matter research over the last years [1]. Due to their chemical structure they are sensitive to high energy radiation. Hence neutron scattering seems an appropriate non-destructive way to study conducting polymer films.

We report first neutron scattering length density measurements on thin conducting polymer films. Materials under investigation have been different novel p-phenylene vinylene polymers (MEH-, MDMO-, M3EH-, and MEH-CN-PPV) and other relevant conducting polymers (F8BT, P3HT, PVK, etc.). For sample preparation, the conduction polymers were dissolved in organic solvents (e.g. toluene, chloroform) and spin coated on glass substrates. We measured the critical edge for these materials using neutron reflectivity (NR). The experiments were performed at the MIRA instrument of the neutron research facility FRM-II. In order to determine the critical edge accurately the measurements were performed at a small q_z range around the critical edge with a high resolution. In order to increase the contrast, the polymer films have also been prepared using deuterated solvents. Improvement in contrast can be attributed to the fact that remaining amounts of solvent might be still embedded in the polymer matrix [2] or a chemical exchange reaction between the polymer and the deuterated solvent occurs.

(1) S. C. Veenstra et. al., Progress in Photovoltaics: Resarch and Application 2007 (15)

(2) J. Perlich, V. Körstgens, E. Metwalli, L. Schulz, R. Georgii, P. Müller-Buschbaum, to be published

M-64 Short Chain Carbohydrate Surfactant with Ethyl Spacer as “Super Hydrogelator”

Vasyl Haramus¹, Götz Milkereit², Mats Almgren³

¹Institute of Material Science/WPS

²Institute of Organic Chemistry, University of Hamburg, Martin-Luther-King-Platz 6, 20146 Hamburg, Germany

³Department of Physical Chemistry, Uppsala University, Box 579, SE-751 23 Uppsala, Sweden

Formation of a thermo-reversible hydrogel formed by a simple sugar based compound with a short alkyl chain (C12), a small ethyl spacer and a disaccharide (lactose) as polar group without any additives and at concentration of about 0.1 % is presented. It is a unique combination of very good gelation properties (lowest gel concentration is 0.03-0.07 wt%) and a much simple molecular structure compared to the classical four component model. Structure of gel has been obtained by SANS and cryo-TEM. The total diameter of fibers (10-11 nm) is 3 times larger than diameter of core (≈ 4 nm) and double length of molecules (≈ 4 nm). One can suppose that this secondary structure consists of 3 thinner fibers of the primary structure.

M-65 On the structural features of polymeric spherulites in solution: a combined wide-Q SANS and microscopy study

Aurel Radulescu¹, Dieter Richter²

¹JCNS at FRM II

²Forschungszentrum Jülich GmbH - JCNS at FRM II

Polymer crystallization from solution occurring by nucleation of micron-size spherulitic-like aggregates was only sporadic studied so far. Since such morphologies are composed of bundles of elongated nano-structures radially oriented or branched and sometimes presenting themselves structural subunits a full understanding of the aggregates formation requires in this case a detailed inspection of wide length scales. Scattering methods that can cover a wide-Q range and thus investigate length scales from Angstroms up to tens of microns are the most suitable tools for such studies. We report results and conclusions of detailed investigations performed on spherulitic-like morphologies formed in solution by the crystalline syndiotactic and alternating crystalline-amorphous isotactic-atactic polypropylenes using three small-angle neutron scattering techniques: the conventional SANS, the mirror-focusing SANS and the ultra-SANS double-crystal diffractometry. Microscopy techniques were complementary used for a better understanding of the morphologies inferred by the scattering data. The ultra-SANS results revealed that the polymeric spherulites present rather a character of dense aggregates with diffuse interfaces than a fractal one.

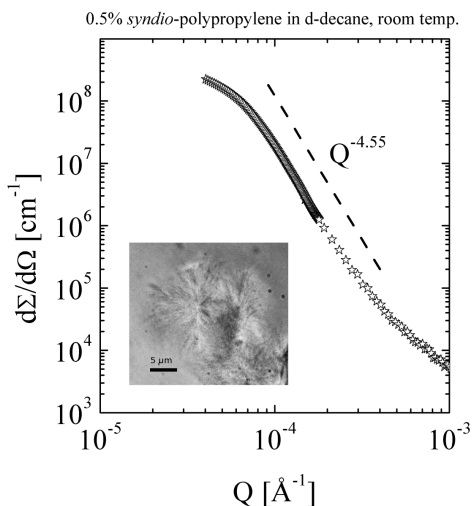


Figure 16.2: Fig.1 - The scattering pattern from syndiotactic-polypropylene spherulites in decane at room temperature measured by ultra-SANS and mirror-focusing SANS. The power-law behavior of the scattered intensity proves that the spherulites - shown by the micrograph - are dense aggregates with diffuse interfaces.

M-66 Small Angle Neutron Scattering of Polyelectrolytes in Solution

Ralf Schweins¹, **Sebastian Lages**², **Klaus Huber**², **Günter Görigk**³, **Fabien Bonnet**⁴, **Francois Boué**⁵, **Eric Buhler**⁶

¹ILL, LSS group

²Uni Paderborn, Physikalische Chemie

³JCNS, IFF, FZ Jülich

⁴CNRS Grenoble

⁵LLB, CEA Saclay

⁶Université Paris 7

Polyelectrolytes dissolve in polar solvents like water by dissociating in small counterions and polyions. The vicinity of equal and therefore repelling charges along the polymer backbone chain leads to stretched conformations. The addition of an inert electrolyte like NaCl screens the Coulomb repulsion and allows for adopting coiled conformations, like neutral polymers in good solvents. As a consequence, the amount of added NaCl determines the quality of the solvent. This is comparable to a change in temperature which governs the solvent quality for neutral polymers in organic solvents.

We performed scattering experiments on poly(sodiumacrylate) [abbrev. as NaPA] in a good solvent. A few percent of sodium ions were replaced by divalent cations like Ca²⁺, Sr²⁺ and Pb²⁺, which specifically interact with the carboxylate groups, leading to a partial neutralisation of the PA chains. As a consequence, a shrinking of coil dimension which is accompanied by a conformational change is induced. Systematic investigations have been done with combined static and dynamic light scattering, small angle neutron and x-ray scattering in order to elucidate the chain conformation and to check for aggregation.

The second system presented here are mixtures of two different polyelectrolytes that exhibit a different rigidity: the sodium salt of Hyaluronan [abbrev. as NaHA] as a negatively charged semi-rigid biopolymer in the presence of the sodium salt of perdeuterated flexible poly(styrenesulfonate) [abbrev. as NaPSS-d]. By use of the contrast variation technique, we succeeded in elucidating the structure of each single component in the mixture. Influences on the rigidity and aggregation tendencies will be discussed.

M-67 The highly fragile glass former Decalin

Stefan Eibl¹, Helmut Schober², Marie Plazenet², Christiane Alba-Simionesco³

¹ILL, Grenoble; University Paris XI, Orsay

²ILL, Grenoble

³University Paris XI, Orsay

A molecular liquid can be supercooled below its melting temperature, T_m , and form a glass, an amorphous solid, at temperature T_g . The way its dynamical properties (viscosity or relaxation time $\tau\alpha$) evolve with T above T_g provides a criterion to classify it among other liquids differing by their configuration or chemical interactions. This criterion is called fragility, m , or steepness index, as introduced by Angell in 1985 [1]; it focuses on data close to T_g showing how fast the dynamics increase approaching the structural arrest at T_g . It varies from 50 to 90 for most molecular liquids (aromatic, ionic, hydrogen bonded). The relevance of this classification is related to its universality, and several phenomenological attempts have been made in the past to relate it to either microscopic interactions controlling the dynamics via an interaction potential, or vibrational properties of their corresponding glasses. Whereas a number of highly fragile glassformers are found for polymeric materials, only very few examples of molecular liquids have been reported. Among them Decahydronaphthalene (Decalin) plays a central role. It seems to be one of the rare systems in which fragility can be tuned by isomeric mixing ratio [2,3].

Decalin has been investigated using among others elastic and inelastic neutron scattering techniques as well as molecular dynamics simulations. The inelastic data acquired on the neutron spin echo machines allow us to study the relaxation and compare it to predictions of different theories. Other inelastic measurements as well as neutron diffraction experiments were compared to the simulations and give good results as shown in Fig.1.

[1] C.A. Angell, *J non Cryst. Sol.*, 73 (1985) 1-17

[2] K. Duvvuri, R. Richert, *J Chem. Phys.*, 117 (2002) 4414-4418

[3] L. Wang, C.A. Angell, R. Richert, *J Chem. Phys.*, 125 (2006)

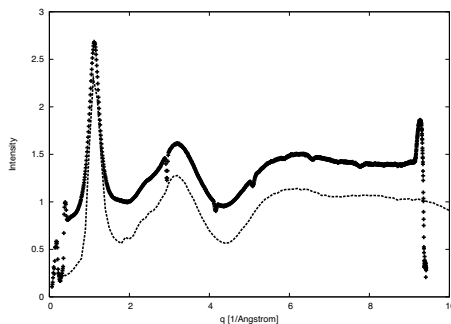


Figure 16.3: Structure of liquid cis-Decalin (crosses) at ambient and $S(q)$ extracted from a corresponding molecular dynamics simulation.

M-68 Molecular Dynamics and Viscoelasticity of Polymer Chains in Presence of Nano Particles

Gerald Johannes Schneider¹, Klaus Nusser², Wim Pyckhout-Hintzen², Andreas Wischniewski², Lutz Willner², Dieter Richter²

¹IFF/JCNS

²IFF

Polymer based nano composites play a crucial role in various applications. Thus, it is not surprising that the research on such materials is continuously increasing. The reason for this is explained by the unique properties, which are not only of interest for the classical field of rubber technology. Meanwhile there are several new applications in the area of micro electronics, such as organic batteries. Due to the blending of nano particles with polymers the composites exhibit improved features. For example, silica-rubber blends show improved tensile properties and silicate-plastics are fire retardant. In order to develop new materials with desired features, a precise knowledge of the dynamics at the microscopic length scale is essential. Although, a lot of studies exist, up to now the relationship between the properties of nano particles and the macroscopic behavior of the blends has not been understood.

In our contribution we present the first results of experiments on the segmental dynamics, and the macroscopic properties of Poly(ethylene-alt-propylene) (PEP)-silica nanocomposites. We will show results of Neutron spin echo (NSE) experiments, which provide the unique possibility to explore the molecular dynamics [1]. Since the coherent single chain dynamic structure factor $S(q,t)$ is measured directly, the NSE experiment is ideally suited to study the influence of nano-particles on the segmental dynamics of the chains. In order to obtain a complete survey of the microscopic situation we performed small-angle neutron scattering and small angle X-ray scattering experiments, which unravel the chain conformation and the size and dispersion of the nanoparticles, respectively.

The microscopic results will be compared to the viscoelastic, i.e. the macroscopic, properties of the blend, which we obtained by means of rheological experiments. The results allow to draw first conclusions. In particular, both neutron scattering and rheological experiments will be discussed in terms of existing models.

[1] D. Richter, M. Monkenbusch, A. Arbe, and J. Colmenero, *Adv. Polym. Sci.* 174, 1, (2005)

M-69 Structure and dynamics of (polyethylene oxide) / layered silicate nanocomposites studied by neutron scattering

Xiuli Jiang¹, Henrich Frielinghaus¹, Wim Pyckhout-Hintzen², Dieter Richter²

¹Jülich Centre für Neutron Science

²Institut für Festkörperforschung

Nanocomposites formed by polymers mixed with filler particles present superior material properties and are attracting more and more interest in polymer science. Research on these nanocomposites has been extended from spherical silica fillers to layered silicates [1]. Meanwhile polymer / layered silicate nanocomposites provide model systems to study the dynamics of confined polymer chains, as the polymers are intercalated into the confined space between the parallel aligned silicate platelets.

Here we present neutron scattering studies on (polyethylene oxide) / Laponite nanocomposites prepared via solution intercalation [2]. By using a protonated / deuterated polymer blend, we should be able to eliminate the scattering contrast between the silicate phase and the polymer phase, if the average scattering length density of the polymer phase is matched to that of the silicate. Debye scattering was expected in small-angle neutron scattering, however, it was not achieved even in the contrast matched samples, due to unavoidable microphase separation between the protonated and the deuterated polymers. The small number of polymers adsorbed on single Laponite particle in solution might be associated with strong composition fluctuations, and these initial deviations from ideal mixing might be amplified by further phase separation during the drying process. To reduce phase separation and investigate further on the reasons for phase separation, a mixture of two random copolymers with different deuterium contents will be used instead of two homopolymers. First results of the dynamics of these confined polymers were also obtained from inelastic neutron scattering experiments, and will be extended in the future.

[1] S. S. Ray and M. Okamoto, *Prog. Polym. Sci.* 28, 1539 (2003).

[2] Z. Shen, G. P. Simon and Y.-B. Cheng, *Polymer* 43, 4251 (2002).

M-70 The volume phase transition of microgels and core-shell hybrid microgels followed by Small Angle Neutron Scattering

Matthias Karg¹, Stefan Wellert², Isabel Pastoriza-Santos³, Jorge Pérez-Juste³, Alain Lapp⁴, Astrid Brandt², Dirk Wallacher², Luis M. Liz-Marzán³, Thomas Hellweg⁵

¹TU Berlin, Stranski-Laboratorium

²Helmholtz-Zentrum Berlin für Materialien und Energie GmbH

³Universidade de Vigo, Departamento de Química Física

⁴Laboratoire Léon Brillouin, CEA de Saclay

⁵Universität Bayreuth, Physikalische Chemie I

Microgels made of the monomer N-isopropylacrylamide (NIPAM) undergo a volume phase transition at a temperature of around 32-33°C. Recently, hybrid microgels containing poly-NIPAM and inorganic nanoparticles such as silica, gold or silver ones have attracted much interest. The main motivation for the preparation of such a composite is the advantage to combine smart behavior of a polymer with the unique properties of nanoparticles in one material.

The overall size of such hybrid particles and also the volume phase transition is typically investigated by dynamic light scattering measurements. Additionally imaging techniques like electron microscopy and atomic force microscopy can be used for particle characterization.

We employed SANS in order to characterize the internal structure of the polymer component in terms of the correlation length ζ , which is not available from light scattering experiments. Measurements at temperatures in the vicinity of the volume phase transition of poly-NIPAM provided the evolution of ζ as a function of temperature. In good agreement to theoretical predictions we found a scaling behavior with a scaling exponent close to 0.625, which corresponds to the 3D Ising prediction for this kind of collapsing network.

Hybrid microgels are possible candidates for many applications such as sensors, photonic crystals, actuators on nm scale, and smart drug carriers. Therefore, understanding of the swelling behavior and the internal structure as well as a comparison to the behavior of pure polymer microgels is essential and a prerequisite to customize their properties in a desired way.

[1] K. Kratz, T. Hellweg, W. Eimer, *Polymer* 2001, 42, 6631-6639

[2] M. Karg, S. Wellert, I. Pastoriza-Santos, A. Lapp, L. M. Liz-Marzán, T. Hellweg, submitted to PCCP

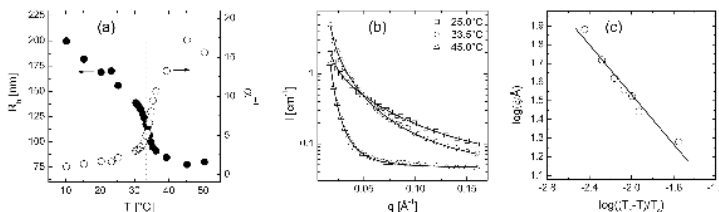


Figure 16.4: Figure 1: Scattering study of a silica-poly-NIPAM core-shell microgel with a core diameter of ≈ 60 nm. a) Hydrodynamic radii and inverse swelling ratio α^{-1} as a function of temperature determined by DLS measurements. b) SANS profiles at three different temperatures. c) Scaling-plot for the correlation length ζ . The linear fit leads to a scaling exponent of -0.67. This is close to the 3D Ising prediction (-0.625).

M-71 Dynamical and structural properties of microemulsions for decontamination of toxic compounds

Stefan Wellert¹, **Matthias Karg**², **Hans-Jürgen Altmann**³, **Andre Richardt**³, **Alain Lapp**⁴, **Bela Farago**⁵, **Thomas Hellweg**⁶

¹BENSC, Helmholtz-Zentrum Berlin, Glienicker Str.100, D-14109 Berlin

²TU Berlin, Stranski-Laboratorium, f. Physikalische und Theoretische Chemie, Strasse des 17.Juni 124, D-10623 Berlin

³Bundeswehr Scientific Institute for NBC-Protection, Humboldtstr. 1, D-29633 Munster

⁴Laboratoire Leon Brillouin, C.E.A.-C.E.N. Saclay, 91191 Gif sur Yvette Cedex, France

⁵Institute Laue-Langevin, B.P. 156, 38042 Grenoble, France

⁶Universität Bayreuth, Physikalische Chemie I, Universitätsstrasse 30, D-95440 Bayreuth

Currently, considerable efforts are being made to develop new media for the decontamination of a variety of toxic compounds. For example, the decontamination of varnished metal surfaces of exterior and interior equipment is very difficult since hydrophobic contaminants have to be extracted from the contaminated surface and brought into contact with hydrophilic reactive agents in order to decompose the toxic compound. In this contribution, we briefly present the phase behavior of the system water-perchloroethylene-IHF-2-propanol. Bicontinuous microemulsions were identified as promising systems on the basis of properties like wetting behavior, extraction capability and decontamination efficiency [1].

These microemulsions were characterized by SANS and NSE measurements. The structural properties of the microemulsions were measured with SANS by a variation of the alcohol content within the bicontinuous region. We discuss the influence of the 2-propanol on the curvature of the amphiphilic film. Additional NSE measurements allowed for the determination of the bending elastic constant based on the theoretical approach of Zilman and Granek [2]. Results obtained from these measurements are discussed with respect to the mentioned application.

[1] S. Wellert, H. Imhof, M. Dolle, H.-J. Altmann, A. Richardt and T. Hellweg: *Coll. & Polym. Sci.*, 286, 417-426 (2008)

[2] A. G. Zilman and R. Granek: *Phys. Rev. Lett.* 77, 4788 - 4791 (1996)

M-72 Anchor architecture in tBLMs

Ann Falk¹, Ingo Köper¹

¹MPI for Polymer Research

Tethered bilayer lipid membranes (tBLMs) are model systems mimicking the structural composition and function of biological membranes. In principal, they consist of a lipid bilayer that is covalently attached to a solid support via an oligomeric spacer group [Raguse1997].

They provide a stable solid supported model architecture to study basic membrane related processes. Furthermore, a highly sensitive and robust artificial membrane could allow for biosensing applications. In biological membranes, the "sensing" part is executed by various membrane proteins. Therefore, the successful integration of such compounds is of great importance. Consequently the molecular architecture of tBLMs is vital to their performance and hence has to be examined and modelled accurately.

For example, the space beneath the membrane which is important for water and ion incorporation but also provides room for larger proteins is usually rather small in tethered membranes.

Also the membrane composition, and hence the fluidity, is not satisfactory solved in this architecture. Biological membranes are composed of various lipids that can change position if necessary. Artificial membrane are usually to unilateral and inflexible, this sometimes proves problematic when larger proteins have to be incorporated. To remedy those drawbacks and still assemble membranes with agreeable sealing properties and membrane fluidity, we tried different approaches (see figure):

- increasing the spacer length of the tether lipids
- tethering lipids with a bulky anchor
- increasing the lateral space of the lipids in the monolayer

We observed that the water content in the sub-membrane space was very sensitive to the packing density of the anchor groups. Additionally, architectures with increased lateral space showed much higher water incorporation then extending the spacer length.

[Atanasova2007] Petia P. Atanasova A molecular approach towards tethered bilayer lipid membranes: Synthesis and characterization of novel anchor lipids, PhD thesis, Universität Mainz (2007)

[Raguse1997] Tethered Lipid Bilayer Membranes: Formation and Ionic Reservoir Characterization Raguse, B., Braach-Maksvytis, V., Cornell, B.A., King, L.G., Osman, P.D.J., Pace, R.J., and Wieczorek, L. *Langmuir*, 14, 3, 648 - 659, 1998, 10.1021/la9711239

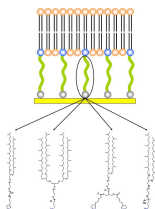


Figure 16.5: Different anchor molecules used in tBLMs synthesised in our group [Atanasova2007].

M-73 Dynamics of Room Temperature Ionic Liquids by QENS

Jan Peter Embs¹

¹Laboratory for Neutron Scattering

In this contribution we present results on cation dynamics in Room Temperature Ionic Liquids (RTILs) obtained by using QENS. It turns out that the dynamics in our RTILs can be described as a confined one. The confining is due to the surrounding ions. The size of confining region increases with increasing temperature. The dynamics inside the confinement can be described using a simple jump diffusion process. Our data can be fitted with one delta-function and one Lorentzian using 6 Angstrom neutrons [2]. The linewidth of the Lorentzian shows a plateau up to a certain wavenvector Q^* while above this Q^* the linewidth increases. This finding is a clear signature of a confining. Using different incident wavelength we can also observe a rotational contribution.

To describe the dynamics inside the confinement there are different models that can be found in literature [3]. We will discuss our data using different approaches and we will show how the size of the cation in our samples will influence the cation-dynamics. Furthermore we will compare our findings to existing MD-simulation data.

[1] F.Volino and M.Dianoux, Mol.Phys. 41, 1980, pp.271

[2] J.P.Embs, E.Reichert, R.Hempelmann, Swiss Neutron News 32, 2007, pp. 4-9

[3] J.P.Embs, in preparation

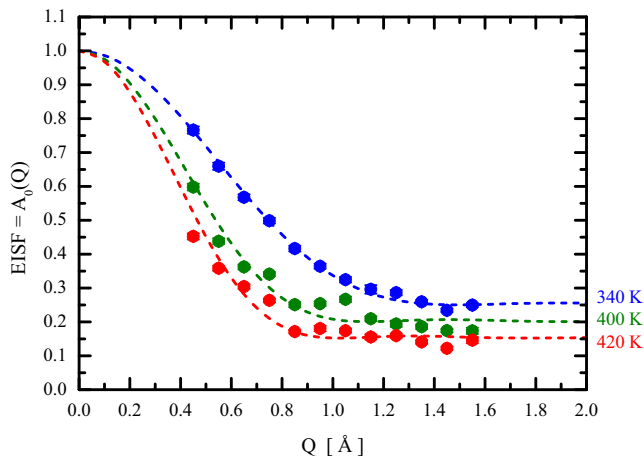


Figure 16.6: Elastic incoherent structure factor for three different temperatures and corresponding fits using the "diffusion-in-a-sphere" model proposed by Dianoux and Volino [1].

M-74 Comparing experiment and theory to understand Pd-NHC catalytic activity in solution

Florian Kargl¹, Gregory A. Chass², Christopher J. O'Brien³, De-Cai Fang⁴, Michael G. Organ⁵

¹IMAPS, Aberystwyth University, Aberystwyth, SY23 3BZ, UK

²School of Chemistry, Bangor University, Bangor, LL57 2UW, UK

³Department of Chemistry and Biochemistry, The University of Texas at Arlington, Arlington, Texas 76019-0065, USA

⁴College of Chemistry, Beijing Normal University, Beijing, 100875, China

⁵Department of Chemistry, York University, 4700 Keele Street, Toronto, Canada M3J 1P3

Pd-catalysed reactions represent a major area of research activity in the molecular sciences. Standard phosphine ligands (P(R)₃) are now challenged by N-heterocyclic carbenes (NHC) of high catalytic activity. The basis of this increased activity is still unknown. Our recent works have provided thermodynamic amendments to the simplified mechanistic picture for alkylzinc couplings devised in literature. These amendments are based on the inclusion of large entropic contributions. Further, a novel Pd-Zn interaction was identified, persisting beyond reductive elimination. It was established that a Pd-center ligated with a bulky NHC, either prepared in-situ[1] or produced by a well-defined complex[2], efficiently mediates a challenging room temperature alkyl-alkyl Negishi cross-coupling of unactivated substrates.

A recent study of Pd-NHC employing AIM-analysis[3] suggested that the motions of the ligand methyl groups are responsible for the level of activity, as is the degree of NHC saturation, effectively retarding/accelerating methyl group movements. Hence this would mean that the catalytic efficiency is intimately coupled to the low energy dynamics of the alkyl-groups. Moreover, it was shown that truncated models are not representative for full model systems[4,5] and that DIMes-Pd and IPr-Pd full model systems reproduce experimental yields within a few % [5].

Here we experimentally underpin these findings by studying the temperature and ligand dependence of methyl group dynamics using neutron spectroscopy. Four Pd-NHC catalysts were investigated using fully-deuterated tetrahydrofuran as solvent. Ligand motions were characterised and activation energies for methyl group rotation were derived. Differences in activation energies for the catalysts are reported and discussed in comparison to results from theory[6].

[1] C. J. O'Brien, E. A. B. Kantchev, C. Valente, N. Hadei, G. A. Chass, A. Lough, A. C. Hopkinson, and M. G. Organ, *Chem. Eur. J.* 12 (2006), 4743.

[2] C. J. O'Brien, E. A. B. Kantchev, G. A. Chass, N. Hadei, A. C. Hopkinson, M. G. Organ, D. H. Setiadi, T.-H. Tangc, and D.-C. Fang, *Tetrahedron* 61 (2005), 9723.

[3] R. F. W. Bader, *Atoms in Molecules, a Quantum Theory*, 1990 (Clarendon Press: Oxford, UK); R. F. W. Bader, and D.-C. Fang, *J. Chem. Theo. Comput.* 1 (2005), 403.

[4] M. G. Organ, G. A. Chass, D.-C. Fang, A. C. Hopkinson, C. Valente, *Synthesis* (in press).

[5] G. A. Chass, C. J. O'Brien, E. A. B. Kantchev, W.-H. Mu, D.-C. Fang, M. G. Organ, A. C. Hopkinson, and I. G. Csizmadia, *Ang. Chem. Int. Ed.* (submitted).

[6] F. Kargl, D.-C. Fang, C. J. O'Brien, M. M. Koza, M. G. Organ, and G. A. Chass, *Ang. Chem. Int. Ed.* (submitted).

M-75 Methyl group dynamics in glassy, polycrystalline, and liquid coenzyme Q10 studied by QENS

Christoph Smuda¹, Sebastian Busch¹, Bernd Wagner², Tobias Unruh¹

¹FRM II

²Physik-Department E21, TU München

A quasielastic neutron scattering (QENS) study on the methyl group rotation of coenzyme Q10 confined in nanosized droplets is presented. Q10 as an oligoisoprene derivative with ten isoprene units can easily be supercooled in nanodroplets. Fixed window scans and QENS spectra at several temperatures of glassy Q10 were recorded to study the methyl group rotation which can be described by a logarithmic Gaussian distribution of hopping rates for temperatures below the glass transition temperature ($T_g \approx 200$ K). A mean activation energy of 4.8 kJ/mol with a distribution width of 2.1 kJ/mol was obtained from the evaluation of the QENS spectra. A corresponding analysis of a fixed window scan yielded an average activation energy of 5.1 kJ/mol with a distribution width of 1.8 kJ/mol. The results are compared and discussed with those of chain deuterated polyisoprene-d5.

For polycrystalline Q10, the QENS spectra could be described by the same model yielding a similar average activation energy as found for glassy Q10. However, no temperature dependence of the distribution width was observed.

Based on the performed low-temperature measurements, the correlation times for the methyl group rotation were extrapolated to temperatures of liquid Q10. The complex dynamics of liquid Q10 could be described by a model yielding an apparent diffusion coefficient, the jump rate of the methyl groups as well as an overall molecular rotational diffusion coefficient. The correlation times of the methyl group rotation in liquid Q10 at a given temperature T_0 coincide with values determined in the glassy phase and extrapolated to T_0 [1]. The activation energy in the liquid phase was found to be essentially zero in agreement to recent studies on methyl group rotation in molecular liquids of small organic molecules [2].

[1] C. Smuda, S. Busch, B. Wagner, and T. Unruh, *J. Chem. Phys.*, submitted

[2] C. Smuda, G. Gemmecker, T. Unruh, *J. Chem. Phys.* 218, 194502 (2008)

M-76 Nanostructures at interfaces: Grazing incidence small angle neutron scattering (GISANS)

Peter Busch¹, Denis Korolkov¹, Emmanuel Kentzinger², Thomas Brückel¹

¹Forschungszentrum Jülich GmbH, Jülich Centre for Neutron Science

²Forschungszentrum Jülich GmbH, Institut für Festkörperforschung

The trend towards miniaturization of functional coatings has pushed the fabrication of nanometer scaled periodic structures at surfaces or interfaces in different fields such as semiconductor industry, magnetism, chemistry, physics and biology. State-of-the-art characterization techniques of the structure of these thin films or nanoparticles include scanning probe microscopy or reflectometry either by X-rays or neutrons. These techniques are however limited to either surface sensitivity, the local structure of a small area or structure variations along the film normal. Grazing incidence small angle scattering either with X-rays (GISAXS) [1] or neutrons (GISANS) [2] are evolving techniques for the structural characterization of both vertical and lateral density variations at interfaces. While with GISAXS mainly structures of supported films or nanoparticles at surfaces are accessible[1,3], GISANS also allows the access to the solid/liquid interface[2a].

On this poster we will present first GISANS results on the small angle scattering instrument KWS-2 of the Juelich Centre for neutron science at the FRM II in Garching. A thin film of a lamellar poly(styrene-*b*-methyl methacrylate) block copolymer was investigated. Additionally the option of polarized neutrons with polarization analysis, which will be available at the second small angle scattering instrument KWS-1 in 2009, will be presented.

[1] D.-M. Smilgies, P. Busch, C. M. Papadakis and D. Posselt, *Synchrotron Radiation News*, 2002, 15, 35-42.

[2] a)Wolff, M. Magerl, A. Zabel, H., *Phys. Rev. Lett.*, 2004, 92, 255501.b) P. Müller-Buschbaum, J. Gutmann, M. Stamm, R. Cubitt, S. Cunis, G. von Krosigk, R. Gehrke and W. Petry, *Physica B*, 2000, 283, 53.

[3] P. Müller-Buschbaum, *Anal. Bioanal. Chem.*, 2003, 376, 3-10.

M-77 Looking closer to the interface: Investigation of polymer dynamics with grazing incidence neutron scattering

Marco Walz¹, Nicole Voss¹, Maximilian Wolff², Hartmut Zabel², Andreas Magerl¹

¹Lehrstuhl für Kristallographie und Strukturphysik

²Lehrstuhl für Experimentalphysik IV/Festkörperphysik

In more complex fluids the conventional non-slip boundary condition becomes microscopically void, and the slip length b may become macroscopic. For a deep understanding of boundary slip the structural and dynamical properties of interfaces on short length scales are essential. Experimental methods with pronounced interfacial feedback are needed. To highlight the properties of the boundary layer we carried out for the first time a neutron spin-echo experiment under condition of grazing incidence (GINSE). With an aqueous solution of a tri-block copolymer with micellar orderings we could verify that the investigation of the dynamics of the sample with GINSE is well feasible and we will present a first data set taken near the critical angle of total reflection.

The authors gratefully acknowledge the financial support by the DFG grants MA801/12-2 and ZA161/18-2 within the priority program SPP 1164 and the BMBF grant ADAM 03ZA7BOC.

M-78 Structural analysis of self-organized diblock copolymers using GISANS

Denis Korolkov¹, Peter Busch¹, Lutz Willner², Emmanuel Kentzinger², Thomas Brückel¹

¹IFF, JCNS

²IFF

Recent success in the production of nanostructures created an interest in scattering techniques as a tool to obtain an averaged characterization of the structural units from a large area of the sample. Grazing incidence small angle neutron scattering is used to obtain information about the correlations in-plane and perpendicular to the plane of the investigated thin film in nanoscale and micrometer scale ranges. GISANS has been applied for various systems such as block copolymers [1] and polymeric systems at the liquid/solid interface [2]. Together with polarized neutron scattering and polarization analysis it gives also access to the in-plane and perpendicular to plane magnetic correlations in complex magnetic systems [3].

In this work we give a theoretical description of GISANS cross-section by means of the distorted wave Born approximation [4]. In order to compare these theoretical approaches with the experimental examples, patterns obtained from self-organized dPS-PB diblock copolymer with cylindrical and lamellar phase are shown. The instrumental smearing effects, obtained directly from the geometry parameters of the instrument and represented by a three-dimensional resolution function, are included in our calculations [5].

[1] Müller-Buschbaum, P. Cubitt, R. Petry, W. (2003). *Langmuir*, 19, 7778

[2] Wolff, M. Magerl, A. Zabel, H. (2004). *Phys. Rev. Lett.*, 92, 255501

[3] Kentzinger, E. Frielinghaus, H. Rücker, U. Ioffe, I. Richter, D. and Brückel, Th. (2007). *Physica B*, 397, 43

[4] Sinha, S. K. Sirota, E. B. Garoff, S. Stanley, H. B. (1988). *Phys. Rev. B*, 38, 2297

[5] Harris, P. Lebeck, B. Pedersen, Jan Skov (1995). *J. Appl. Cryst.*, 28, 209

M-79 Molecular mobility of spider dragline and silkworm silk as a function of humidity studied by neutron spectroscopy techniques

Tilo Seydel¹, Daniel Sapede², Wiebke Knoll³, Imke Diddens⁴, Michael M. Koza¹, Cedric Dicko⁴, Fritz Vollrath⁴, Christian Riekkel⁵, Martin Müller⁶

¹ILL

²ILL + ESRF

³ILL + IEAP, Uni Kiel

⁴Zoology, University of Oxford, U.K.

⁵ESRF

⁶IEAP, Uni Kiel

In the pursuit of contributing to a further understanding of the extraordinary mechanical properties of silk fibres using scattering techniques [1,2,3], we have investigated the molecular mobility of spider dragline silk [4] as well as silkworm silk and adsorbed water in oriented silk fiber bundles. Using cold neutron spectroscopy techniques, information on quasi-elastic scattering arising from molecular diffusion, polymer chain mobility or relaxed relaxation phenomena as well as information on inelastic scattering arising from molecular vibrations has been obtained as a function of the scattering vector. Thus time scales from a few nanoseconds down to below picoseconds and length scales from approximately 0.3 to 1.5nm have been accessed. The interpretation of the results takes into account previously obtained information on the water-accessibility of different structural elements of the silk.

The spectroscopic response of spider silk is discussed in the context of the known behavior of hydrated proteins. To some extent, the behavior of spider silk resembles to the response of a glass-like harmonic solid. The results further indicate that the presence of water leads to slower relaxations in humid spider silk as compared to dry silk. The results also corroborate the enhancement of nanosecond polymer motions in the presence of water. The water mobility inside the polymer matrix is characteristic of a strong confinement in a broad pore size distribution. A comparison is done with the morphologically very similar and more abundant silkworm silk.

[1] D. Sapede, T. Seydel, V.T. Forsyth, M.M. Koza, R. Schweins, F. Vollrath, C. Riekkel; *Macromolecules* 38, 8447 (2005).

[2] T. Seydel, K. Kölln, I. Krasnov, I. Diddens, N. Hauptmann, G. Helms, M. Ogurreck, S.-G. Kang, M.M. Koza, M. Müller; *Macromolecules* 40, 1035 (2007).

[3] I. Krasnov, I. Diddens, N. Hauptmann, G. Helms, M. Ogurreck, T. Seydel, S. S. Funari, M. Müller; *Phys.Rev.Lett.* 100, 048104 (2008).

[4] T. Seydel, D. Sapede, M. M. Koza, M. Müller, F. Vollrath, C. Riekkel; Molecular mobility of spider dragline silk and confined water studied by neutron spectroscopy techniques; submitted.

M-80 Investigation of micellar crystallization in salted solutions

Nicole Voss¹, Marco Walz¹, Max Wolff², Hartmut Zabel², Andreas Magerl¹

¹Lehrstuhl für Kristallographie und Strukturphysik, Universität Erlangen-Nürnberg

²Lehrstuhl für Experimentalphysik / Festkörperphysik, Ruhr-Universität Bochum

Micellar aqueous solutions of tri-block copolymers are an excellent model system for the study of crystallization in soft matter, since they have well-known and rich phase diagrams. The phases can be controlled by varying temperature or polymer concentration, and furthermore the aggregation and crystallization is highly sensitive to the presence of ions.

The addition of alkalimetal-halogenide compounds modifies the attraction between hydrocarbon chains and water, resulting in a linear shift of all phase lines to lower temperatures.

We investigated the influence of CsCl with concentrations up to 1.5 mol/L on the phase diagram of the tri-block copolymer Pluronic P123 which consists of a central part of 70 propylene oxide units terminated by two end groups of 20 ethylene oxide units (EO(20)-PO(70)-EO(20)).

The strong correlation of macroscopic viscosity and structural properties enables a localization of the phases using rheometry, but neutron scattering methods are required to obtain a deeper insight into micellar crystallization processes.

Following this line we performed Grazing Incidence Small Angle Neutron Scattering (GISANS) to investigate the structural properties of the crystalline phases which exist in higher concentrated solutions.

With the objective of correlating these results with micellar form and shape we measured the micellar form factor using Small Angle Neutron Scattering (SANS) at dilute solutions.

In this presentation we combine the results of these complementary techniques, which allows a correlation of macroscopic viscosity, structural properties and intermicellar distance in the crystalline phase, and micellar size and shape.

The work was in part supported by the DFG priority program SPP 1164.

G. Wanka et al., *Macromolecules* 27, 4145, (1994)

Y. Sasanuma, *Macromolecules*, 28, (1995)

C. Guo et al., *Colloid Polym. Sci.*, 277, (1999)

C. Guo et al., *Langmuir*, 15, (1999)

K. Mortensen, *J. Phys.: Condens. Matter*, 8, (1996)

J.-h. Ma et al., *Langmuir*, 23, (2007)

M. Walz et al., *Superlatt. and Microstruct.*, 41, (2007)

M-81 Wasser-in-Öl-Mikroemulsionen - Modellsysteme zur Untersuchung der Dynamik in eingeschränkte Geometrie?

Tinka Spehr¹, Bernhard Frick², Bernd Stühn³

¹ILL / TU Darmstadt

²ILL

³TU Darmstadt

Wir untersuchen die Dynamik von Wasser, AOT- Tensid, Öl Mikroemulsionen (mit Toluol, Dekan oder Heptan) die über einen grossen Bereich stabile Tröpfchen bilden, wobei ein Tröpfchenradius von 0.1- 6 nm über das molare Wasser/Tensid Verhältnis eingestellt werden kann [1]. Da sich das Wasser in kleinen Tröpfchen unterkühlen lässt, könnte dies ein ideales System sein die Dynamik von Wasser in "weicher" eingeschränkter Geometrie zu untersuchen.

Neben temperaturabhängigen KWS Experimenten haben wir Flugzeit und Rückstreuexperimente an partiell deuterierten Mikroemulsionen durchgeführt. Mit KWS finden wir daß kleine Tröpfchen weiter unterkühlt werden können bevor sie abrupt schrumpfen als grössere Tröpfchen. Mit elastischen Scans in Rückstreuung finden wir daß das Wasser im gleichen Temperaturbereich einfriert in dem auch die Tröpfchen schrumpfen [2]. Spektroskopische Messungen (TOF, BS) zeigen eine Verlangsamung der Dynamik des unterkühlten eingeschlossenen Wassers im Vergleich zu normalem Wasser [3]. Modellfits legen nahe, dass die Translation des Wassers stärker von der eingeschränkten Geometrie beeinflusst ist als die Rotation.

[1] S-H Chen, Ann. Rev. Phys. Chem 37, (1986) 351 and references therein.

[2] T Spehr, B Frick, I Grillo and B Stühn, JPCM 20, (2008) 104204

[3] J Teixeira, M-C Bellissent-Funel, S-H Chen and AJ Dianoux, Phys. Rev. A 31, (1985) 1913

M-82 Dynamics of Phospholipids used as Stabilizers in Colloidal Dispersions studied by Quasielastic Neutron Scattering

Sebastian Busch¹, Christoph Smuda¹, Tobias Unruh¹

¹Forschungsneutronenquelle Heinz Maier-Leibnitz (FRM II), Technische Universität München, Lichtenbergstr. 1, D-85748 Garching bei München; and Physik Department E13, Technische Universität München, James-Franck-Str. 1, D-85747 Garching bei München.

Many modern drugs are not water-soluble. To facilitate their intravenous applicability, a drug carrier has to be employed. Phospholipid vesicles or dispersions of lipid nanoparticles stabilized by phospholipids such as dimyristoylphosphatidylcholine (DMPC) are promising candidates. It has been shown that not only the drug release rate but also the storage stability of these systems highly depends on the properties of the stabilizer (Westesen 1997, Bunjes 2003, Bunjes 2007). These properties were investigated i. a. by SAXS (Unruh 2007), revealing that the structure of the monolayer is clearly distinct from what one would expect from the well-known structure of bilayers: It is thinner and the peaks in the electron density profile are less pronounced.

A series of experiments aiming to determine the dynamic characteristics of DMPC in mono-, bi- and multilayers is performed at the time-of-flight spectrometer TOFTOF at the FRM II. A major goal is to link the molecular dynamics with the before-mentioned macroscopic properties like storage stability. First experiments were done comparing the picosecond-dynamics in a dispersion of vesicles, serving as model for phospholipid bilayers, with the one of a stabilizing phospholipid monolayer in an emulsion of deuterated hexadecane in D₂O.

Increased dynamics was observed in the monolayer which can intuitively be correlated with the looser molecular arrangement of the phospholipid molecules in the monolayer (Unruh 2007). Experiments investigating the influence of stabilizing co-emulsifiers on the phospholipid dynamics will also be addressed.

K. Westesen and B. Siekmann; *Int. J. Pharm.*, 151 (1997) 35

H. Bunjes, M. H. J. Koch, and K. Westesen; *J. Pharm. Sci.*, 92 (2003) 1509

H. Bunjes, F. Steiniger, and W. Richter; *Langmuir*, 23 (2007) 4005

T. Unruh; *J. Appl. Cryst.*, 40 (2007) 1008

M-83 Water Uptake in Polyelectrolyte Multi Layers with different charge densities Studied by Neutron Reflectometry

Ralf Köhler¹, Ingo Dönch², Patrick Ott³, André Laschewsky³, Andreas Fery⁴, Rummen Krastev³

¹Helmholtz-Zentrum Berlin

²Max-Planck Institut für Kolloid- und Grenzflächenforschung Potsdam

³Fraunhofer IAP Potsdam

⁴Universität Bayreuth, Physikalische Chemie II

Due to their high potential for application polyelectrolyte multilayer systems (PEM) gained increasing recognition since they were introduced in the 90's. Exploiting the fact that polyelectrolytes adsorb onto surfaces of opposite charge (reversing surface charge), an easy and reproducible preparation technique has been established. This Layer-by-Layer technique (LbL) allows for tuning thickness, density and roughness of PEM in nanometre range.

Exposure to solvent vapour (water) leads to swelling of the whole system mirroring the interplay of the intermolecular forces in the PEM, e.g. ionic and hydrogen bonding, and molecular entanglement. Most studies examining the solvent uptake of PEM have probed only two states: dry PEM and PEM in contact with bulk water. Present neutron reflectometry (NR) study shows results on swelling of PEM at different vapour pressures. Here, NR-technique can play out its strengths to provide independently and simultaneously information on thickness change of the PEM and on its water content (computed from the change of SLD).

The PEM were prepared from deuterated poly-(sodium 4-styrenesulfonate) (dPSS) used as a polyanion and different poly-(diallyldimethylammonium chloride)-derivatives (PDAD-MAC) with charge densities of 100%, 89% and 75% used as polycations, 6 bilayer of PE were deposited (sprayed) onto quartz wafers.

In our study was found that the water content of PEM follows almost linear the relative humidity of surrounding vapours, but swelling rate (swollen divided by dry film thickness) depends nonlinearly from the amount of incorporated water in the multilayers. No significant dependence of swelling and water uptake on charge density was observed in ultra-thin PEM. Instead of proportional relation between swelling and water content, a two-fold swelling behaviour was found, showing two different modes of volume increase with respect to water content. They can be interpreted as a "filling-like" and a "displacement-like"-swelling mode, giving strong hints on a phase separation at higher water contents in PEM.

M-84 Buried structures in thin block copolymer films – time-of-flight neutron reflectometry

Zhenyu Di¹, Lutz Willner², Reinhard Kampmann³, Martin Haese-Seiller³, Christine Papadakis¹

¹Physikdepartment E13, TU München

²Institut für Festkörperforschung, Forschungszentrum Jülich

³Institut für Werkstofforschung, GKSS, Geesthacht

Diblock copolymers form spontaneously oriented structures in thin film geometry, which are of great use for a number of applications, such as the creation of nanoporous films. The aim of our investigation was to gain detailed information on the lamellar structure in thin diblock copolymer films. In supported films of a high molar mass poly((d-styrene)-b-butadiene) (dPS-PB) diblock copolymer, we have observed that the lamellae are perpendicular to the substrate, in agreement with our results on non-deuterated PS-PB [1]. However, one may anticipate a thin overlayer of PB because of its lower surface tension than dPS or a buried layer of dPS or PB near the substrate surface (inset of Fig. 1a). The existence of such layers is important for the accurate calculation of the free energy of the films, which allows the prediction of their orientation [2]. In the case of block copolymers, such a layer is expected to have a thickness of approximately a quarter of the lamellar thickness. To detect possible buried layers or overlayers, we carried out time-of-flight neutron reflectometry (NR).

A thin film was prepared from dPS-PB (molar mass 150 kg/mol) by spin-coating from toluene solution onto a Si wafer with a native oxide layer. The lamellar thickness is 920 Å. NR experiments were carried out at the ToF-reflectometer REFSANS at FRM II with a sample-to-detector distance of 10 m and three incident angles between $\theta_i = 0.40^\circ$ and 1.50° .

The NR curve (Fig. 1) measured over a dynamic range of 10⁻⁵ reveal a high number of well-resolved Kiessig fringes. Fits of different layered structures revealed that the overall film thickness is 3710 Å. The film consists of a near-substrate layer of dPS having a thickness of 192 Å and a mixed layer of dPS and PB on top, i.e. perpendicular lamellae, as previously evidenced using grazing-incidence small-angle X-ray and neutron scattering. We conclude that a near-substrate layer of dPS persists which could be detected in high-resolution ToF-NR experiments on partially deuterated samples.

1. D.-M. Smilgies, P. Busch, C.M. Papadakis, D. Posselt, *Synchr. Rad. News* 15, no. 5, p. 35 (2002). P. Busch, D. Posselt, D.-M. Smilgies, B. Rheinländer, F. Kremer, C.M. Papadakis, *Macromolecules* 36, 8717 (2003). C.M. Papadakis, P. Busch, D. Posselt, D.-M. Smilgies, *Adv. Solid State Phys.* 44, 327 (2004). P. Busch, D. Posselt, M.Rauscher, D.-M. Smilgies, C.M. Papadakis, *Macromolecules* 40, 630 (2007).

2. I.I. Potemkin, *Macromolecules* 37, 3505 (2004). I.I. Potemkin, P. Busch, D.-M. Smilgies, D. Posselt, C.M. Papadakis, *Macromol. Rapid. Commun.* 28, 579 (2007).

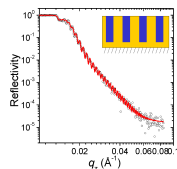


Figure 16.7: Figure 1: ToF-NR curves from the thin dPS-PB film (circles) together with a fit of the layer structure discussed in the text (line). The insert shows the film structure.

M-85 Self-assembly and multi-compartment micellar hydrogel formation of amphiphilic di- and triblock copolymers containing fluorophilic blocks

Christine Papadakis¹, Ruzha Ivanova¹, Tine B. Bonn ¹, Thomas Komenda², Karin L dtke², Kell Mortensen³, P. Klaus Pranzas⁴, Rainer Jordan²

¹Physikdepartment E13, TU M nchen

²Department Chemie, TU M nchen

³KU Life, Copenhagen University

⁴Institut f r Werkstofforschung, GKSS, Geesthacht

Amphiphilic block copolymers in aqueous solution associate reversibly into micelles which offer a large variety of aggregate sizes and shapes, depending on the polymer architecture, composition or structure. Special attention is currently focused on amphiphilic polymers with fluorophilic blocks and especially ABC 'multiphilic' triblock copolymers containing lipophilic, hydrophilic and fluorophilic moieties that have been found to form multicompartment micelles in aqueous solution and, at higher concentrations, micellar networks. Poly(2-oxazoline)s constitute a very versatile system to study the aggregation behavior as a function of the polymer architecture and the hydrophilic-lipophilic balance [1].

We have investigated the self-assembly of novel amphiphilic poly(2-oxazoline) di- and triblock copolymers containing hydrophilic and fluorophilic and/or lipophilic blocks in aqueous solutions by means of small-angle neutron scattering. We have found that the diblock copolymers aggregate into core-shell micelles. The micelles formed by the lipophilic-hydrophilic copolymers are spherical, whereas those formed by the hydrophilic-fluorophilic copolymers are slightly elongated (Fig. 1). In concentrated solution, triblock copolymers aggregate into micellar hydrogels. We could show that the scattering curves of the hydrogels can be described by a coexistence of spherical lipophilic and elongated fluorophilic micellar cores linked by the hydrophilic blocks. Thus the studied poly(2-oxazoline) copolymers have large practical potential as multi-compartment vehicle systems in e.g. medicine or cosmetics.

1. T.B. Bonn , K. L dtke, R. Jordan, C.M. Papadakis, *Macromol. Chem. Phys.* 208, 1402 (2007). C.M. Papadakis, R. Ivanova, K. L dtke, K. Mortensen, P.K. Pranzas, R. Jordan, *J. Appl. Cryst.* 40, s361 (2007). T. Komenda, K. L dtke, R. Jordan, R. Ivanova, T.B. Bonn , C.M. Papadakis, *Polym. Prepr.* 47, 197-198 (2006). T.B. Bonn , K. L dtke, R. Jordan, P. Št p nek, C.M. Papadakis, *Colloid Polym. Sci.* 282, 833 (2004).

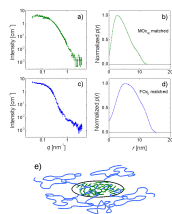


Figure 16.8: (a, c) SANS intensity curves from annealed solutions of hydrophilic/fluorophilic diblock copolymers in D₂O/H₂O and (b, d) corresponding pair distance distribution functions. The lines in (a) and (c) are fits. (a, b) Hydrophilic block matched, (c, d) fluorophilic block matched. (e) Resulting structure of the micelle. Blue: hydrophilic backbone, green: fluorinated side groups.

M-86 Contrast Variation In Small-Angle Neutron Scattering From Magnetic Fluids As Polydisperse Superparamagnetic Systems

Artem Feoktystov¹, Mikhail Avdeev², Victor Aksenov³, Leonid Bulavin⁴, Doina Bica⁵, Ladislau Vekas⁵, Vasil Garamus¹, Regine Willumeit¹

¹GKSS Research Centre, Germany

²Joint Institute for Nuclear Research, Russia

³Russian Research Center "Kurchatov Institute", Russia

⁴Taras Shevchenko Kyiv National University, Ukraine

⁵Centre For Fundamental and Advanced Technical Research, Romania

The contrast variation method in experiments on small-angle neutron scattering (SANS) is a powerful technique, which is now widely applied for studying colloidal systems. It is based on the detection of changes in the scattering from the system when varying the contrast (difference between the mean scattering length densities of the studied particles, and the solvent, where these particles are located). The latter is achieved by partial substitution of hydrogen with deuterium in the solvent. The classical approach [1] deals with systems of monodisperse multicomponent and non-magnetic nanoparticles. For magnetic fluids, which are polydisperse and superparamagnetic systems, the method of the contrast variation requires some modifications [2].

In the present work SANS curves obtained at different contrasts for two kinds of magnetic fluids (magnetite/myristic acid/benzene and magnetite/oleic acid/benzene) are treated in terms of modified basic functions approach [2]. Analysis of the obtained basic functions makes it possible to conclude about the inner structure of nanoparticles in magnetic fluids together with the size polydispersity function. Also, the cluster formation effect is considered. Dependence of the apparent radius of gyration as a function of the inverted contrast gives information about the characteristic radius of the whole (magnetite plus surfactant) particle in the fluid. For magnetic fluid with oleic acid this radius (10.3 nm) is twice larger compared to that for the fluid with myristic acid (5.1 nm), which is in agreement with the data of polarized neutrons scattering [3]. It is shown that the used approach can be efficiently used as a method complementary to the direct modeling of the SANS curves.

[1] H.B. Stuhrmann, In: Small-angle X-ray scattering, Eds. O. Glatter, O. Kratky, London: Acad. Press, 1982.

[2] M.V. Avdeev, *J. Appl. Cryst.*, 40 (2007) 56.

[3] M.V. Avdeev, D. Bica, L. Vékás, et al., *J. Mag. Mag. Mater.*, 311 (2007) 6.

M-87 Lubrication in model joints – a study on shear dependence

Martin Kreuzer¹, Thomas Kaltofen², Roland Steitz¹, Reiner Dahint²

¹Helmholtz-Zentrum Berlin, Methoden und Instrumente (SF1)

²Uni-Heidelberg, Physikalisch-Chemisches Institut

In the last decade, the search for biocompatible materials has become a major topic in medical research. The development of movable and mechanically stressed implants, such as artificial joints, requires optimization of lubrication under shearing forces and pressure. Nowadays researchers try to copy the principles of lubrication observed in natural joints (1). Here, two opposing components are coated by lipids and separated by a liquid phase, which consists mainly of hyaluronic acid (HA). It is generally accepted, that HA plays an important role for the low friction observed. Furthermore it is assumed, that surface active lipids participate in the lubrication (2).

However, the mechanisms and physicochemical parameters to reduce friction are not yet clear and subject of controversial discussions. For achieving closer insight, we represented the biological interface by suitable model systems and employed NR with a shear setup for studying relevant structural features on the molecular scale. As system of choice we used a polyelectrolyte multilayer (PEM) film on a silicon substrate and subsequently attached a lipid bilayer to it by vesicle fusion. As liquid phase we either used pure D2O or a solution of HA in D2O. In a first round of experiments on pure PEM film against D2O or HA in D2O we found that thickness and composition, i.e. scattering length density, of the PEM cushion did not change with applied shear. In a second round we studied the more elaborated system with attached lipid bilayer. Again, by shearing D2O against the system, we did not see any structural changes with applied shear force. In contrast, by shearing an HA solution against the PEM film + lipid bilayer the system responded to shear with a change in thickness and composition.

(1) A. Unsworth, *Phys. Med. Biol.* 52 (2007) 197-212

(2) T. Kawano, *ARTHRITIS & RHEUMATISM* 48 (2003) 1923-1929

M-88 Anomalous changes in the mesostructure of hydrated zirconia xerogels in the vicinity of the point of zero charge

Gennady Kopitsa¹, Vladimir Ivanov², Sergey Grigoriev¹, P. Klaus Pranzas³, Vasyil Haramus³

¹Petersburg Nuclear Physics Institute, Gatchina, Russia

²Institute of General and Inorganic Chemistry, Moscow, Russia

³GKSS Research Centre, Geesthacht, Germany

In the present work, the small angle neutron scattering (SANS), ultra-small angle neutron scattering (USANS) and low temperature nitrogen adsorption techniques have been used to study the fractal properties of Zr-based amorphous xerogels synthesized by the precipitation from the solution of zirconyl nitrate at different pH values. The series of the samples of ZrO₂ xerogels with pH = 3, 4, 5, 6, 7, 7.5, 8 and 9 as well as products of thermal decomposition and hydrothermal treatment of the xerogels were investigated. The SANS measurements were carried out on the SANS-1 and SANS-2 scattering facilities (FRG-1 research reactor, Geesthacht, Germany).

The analysis of SANS, USANS and low temperature nitrogen adsorption data allows to reveal an anomalous effect of the acidity of medium both on the fractal dimension of the xerogels ZrO₂ and the size of the monodisperse particles and their aggregates. It was found that the transition from the pore structure with practically sharp boundaries (DS = 2) to that one with fractal surface (DS = 2.6) occurs with the increasing pH from 3 (acid medium) to 9 (alkaline medium). Moreover, it was shown that similar effect is observed for Hf-based amorphous xerogels [1], which is chemical analog of zirconium. We suggest that the same influence may occur for the rows of the xerogels of transition element hydroxides.

Finally, the influence of the fractal properties of xerogels on the mesostructure of nanocrystalline zirconia powders formed upon annealing and hydrothermal treatment of xerogels was demonstrated.

[1] G.P. Kopitsa, V.K. Ivanov, S.V. Grigoriev, P.E. Meskin, O.S. Polezhaeva and V.M. Haramus, JETP Letters., V.85(2), p.132, 2007.

M-89 Ultrasound-induced changes in mesostructure of amorphous iron (III) hydroxide xerogels: a SANS study

Gennady Kopitsa¹, Vladimir Ivanov², Sergey Grigoriev¹, Alexandr Baranchikov², P. Klaus Pranzas³

¹Petersburg Nuclear Physics Institute, Gatchina, Russia

²Institute of General and Inorganic Chemistry, Moscow, Russia

³GKSS Research Centre, Geesthacht, Germany

Structure and thermal properties of iron(III) hydroxide xerogels obtained under high intensity ultrasonic treatment were studied by means of small-angle neutron scattering (SANS) and heat flux calorimetry. It was established that sonication affects the mesostructure of amorphous xerogels (i.e. increase their homogeneity, surface fractal dimension and the sizes of monomer particles and their aggregate structure) as opposed to the commonly accepted point of view that ultrasonic action cannot lead to notable changes in structure of powders, consisting of nanometer size particles. Ultrasonically-induced structural changes in xerogels are evidently confirmed via their notably different reactivity at thermal decomposition under hydrothermal conditions.

M-90 Neutron Reflectometry - A unique tool to Investigate Diffusion Processes in Solids on the Nanometre Scale

Harald Schmidt¹

¹Institut für Metallurgie/ AG Materialphysik

Self-diffusion is a fundamental matter transport process in solids, which controls various kinetic processes (crystallization, precipitation, growth or creep) important for technological applications. It is also essential for the thermal stability of materials. For a characterization of metastable materials like amorphous or nano-crystalline solids, conventional methods of diffusivity determination (e. g. radioactive tracers) are often not sufficient for a proper characterization. Here, the detection of self-diffusion processes on the scale of 1 nm and below is necessary, which can be achieved by neutron reflectometry [1, 2].

Using our method, the destruction of the artificial order of so-called isotope heterostructures is detected. Isotope heterostructures are chemically homogeneous but periodically isotope modulated layers (e. g. [57Fe(5 nm)/Fe(10 nm)]₁₀), which are produced by magnetron sputtering or molecular beam epitaxy in form of thin films. Due to the different coherent neutron scattering lengths of the stable isotopes, interference effects like fringes or Bragg peaks occur in the reflectivity spectrum. Due to interdiffusion of the isotopes after annealing at elevated temperatures the reflectivity is modified, where from diffusivities can be determined.

We will illustrate this technique and its possibilities for typical model systems like single crystalline Ge, amorphous Si-C-N, and nano-crystalline Fe. Especially, the possibility to determine ultra low self-diffusivities (10^{-25} m²/s), to characterize defect mediated structural relaxations and to measure grain boundary diffusion close to room temperature is demonstrated.

[1] H. Schmidt et al. Phys. Rev. Lett. 96 (2006), 055901.

[2] H. Schmidt et al. Acta Mater. 56 (2008), 464.

M-91 Hydration behavior of casein micelles in thin film: GISANS study

Ezzeldin Metwalli¹, Marie-Sousai Appavou², Ronald Gebhardt³, Jean-Francois Moulin⁴, Volker Körstgens¹, Robert Cubitt⁵, Alexander Tolkach⁶, Ulrich Kulozik⁶, Wolfgang Doster⁷, Peter Müller-Buschbaum⁷

¹Physikdepartment E13, Technische Universität München, D-85747 Garching, Germany

²JCNS-FRM-II, Technische Universität München, D-85747 Garching, Germany

³European Synchrotron Radiation Facility, Grenoble, France

⁴Institut für Werkstofforschung, GKSS-Forschungszentrum Geesthacht GmbH, Germany

⁵Institut Laue-Langevin, 38042, Grenoble, France

⁶Chair for Food Process Engineering and Dairy Technology, TU München, 85354, Weihenstephan, Germany

⁷Physikdepartment E13, Technische Universität München, D-85747 Garching, Germany

Casein micelles in thin films have interesting applications in labeling of glass containers and adhesion technology. Thin dry casein micelles films were prepared via spin coating method [1,2] and allow good access to study water-content of casein micelle in absence of the hydrodynamic hydration water. Using grazing incidence small-angle neutron scattering (GISANS), in situ D₂O vapor swelling of native and Ca-free casein micelles was investigated at different times and temperatures to get insight into the casein micelles structure as a function of water-uptake. The lateral correlation between the micelles at the nano-meter length scale was resolved over 1 minute time scans during the swelling experiment. Our results are discussed and compared with various proposed models on the casein micelle structures. The relatively high water-uptake into the casein micelles thin films favourably supports the coat-core structural model. With no free water exists between the micelles in the dry film, the water-uptake by the protein molecules was tightly bound as monolayer of water at the surface of the micelles.

[1] P. Müller-Buschbaum, R. Gebhardt, E. Mauer, E. Bauer, R. Gehrke, W. Doster, *Biomacromolecules* 7, 1773 (2006).

[2] P. Müller-Buschbaum, R. Gebhardt, S.V. Roth, E. Metwalli, W. Doster, *Biophys. J.* 93, 960 (2007).

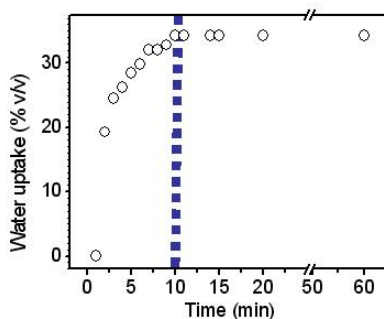


Figure 16.9: Time resolved GISANS scans on casein protein films in D₂O vapor were performed and the water uptake upon swelling is plotted vs time (min). An equilibrium in the overall water content is reached after 10 min.

M-92 Reversible activation of a polyelectrolyte brush: Responsive monolayers.

Roland Steitz¹, **Vasiliki Papaefthimiou**², **Jens-Uwe Günther**³, **Christiane A. Helm**³, **Gerhard G. Findenegg**²

¹Helmholtz Zentrum Berlin für Materialien und Energie

²TU Berlin

³Ernst-Moritz-Arndt Universität Greifswald

Polyelectrolytes anchored on surfaces are important in various applications and are also a challenging topic for fundamental studies. In this work, a monolayer of the PEE114PSS83 [(poly(ethyl ethylene)114 poly(styrene sulfonic acid)83] diblock copolymer was transferred from the air/water interface to a deuterated polystyrene coated silicon (dPS/Si) surface, for evaluation as a tunable polyelectrolyte brush containing system. The grafting density of the polymer film was controlled by changing the lateral pressure during the depositions. X-ray Reflectivity and AFM measurements showed that a homogeneous layer of the block copolymer was formed, whose thickness (maximum 8 nm) increased with increasing grafting density. Neutron reflectivity studies against aqueous solutions revealed a hydrophobic PEE layer attached on the dPS/Si surface, and a carpet/brush polystyrene sulfonate (PSS) double layer in water. The effect of salt concentration on the brush nanostructure was investigated in aqueous solutions containing 0-1 M NaCl. It was found that the brush thickness decreases for salt concentrations above 0.1 M. In addition, reversible activation of the brush by changing the ionic strength of the sub-phase was demonstrated. These results confirm a potential use as a stimuli-responsive polymer for both fundamental studies and biological applications.

M-93 Mineralization in the Presence of Proteins – an Exploration with Small Angle Neutron Scattering using Contrast Variation

Dietmar Schwahn¹

¹Neutronentreuung

Early stages of time resolved mineralization of calcium carbonate and phosphate in the presence of the proteins was explored by SANS using the technique of contrast variation [1-3].

Mineralization of calcium carbonate in the presence of the egg-white protein ovalbumin followed Oswald's law by a step-by-step formation from less stable to more stable polymorphs. The formation of the amorphous mineral polymorph occurred in parallel to denaturation and aggregation of the protein. After about 6h from starting the mineral transformed to the more stable vaterite, and finally after about 10h to the even more stable aragonite. Calcite as the most stable polymorph was not detected within the experimental time [1].

The other protein was fetuin-A which acts as an inhibitor of calcium phosphate mineralization [2,3]. The mineral particles formed in a two-stage process. During the first stage particles of about 300Å were observed immediately after mixing and were stable for about 5 hours. Between 5 and 10 hours the particles slowly increased their size to the order of 1000Å diameter representing the second stage which became stable within the maximum experimental time of about 24 hours. The mineral-organic structure of the particles within their second stage was further analyzed by contrast variation. We found an octacalcium phosphate core and a dense monolayer of the protein, which protects the mineral from further growth until sedimentation takes place.

Acknowledgements: This work was performed within the priority program "Principles of Biomineralization" funded by the German Science Foundation.

1. Vitaliy Pipich, Matthias Balz, Wolfgang Tremel, and Dietmar Schwahn, *J. Am. Chem. Soc. (JACS)* 130 (2008) 6879.
2. A. Heiss, W. Jahnhen-Dechent, H. Endo, and D. Schwahn, *Biointerphases* 2 (2007) 16.
3. Alexander Heiss and Dietmar Schwahn, Chapter 24, pp. 415-433 in *Handbook of Biomineralization, Vol. 1: The Biology of Biominerals Structure Formation* (E. Bäuerlein, P. Behrens, M. Eppe, (eds.), Wiley-VCH, Weinheim) (2007).

M-94 Intrinsic bulk vortex lattice dynamics revealed by time resolved small angle scattering

Sebastian Mühlbauer¹, Peter Böni¹, Christian Pfeleiderer¹, Albrecht Wiedenmann², E.M. Forgan³

¹TUM, Physikdepartment E21

²ILL, HMI

³University of Birmingham

Until nowadays, the access to intrinsic vortex lattice (VL) dynamics in superconductors (SC) as for instance VL melting or Bragg glass transitions was only possible by macroscopic bulk methods, for example by transport measurements or surface sensitive measurement techniques. Therefore, usually thin SC films are used for VL dynamics measurements. A direct consequence of using thin films is the strong influence of surface effects and defects, sample quality and geometry effects on the VL properties of the materials.

We succeeded to combine time resolved stroboscopic small angle neutron scattering (SANS) with an advanced, time varying magnetic field setup allowing to extend the time window for slow dynamical processes from 10 microseconds with TISANE [1] to the range of 10 ms up to several minutes with stroboscopic SANS. The new results demonstrate that it is possible to observe the intrinsic dynamics of the VL in a bulk niobium single crystal on a microscopic scale without any limitations due to surface effects. Field and temperature dependent relaxation times of the VL from 20 to 500 ms could be observed for the first time, allowing to directly measure the Ginzburg-Landau parameters of the system. This new experimental technique provides the possibility to study also the bulk dynamical magnetic properties of various strongly correlated electron systems.

[1] A. Wiedenmann, et al, PRL, 97, 057202, (2006)

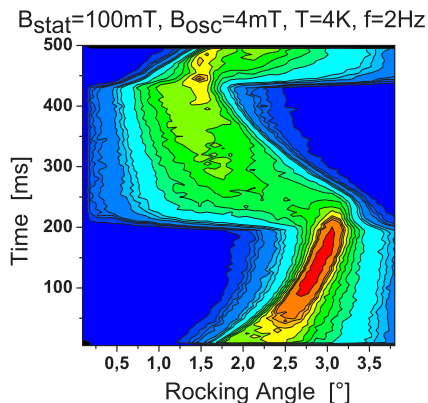


Figure 16.10: Vortex lattice rocking scan showing the relaxation of a VL in superconducting Niobium at 4K between two field-generated equilibrium positions as a function of time, obtained by stroboscopic SANS. The two equilibrium positions are generated by overlaying 100mT static field with 4mT oscillating field in perpendicular geometry. The cycle frequency is 2Hz.

Abstracts: Posters II (Tuesday)

Instrumentation and methods II: T1 - T18
Magnetism II: T19 - T37
Material science and Engineering: T38- T59
Structure research: T60 - T82
Dynamics: T83 - T94

17 Instrumentation and methods II

T-1 Perspectives for Materials Investigations at the Structured Pulse Engineering Spectrometer (SPES) Proposed by GKSS to be Built at ILL or FRM II

Reinhard Kampmann¹, Martin Haese-Seiller¹, Valeri Kudryashov², Andreas Schreyer¹

¹GKSS Forschungszentrum

²PNPI, St. Petersburg

One important goal of modern engineering investigations is to improve our understanding of materials behaviour and failure on a microstructural basis. This requires e.g. measurements of three-dimensional maps of stresses and textures within engineering components or in-situ studies of fatigue behaviour or stresses in rotating machinery. Such experiments are currently extremely time consuming and can thus not be performed to the required extend at modern instruments such as SALSA at ILL or Stress-Spec at FRM II. This results especially from the neutron flux at the continuous sources. New perspectives for engineering applications will be offered by new instruments at MW spallation sources such as VULCAN at SNS.

Against this background the GKSS-Research Centre has recently proposed to build a novel structured pulse engineering spectrometer (SPES) at ILL or at FRM II which is expected to be competitive in performance with Vulcan at SNS for the case of analyses of textures and residual stresses in highly symmetric materials such as Al-alloys or steel. The instrument will be based on a novel ToF-design comprising both a coarse and a fine chopper system. The coarse chopper allows of very high transmission of typically 10% due to its low resolution and will form long pulses. The fine chopper is located close to the reactor wall at a distance of $\approx 40\text{m}$ from the sample and is used to achieve high resolution (up to $\delta_d/d \approx 2 \cdot 10^{-3}$) by modulating the coarse pulses. Despite of its high transmission and resolution the SPES-chopper will allow for measurements without pulse overlap and will thus offer excellent conditions for engineering investigations comprising strain and texture measurements. The design of the instrument will be presented and its expected performance will be compared especially with VULCAN at SNS.

T-2 New Larmor precession based techniques

Erwin Jericha¹, Gerald Badurek¹

¹Atominstytut der Österreichischen Universitäten

We present the concepts of two novel techniques which are based on neutron spin rotation. Dynamical Neutron Polarization (DNP) aims at the loss-free polarization of thermal and cold neutron beams. Contrary to conventional methods which remove one spin state from the incident beam DNP manipulates both spin states differently and achieves full beam polarization with virtually no loss of neutron intensity. The method is based on a small shift in neutron energy in an NMR-like arrangement of crossed static and radiofrequency magnetic fields, followed by time-dependent spin rotation in a homogeneous magnetic precession field. The strength of this field is precisely varied in time and synchronized with a time modulated spin turning device at the exit position which allows to stop the precession when both spin states are aligned parallel.

Spin rotation also plays a decisive role when neutrons pass through a ferromagnetic solid. Polarization control of the incoming and polarization analysis of the transmitted beam combined with tomographic methods in neutron interferometry or 3D polarimetry enables the reconstruction of the magnetic structure. As a result one can expect a complete 3D representation in real space of the magnetization distribution inside the sample. While the concept is comparable to absorption and phase contrast tomography, this technique involves tensorial computation and requires specific reconstruction algorithms due to path-ordering effects contained in the measured projections.

We present conceptual calculations and simulation results for both methods and discuss their potential as well as the technological challenges involved in their realization.

G. Badurek, C. Hartl, E. Jericha, Nucl. Instr. Meth. A 586 (2008) 95

E. Jericha, R. Szeywerth, H. Leeb, G. Badurek, Nucl. Instr. Meth. A 586 (2008) 119

T-3 Performance of the Horizontal ToF-Neutron Reflectometer REFSANS at FRM II Munich, Highlighted by Recent Experimental Results

Reinhard Kampmann¹, Martin Haese-Seiller¹, Jean-Francois Moulin¹, Matthias Pomm¹, Bert Nickel², Andreas Schreyer¹

¹GKSSForschungszentrum Geesthacht

²Ludwig-Maximilians-Universität München

The horizontal neutron reflectometer REFSANS allows to perform comprehensive analyses of vertical and lateral surface and interface structures by means of specular and off-specular neutron reflectivity as well as small-angle neutron scattering at grazing incidence (GI-SANS). All measurements can be performed on the air-water interface (horizontally aligned sample). The design of this novel ToF-instrument is presented and its performance is highlighted by means of recent measurements of weak off-specular scattering, GI-SANS and very low specular reflectivity.

T-4 First experimental test of tensorial neutron tomography

Erwin Jericha¹, Gerald Badurek¹, André Hilger², Nikolay Kardjilov², Ingo Manke², Markus Strobl³

¹Atominstitut der Österreichischen Universitäten

²Helmholtz Zentrum Berlin für Materialien und Energie

³Ruprecht Karl Universität Heidelberg

Tomographic methods and 3D neutron polarimetry allow for a reconstruction of 3D distributions of magnetic fields in principle. This technique exhibits attractive potential for the study of magnetization distributions in ferromagnetic solids. So far the concept has only been pursued with simulations and model calculations. Now we have performed an experiment on the V7 instrument CONRAD at HMI with full polarization control of the incident and full polarization analysis of the outgoing neutron beam. We used a small coil as a model structure for ferromagnetic domains. The tomographic projections were recorded with a 2D position sensitive detector. We present the experimental set-up and the results obtained by this novel technique and by corresponding model calculations. The issue of reconstruction is discussed together with the limitations imposed by present-day neutron source power and detector capabilities. With respect to the joint character of the meeting this work is a concrete example for a lively German-Austrian collaboration in neutron scattering.

E. Jericha, R. Szeywerth, H. Leeb, G. Badurek, Nucl. Instr. Meth. A 586 (2008) 119

H. Leeb, M. Hochhold, G. Badurek, R.J. Buchelt, A. Schrickler, Aust. J. Phys. 51 (1998) 401

T-5 A wedge-shaped polarizing analyzer - ray-trace MC simulations and experimental analysis

Ralf Ackermann¹, Uwe Filges¹, Michael Schneider¹, Jan Peter Embs¹, Rolf Hempelmann²

¹Paul Scherrer Institut

²Universität des Saarlandes

We are developing a polarization option for the cold neutron time-of-flight (TOF) spectrometer FOCUS at the Swiss Spallation Neutron Source SINQ at Paul Scherrer Institut (PSI). For polarization analysis covering the entire scattering region of 120 degree, a novel neutron optics component, i.e. a wide-angle polarizer, is required. Our design concept is based on a wedge-shaped stack of polarizing magnetized supermirrors horizontally bent in a mechanical guide. In our setup, we use remanent magnetized FeCoV/NiN supermirrors with $m = 3$ built at PSI surrounded by a magnetic guide field of about 2 mT. As a first crucial part of our development, we performed test measurements on an analyzer prototype consisting of a stack of 30 mirrors covering about 2 degrees. The polarized beam we used was 1 mm x 40 mm in size and could be varied in wavelength. As a result, we measured a polarization up to 90%. In addition, we analyzed our design concept using neutron ray-trace Monte-Carlo simulations packages McStas and Vitess. Keeping mirror distance and radius of curvature as constant, we calculated polarization and transmission properties of a 4.8 degree section as function of the neutron wavelength, the sample size, and the supermirror length. Values for supermirror reflectivity were obtained both from simple model functions and from experimental data. Assuming a realistic sample width of 10 mm and a mirror length of 137 mm, our calculations result in a polarization better than 98% for wavelengths between 2 Å and 6 Å and a transmission better than 79% for a wavelength of 4 Å. An additional result for this wavelength is the estimated vertical acceptance of our device of about 10 mm, which corresponds approximately to our standard sample size. This work is supported by the German Ministry of Education and Research (BMBF) under grant 03HE7SAA.

T-6 New polarized time-of-flight spectrometer DNS at FRM-II

Y. Su¹, W. Schweika², R. Mittal¹, E. Küssel², F. Gossen¹, B. Schmitz², K. Bussmann², P. Harbott², M. Skrobucha³, R. Möller⁴, M. Wagener⁴, M. Drochner⁴, H. Kleines⁴, A. Iffoe¹, Th. Brückel¹

¹JCNS, Outstation at FRM II, Garching

²IFF, Forschungszentrum Jülich, Jülich

³ZAT, Forschungszentrum Jülich, Jülich

⁴ZEL, Forschungszentrum Jülich, Jülich

DNS is a new cold neutron multi-detector time-of-flight spectrometer with polarization analysis at FRM-II. It has the capability to allow the unambiguous separation of nuclear-coherent, spin-incoherent and magnetic scattering contributions simultaneously over a large range of scattering vector Q and energy transfer E . With its compact size DNS is optimized as a high intensity instrument with medium Q - and E - resolution. DNS is therefore ideal for the studies of magnetic, lattice and polaronic correlations in highly frustrated magnets and strongly correlated electrons. With its unique combination of single-crystal time-of-flight spectroscopy and polarization analysis, DNS is also complimentary to many modern polarized cold neutron triple-axis spectrometers. The first construction phase of DNS has been completed recently. Since then, we have been able to provide intense polarized neutron beams and polarization analysis to both internal and external user groups on the investigations of a wide range of condensed matter materials. Recent highlights on the investigations of spin ice, kagome spin systems and strongly correlated electrons via neutron polarization analysis will be given.

T-7 The innovative upgrading of the SANS instrument D11 at ILL

Peter Lindner¹, Ralf Schweins¹, Antonio Perillo-Marcone¹

¹ILL

The SANS instrument D11 at ILL has undergone a major refurbishment over the past 2 years. For the whole range of collimation distances significant flux gains are expected with a new guide design, as confirmed by MC simulations. The 39 metres of straight glass guides (formerly with constant cross section 30 x 50 mm, width x height) have been replaced by an innovative guide system. It consists of a first diverging section, widening the guide width over the first metres by about 50%. After a 28.5 metres long straight section of 45 x 50 mm width x height, a focusing section has been installed over the last few metres. These changes have been realised in conjunction with the ongoing Millennium Project "D11 Revised" (2005 – 2008).

This important project also includes the development of a larger and faster SANS detector being installed in a new Aluminum detector tube with larger diameter and length, thus increasing the dynamic range and the resolution of the instrument by 100% each. Considerably higher count-rates than at present will be possible (decrease of the detector dead time) and the range of available momentum transfer Q , both towards higher Q as well as to lower Q , will be significantly extended.

K. Lieutenant, P. Lindner, R. Gähler (2007), *J. Appl. Cryst.*, 40, 1056-1063

P. Lindner, R. Schweins (2006) ILL Technical Report ILL06LI02T

T-8 State of art of experimental analysis at the PGAA facility in FRM II

Lea Canella¹, Petra Kudejova², Ralf Schulze³, Nigel Warr³, Andreas Türler¹, Jan Jolie³

¹Institut für Radiochemie, TUM

²Institut für Kernphysik, Universität zu Köln - Institut für Radiochemie, TUM

³Institut für Kernphysik, Universität zu Köln

The Prompt Gamma-ray Activation Analysis (PGAA) is a nuclear analytical technique using the (n,gamma) reaction to determine non-destructively the elemental or isotopic composition of various samples. A new PGAA instrument [1] has been built at the research reactor, FRM II, in Garching near Munich.

The advantage of PGAA to the other comparable techniques is the easy preparation of samples and the quick measurements, thanks to the high neutron flux available. In principle, a complete analysis can be done in 1 day.

Actually, the first samples that arrived at the facility come from industry and different science field, i.e. material science, geochemistry, archaeology, ecology and medicine. This shows a really wide application of this non-destructive analysis.

An important starting point for a reliable analysis is the study of the radiation background during the sample irradiation - also called beam background - due to shielding and structure materials of the instrument.

In January 2008, shielding materials were improved for the two measuring positions available. The total background count-rate for the first position was suppressed to 650 cps with a cold neutron flux of 2.26×10^9 n/cm²s, and a background count-rate of 350 cps was achieved for the second position (with the "elliptical nose") with a neutron cold flux reduced to 0.5×10^9 n/cm²s [2].

First samples analysed are new single-crystal intermetallic compounds, i.e. Mn₃Si, Fe₂TiSn, Ni₃Al and NbFe₂. As an example, a PGAA spectrum for one of these samples is shown in Figure 1.

Other interesting samples analysed by the PGAA facility are iron oxide nanoparticles with boron inside and, concerning boron determination as well, very pure silicon wafers used in electronics. At the moment the detection limit measured for this element is around 1 ppm. To improve this detection limit, further efforts in lowering the background must be carried on.

1] P. Kudejova and G. Meierhofer and K. Zeitelhack and J. Jolie and R. Schulze and A. Türler and T. Materna, The new PGAA and PGAI facility at the research reactor FRM II in Garching near Munich, JRNC in press

2] L. Canella, P. Kudejova, R. Schulze, N. Warr, A. Türler, J. Jolie, Zs. Revay, T. Belgva, First experiments at the new PGAA facility at the research reactor FRM II, Contribution at NRC 7, Budapest 24-29 August 2008.

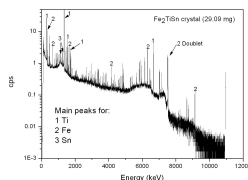


Figure 17.1: Fig.1: Prompt-gamma spectra of a sample of Fe₂TiSn. The sample has a weight of 29.09 mg. The spectrum was acquired in the first measuring position with a cold neutron flux of 2.26×10^9 n/cm²s. Acquisition time was 1200 s.

T-9 SALSA at ILL: flexible beam optics for a large variety of applications

Thilo Pirling¹, Darren Hughes¹

¹ILL

The strengths of the strain imager SALSA at ILL are the capability of extremely flexible sample positioning, and the various adaptable beam optics devices. The load capacity of the robotic sample stage is 1000 kg, providing tilts of 30° and a positioning accuracy of 10 micrometres. The optical devices, comprising radial focussing collimators and automated variable slit systems allow measurements even in large samples with high lateral resolution.

One application, that requires these options, comes from collaboration with SKF on a roller bearing for wind turbines. The central bearing of the drive axis is a key component. It experiences complex stress states, both in the bulk and on the surfaces in contact with the shaft on one side and the rollers on the other. These commonly lead to fatigue failure. The bearing has a diameter of 600 mm and weights 120 kg. In order to align the surfaces, the bearing had to be tilt by 11°. The figure shows the bearing aligned for the measurement of the radial strain component. The 0.6 mm focus radial collimators allowed measurements 60 micrometres close to the surface and provided the necessary penetration.

A new set of collimators provide 2 mm beam width at a focal distance of 380 mm. This leaves room for scanning samples such as the above described bearing in all orientations required for tri-axial stress determination.

All optical components of SALSA can be combined: collimators with 0.6 mm and 2 mm focus, as well as variable automated slit systems ranging from 0.1 mm to 5 mm beam width and 1 mm to 20 mm beam height. The options on SALSA are not only advantageous for large samples but as well for in-situ experiments in sample environment such as stress rigs, cryostats and furnaces.



Figure 17.2: SALSA hosting a 600 mm diameter bearing of a wind turbine for tri axial stress determination in bulk and very near surface.

T-10 IN16B - der Aufbau eines neues Rückstreuспекtrometers am ILL

**Bernhard Frick¹, Tilo Seydel¹, Lambert van Eijck¹, Barthelemy Jean-François¹,
David Bazzoli¹**

¹ILL

Wir berichten über den neuesten Stand des Baus eines Hochfluß-Rückstreuспекtrometers unter Benutzung eines Phasenraum Transformationschoppers (PST) am Ende eines neuen kalten Neutronenleiters H112 am Institut Laue Langevin. Ein neuer ballistischer Leiter wird IN16B mit Neutronen versorgen und sollte einen Neutronenfluß von etwa 10^{10} n/cm⁻²s⁻¹ am PST liefern. Das Sekundärspektrometer wird in einer mobilen Vakuumkammer untergebracht und im Vergleich zu IN16 ist eine Verdoppelung der Analysatorfläche vorgesehen. Neu entwickelte Kristallkassetten haben ausgedehnte Beschleunigungstest bestanden, wobei ein neuer Rekord in der Kristallbeschleunigung aufgestellt wurde. Phasenraumtransformator und Vakuumkammer sind jetzt in der Konstruktionsphase. Eine Besonderheit des IN16B wird seine aussergewöhnliche Flexibilität sein, die es erlaubt am Leiterende im PST Modus mit hohem Fluss oder aber an der Seitenposition mit Deflektor und mit niedrigem Untergrund zu arbeiten. IN16B soll 2011 in Betrieb gehen und sollte dann das Reaktor-Rückstreuспекtrometer mit höchstem Fluss sein.

T-11 The reflectometer Super ADAM at the ILL

Maximilian Wolff¹, Kyryl Zhernenkov¹, Hartmut Zabel¹, Boris P. Toperverg¹, Andrew Wildes², Andrian Rennie³, Björgvin Hjörvarsson³

¹Lehrstuhl für Festkörperphysik

²Institute Laue-Langevin

³University Uppsala

The angle dispersive neutron reflectometer ADAM at the ILL offers high flux combined with an excellent Q resolution and full polarization analysis. We will briefly present some results obtained by the Bochum group during the last years:

1. Exchange bias: The asymmetry in the first and second magnetization reversal of CoO/Co bilayers has been related to nucleation or domain wall movement and magnetization rotation, respectively.
2. Domain walls: Banana shape off-specular scattering has been explained by a simple optical model including refraction at domain walls.
3. Quantum spin states of neutrons: From the intensity at the total reflection edges of a magnetic film the quantum spin state of neutrons inside magnetic samples has been proven.
4. Lateral structures: Correlated magnetic reversal in magnetic stripe arrays was resolved by specular and off-specular neutron reflectivity.
5. Crystallization of micelles: Preferred crystallization of micelles was found close to an attractive interface while crystallization is suppressed close to a repulsive interface.

To further improve the performance of the instrument and remain competitive with recently built reflectometers ADAM is presently reconstructed. The flux will be increased due to a new monochromator and optimised collimation. Optional neutron optic devices will push the limit with respect to the samples size aiming at 1x1 mm² samples. For the polarization analysis contact free flippers and an efficient area polarizer and analyzer will be used. Magnetic fields up to 5 Tesla will be available at the sample position. We expect unique possibilities for the investigation of magnetic thin films due to the high flux (10⁸ without collimation), the low background (9 orders of magnitude dynamic range) and excellent polarization analysis.

Super ADAM is a joint project of the University of Uppsala and the Ruhr-University Bochum supported by the BMBF under contract no.: 03ZA7BOC.

T-12 In-situ SEOP polarized 3He for PA on a polarized reflectometer

Earl Babcock¹, Stephen Boag², Maximillian Skoda², Steve Parnell³, Tim Charlton², Wangchun Chen⁴, Rob Dalgliesh², Chris Frost², Ken Andersen⁵, Thomas Gentile⁴, Shawn Langridge², Ricardo Lopez-Anton², Alexandre Petoukhov⁵

¹JCNS / ILL

²ISIS

³ISIS/University of Sheffield

⁴NIST

⁵ILL

An in-situ 3He polarization system based on the spin-exchange optical pumping method, SEOP, was installed in place of the normal SM analyzer on the polarized reflectometer CRISP at ISIS. The SEOP polarizer was originally constructed to explore the feasibility of using such a system to provide steady-state 3He polarization for particle physics experiments on the PF1B fundamental physics beam line at the ILL. The system utilizes a rectangular mu-metal magneto static cavity similar to the 'magic box' used at the ILL but has been modified to accommodate in-situ SEOP polarization. Two frequency narrowed diode array bars with a maximum output of 60W each provide the optical pumping light. Further the system has an integrated 3He AFP flipper that allows one to reverse the 3He polarization with a simple 5V state signal provided by the CRISP control computer while continuously polarizing the 3He. Relative 3He polarization can be monitored independent of the neutrons via a compact USB-daq based NMR FID system. A 11cm diameter cell containing 1.4 bar/liters of 3He provided by NIST was used. The apparatus was installed in the space where the SM analyzer would otherwise be installed for polarized mode. No modifications, other than installation of a laser security system, were made to the standard instrument, sample environment, or detector configuration. The system was operated continuously for 6 days including 3 days of measurement time with neutrons. A maximum 3He polarization of 66% was observed, and polarization over 61% was maintained over the entire duration of the experiment. It is believed the polarization was limited below the 70%+ maximum obtainable for this cell due to simple optical problems which are easily corrected in the future. Two test samples were measured. A supper mirror fragment, magnetized with the 1T Newport sample magnet, was measured using the point detector to show the angular acceptance of the device and calibrate the efficiency of the devices. Next a magnetized Fe-Fe58 superlattice grating was measured using the line detector to show performance for spin-flip and off-specular spin-flip scattering. Analyzed data from both samples will be presented. It is currently planned to construct a similar system for incident beam neutron polarization on LET at ISIS. Recent knowledge from exploring SEOP when exposed to high flux beams and plans for 3He at JCNS will also be presented.

T-13 POLI-HeiDi: the New Polarised Neutron Diffractometer at the Hot Source (SR9) at the FRM II – Project Status

Vladimir Hutanu¹, Martin Meven², Gernot Heger³

¹Institut für Kristallographie Aussenstelle bei FRM

²TU München Forschungsneutronenquelle Heinz Maier-Leibnitz

³Institut für Kristallographie RWTH Aachen

The project to extend the existing single-crystal diffractometer HEiDi at FRM II to have a polarised neutron option, enabling the investigation of magnetic order in single crystals has been ongoing since autumn 2004. The project is being carried out by the Institut für Kristallographie RWTH Aachen and is financed by the BMBF. After a detailed investigation of the available options it was decided to develop and build a second instrument using the HEiDi monocromator. The design chosen includes options for both 3D polarisation analysis and the flipping ration method to allow spin densities to be determined in a high field. The new instrument has been named POLI-Heidi as an abbreviation of Polarisation Investigator at HEiDi (Heisses Einkristal Diffractometer). Two different zero-field polarimeters will be made available for spherical neutron polarimetry (SNP), CryoPAD and MuPAD. Both polarisation and analysis will be done with 3He spin filters. Recent tests have incorporated several new and important components of the instrument. In this report we will present the results of the first tests of these parts and how they fit with the design concept of the whole instrument. The commissioning of the most important components such as the detector analyser unit Decpol, the zero-field sample environment CryoPAD and the controlling electronics is planned for this year. Next year will see the commissioning of the 3D polarisation analysis as well as the first experiments by external users.



Figure 17.3: POLI-HEiDi during the first test measurements on SR9.

T-14 Solid state lens for neutron focusing

Roland Bartmann¹, Nicolas Behr¹, Thomas Krist¹, Jan-Ekkehard Hoffmann¹, János Füzi²

¹HZB-SF1

²BNC

In neutron instrumentation there is the steady need for flux improvement. The possibilities are on the one hand to increase the source and improve the guide system or otherwise to use some focusing technique. One common method to focus neutrons is done by reflection devices. The solid state lens presented here is an example for such apparatus. Situated behind the exit of a neutron guide the lens can focus the full angular divergence of the guide.

The lens consists of an aluminium housing in which two symmetric wafer stacks are integrated. 95 bent silicon wafers on each side with the wafer dimensions of $20 \times 140 \times 0.15 \text{ mm}^3$. The wafers have different lengths increasing from the inside to the outside of the lens. The coating of the wafers is made of $m=2$ NiTi supermirrors by BNC which will reflect the incoming neutrons along the different wafer channel lengths up to 2 times higher critical angle than pure nickel coatings.

This double sided solid state lens was tested at BENSIC at the neutron tomography station V7.[1] A monochromatized neutron beam with 5 \AA wavelength a cross section of $48 \times 32 \text{ mm}^2$ and a divergence of 0.6° was used. The lens was placed at the higher resolution position in front of the 2D scintillation detector of the CONRAD instrument. The Measurements at the focus position 31mm behind the end of the lens show 5.6 times increased intensity in one dimension compared to the direct beam without the lens inserted. The FWHM of the focus was 2.4mm. A simple lens consisting of only one bent wafer stack was tested before. [2]

[1] R.Bartmann, A.Hilger, N.Kardjilov, T.Krist: Double-sided focusing solid state lens, BENSIC Experimental Reports 2007

[2] T.Krist, N.Behr, J.-E.Hoffmann: Focusing lens and polarising supermirror, BENSIC Experimental Reports 2005

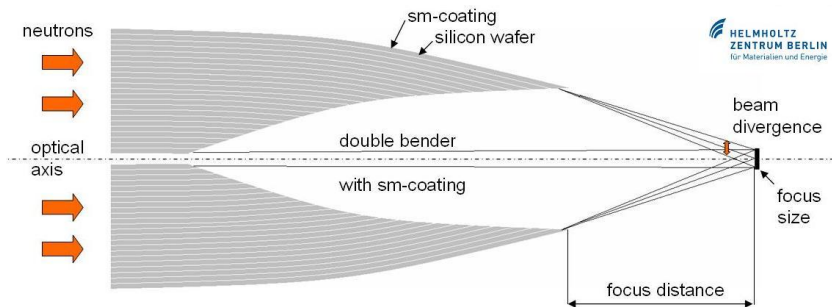


Figure 17.4: Set up of the neutron silicon lens

T-15 A novel analyzer design for the wide angle spin-echo spectrometer WASP

Peter Fouquet¹, Ken Andersen¹, Phillip Bentley¹, Bela Farago¹, Marco Maccarini¹, Gilles Pastrello¹, Iain Sutton¹, Eric Thaveron¹, Frederic Thomas¹, Evgeny Moskvina², Catherine Pappas²

¹ILL

²Helmholtz-Zentrum Berlin

This presentation will give an overview of design recent measurements of the performance of the analyzer bank for the new ILL spin echo spectrometer WASP (Wide Angle SPin echo spectrometer). The aim of the project is to increase flux and acceptance angle of the high signal spectrometer IN11 by changing the design of the magnetic coils.

The design of WASP profits from the experience gained with the novel spectrometer SPAN which has recently been commissioned at the Hahn-Meitner Institute in Berlin, Germany [1,2]. In the SPAN/WASP design nearly perfect 360° field symmetry is achieved by replacing the conventional collinear NSE field solenoids by a pair of anti-Helmholtz solenoids placed above and below the neutron beam plane. Recently we have incorporated genetic algorithms into our design package. Using this tool we have been able to accelerate the rather complex coil design with typically more than 10 free parameters [3].

A critical design change with respect to SPAN and other spin echo spectrometers is the adoption of an analyzer design where supermirrors are magnetized vertically by permanent magnets. This design has been implemented in the diffuse scattering spectrometer D7 at ILL for xyz polarization analysis. Here, we show that this design performs very well for spin echo measurements and can be adopted for WASP.

[1] C. Pappas et al., Physica B 297, 14 (2001).

[2] P. Fouquet et al., J. Neutron Res. 15, 39 (2007).

[3] R. Hölzel, P.M. Bentley and P. Fouquet, Rev. Sci. Instrum. 77, 105107 (2006).

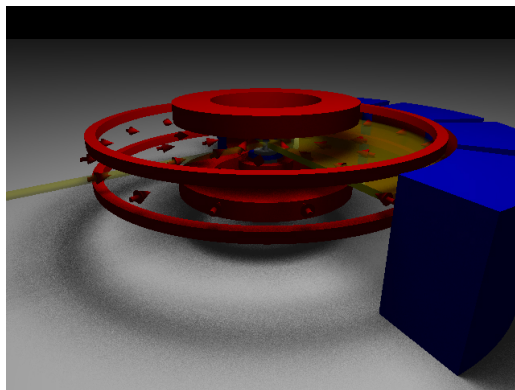


Figure 17.5: Artists view of the WASP neutron spin-echo spectrometer, which is being constructed at the ILL.

T-16 MIRA - New options

Robert Georgii¹

¹FRM-II

MIRA has demonstrated its flexible use as a reflectometer, a small angle scattering instrument and an easy accessible test beam line [1]. Currently we are upgrading MIRA with a second beam port and a HOPG monochromator thus opening the wave length range for neutrons from 3 to 6 Å with an increased flux. Furthermore the MIEZE option of MIRA has been taken into user operation. Progress for both new options will be presented.

R. Georgii et al., Neutron News 18, 25 - 28, 2007.



Figure 17.6: MIRA with the second beam port for neutrons with a wavelength of 3-6 Å .

T-17 The new neutron guide system for the time-of-flight diffractometers at the beamline 7 of the pulsed neutron source IBR-2M Dubna

Christian Scheffzük¹, Walther Kurt¹, Frischbutter Alexander², Bulkin Alexej P.³, Schilling Frank²

¹FU Berlin

²Helmholtz centre GFZ Potsdam

³PNPI Gatchina

Two neutron time-of-flight diffractometers will be operated at the beam lines 7A1 and 7A2 of the pulsed neutron source (5 Hz) at the IBR-2M. They are mainly used for geo-scientific investigations: Strain/stress experiments (EPSILON-diffractometer) and texture is determined (SKAT-diffractometer). The available wide wavelength band offers the possibility to observe diffraction lines with the lattice spacing up to 5.3 Å, simultaneously.

In the past both diffractometers had used a common neutron guide with dimensions of $H \times W = 170 \text{ mm} \times 50 \text{ mm}$ by dividing the neutron beam (lower and upper part), each for $H \times W = 85 \text{ mm} \times 50 \text{ mm}$. Because of variant reasons the neutron flux at sample position was very low.

Besides of the low flux another drawback of the old guide was a large background. He was caused by fast neutrons and the insufficient shielding of the diffractometers. Therefore, it was decided to separate the diffractometers from each other and to install bent guides. The curvature radius was chosen to be 13400 m and to have a length of 85 m. The critical wavelength will be 1.58 Å.

The spatial separation of the diffractometers requires two guides. At the same beam line 7 is installed a further straight guide (7B) providing neutrons for the spectrometer NERA. In order to get an optimal flux for all three facilities a guide splitter will become necessary.

At the neighbouring beamline 8 of the IBR-2M will be installed a cold source, which will partial seen by the beamline 7 too. It is expected a large wavelength band up to $\lambda = 12 \text{ Å}$, the frame overlapping will occur at $\lambda = 7.8 \text{ Å}$. Therefore, a "lambda-chopper" is planed to suppress each second neutron pulse to extend the available diffraction pattern. This will give the possibility to observe low-indexed peaks with very large lattice spacing up to $d = 8.5 \text{ Å}$.

T-18 A quantitative study of neutron scattering related publications of all ENSA members from 2004 to 2006

Helmut Rauch¹, Thomas Oesterreicher¹

¹Atominstitut der Österreichischen Universitäten

One of the future criteria of measurability of science in different scientific fields will be the number of publications and the corresponding number of citations of these publications. For Neutron Scattering Related Topics, including Neutron Scattering, SANS, USANS, Neutron Diffraction, Neutron Radiography, Tomography and Interferometry, Spin-echo, Polarized Neutrons and Neutron Optics, we have analyzed about more than 95% of the publications of the ENSA member countries from 2004 to 2006 that could be reached within the Science Citation Index,-database. With this bibliographic poster we want to present our results, give a short overview for optimized database research and some interesting details.

18 Magnetism and dynamic II

T-19 Magnetism and Superconductivity in Cd-doped CeCoIn₅

Ulrike Witte¹, Oliver Stockert², Michael Nicklas², Roland Schedler³

¹IFP, TU Dresden

²MPI CPfS Dresden

³HMI Berlin

Coexistence and competition between magnetism and superconductivity continue to be of central interest in condensed matter physics. CeCoIn₅ is a heavy-fermion superconductor with one of the highest transition temperatures of $T_C = 2.3$ K among heavy-fermion systems. Doping with cadmium leads in CeCo(In_{1-x}Cd_x)₅ to antiferromagnetic order above a critical nominal Cd concentration of 5 % and superconductivity is successively suppressed until for nominal 15 % Cd doping no more superconductivity is observed. In the intermediate doping regime from 5 % to 15 % the subtle interplay between magnetism and superconductivity can be studied. We performed extensive elastic neutron scattering experiments on 7.5 % Cd doped CeCoIn₅ to study the antiferromagnetic ordering and the possible influence of superconductivity on the magnetism. A strong interplay of both phenomena is expected, since superconducting transition temperature $T_C = 1.7$ K is close to the Néel temperature $T_N = 2.4$ K. We found the magnetic structure to be commensurate with $QAF = (0.5 \ 0.5 \ 0.5)$ below T_N in agreement with results on a 10 % Cd doped sample [1]. The magnetic intensity increases below T_N , displays a kink at T_C and saturates at a reduced value. Hence, a clear effect of superconductivity on the antiferromagnetic order is seen, but still both phenomena do coexist. Data collected at different magnetic fields and temperatures revealed the magnetic (B,T) phase diagram. Our results will be discussed in comparison to other magnetic heavy-fermion superconductors.

[1] M. Nicklas et al. Phys. Rev. B 76, 052401 (2007)

T-20 Twisted magnetization state in an antiferromagnetically coupled Fe/Si multilayer as probed by specular and off-specular polarized neutron scattering

Amitesh Paul¹

¹Helmholtz-Zentrum Berlin für Materialien und Energie GmbH

We have investigated strongly coupled Fe/Si multilayers by polarized neutron scattering in specular and off-specular modes. Using the specular reflectivity patterns as a function of the applied field, we have extracted the magnetization angles for layers buried in the stack. In order to explore the magnetization depth profile across the interfaces the neutron data have been combined with micromagnetic simulations. A rigid/uniform approximation of the layer magnetization is found to describe the data over a considerable range of the applied field, but reveals significant shortcomings around an intermediate field between remanence and saturation. For these intermediate field values, we found: (i) a close agreement of the magnetization state with a twisted state model, which indicates the formation of exchange-spring type spin structure, (ii) depending upon the magnetic history of the specimen, an enhanced off-specular magnetic scattering of neutrons at the antiferromagnetic Bragg-peak positions, which indicates the presence of buried domains. However, an extraction of the state of magnetic chirality within a single ferromagnetic layer is in itself challenging and is further complicated as the length scale of these domains becomes smaller than the neutron coherence length [1].

[1] Amitesh Paul, Mathias Buchmeier, Daniel Bürgler, Ulrich Rücker, Claus Schneider Phys. Rev. B, 77, 184409, 2008.

T-21 Reversal Mechanism and Suppression of Training in Exchange Coupled System

Amitesh Paul¹

¹Helmholtz-Zentrum Berlin für Materialien und Energie GmbH

We show that the extent of training in exchange biased systems can be strongly influenced by the field cooling procedure. This phenomenon is revealed by comparing the behavior of the system in two different magnetic configurations: cooling the system in a remanent state without an external magnetic field (state I) results in a suppression of the training effect, whereas the same sample being field-cooled (state II) exhibits a clear training response. Interestingly, by cooling the sample in a critical field H_{FC} close to the coercive field H_C of the ferromagnet, we find a peculiar situation with a coexistence of states I and II. By using a depth-sensitive polarized neutron reflectivity technique, we can establish a clear correlation of the reversal mechanism with either the untrained or the trained state [1].

[1]Amitesh Paul, Claus M. Schneider, Jochen Stahn Phys. Rev. B, 76, 184424, 2007.

T-22 Homogeneity and inhomogeneity in Dilute Magnetic Semiconductors

Amitesh Paul¹

¹Helmholtz-Zentrum Berlin für Materialien und Energie GmbH

We investigate chemical and magnetic homogeneity of Ge based dilute magnetic semiconductors (DMS) by polarized neutron reflectivity. We find our DMS films to be fairly homogeneous throughout the depth of the film, in contrast to the inhomogeneity identified by transmission electron microscopy technique or indicated by their magnetization behavior. Sensitive depth profiling for such low concentration of magnetic-ions, is largely challenged by the low signal-to-background ratio over a large dynamical range of momentum transfer [1].

[1]Amitesh Paul, Timothy Charlton (to be published).

T-23 Magnetic Excitations in Rare-Earth Superlattices studied with Three-Axis-Spectroscopy

Alexander Grünwald¹, Elena Tartakovskaya², Andrew Wildes³, Wolfgang Schmidt⁴, Katharina Theis-Bröhl⁵, Roger Ward⁶, Peter Link⁷, Andreas Schreyer¹

¹GKSS Research Centre

²Institute of Magnetism NAS of Ukraine

³Institut Laue-Langevin

⁴Jülich Centre for Neutron Science

⁵University of Applied Sciences Bremerhaven

⁶University of Oxford

⁷Forschungsneutronenquelle Heinz Maier Leibnitz

Magnetic multilayers are of great interest for tailor-made magnetism and to understand new properties of magnetism and spin dynamics in confined structures and quasi 2-D nanostructures. Several characteristics can be derived from the dispersion of fundamental magnetic excitations – spin waves. Our theory predicts discrete energy levels and Brillouin zone folding effects for spin waves propagating normal to the interfaces in long-range exchange-coupled rare-earth superlattices due to the periodic sample structure. Inelastic neutron scattering is the most versatile technique to study spin dynamics and magnetic excitations, and a well-established method to investigate bulk materials. In the past we have shown that, despite the small amount of magnetic material in the beam, three-axis-spectroscopy can be used to study magnetic excitations in rare-earth superlattices [1].

Here we report on magnetic excitations in Gd/Y and Dy/Y superlattices investigated with cold three-axis-spectroscopy on the high flux instruments PANDA (FRM-II), IN12 and IN14 (ILL). The ferromagnetic Gd slabs show simple antiferromagnetic coupling between the layers and a weak signal is observed from low energy excitations. A ferromagnetic order of the Gd layers can be induced with a moderate, applied magnetic field. In this phase a spin wave gap opens up at the Brillouin zone center. In the Dy/Y superlattice the Dy exhibits an incommensurate, long-range helical order which is coherent over many bilayers. The observed inelastic signals are broad in energy. Similar results have been obtained on a (thick) Dy film, consistent with previously published results on bulk Dy [2], suggesting that a broad width is intrinsic and not purely due to the superlattice structure. In both superlattice compounds, clear dispersive modes from magnetic excitations propagating normal to the interfaces have been followed and indications on discrete energy levels have been found.

[1] A. Schreyer et al., J. Appl. Phys. 87, 5443 (2000)

[2] R.M. Nicklow, J. Appl. Phys. 42, 1672 (1971)

T-24 Do antiferromagnetism and superconductivity coexist in 2% and 10% Ge doped CeCu_2Si_2 ?

Julia Arndt¹, **Oliver Stockert**¹, **Robert Borth**¹, **Enrico Faulhaber**², **Karin Schmalzl**³, **Astrid Schneidewind**², **Hirale Jeevan**¹, **Christoph Geibel**¹, **Michael Loewenhaupt**², **Frank Steglich**¹

¹Max-Planck-Institut für Chemische Physik fester Stoffe, Dresden

²Institut für Festkörperphysik, TU Dresden

³Institut für Festkörperforschung, FZ Jülich GmbH, Jülich Centre for Neutron Science at ILL, Grenoble

The heavy-fermion compound CeCu_2Si_2 exhibits different ground states in subtle dependence on the stoichiometry: Incommensurate magnetic order (A), superconductivity (S), or both phenomena (A/S). Ge doping decreases the hybridisation between the localised Ce 4f and the conduction electrons, and therefore allows for studying the evolution of superconductivity in the presence of a stabilised magnetic A phase. NQR and μSR measurements on polycrystals suggest coexistence of superconductivity and antiferromagnetism in 2% and 10% Ge doped CeCu_2Si_2 . We performed heat capacity, ac susceptibility, and elastic neutron scattering measurements on single crystals at different temperatures and magnetic fields. The zero field transition temperatures in 2% Ge doped CeCu_2Si_2 are still close to those in A/S CeCu_2Si_2 ($T_c = 500$ mK, $T_N = 700$ mK), whereas in 10% Ge doped CeCu_2Si_2 $T_c = 120$ mK and $T_N = 1.3$ K differ by an order of magnitude. Our neutron scattering results show that, while a phase separation between magnetic and superconducting volumes takes place in 2% Ge doped CeCu_2Si_2 , antiferromagnetism and superconductivity coexist on the microscopic scale in 10% doped CeCu_2Si_2 . These results might indicate that a stabilised magnetism is favourable for its coexistence with superconductivity.

T-25 Nature of magnetic correlations at the martensitic transformation in Ni-Mn-based Heusler systems studied by neutron polarization analysis

Seda Aksoy¹, Mehmet Acet¹, Pascal Deen², Lluís Manosa³, Antoni Planes³

¹Universität Duisburg-Essen, Germany

²Institut Laue-Langevin, France

³Universitat de Barcelona, Catalonia, Spain

In Ni-Mn-based Heusler alloys undergoing martensitic transformations, a sudden drop in the magnetization just below the transformation is observed. This loss in magnetization is thought to be related to the development of either a reentrant paramagnetic state or to the development of anti-ferromagnetic short-range ordering. To resolve this issue we employ polarization analysis and find indeed the presence of antiferromagnetic correlations below martensitic transformation in Ni-Mn-Sb and Ni-Mn-Sn.

T-26 Study of the Self-Ordering of Cobalt Nanoparticles by PNR and Polarized SANS and GISANS

Katharina Theis-Bröhl¹, Maximilian Wolff², Boris P. Toperverg², Charles D. De-whurst³, Inga Ennen⁴, Britta Vogel⁴, Andreas Hütten⁴

¹University of Applied Science, 27568 Bremerhaven

²Ruhr-University Bochum, D-44780 Bochum, Germany

³Institut Laue-Langevin, F-38042 Grenoble, France

⁴Bielefeld University, D-33615 Bielefeld

Magnetic nanoparticles are potential candidates for future data storage as well as vehicles for biomedical, e.g., in therapy and diagnosis, applications. From this point of view nanoparticles with high magnetic moments are under consideration as a new magnetic particle generation and deserve detailed and comprehensive investigation using various physical methods.

In this study a combination of polarized neutron reflectometry (PNR) and polarized small angle scattering (POLSANS), partly applied under grazing incidence (POLGISANS), was employed to deduce the structural and magnetic arrangement of cobalt-oleyl amine nano-complexes prepared by layer-by-layer dropping on a silicon substrate. For this study we prepared a film of 20 layers of Co nanoparticles with a diameter of 13 nm. The nanoparticle film shows a ferromagnetic hysteresis loop already at room temperature as was measured by alternating gradient magnetometry.

The ferromagnetic properties are expressed in the PNR curves via a certain splitting between the R₊₊ and the R₋ reflectivities. Fitting the PNR data leads to the result that the magnetization of the Co nanoparticles maintains its saturation value. For the out-of-plane ordering of the nanoparticles on the Si substrate we expected a layering manifested by a Bragg peak due to the periodic superstructure. Such a layering, however, was not found, at least not in a range higher than the lateral coherence length of about 100 μm. Nevertheless, via fitting of the PNR data we were able to deduce the film thickness and the nuclear (Nb) and magnetic (Np) scattering length densities of the Co-oleyl amine complex. Comparing Nb and Np leads to the conclusion that the Co nanoparticles are surrounded by a CoO shell. From the POLSANS and the POLGISANS maps we find a Debye-Scherrer ring, mostly pronounced in the spin asymmetry between I₊ and I₋. From this we conclude that the nanoparticles are self-organized into a 3D paracrystalline-like lattice with the positional order well defined over a few inter-particle spacings.

We acknowledge funding by BMBF (O3ZA6BC1) and by ILL. Furthermore we would like to thank C. Waltenberg and D. Meißner for the synthesis of the nanoparticles.

T-27 Neutron scattering study of $\text{Ce}_2\text{Pd}_{(1-x)}\text{Co}_x\text{Si}_3$ ($x = 0.0, 0.8, 1.0$)

Wolf-Dieter Stein¹, Peter Link², Matthias Frontzek¹, Marek Koza³, Jens-Uwe Hoffmann⁴, Nadja Wizent⁵, Wolfgang Löser⁵, Michael Loewenhaupt¹

¹IFP, TU-Dresden

²FRM2, TU-München

³ILL, Grenoble

⁴HMI, Berlin

⁵IFW, Dresden

Compounds of the type R_2PdSi_3 (R = rare earth) with AlB_2 -derived structure have gained much interest in the last years due to their interesting magnetic properties. The interplay of crystalline-electric-field (CEF) and indirect exchange [Ruderman-Kittel-Kasuya-Yosida (RKKY)] of the $4f$ magnetic moments in combination with the Kondo effect in Ce-based systems was the motivation for new investigations of related systems. In the solid solution system $\text{Ce}_2\text{Pd}_{1-x}\text{Co}_x\text{Si}_3$ a quantum critical point arises at $x \approx 0.8$ between the antiferromagnetically ordered Ce_2PdSi_3 with $T_N \approx 3\text{K}$ and the non-magnetic Kondo lattice Ce_2CoSi_3 . Detailed knowledge of the magnetic structure and the CEF-effect is fundamental for understanding the nature of the magnetic properties in these compounds.

Ce_2PdSi_3 crystallizes in the AlB_2 structure (P6/mmm) with the magnetic Ce atom occupying the Al position and the non-magnetic Pd and Si atoms distributed over the B positions [Szytula1999a,Wawrzynska2004a]. The anti-ferromagnetic structure has been investigated by neutron diffraction on powder samples, however, the structure is still matter of debate. For clarification, we performed neutron diffraction experiments on single crystals at E2 (HMI, Berlin) and Panda (FRM2, Garching).

The magnetic, thermal and transport properties of this compound have been studied on poly-crystalline samples [Szytula1999a,Mallik1996a] and on single crystals [Saha2000a,Saha2000b]. Large anisotropies in the transport and magnetic properties are mainly associated to the CEF-effect. From inverse susceptibility measurements a CEF-model was proposed with excited crystal field levels at 2.3 meV and 10.8 meV.

We performed inelastic neutron scattering experiments with polycrystalline samples on IN4 and IN6 (ILL, Grenoble) for the study of the CEF-excitations in the the solid solution system $\text{Ce}_2\text{Pd}_{1-x}\text{Co}_x\text{Si}_3$ ($x= 0.0, 0.8, 1.0$). While in the pure Pd-compound CEF-excitations could be observed, in the two Co-containing systems no CEF-excitations were found in the range from 0.2 to 20 meV.

A. Szytu a et al.; J. Magn. Magn. Mater. **202**, 365 (1999). E. Wawrzyska et al.; J. Alloys Comp. **373**, 73 (2004). R. Mallik et al.; J. Magn. Magn. Mater. **164**, L13 (1996). S. R. Saha et al.; Phys. Rev. B **62**, 425 (2000). S. R. Saha et al.; Physica B **281/282**, 116 (2000).

T-28 Magnetic Excitations of a Distorted Kagome Antiferromagnet

Richard Mole¹, **Paul Wood**², **Gerald Weldon**², **John Stride**³, **Tobias Unruh**¹, **Paul Henry**⁴

¹Technische Universität München, Forschungsneutronenquelle Heinz Maier-Leibitz (FRM II), D-85747 Garching

²University of Cambridge

³UNSW

⁴ILL

Strongly frustrated systems in two dimensions have been much studied due to the possibility of exotic ground states and unusual excitation spectra. The kagome lattice is a good example of this, being a two dimensional lattice with a large number of frustrating interactions. Here we present the first results of the neutron diffraction and inelastic neutron scattering (INS) of a distorted kagome lattice with classical $S = 5/2$ spins, $\text{Mn}_3(\text{C}_6\text{H}_3(\text{COO})_3)_2$. The data obtained shows that the system shows some properties of the compound are indicative of a ferrimagnetic ground state, whereas the INS shows characteristics of a more strongly frustrated system. All results highlight a possible misinterpretation of the recently published susceptibility data (1) on this compound.

1. Partha Mahata, Diptiman Sen and Srinivasan Natarajan, Chem. Commun., 2008, 1278

T-29 Spin dynamics in superconducting CeCu₂Si₂

Oliver Stockert¹, Julia Arndt¹, Karin Schmalzl², Hirale S. Jeevan¹, Christoph Geibel¹, Michael Loewenhaupt³, Frank Steglich¹

¹Max-Planck-Institut CPfS, Dresden

²IFF, FZ Jülich, JCNS at ILL, Grenoble

³Institut für Festkörperphysik, TU Dresden, Dresden

Continued experimental and theoretical interest in the prototypical heavy-fermion compound CeCu₂Si₂ arises from the interplay between antiferromagnetic order and superconductivity. Superconductivity occurs in the vicinity of the quantum phase transition where magnetic order vanishes as a function of an external control parameter. Pressure as well as chemical composition can act as such control parameters. The complex chemical phase diagram of CeCu₂Si₂ results in different ground states: magnetically ordered, superconducting or exhibiting both, antiferromagnetism and superconductivity.

We will report on elastic and inelastic neutron scattering experiments on CeCu₂Si₂ to elucidate the antiferromagnetic order and its interplay with superconductivity. The magnetic order with a quite small ordered moment is an incommensurate spin-density wave determined by the nesting properties of the Fermi surface. Our experiments on single crystalline samples clearly revealed that antiferromagnetism and superconductivity exclude each other on a microscopic scale. In the superconducting state of CeCu₂Si₂ for the first time a spin excitation gap with an inelastic peak has been observed in the excitation spectrum. This gapped excitation shows dispersion. In addition, elastic short-range magnetic correlations seem to survive in the superconducting state. Since we probe the 4f spin dynamics by inelastic neutron scattering, this is again an indication that the Ce 4f electrons are involved in the Cooper pair formation of the superconducting state. Entering the paramagnetic state of CeCu₂Si₂ the magnetic response becomes quasielastic. Our results will be discussed in comparison to other heavy-fermion compounds and high temperature superconductors.

T-30 Magnetic ordering in MnSe studied using polarized neutrons

A. Das¹, R. Mittal², Y. Su², J. B. C. Efre³, K. R. Priolkar³, W. Schweika⁴, Th. Brückel⁵

¹Solid State Physics Division, Bhabha Atomic Research Centre, Mumbai, India 400085

²Jülich Centre for Neutron Science, Institut für Festkörperforschung, Forschungszentrum Jülich, Outstation at FRM-II, Lichtenbergstrasse 1, D-85747 Garching, Germany

³Department of Physics, Goa University, Goa 403206, India

⁴Institut für Festkörperforschung, Forschungszentrum Jülich GmbH, D-52425 Jülich, Germany

⁵Jülich Centre for Neutron Science, Institut für Festkörperforschung, Forschungszentrum Jülich, Outstation at FRM-II, Lichtenbergstrasse 1, D-85747 Garching, Germany; Institut für Festkörperforschung, Forschungszentrum Jülich GmbH, D-52425 Jülich

Manganese chalcogenides, MnS, MnSe, MnTe etc., are anti ferromagnetic compounds. MnSe crystallizes in cubic NaCl structure. Magnetic susceptibility of MnSe exhibits anomalous behavior at 160 K. This anomalous behavior had been attributed to structural transition. Our earlier reported study, using unpolarized neutron diffraction technique, indicate that at low temperatures MnSe has two coexisting crystal structures, cubic NaCl and hexagonal NiAs [1]. NiAs phase appears below 266 K and is antiferromagnetically ordered at all temperatures while the NaCl phase orders antiferromagnetically at 130 K. However, there were limitations in this study as there were overlapping nuclear and magnetic reflections. Therefore we have made xyz polarization analysis to separate the magnetic scattering from nuclear and spin incoherent scattering. The measurements were carried out DNS spectrometer at FRM-II reactor. An incident neutron beam of 4.74 Å was used for the measurements. Polarized neutron diffraction data was collected at six temperatures in the temperature range 2 K to 300 K. At 300 K, only the non spin flip (NSF) Bragg scattering is observed. At 225 K, super lattice reflections are observed. Spin flip (SF) contribution to NiAs phase reflections in addition to NSF is observed. For $T \approx 110$ K, SF contribution to reflections indexed to cubic NaCl phase is observed. This study confirms our conclusions regarding structural and magnetic transitions in this compound arrived at using unpolarized neutrons diffraction technique.

[1] J B C Efre³ et al., Pramana , Journal of Physics, 63 227 (2004).

T-31 Magnetic excitations in R_2PdSi_3 studied by inelastic neutron scattering

Fei Tang¹, Peter Link², Matthias Frontzek¹, Astrid Schneidewind¹, Irina Mazilu³, Michael Loewenhaupt¹

¹Institut für Festkörperphysik, TU Dresden

²FRM II

³Leibniz-Institut für Festkörper- und Werkstoffforschung Dresden

R_2PdSi_3 compounds have been found to exhibit rich magnetic phenomena arising from the interplay between RKKY interaction, crystal electric field effects and geometric frustration due to the derived hexagonal AlB_2 structure. The observed crystallographic superstructure further complicates the CEF effects. Except for Ho_2PdSi_3 compound the second order crystal electric field parameter dominates the magneto-crystalline anisotropy.

Inelastic neutron scattering measurements on single crystals of Ho_2PdSi_3 , Tm_2PdSi_3 and Er_2PdSi_3 have been performed at the cold triple axis spectrometer PANDA in FRM-II. All three compounds order antiferromagnetically at T_N 7.7 K, 7 K and 2.1 K respectively; Both Ho_2PdSi_3 and Er_2PdSi_3 undergo a second phase transition at $T_2 \approx 2$ K. Low lying CEF excitations (below 10 meV) were observed in all three compounds measured. The lowest excitation in Ho_2PdSi_3 (1 meV) and Er_2PdSi_3 (3.5 meV) show dispersion in the order of 0.5 meV below the Neel temperature, while the effect in Tm_2PdSi_3 is less pronounced in agreement with the lower ordering temperature. Measurements in magnetic fields up to 13 T show Zeeman splitting of the CEF excitations.

In this contribution we will present and discuss the results of the inelastic neutron scattering experiments and try to entangle the CEF level scheme.

[1] M. Frontzek, A. Kreyssig, M. Dörr, M. Rotter, G. Behr, W. LÄoser, I. Mazilu, and M. Loewenhaupt, *J. Magn. Magn. Mat.* 301 (2006) 398

[2] M. Frontzek, A. Kreyssig, M. Dörr, A. Schneidewind, J.-U. Hoffman, and M. Loewenhaupt, *J. Phys.: Condens. Matter* 19 (2007) 145276

T-32 Diffuse scattering from polarizing supermirrors

Anke Teichert¹, Thomas Krist², Roland Steitz²

¹SF1

²Helmholtz Zentrum Berlin für Material und Energie

Si-Fe supermirrors are frequently used as neutron polarizers. Optimum performance requires low roughness, minimal interface layer thickness and low stress in the layers. An additional aspect is diffuse scattering, which can be due to structural or magnetic roughness. The latter one cause spin flips and thus reduces the polarizing effect of the supermirror.

Polarising Si-Fe supermirrors with $m=2$ to 2.6 were investigated by specular and off-specular (diffuse) neutron scattering. Samples with high stress (i.e. low bending radius ($R<50\text{m}$)) were coated on one side, samples with low stress (i.e. high bending radius ($R>50\text{m}$)) were coated on both sides.

It was found that supermirrors with low and large internal stress showed similar performance of 92% reflectivity and a flipping ratio of 63 at a field of 300G. Both sample types exhibited strong diffuse scattering in reflection as well as in transmission at a magnetic field of 200G.

However, at a magnetic field up to 1030G the diffuse scattering was reduced for the low stress samples for about 25%, while for samples with large internal stress no reduction of diffuse scattering was observed. Above 1030G there was no further improvement. At an incident angle of 0.8deg samples with $R>50\text{m}$ and tensile stress showed a broader rocking peak than samples with compressive stress.

Strong bending of samples correlated with the stress and bias voltage. Compressive stress reduced with higher Bias and rocking peak width decreased simultaneously.

We conclude that both structural and magnetic roughness cause diffuse scattering and occur in different proportions for different supermirrors. The quality of supermirrors can strongly be enhanced by optimising production parameters and/or applying large enough external magnetic fields.

T-33 PNR reflectometry on Fe/ CoO films

Anke Teichert¹, Roland Steitz², Claudia Fleischmann³, Kristiaan Temst³

¹SF1

²Helmholtz Berlin Zentrum für Material und Energie

³Katholieke Universiteit Leuven, Belgium

Nowadays exchange bias systems find application in magnetic storage technology such as hard disks. They consist of ferromagnetic and antiferromagnetic layers and the coupling at the interface between these both layers lead to a broadening and a unidirectional shift of the hysteresis loop. In this paper we report on structural and magnetic properties of Fe/CoO films prepared by molecular beam epitaxy and in-situ oxidation. A Ag buffer layer is used to change the microstructure of the AF/F interface. The thickness of the buffer Ag layers varies between 2 and 50nm, where an increase in the Ag film thickness leads to an increase in roughness.

First a 2nm thick Co layer is grown on oxidized Si substrate, which is then oxidized in an oxygen environment. The thin CoO layer is subsequently covered with a 20nm thick Fe layer. The films are protected against oxidation with a Au capping layer of a thickness of 6nm. The CoO/Fe films were investigated with scanning tunneling microscopy (STM), vibrating sample magnetometry (VSM) as well as x-ray and polarized neutron reflectometry (PNR).

VSM measurements showed a strong asymmetric loop for the samples without the Ag layer. This asymmetry vanishes with increasing Ag layer thickness. The reasons are the two different reversal mechanisms, which are active in the respective hysteresis loops. We found domain wall nucleation and motion for the descending branch and domain rotation for the ascending branch.

Spin-analyzed PNR are performed on samples without buffer layer and with 18nm thick Ag buffer layer at V6, BENSC, at 12K. The four cross sections (R_{++} , R_{-} , R_{+-} , R_{-+}) for the initial and trained loop in the ascending and descending branch were measured in an increasing magnetic field.

For the sample without the Ag layer the spin-flip signal for the descending branch in the initial loop was low, whereas all other branches showed a significant spin-flip signal. The results are consistent with the VSM measurements.

Controversially to the VSM and AMR measurements the PNR measurements on the sample with 18nm Ag buffer layer revealed that for all branches the reversal mechanism is dominated by domain wall nucleation and motion. This might be related to the different information depth of the applied techniques.

T-34 Dynamical Properties of Ferromagnetic Shape Memory Alloys

Tetiana Dadakova¹, Klaudia Hradil², Peter Link², Tarik Mehaddene¹, Jürgen Neuhaus², Winfried Petry², Reiner Schneider³

¹Technische Universität München

²Forschungs-Neutronenquelle Heinz Maier-Leibnitz (FRM II)

³Helmholtz-Zentrum Berlin für Materialien und Energie

Magnetic shape memory (MSM) alloys can achieve large reversible deformations, which can be controlled by magnetic field. Magnetic field offers faster response in comparison to temperature driven shape memory. Also, the maximum strains obtained from MSM alloys is by far larger than in the ordinary magnetostrictive materials, and results to deformations up to 10%. This effect is connected to martensitic transition, the dynamics of which can be investigated by inelastic neutron scattering.

Dynamical properties of magnetic shape memory alloy Ni₄₉Mn₃₂Ga₁₉ have been investigated by means of inelastic neutron scattering on single crystal using the three-axis spectrometers PUMA and PANDA at Forschungs-Neutronenquelle Heinz Maier-Leibnitz (FRM II).

The measurements have been done for austenitic (cubic) as well as for martensitic (tetragonal) phases of MSM alloy Ni₄₉Mn₃₂Ga₁₉. To do so a single crystal was transformed uniformly in a single 5M variant of the martensite phase. The martensitic 5M structure has a tetragonal unit cell with a periodic stacking sequence of (110) atomic layers along [1-10].

Using the slopes of phonon branches, the calculations of the elastic constants for cubic and tetragonal phases were done. The results can be used as input parameters for ab-initio calculations. There is a dip in the TA [110] branch of the 5M structure, that means that this structure may transfer to another modulated structure on further cooling.

This project is funded by the DPG, SPP 1239, "Änderung vom Mikrostruktur und Form fester Werkstoffe durch äußere Magnet Felder"

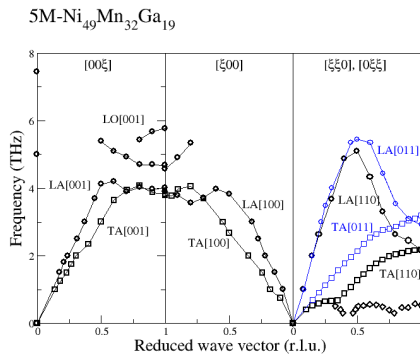


Figure 18.1: Phonon dispersion curves of the martensitic 5M structure of Ni₄₉Mn₃₂Ga₁₉.

T-35 PtMn-Behaviour in exchange biased CoFe/PtMn systems-studied using Neutron Scattering

Danica Solina¹, Dieter Lott¹, Wolfgang Schmidt², Cornelia Krien³, Yu- Chang Wu⁴, Jochen Fenske¹, Ulrike Starke³, Rainer Kaltfofen³, Chih-Huang Lai⁴, Andreas Schreyer¹

¹GKSS Forschungszentrum, Geesthacht, Germany

²ILL, Grenoble, France

³IFW, Dresden, Germany

⁴Dept. Materials Science, National Tsing Hua University, Taiwan

Neutron scattering studies have been carried out on single crystal bilayers of exchange biased PtMn(001)/CoFe grown epitaxially on MgO[001] using sputtering. Polarized neutron diffraction measurements taken around the hysteresis loop with sample aligned along the bias direction show changing peak shape and width for the 101 reflections while the 100 reflection only show weak intensity changes. This suggests a domain size change out-of-plane whereas in-plane the domain size remains constant. The data has been simulated with a partial twist at the turning points of the hysteresis loop with resulting relaxation and spin reorientation at saturation to comply with experimental observations.

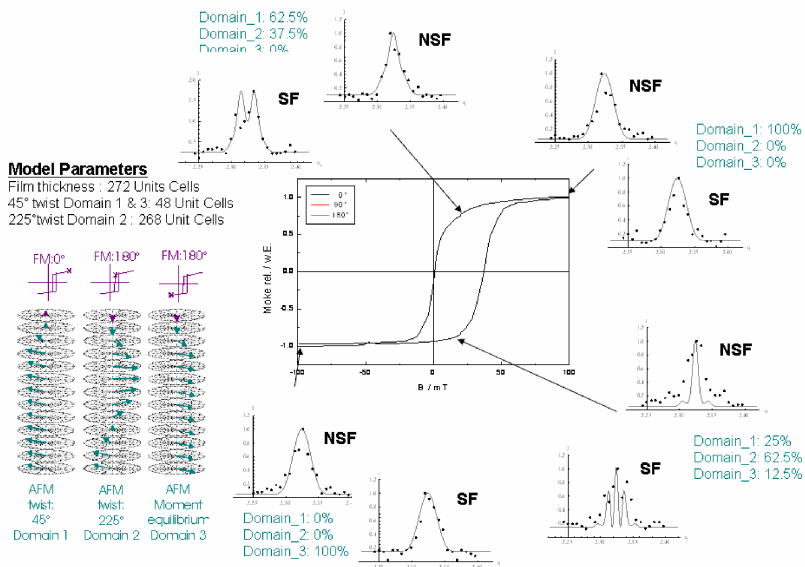


Figure 18.2: Simulation (line) for experimental polarized neutron diffraction data (dots) obtained around hysteresis loop for a triple domain model (domains illustrated). Total unit cells: 272

T-36 Dimensionality crossover upon magnetic saturation in the itinerant ferromagnets Fe, Ni and Co

Andreas Hoser¹, Ulrich Köbler², Klaus Habicht³

¹HZB SF2

²HZB BENSC

³HZB SF1

One of the main experimental tests of conventional spin wave theory [1] has been tried in 1963 on ferromagnetic iron [2]. This experiment has, however, not provided a positive proof due to a number of intricate problems. 1.) Typical for the atomistic character of spin wave theory is that the thermal decrease of the spontaneous magnetization is described by a power series of temperature [1]. Since power functions are not orthogonal basis functions it is practically not possible to evaluate exponent and pre-factor of the leading term ($\approx T^{3/2}$) unambiguously. 2.) It was noticed in 1972 [3] that the spontaneous magnetization of iron measured in zero field either using ^{57}Fe NMR or Mössbauer spectroscopy on the one hand and measured by conventional magnetization measurements, i.e. in the magnetically saturated state on the other hand has different temperature dependence. The question therefore is which method measures the spontaneous magnetization correctly. One explanation for this discrepancy was to assume a temperature dependent hyperfine coupling constant [3]. 3.) Paramagnetic impurities can disturb the macroscopic measurements in particular at low temperatures where deviations from saturation are small.

We present experimental evidence that the symmetry change from three dimensional in the zero field ground state to axial in the magnetically saturated state is relevant in the sense of renormalization group (RG) theory [4] and therefore associated with a crossover. Fig. 1 shows this dimensionality crossover (DC) for hcp cobalt observed with neutron scattering (E1/HMI). Surprisingly, the scattering intensities decrease instead of increasing upon application of a vertical field. Our conclusion is that in the magnetically saturated state Fe, Ni and Co are one dimensional in spite of a normal saturation of the macroscopic magnetization [5]. The observed dimensionality change cannot be understood assuming that magnons are the relevant excitations.

[1] F.J. Dyson, Phys. Rev. 102 (1956) 1230.

[2] B.E. Argyle, S.H. Charap, E.W. Pugh, Phys. Rev. 132 (1963) 2051.

[3] M.A. Butler, G.K. Wertheim, D.N.E. Buchanan, Phys. Rev. B 5 (1972) 990.

[4] K.G. Wilson, J. Kogut Phys. Reports 12C (1974) 75.

[5] U. Köbler, A. Hoser, Physica B 362 (2005) 295.

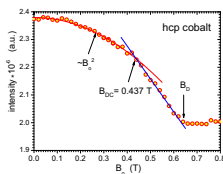


Figure 18.3: Bragg intensity (100) vs. vertical field (spherical sample)

T-37 Determination of the Magnetic Structure of MnNCN

Manuel Krott¹, Andreas Houben¹, Paul Müller¹, Jens Walter², Werner Schweika³, Yixi Su³, Richard Dronskowski¹

¹Institut für Anorganische Chemie, RWTH Aachen University, D-52056 Aachen

²Mineralogisch-Petrologisches Institut, Universität Bonn, D-53115 Bonn

³Jülich Center for Neutron Science at FRM II, D-85747 Garching

MnNCN, the first carbodiimide of a magnetic transition metal, has been synthesized and characterized by single-crystal X-ray diffraction three years ago. MnNCN crystallizes in space group $R\bar{3}m$ with the lattice parameters $a = 3.3583(4)$ Å and $c = 14.347(2)$ Å^[1]; the spatial parameters are given in Table 1.

Table 18.1: Positional and isotropic displacement parameters for MnNCN with standard deviations in parentheses.

Atom	Position	x	y	z	U_{iso} (Å ²)
Mn	$3a$	0	0	0	0.0092(4)
C	$3b$	0	0	$\frac{1}{2}$	0.0085(11)
N	$6c$	0	0	0.5855(3)	0.0115(8)

Magnetic measurements show a Néel point at about 28 K and a Curie-Weiss behavior for higher temperatures. The first neutron powder diffraction measurements were performed, immediately after synthesis, at room temperature and below the Néel point using the SV-7 instrument at Forschungszentrum Jülich. Although there was evidence for magnetic ordering, the weak magnetic reflections did not allow the solution of the complete magnetic structure. Recently, better resolved data were collected below the transition temperature by use of the DNS instrument and polarized neutrons at FRM II in Garching. The advantage of the DNS instrument in detecting magnetic peaks in a powder sample is obvious from Figure 1. Temperature-dependent measurements showed a significant difference in the intensity loss of the first two magnetic reflections upon increasing the temperature, indicative of two different spin arrangements. Just below 28 K, the c axis becomes doubled due to the formation of antiferromagnetically ordered sheets of manganese atoms such that the spins are coupled ferromagnetically in the ab plane with a spin direction perpendicular to the c axis. This leads to two magnetic reflections with Q values of 0.65 and 1.95 Å⁻¹. Below 20 K, three additional magnetic peaks arise, indicative of another transition to a presently unknown magnetic ordering type.

X. Liu, M. Krott, P. Müller, C. Hu, H. Lueken, R. Dronskowski, Inorg. Chem. 2005, 44, 3001.

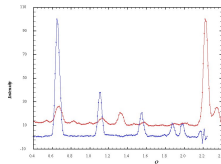


Figure 18.4: SV-7 scan (red curve) and DNS scan (blue curve) (polarized neutrons) at 4.5 K. For the DNS data, only magnetic peaks are shown.

19 Materials Science and Engineering

T-38 Investigations Of Lattice Spacing On In718 Via Neutron Larmor Diffraction

Julia Repper¹, Michael Hofmann¹, Christian Krempaszky², Thomas Keller³, Winfried Petry¹, Ewald Werner⁴

¹Forschungsneutronenquelle Heinz Maier-Leibnitz (FRM II), TU München, D-85747 Garching, Germany

²Christian-Doppler-Laboratory of Material Mechanics of High Performance Alloys, TU München, D-85748 Garching, Germany

³Max-Planck-Institute for Solid State Research, D-70569 Stuttgart, Germany

⁴Institute for materials science and mechanics of materials, TU München, D-85747 Garching, Germany

The residual stress analysis via conventional diffraction methods is based on the comparison of the lattice spacing d of a stressed component with the lattice spacing d_0 from a macroscopically stress free reference sample. In neutron Larmor diffraction the lattice spacing d is encoded in the spin precession of a polarized monochromatic neutron beam scattered at the sample. In contrast to conventional neutron diffraction methods Larmor diffraction is independent of the divergence of the initial beam, the spread of the wavelength and the scattering angle 2θ [1]. Based on this, the Larmor technique is relatively insensitive to alignment errors of the sample, which cause large shifts in measured 2θ -values in conventional diffractometer techniques. Hence, the method enables the measurement of reference values d_0 with a very high accuracy (in the order of 10^{-5} Å) hitherto not possible using classical diffractometers [2]. In addition Larmor diffraction provides the unique possibility to resolve the fluctuation of the lattice spacing resulting from a variation of the stress state within the sample over the whole gauge volume [3]. Therefore, this method allows to determine particularly in the case of complex, high performance superalloys micro stress levels and their fluctuations over the sample geometry and to study their influence on macroscopic stress analysis.

In this contribution first results are presented, which were achieved with the new neutron Larmor diffraction method carried out at the spin echo triple axis spectrometer TRISP on the industrial employed Ni based multiphase superalloy Inconel 718.

[1] M.T. Rekveldt, T. Keller, W.H.Kraan, Europhys. Lett, 54, 342-346 (2001).

[2] C. Pfeleiderer, P. Böni, T. Keller, U.K. Röbber, A. Rosch, Science, 316, 1871-1874 (2007).

[3] M.T. Rekveldt, W.H.Kraan, J. Neutron Research, 8, 53-70 (1999).

T-39 Effect of residual stresses on in-service performance of friction stir welded joints

Torben Fischer¹, Peter Staron¹, Jorge dos Santos¹, Yu-E Ma², Andreas Schreyer¹

¹GKSS Research Centre

²Cranfield University

Friction stir welding (FSW) is a proven technology for use in airframes. It has been shown that even for simple applications like longitudinal fuselage joints weight savings of up to 15% and cost savings of 20% can be achieved. FSW is now seen as a key element for producing cost effective integral metallic structures in future airframe applications. By further understanding and development of the FSW process new applications can be realized leading to further cost and weight benefits for metallic airframe structures, which will make these structures more competitive in the future [1-2]. Of particular importance is the understanding of the effect of residual stress on the performance of the welded components. In order to investigate the influence of the sample dimensions on maximum residual stresses and mechanical properties, three fatigue test samples with different sizes of a batch of friction stir welded AA 2195 sheets were tested. The sheets were welded in butt-joint configuration and have a thickness of 8 mm. The notch of the samples was perpendicular to the weld line and was inserted on the advancing side of the weld. Residual stress measurements have been carried out with the neutron diffractometer ARES-2 at Geesthacht Neutron Facility (GeNF) at GKSS. Neutrons of 0.164 nm wavelength were chosen with a Silicon (311) monochromator. The three independent strains were measured in longitudinal, normal, and transverse direction. The gauge volume was placed at the middle of the sheet thickness. The approximation of a biaxial stress state was made for the calculation of stress-free lattice parameters and stresses.

This work will explore the influence of residual stress fields and the orientation of the crack to the weld line in a series of tests in which the residual stress fields in the samples are monitored and will be related to the observed crack growth behaviour. First results show that the residual stresses depend strongly on the specimen size.

[1] J.F. dos Santos (editor): Proceedings of the 1st international seminar on FSW modelling and flow visualisation. 24-25 February 2003, Geesthacht, Germany.

[2] J.F. dos Santos (editor): Proceedings of the 2nd international seminar on FSW modelling and flow visualisation, 31 January - 1 February 2005, Geesthacht, Germany.

T-40 In-situ Strain Measurements in Composite Castings using Neutron Diffraction

Uwe Wasmuth¹, Michael Hofmann²

¹utg

²FRM II

Due to different thermal expansion of the casting material and the material of the insert residual stresses occur during solidification of composite castings. These residual stresses can reduce fatigue strength and lead to distortions of the part. They can be minimised by constructive measures. Casting simulation is a suitable method to predict residual stresses and distortions and thus to optimise design of parts. To improve the accuracy of stress simulation composite castings were investigated experimentally using conventional strain gauge methods and neutron diffraction. The use of neutron diffraction enabled to obtain, non-destructively, stress distributions within the bulk of the specimen [1]. In-situ neutron diffraction strain experiments during solidification of the composite castings made it further possible to measure thermal and mechanical strains up to solidus temperature of the casting material. The results are used to verify and optimise the residual stress simulation. In the end this enables an optimised construction of composite castings.

[1] U. Wasmuth, M. Hofmann et al, Optimisation of Composite Castings by Means of Neutron Measurements, Annals of the CIRP Vol. 57/1/2008

T-41 In-situ SANS investigation of strained conductive polymer-carbon composites

Florian Spieckermann¹, Manfred Prem¹, Harald Renzhofer¹, Maris Knite², Gerhard Krexner¹, Adél Len³

¹Uni Wien

²Riga Technical University

³BNC Budapest

Conductive polyisoprene-carbon nano-composites were recently found to exhibit a change of electrical resistivity by more than four orders of magnitude on applying a moderate uniaxial strain of up to about 20 percent [1,2]. The occurrence of this giant tenso-resistive effect has been observed for various filler materials such as carbon black (CB), single wall and multiwall carbon nanotubes (SWCNT, MWCNT) and can be described as a percolation-like transition due to rearrangements of the embedded carbon particles in the strained polymer matrix [3].

SANS experiments on nano-composites were carried out at the Budapest Neutron Center (BNC) as a function of uniaxial strain applied in situ. Composition of the samples differed with respect to the amount and the structure of the carbon particles dispersed in the polyisoprene matrix: 10.89wt% MWCNT, 6.05wt% MWCNT and 6.05wt% SWCNT, respectively. In order to cover a wide q-range neutron wavelengths of 3.38Å, 7.51Å and 22.44Å were chosen. The sample-to-detector distance was fixed at 5.6 meters. Uniaxial strains of 0%, 15%, 30% and 45% were applied to the samples by a computer-controlled tensile testing machine. Changes in electrical resistivity were recorded in-situ with an electrometer.

The SANS spectra reveal two non-integer power law regions related to a) the mass fractal nature of the filler particles and b) to the surface fractal nature of the inner surfaces of the MWCNT and the nanotube bundles, respectively. This contrasts with earlier findings on carbon black composites where two regions of mass-fractal behavior could be distinguished [3,4] corresponding to the dispersion/agglomeration of the respective particles. Measurements at 22.44 Å showed anisotropic SANS patterns for all nanotube samples indicating a slight reorientation of the tubes with increasing strain. The results are discussed with respect to the mechanisms governing the strain-induced conductivity changes in samples containing CB and carbon nanotubes, respectively.

[1] Knite, M.; Teteris, V.; Kiploka, A. & Kaupuzs, J. (2004), 'Polyisoprene-carbon black nanocomposites as tensile strain and pressure sensor materials', *Sensors and Actuators A: Physical* 110(1-3), 142 - 149.

[2] Knite, M.; Tupureina, V.; Fuith, A.; Zavickis, J. & Teteris, V. (2007), 'Polyisoprene-multiwall carbon nanotube composites for sensing strain', *Materials Science and Engineering: C* 27(5-8), 1125 - 1128.

[3] Allmann, S. (2006), 'Neutronenkleinwinkelstreuung an leitenden Polyisoprene-Carbon Black Nanocomposites bei Dehnung in situ zur Untersuchung des Tenso-Resistiven Effekts', diploma thesis, Technical University Graz.

[4] Allmann S., Prem M., Knite M., Krexner G., Len A., SANS Investigation of Conducting Polyisoprene Nanocomposites and the Tensoresistive Effect, in preparation.

T-42 Phase Transition Kinetics in Austenitic Ductile Iron (ADI)

Michael Hofmann¹, Leopold Meier², Günther Reithmeier¹, Wasmuth Uwe², Peter Schaaf³, Bamberger Menachem⁴

¹FRM II

²UTG, TU München

³TU Ilmenau

⁴Technion Haifa, Israel

Austempered Ductile Iron (ADI) is a high-performance casting material. Its microstructure consists of spheroidal graphite and a matrix of high carbon austenite and bainitic ferrite which is formed by a special austempering heat treatment. The final properties of ADI are very sensitive to chemical composition, as-cast microstructure and heat treatment conditions, making it possible to produce a family of ADIs. They offer a range of mechanical properties superior to those of other cast irons, and show excellent competitiveness with aluminium alloys and steels in terms of mechanical properties, manufacturing cost, physical properties and weight saving.

ADI samples were austempered (heat treated) and the phase transitions were monitored in situ during the process and ex-situ after interrupted austempering using neutron diffraction on STRESS-SPEC, FRM-II. These measurements yielded the phase kinetics, the change of austenite carbon content and phase fractions (austenite, ferrite, martensite, cementite, graphite, etc.), which are compared to results derived using other methods, like dilatometry, nanoindentation, XRD, SEM, TEM and Mössbauer spectroscopy.

T-43 Vortex Structure in NbTi/Nb multilayers

Wolfgang Donner¹

¹Materialwissenschaften/Strukturforschung

NbTi alloys are the Industrially most relevant superconductors. Several strategies to enhance their critical current by introducing artificial pinning centers are being used, like rolled multilayer sheets, drawn microwires and thermal processing of bulk alloys [Cooley 99]. Since the early 1980's artificially multilayered structures are being used as model systems in order to study the effect of interfacial pinning on well-defined samples. Very high critical currents have been found in multilayers containing NbTi/Nb [McCambridge 95], NbTi/Ti [Cooley 99b]. Different models involving the static [McCambridge 95] or dynamic pinning [Gurevich 96] of vortices that run parallel to the surface of the multilayer have been proposed.

The observation of vortex lines can be done directly by magneto-optical techniques [Baseljevich 03], or by diffraction [Riseman 98]. In the case of vertically stacked vortex lines in a thin film multilayer, both methods fail for geometric reasons. The method of choice here is spin-polarized neutron reflectivity (SPNR), which allows to extract the vertical magnetic scattering length profile on a nm scale. SPNR has been used to look at YBCO [Lauter 99] thin films and Nb/Al multilayers [Han 03]. In both cases it was possible to demonstrate that the magnetization profiles of the samples change under an applied magnetic field and the profiles had been compared to existing models of flux penetration. In the Nb/Al case, no evidence of a matching effect between the vortex structure and the multilayer periodicity had been found so far.

This project will use NbTi/Ti multilayers as model systems, mainly because they show the largest effect of the multilayer structure on the critical current and they have been sufficiently studied by other methods.

We will report on recent experiments carried out at NREX+ at the FRM2.

[Cooley 99] L.D. Cooley, L.R. Motowidlo, *Superconductor Science and Technology* 12, R135 (1999)

[Lauter 99] V. Lauter-Pasyuk, H.J. Lauter, M. Lorenz, V.L. Aksenov, P. Leiderer, *Physica B* 267, 149 (1999)

[Han 03] S.W. Han, J. Farmer, P.F. Miceli, G. Felcher, R. Goyette, G.T. Kiehne, J.B. Ketterson, *Physica B* 336, 162 (2003)

[Cooley 99b] L.D. Cooley, C.D. Hawes, P.J. Lee, D.C. Larbalestier, *IEEE Transactions on Applied superconductivity* 9, 1743 (1999)

[McCambridge 95] J.D. McCambridge, N.D. Rizzo, X.S. Ling, J.Q. Wang, D.E. Prober, *IEEE Transactions on Applied superconductivity* 5, 1697 (1995)

[Gurevich 96] A. Gurevich, E. Kadyrov, D.C. Larbalestier, *Physical Review Letters* 77, 4078 (1996)

[Riseman 98] Observation of a square flux line lattice in the unconventional superconductor Sr₂RuO₄, T.M. Riseman et al., *Nature* 396, 242 (1998)

[Baziljevich 03] M. Baziljevich, P. E. Goa, H. Hauglin, E. Il'Yashenko, T. H. Johansen, *Advances in Science and Technology* 38, 377 (2003)

T-44 In situ temperature and stress-dependent measurements of Ni_{50.14}Ti_{49.86} shape memory alloy.

Casjen Merkel¹, Ahmed Afandi¹, Markus Hölzel², Heinz-Günter Brokmeier³, Jan Frenzel⁴, Wolfgang Schmahl¹

¹Kristallographie, LMU

²TU Darmstadt

³TU Clausthal

⁴Ruhr-Universität Bochum

Martensitic twin reorientations allow deformed NiTi alloys to recover their pristine shape by thermal treatment. This shape memory effect is based on deformation by ferroelastic switching of the twin domain structure of the monoclinic phase under stress. This twin structure remains stable when the stress is released. Heating transforms the material into the cubic B2 phase. This phase transforms to the monoclinic phase with random twinning, recovering the original shape upon cooling in a stress-free environment. Shape memory alloys (SMA) provide a tunable martensitic transition temperature which varies strongly with Ni-content. This makes the material especially relevant for a widespread of medical and engineering applications such as mobile phone antennas, durable frames, arterial implants, micro actuator valves, pipe fittings, and orthodontic wires.

High resolution neutron diffraction is required to access the crystallographic properties and textures of these alloys. Rietveld refinement using the spherical harmonics description for the texture adjustment allows us to obtain the phase state and lattice parameters of coarse grained polycrystalline samples as used in industrial applications with high accuracy. In situ temperature dependent measurements of these alloys have been performed from 5 K to 440 K to obtain the order parameters for a Landau description of a Ni_{50.14}Ti_{49.86} SMA. Moreover in situ stress-dependent measurements have been carried out which give rise to stress-strain parameters in the Landau description. The measurements reveal that a and c parameters increase, while b and β decrease with increasing temperature. The spherical harmonics (SH) description of the textured sample are consistent with previously measured stress-dependent variations in SMAs. Moreover the SH description has been validated by a classical full texture determination. This series of measurements in temperature-stress-space on the same samples will lead to a complete description of the phase transformation of monoclinic to cubic Ni_{50.14}Ti_{49.86} SMA.

T-45 Texture gradient in a bone-like extrusion profile of Mg-Ze10 alloy

Heinz-Günter Brokmeier¹, Jan Bohlen², Peter Spalthoff², Christian Randau¹, Ulf Garbe³

¹IWW-TU Clausthal

²GKSS-Forschungszentrum

³Bragg Institute, ANSTO

STRESS-SPEC measurements were carried out to investigate the texture gradient of a bone-like extrudate. The gradient results from the anisotropic extrusion die to produce a bonelike extrusion profile. Round extrusion and rectangular extrusion show very typical texture with basal plane orientations to the macroscopic glide plane. Two different types of experiments will be compared, carried out at STRESS-SPEC, using on hand a step scan method (equal angular scanning) and on the other hand a continuous scanning around phi. In both cases complete pole figures of a set of reflections were obtained to calculate the orientation distribution function with the iterative serious expansion method. The advantages of the continuous scanning method, which is a new technique for neutron diffraction, will be discussed in another paper on this conference in detail. Only one point of interest has to be mentioned that is a strong reduction in the total counting time.

A texture gradient results particular in the intermediate region between the inner part and the top and bottom part. In the middle part a texture type close to a rectangular extruded sample with an orthorhombic sample symmetry was obtained, while in the transition zone this high sample symmetry is lost. The round part of the bonelike structure (bottom and top) shows a strong <10.0> fibre texture.

T-46 Structure aspects of stabilization of ferrofluids by small-angle neutron scattering

Mikhail Avdeev¹, Vasil Garamus², Regine Willumeit², Artem Feoktystov², Ladislau Vekas³, Victor Aksenov⁴

¹Joint Institute for Nuclear Research

²GKSS Research Centre

³Center for Fundamental and Applied Technical Research, Timisoara branch of Romanian Academy

⁴Russian Research Center

It is well known that one of the best molecules for stabilizing magnetite nanoparticles in organic non-polar liquids is oleic acid, a non-saturated mono-carboxylic (fatty) acid, which has a C18 tail with a double bond kink in the middle. Despite wide use of this surfactant in stabilization procedures of magnetic fluids, still there is no full understanding what factors responsible for the resulting stabilization distinguish oleic acid from its saturated analogue, stearic acid, which is always considered as a poor stabilizer. Here, we investigate the structure of magnetic fluids based on decahydronaphthalene and stabilized by various chain length molecules from a series of saturated fatty acids, namely lauric (LA), myristic (MA), palmitic (PA) and stearic (SA) acids with C12, C14, C16, C18-tails, respectively, and compared them with the classical fluid stabilized by oleic acid (OA). The structure of stabilized magnetic particles is obtained by small-angle neutron scattering (SANS) performed for H- and D-carriers. It is shown that for all saturated acids magnetite is dispersed in the carrier approximately with the same particle size distribution whose mean value and width are significantly less than in the OA case. Along with it, these acids exhibit different initial dispersing efficiency. A dependence of the thickness of the stabilizing shell around magnetite on the surfactant type was observed, which is discussed with respect to stabilizing properties of saturated fatty acids.

The work is done in the frame of the project RFBR-Helmholtz (HRJRG-016).

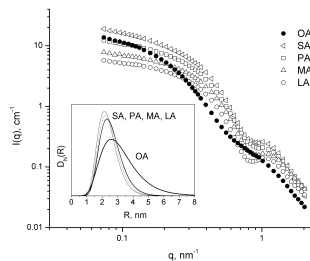


Figure 19.1: SANS curves from magnetite nanoparticles dispersed in deuterated decahydronaphthalene (volume fraction 0.6 %) and stabilized by different mono-carboxylic acids including non-saturated oleic acid (OA) and saturated stearic (SA), palmitic (PA), myristic (MA) and lauric (LA) acids. Inset shows determined particle radius distribution functions of magnetite for different stabilization. Significant difference is seen for saturated acids as compared to oleic acid. At the same time, modulation of the curves for saturated acids with the surfactant length reflects different thickness of the stabilizing layer.

T-47 In-situ high-temperature characterization of intermetallic precipitates in a new nickel-based superalloy

Gerald Andreas Zickler¹, Ronald Schnitzer¹, Ralf Schweins², Harald Leitner¹

¹Christain Doppler Laboratory ESOP, Dept. Phys. Metallurgy & Mater. Testing, University of Leoben, Austria

²Institut Laue - Langevin, Grenoble, France

For several years nickel-based alloys, so-called superalloys, have been extensively used for high-duty components of combustion engines, aerospace engines, gas turbines, and nuclear reactors. The improvement of conventional materials and the development of new advanced alloys require comprehensive understanding of the occurring microstructural reactions and solid-state phase transformations and their effects on macroscopic properties, e.g. mechanical properties. In recent decades much effort has been made to develop a new commercial nickel-based superalloy with higher temperature capabilities, improved properties, and lower costs than that of classical alloys. As a part of this effort, the new ATI Allvac(R) 718Plus(TM) alloy was developed. The nominal chemical composition (wt%) is given by: base Ni, 0.025 % C, 18.0 % Cr, 2.70 % Mo, 1.0 % W, 9.0 % Co, 10.0 % Fe, 5.40 % Nb, 0.70 % Ti, 1.45 % Al, 0.007 % P, and 0.004 % B. The alloy derives its strength essentially from precipitation hardening by intermetallic phases. The aim of the present study is gaining fundamental knowledge of the precipitation kinetics of intermetallic phases as function of heat treatment temperature and ageing time. Small-angle neutron scattering (SANS) was applied as an appropriate investigation technique to study size, shape, and volume fraction of the nanometer-sized precipitates. The experiment was performed in-situ at isothermal temperatures between 775 and 925°C in the time range of up to 3 h by using a special high-temperature furnace. The SANS patterns were analyzed by applying a microstructural model of densely packed spheres (hard-sphere potential), yielding least-square fitted microstructural parameters. The outcomes of the experiment were combined with results of electron microscopy, atom probe tomography, and mechanical testing. This multi-method approach leads to a deeper understanding of precipitation reactions and phase transformations in the investigated nickel-based superalloy.

T-48 Probing polymer interfaces using time-of-flight grazing incidence small-angle neutron scattering

Ezzeldin Metwalli¹, Jean-Francois Moulin², Uwe van Bürck¹, Gunar Kaune¹, Matthias Ruderer¹, Peter Müller-Buschbaum¹

¹Physikdepartment E13, Technische Universität München, D-85747 Garching, Germany

²Institut für Werkstofforschung, GKSS-Forschungszentrum Geesthacht GmbH, Germany

Time-of-flight grazing incidence small-angle neutron scattering (TOF-GISANS) has the advantage to monitor a wide range of momentum transfer (q) in a single experiment without the need to alter the incident angle, the collimation or the sample-to-detector distances. In a single TOF-GISANS measurement, we have simultaneously spanned a q range from 0.02 to 0.4 nm⁻¹ and followed the wavelength dependent scattering of poly(styrene-*b*-isoprene), P(S-*b*-I), diblock copolymer thin film. Due to the selected molecular weight and the molecular weight ratio of the styrene and the isoprene block a lamellar morphology with lamella thickness of 53 nm is installed. With TOF-GISANS the lamellar structures of the thin diblock copolymer films is detected to be oriented parallel to the substrate surface. Two Bragg peaks in the scattering plane are discriminated from the Yoneda peak and the specular reflection at different wavelengths. The position of the Bragg peaks is modeled as a function of wavelength, taking into account the refraction at the film surface and reflection at the film-substrate interface. Including instrument-dependent corrections, a good agreement between experimental and modeled data is achieved.

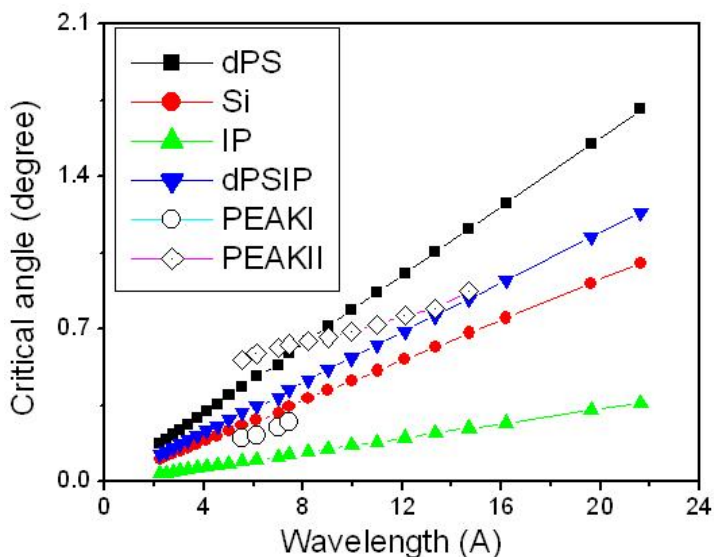


Figure 19.2: The figure shows the calculated critical angle versus the wavelength for polymers and silicon substrate (filled markers). The unfilled markers are the experimental exit angle. Peak I (open circles) represents the Si critical angle while Peak II (open diamond) indicates the Bragg reflection of surface-parallel lamellae.

T-49 Water storage in novel undeformable hydrogel thin films as probed with in-situ neutron reflectivity

Weinan Wang¹, Ezzeldin Metwalli¹, Jan Perlich¹, Kordelia Troll¹, Christine Papadakis¹, Robert Cubitt², Peter Müller-Buschbaum¹

¹TU München, Physik - Department E13, James-Franck-Str. 1, D-85747 Garching, Germany

²Institut Laue Langevin (ILL), 6 Jules Horowitz, 38042 Grenoble, France

Responsive hydrogel systems that can be interconverted by different external stimuli constitute a field of increasing interest, with potential applications in drug delivery systems, electrical and optical switching devices. In the thin film geometry a swelling of the hydrogel film is accompanied with an increase in the film thickness.[1] However, for many applications such changes in the film thickness are less advantages and water storage without changes in the film thickness would be desirable. Within the presented investigation we follow the bulk approach of Poly(N-isopropylacrylamide) (PNIPAM) based block copolymers with a long hydrophobic PS block. PNIPAM is chosen as it is one of the most studied thermosensitive polymers in many applications. We select the model system of P(S-b-NIPAM) diblock copolymer with a PNIPAM volume fraction of 0.276 and thin films are prepared on silicon substrates. We demonstrate the water storage capacity of these films instead of a normal swelling capacity in contact with saturated water vapour. The water storage mechanism is discussed. In storage and de-storage cycles we investigate aging effects of the storage capacity giving insights in the applicability of the novel undeformable hydrogel films (see Fig. 1). The investigation is based on in-situ neutron reflectivity experiments in combination with the usage of deuterated water vapour to generate contrast with the copolymer film.[2] Finally, X-ray reflectivity, atomic force microscopy and IR measurements complete the investigation.

[1] W. Weinan, K. Troll, G. Kaune, E. Metwalli, M. Ruderer, K. Skrabania, A. Laschewsky, S. V. Roth, C. M. Papadakis, P. Müller-Buschbaum, *Macromolecules*, 2008, 41, 3209-3218.

[2] P. Müller-Buschbaum, E. Bauer, E. Maurer, A. Nelson, R. Cubitt, *Phys. Stat. Sol. (RRL)*, 2007, 2, R68-R70.

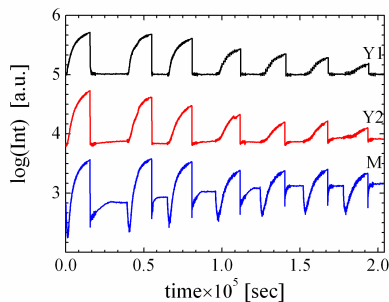


Figure 19.3: Figure 1. The integrated areas Y1, Y2, and M are representing the Yoneda peak of deuterated material, the Yoneda peak of protonated material and the first minimum of the reflectivity, respectively. On a logarithmic intensity axis 7 repetition cycles are shown. The curves are shifted along the y-axis for presentation.

T-50 Microstructural Stability of Co-Re alloys at 1000°C measured by in-situ SANS

Debashis Mukherji¹, Pavel Strunz², Ralph Gilles³, Joachim Rösler¹

¹Technical University Braunschweig, Germany

²Research Centre Rez, Czech Republic

³Technical University Munich, Germany

New generation Co-Re-based alloys are being developed for applications at high temperatures ($\approx 1200^\circ\text{C}$) beyond Ni-base superalloys. These alloys are strengthened by carbides and/or a Re-rich second phase (σ) and the high temperature stability of the strengthening phases are critical for the alloy development. The chromium carbides have different morphologies and their distribution is an important parameter for the effective strengthening. A typical microstructure of the carbides is shown in Fig. 1. In-situ SANS experiment by heating experimental Co-Re alloy was performed with the aim to test the microstructural stability. Structural characterization on different alloys was made at the temperature of 1000°C for up to 20 hours hold time. In-situ SANS result was complementary to the measurement performed with synchrotron radiation and electron microscopy.

The measured scattering curves (SANS) were modeled and fitted in accordance with the electron microscopy results on samples measured at room temperature. Two microstructural models are necessary to describe the in-situ SANS data in the broad Q-range. One of them is a plate-like phase with mean plate thickness of 45-75 nm, which increases with the hold time (up to 20 h) at nearly constant volume. The second type of particle describes the large precipitates (blocky carbides and σ phase) and is modeled by spherical particles of 800 nm diameter. The combination of SANS and synchrotron data indicates the grain boundary and the large blocky carbides start dissolving in the first hours of the exposure. The increase of the scattering curves at very low Q magnitudes indicates formation of σ phase. No sudden change in the scattering curves was observed with increase in temperature to 1000°C or on hold. It is therefore, quite likely that the plate-like carbides and the σ plates coexist during the hold at the high temperature.

1. J. Rösler, D. Mukherji, T. Baranski: *Adv. Engg. Mater.* 9 (2007) 876.

2. D. Mukherji, M. Klauke, P. Strunz, I. Zizak, G. Schumacher, A. Wiedenmann and J. Rösler: High temperature stability of Cr-carbides in an experimental Co-Re-based alloy, *Metal. Mater. Trans.* (2008) submitted.

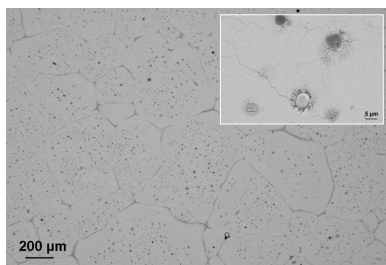


Figure 19.4: Different morphologies of Cr-carbides in Co-17Re-23Cr-2.6C alloy (in at%): grain boundary carbides, blocky carbides and lamellar carbides (see inset).

T-51 Neutron Diffraction Measurement of a AZ31B Magnesium Alloy Sheet Biaxially Deformed at Warm Temperatures

Ibai Ulacia¹, Gurutze Arruebarrena¹, Peter Spalhoff², Christian Randau³, Iñaki Hurtado¹

¹Dept. of Manufacturing, MGEP, Mondragon Unibertsitatea, Spain

²Institute for Materials Research, GKSS, 21502 Geesthacht, Germany

³Institute of Materials Science and Engineering, TU Clausthal,

Magnesium alloys present high potential for automotive applications due to their lower density in comparison with other widely used structural materials. This property could allow reductions in vehicle weight, but also improvements in dent resistance and shell resistance behaviour by increasing thickness in structural sheet applications. However, as it has been reported by many researchers, some limitations emerge when forming magnesium sheet parts. It is well known that due to their hexagonal close-packed (hcp) microstructure, magnesium alloys present low formability at room temperature. Increased forming temperatures improves the formability of magnesium alloys. Therefore, in the present study deep drawing experiments were carried out at warm temperatures up to 250°C that show the formability improvement.

Neutron diffraction measurements were performed from parts obtained by warm a deep drawing process and the textures from different zones were compared in order to know forming conditions and properties of the final part. The measurements show a similar deformation pattern in two directions of the sheet that means the properties of the final part are influenced by the initial texture.

Finally, orientation distribution function (ODF) of the different samples was calculated from the experimentally measured pole density functions (pole figures). The negligible average deviations between experimental and recalculated pole figures, show the reliability of the neutron diffraction measurements.

T-52 Effect of compressive and tensile residual stresses on constraint in fracture of welded components

Simon Kamel¹, Robert Wimpory², Noel O'Dowd³, Kamran Nikbin¹

¹Imperial College London

²Helmholtz Zentrum Berlin

³University of Limerick

Residual stress is a key feature in welded pipe and plate components containing defects that needs to be quantified and modelled in order to improve component lifing at low temperatures. In this work experimental and numerical investigations have been performed using blunt-notched compact tension C(T) specimens, of 347 stainless steel weld material, to examine the effect of tensile and compressive residual stress on fracture. The residual stress is introduced into the C(T) specimens by a tensile or compressive mechanical preload to produce, respectively, a compressive or tensile residual stress ahead of the notch. Neutron diffraction measurements are performed on the preloaded specimens, prior to introduction of a crack, and compared with predictions of the residual stress from finite element analyses of the preloaded C(T) specimens using tensile properties derived at room temperature. A crack is subsequently introduced ahead of the notch using Electro Discharge Machining. Initial fracture tests on the as-received specimens suggests that the ductile nature of 347 weld at room temperature will eradicate any variation in fracture toughness that may exist between the pre-compressed and pre-tensioned specimens and the as-received material.

T-53 SANS investigation of irradiation-induced phase separation in binary Fe-Cr-alloys

Andreas Ulbricht¹, Frank Bergner¹, Cornelia Heintze¹, Helmut Eckerlebe²

¹Forschungszentrum Dresden-Rossendorf

²GKSS Forschungszentrum

Ferritic-martensitic chromium steels are candidate materials for future applications in both Gen-IV and fusion technology. Investigations of related binary Fe-Cr alloys will significantly contribute to the understanding of the behaviour of more complex alloys. The presented SANS results are focused on a Fe-9at.% Cr alloy neutron-irradiated up to a dose of 1.5 displacements per atom (dpa).

We have observed a pronounced increase of scattering intensities for two different irradiation conditions at scattering vectors $Q > 0.2 \text{ nm}^{-1}$ for both magnetic (figure (a)) and nuclear scattering. The reason for the increased intensities are irradiation-induced clusters with size distributions presented in figure (b). The A-ratio is about 2.8 for both irradiation conditions. This value is far from a value of 1.45 corresponding to nanovoids as scattering objects. This indicates that the irradiation-induced clusters are different from pure nanovoids and must contain Cr-atoms with the same or very similar average composition for both irradiation conditions. These clusters are interpreted as α' -phase. The volume fraction of clusters of this type increases slightly with neutron dose.

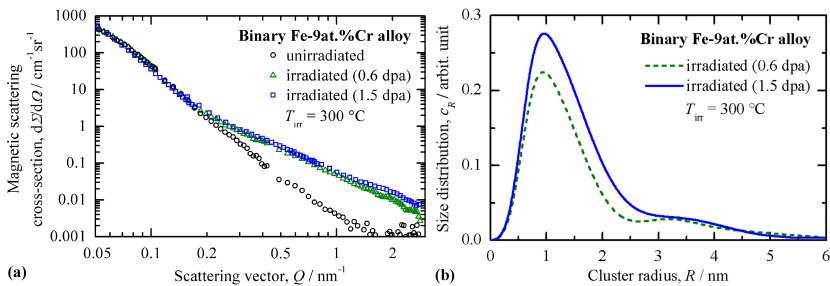


Figure 19.5: (a) Magnetic SANS cross-section as function of scattering vector for different conditions of a binary Fe-9at.% Cr alloy. (b) Distribution of the volume fraction of irradiation-induced clusters in a Fe-9at.% Cr alloy, identified as a Cr-enriched α' -phase.

T-54 Neutron diffraction study of texture evolution of ECAPed magnesium alloys

Tatiana Lychagina¹, Heinz-Günter Brokmeier², Dimmitry Nikolayev¹, Weimin Gan³

¹Frank Laboratory of Neutron Physics, Joint Institute for Nuclear Research, Dubna

²TU-Clausthal

³TU-Claustahl

Deformed magnesium alloys find wide application in various branches of mechanical engineering and, first of all, in aerospace, automobile and electronic industries. Plasticity of semifinished products from these alloy is not rather high [1] especially at temperatures of deformation below 250°C in spite of the high alloys strength. It is connected in many aspects to features of the structure and texture formation during plastic deformation of the given alloys. Situation can considerably be improved if to find ways of magnesium products deformation allowing generating in these materials the equiaxed fine-grained structure and diffuse or tilted basal texture. One of the promising ways to solve the problem is application of the severe plastic deformations with the help of equal channel angular pressing (ECAP) [2-3]. The ECAP process is characterized by the development of characteristic deformation textures. Moreover, plastic deformation of magnesium alloys strongly affected by the crystallographic texture [4]. In this work texture evolution of ECAPed samples from alloys AZ31 and MA2-1 (Mg-4.5% Al-1% Zn) has been investigated by means of neutron diffraction. The texture measurements were carried out at TEX-2 instrument situated at reactor FRG-1(GKSS). The deformation experiments were done following the three important routes of ECAP, namely A, Bc and C up to six passes in a 90° die. Texture evolution with a double initial fiber was analyzed and related to the processing routes.

1.K.Xia, J.T. Wang, X.Wu, G.Chen, M.Gurvan, Mater.Sci.Eng. A 410-411, 324-327 (2005)

2.Z.Horita, T.Fujinami and T.G. Langdon, Mater.Sci.Eng., A318, 34 (2001)

3.R.Z.Valiev, R.K. Islamgaliev and I.V. Alexandrov Prog.Mater.Sci., 45, 103 (2000)

4.Suwas S., Gottstein G., Kumar R. Mater. Sci. Eng. A, 2007, 1-14

T-55 Bridging the gap between synchrotrons and neutrons in non destructive testing at the surface

Robert Wimpory¹, Tobias Poeste², Mirko Boin¹, Stefan Flemming¹, Ingwer Denks¹, Christoph Genzel¹, Rainer Schneider¹

¹Helmholtz-Zentrum Berlin für Materialien und Energie

²University of Kassel

In this presentation we would like to give a brief overview of the measurement of strains at surfaces of materials using diffraction, tackling the so-called surface effect [1]. New instrument up-grades concerning optics and detection can have a profound influence on the observed surface effect when strain scanning. Since May 2007 a new perfectly bent silicon monochromator on E3 [2] (at BENSC at the Helmholtz Centre Berlin for Materials and Energy) has provided a significant boost to the efficiency and number of measurements that can be performed. This increase in speed of measurement renders strain determination more feasible. Recent measurements on E3 have shown that for ferritic steel (using the hkl 211 reflection on a specimen previously measured on EDDI [3]), the surface effect appears to be very small at its normal optimal conditions without adjusting the bending radius of the monochromator [4]. Results from these measurements will be presented and discussed. As a conclusion, discussion of how to interpret the data and the precautions that need to be taken will be made.

[1] P. J. Webster et al, 'Impediments to efficient through-surface strain scanning', Journal of Neutron Research, 3:4, pp 223 - 240 (1996).

[2] R.C. Wimpory et al, 'Efficiency Boost of the Materials Science Diffractometer E3 at BENSC: One Order of Magnitude Due to a Horizontally and Vertically Focusing Monochromator', Neutron News, Volume 19, Issue 1 January 2008, pages 16 - 19

[3] I.A. Denks and Ch. Genzel 'Enhancement of energy dispersive residual stress analysis by consideration of detector electronic effects, Nuclear Instruments and Methods in Physics Research B 262 (2007) 87-94

[4] Miroslav Vrβna, P. Mikula 'Suppression of Surface Effect by Using Bent-Perfect-Crystal Monochromator in Residual Strain Scanning' Material Science Forum Vols. 490-491 (2005) pp 234-238

T-56 Neutron Diffraction Measurement Of AZ31B Magnesium Alloy Sheet Biaxially Deformed At Warm Temperatures

Ibai Ulaçia¹, Gurutze Arruebarrena¹, Peter Spalthoff², Christian Randau³, Iñaki Hurtado¹

¹MGEP - Mondragon Unibertsitatea

²Institute for Materials Research, GKSS

³Institute of Materials Science and Engineering TU-Clausthal

Magnesium alloys present high potential for automotive applications due to their lower density in comparison with other widely used structural materials. This property could allow for reductions in vehicle weight, but also for improvements in dent resistance and shell resistance behaviour, by increasing thickness in structural sheet applications. However, as it has been reported by many researchers, some limitations emerge when forming magnesium sheet parts. It is well known that due to their hexagonal close-packed (hcp) crystal structure, magnesium alloys present low formability at room temperature. Increasing forming temperature, formability of magnesium alloys is improved. With the aim of quantifying the formability improvement, in the present study, deep drawing experiments were carried out at warm temperatures up to 250°C.

Neutron diffraction measurements were performed in parts produced by warm deep drawing process. The measured textures in different zones of the sample were compared in order to know forming conditions and properties of the final part. Measurements show a similar deformation pattern in two directions of the sheet which means that the properties of the final part (i.e. earing) are influenced by the initial texture.

Finally, orientation distribution function (ODF) of the different samples was calculated from the experimentally measured pole density functions (pole figures). The negligible average deviations between experimental and calculated pole figures show that the neutron diffraction measurements were carried out correctly.

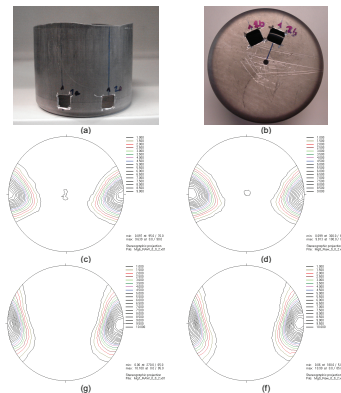


Figure 19.6: Areas of the deformed sheet where texture measurements were carried out, (a) in the flange and (b) in the base. (c), (d), (e) and (f) pole figures for the (002) diffraction peak for the four considered zones.

T-57 Formation and stabilisation of miniemulsions based on the phase inversion concentration (PIC) method

Peggy Heunemann¹, Michael Gradzielski²

¹TC 7

²TC7

A miniemulsion can be obtained by using the phase inversion method (PIC). Normally two immiscible fluids are mixed; thereby one of the fluids is distributed as small droplets into the other [1]. Depending on which fluid generates the droplets, there are two possible forms of emulsions. Direct emulsions are characterized through oil dispersed droplets in an aqueous phase while inverse emulsions are exactly oppositely built. In the PIC-case only o/w-emulsions are possible to create [2]. The formation takes place while adding a high amount of water to a mixture composed of oil, surfactant, cosurfactant, emulsifier and emollients. The generation of such an emulsion is constituted by passing a bicontinuous phase while diluting [3].

The accumulated droplets exhibit very small diameters in the magnitude of 10 – 500nm and were studied with respect to their structure by means of Dynamic Light Scattering (DLS), Small Angle Neutron Scattering and X-Ray Scattering (SANS, SAXS).

Combined Stopped-Flow-SANS (SF-SANS) and -SAXS (SF-SAXS) observations had been done in respect to examine the stability behavior during the formation process, ageing process and breakdown processes whatsoever. The formation and stabilization of o/w miniemulsions in use based on a commercial formulation [3], so that the composition with respect to the surfactant and the contained oil was varied and its effect on the structures and their stability determined. As the systems are electrostatically stabilized we in particular studied the effect of ionic strength on the stability of the formed miniemulsions by means of turbidimetry and SF-SANS.

[1]: J. Bibette, F. L. Calderon, and P. Poulin. Emulsions: basic principles. Reports On Progress In Physics, 969-1033, 1999

[2]: F. Caruso. Colloids and Colloids Assemblies: Synthesis, Modification, Organization and Utilization of Colloid Particles; Wiley-VCH, Weinheim 2004

[3]: Gabriel Polak Jürgen Meyer and Ralph Scheuermann. Preparing pic emulsion with a very fine particle size. Cosmetics & Toiletries magazine, 1-10, 2006.

T-58 Observation of the precipitation behaviour of Fe-25wt%Co-15wt%Mo by in-situ SANS and 3DAP

Elisabeth Eidenberger¹, Erich Stergar¹, Harald Leitner², Peter Staron³, Thomas Schmölzer¹, Helmut Clemens¹

¹Department Metallkunde und Werkstoffprüfung, Montanuniversität Leoben

²Christian Doppler Labor

³Institut für Werkstofforschung, GKSS Forschungszentrum Geesthacht

The precipitation behaviour of a martensitic Fe-25wt%Co-15wt%Mo alloy was investigated by in-situ small-angle neutron scattering (SANS) and three-dimensional atom probe (3DAP). In this alloy, age hardening is achieved by the precipitation of a nano-scaled intermetallic phase instead of secondary hardening carbides. For the optimization of materials properties knowledge of the precipitate reaction is essential. In order to obtain detailed information about the formation, growth and coarsening of precipitates a combination of several characterisation techniques is required. SANS is a powerful tool to gain reliable quantitative analyses of size distributions and volume fraction of precipitates. Furthermore, because of the ferromagnetic nature of the investigated alloy, nuclear and magnetic scattering information can be extracted from the SANS data. In-situ SANS measurements have been performed on preliminarily solution annealed samples. The samples were isothermally annealed at 500°C employing a recently developed furnace placed between the poles of an electromagnet while measuring the scattered intensity in steps of 30 s. The ratio of nuclear and magnetic cross-section, which is sensitive to changes in the chemical composition of precipitates, has been calculated. Complementarily, 3DAP has been conducted to characterize size and shape of the precipitates in the alloy. For further evaluation of SANS data, additional information about chemical compositions of matrix and particles derived from 3DAP measurements was used to calculate the scattering length density difference of matrix and particle and hence the ratio of magnetic to nuclear scattering intensities. For doing so, several assumptions concerning, i.e., mean atomic volume and magnetization of the precipitates have to be taken into account. Combination and comparison of the results of SANS and complementary methods and their interpretation provide the possibility to describe the microstructure of the alloy in detail and lead to a better understanding of the strengths and limitations of each method.

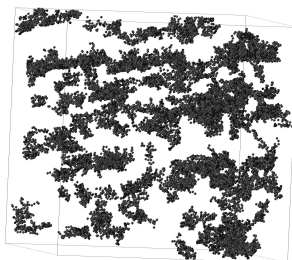


Figure 19.7: 3DAP data analysis: precipitates in a sample annealed at 500°C for 6000sec found by a cluster search algorithm. Fe, Co, Mo Atoms inside the precipitates are depicted. Sample volume 30x30x30nm³.

T-59 Measurement by neutron diffraction of all six components of X-ray elastic factors

Balder Ortner¹, Thomas Antretter¹, Michael Hofmann², Ewald Werner³

¹University Leoben, Austria

²FRM 2, München, Germany

³TU München, Germany

The strain $\varepsilon(\mathbf{r}, hkl)$ measured in direction \mathbf{r} is related to the stress state σ_{ij} and the X-ray elastic factors $F_{ij}(\mathbf{r}, hkl)$ via [1]:

$$\varepsilon(\mathbf{r}, hkl) = \sum_{i,j=1}^3 F_{ij}(\mathbf{r}, hkl) \sigma_{ij}$$

Usually this equation can be used for the measurement of residual stresses, if the matrices F_{ij} are known. The components of the tensor \mathbf{F} are calculated, which is possible, if the texture of the polycrystalline material as well as the elastic properties of the single crystals (grains) are known. On the other hand, measurements of the \mathbf{F} -tensor are scarce and experiments to determine of all components of \mathbf{F} have not been reported so far. This contribution aims to fill this gap by presenting a measurement strategy for obtaining the full tensor.

The principle of the experiment is the following: A cuboctahedrally shaped specimen is set under compressive stress on its seven distinct pairs of parallel planes. This gives seven different stress tensors, with measurement of epsilon in always the same direction \mathbf{r} . Using Eq. 1 a system of linear equations can be established. Since the loading is not uniaxial, the entries of the stress tensor σ have been calculated by the finite elements method. It is demonstrated that the system of linear equations is well conditioned so that the full tensor \mathbf{F} can be calculated.

[1] H. Dölle, J. Appl. Cryst. 12 (1979) 489-501

20 Structure research

T-60 GISANS study of layered TiO₂:polymer films for photovoltaic applications

Gunar Kaune¹, Ezzeldin Metwalli¹, Uwe van Bürck¹, Jean-Francois Moulin², Peter Müller-Buschbaum¹

¹TU München. Physik Department LS E13

²GKSS Forschungszentrum, REFSANS

Photovoltaic energy conversion systems based on an inorganic semiconductor and an organic hole transporting material, so called hybrid solar cells, have emerged to a promising alternative technology for solar light harvesting [1]. In a common device, a nanosized structure with a large interface between the two components is necessary to separate excitons generated by incoming light efficiently. This can be achieved by application of a nanostructured material, whose interspaces are filled with a polymeric hole transporting material.

In our model system, we use porous titanium dioxide (TiO₂) prepared by application of a sol-gel process [2]. On the nanostructured TiO₂ layer, a thin film of poly(N-vinylcarbazole) (PVK), doped with 2,4,7-trinitro-9-fluorenone (TNF), was spin coated from a solution. The resulting structure in the films was studied with grazing incidence small angle neutron scattering (GISANS). For structural characterisation of thin film architectures, GISANS is a powerful tool, it allows to determine characteristic length scales in perpendicular as well as lateral direction to the film plane [3]. The experiments were carried out at REFSANS at FRM II, composite films consisting of TiO₂ and a PVK:TNF blend in different blending ratios were compared with single PVK:TNF blend films. For additional structural characterisation, X-ray reflectivity and atomic force microscopy measurements were done.

[1] U. Bach, D. Lupo, P. Comte, J. E. Moser, F. Weissörtel, J. Salbeck, H. Spreitzer, M. Grätzel, *Nature* 395, 583 (1998)

[2] G. Kaune, W. Wang, E. Metwalli, M. Ruderer, R. Roßner, S. V. Roth, P. Müller-Buschbaum, *Euro. Phys. J. E* 26, 73 (2008)

[3] P. Müller-Buschbaum, J. S. Gutmann, R. Cubitt, W. Petry, *Physica B* 350, 207 (2004)

T-61 Complex Metals and alloys: Neutrons for determining transition metal ordering

Bjørn Pedersen¹, Thomas Weber², Friedrich Frey³

¹Forschungsneutronenquelle Heinz Maier-Leibnitz

²Laboratorium fuer Kristallographie, ETH-Hoenggerberg, Zürich

³Sektion Kristallographie, Geo-Department, LMU München

The question of transition metal (TM) ordering in complex alloys is often difficult to access with x-ray diffraction methods. Neutrons can be very helpful due to their different scattering power contrasting almost isoelectronic atoms. In this contribution we report about results from a quasicrystalline Al-Co-Ni alloy, Al₇₀Co₁₀Ni₂₀, where combined x-ray and neutron diffraction give clear indication of pronounced TM ordering [1]. The structure solution could be accomplished with the "charge-flipping"-method [2]. Neutron data were collected at instrument RESI/FRM2 where we took profit from the image plate recording technique [3].

[1] Weber Th., Pedersen B., Gille P., Frey F. and Steurer W., Z.Krist., accepted.

[2] Oszlanyi G., Suto, A., Acta Crystallogr. A64 (2008) 123-134. Palatinus, L., Chapuis, G., J. Appl. Cryst. 40 (2007) 786-790.

[3] Pedersen B., Frey F., Scherer W., Gille P., Meisterernst G. Physica B 385-386 (2006) 1046-1048. Pedersen, B., Frey, F., Scherer, W., Neutr. News 18 (2007) 20-22.

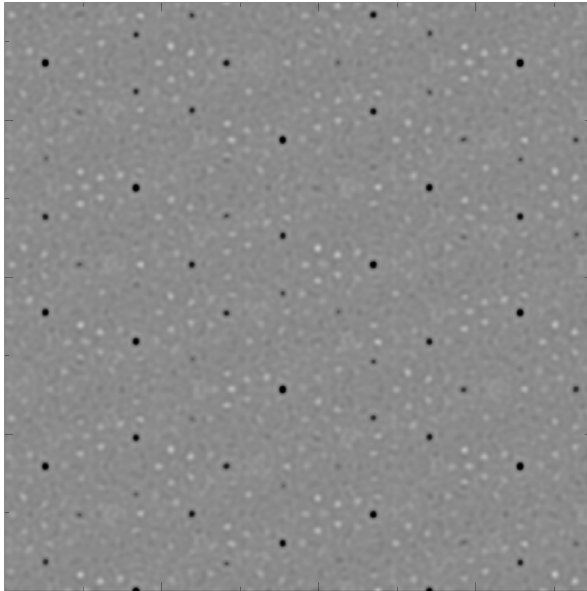


Figure 20.1: n-X difference plot of real space scattering length density. The dark spot are Co-rich positions, the bright spots are Ni-rich.

T-62 Investigation of crystal and magnetic structure of multiferroic GaFeO₃ doped with manganese

M. Bakr¹, A. Senyshyn¹, H. Ehrenberg¹, H. Fieß¹

¹Material science

Gallium iron oxide (GaFeO₃) is one of the multiferroic materials with ferrimagnetic and ferroelectric properties [1-3]. Single phase GaFe_{1-x}MnxO₃ polycrystalline have been synthesized to study the influence of Mn substitution on their crystal and magnetic structures. From XRD analysis it is seen that Mn substitution does not affect the crystal structure of the system but influences the magnetization. Neutron powder diffraction were obtained by using SPODI diffractometer. Refinement of the crystal and magnetic structure of GaFe_{1-x}MnxO₃ will be presented.

[1] R. B. Frankel ,et al , Phys. Rev. Lett. 15, 958 (1965).

[2] T. Arima, et al., Phys. Rev. B 70, 064426 (2004).

[3]Z H Sun,et al , J. Phys. D: Appl. Phys. 39 (2006) 2481-2484.

T-63 Magnetic Structure of the Inverse Perovskite (Ce₃N)In

Frank Gäbler¹, Rainer Niewa¹, Anatoliy Senyshyn²

¹Dept. Chemistry, TU München

²Materialwissenschaft, TU Darmstadt; FRMII, TU München

In recent years a number of new metal-rich Perovskites were described, indicating a similar variety in terms of compositions and crystal structures as is known from normal oxide Perovskites. However, chemical and physical properties differ substantially. For example, Perovskite nitrides of the general composition (Ca₃N)E with E = P, As, Sb, Bi, Ge, Sn, Pb, Tl cover electronic properties from semiconductors to metals [1, 2]. Substitution of the alkaline-earth metals by rare-earth metals influences the electronic balance and gives the possibility to introduce localized magnetic moments [3, 4].

Measurements of the isotherm magnetization of (Ce₃N)In (space group Pm-3m, Z = 1) at 1.8 K show a step-like metamagnetism [5]. To obtain a deeper insight in the origin of this behavior we have performed neutron diffraction on a microcrystalline sample at the SPODI powder diffractometer of FRMII with the aim to derive the magnetic structure of (Ce₃N)In below T_N = 9(1) K without application of an external magnet field. Below T_N the diffraction pattern contain additional reflections due to antiferromagnetic order. A propagation vector of $k = (0, 0.5, 0.5)$ was derived. The magnetic structure can be described by three independent magnetic substructures with moments localized on Ce atoms orientated each parallel to one of the three perpendicular crystallographic axes. All three magnetic substructures are internally antiferromagnetically ordered, resulting in a net magnetic moment of zero. The magnetic moment at Ce for the lowest temperature of 1.8 K refines to 1.75(8) μ_B .

[1] M. Y. Chern, D. A. Vennos, F. J. DiSalvo, J. Solid State Chem. 1992, 96, 415.

[2] R. Niewa, W. Schnelle, F. R. Wagner, Z. Anorg. Allg. Chem. 2001, 627, 365.

[3] M. Kirchner, F. Gäbler, W. Schnelle, F. R. Wagner, R. Niewa, Z. Kristallogr. 2006, 221, 543.

[4] M. Kirchner, W. Schnelle, F. R. Wagner, R. Niewa, Solid State Sci. 2003, 5, 1247.

[5] F. Gäbler, W. Schnelle, A. Senyshyn, R. Niewa, Solid State Sci. in press.

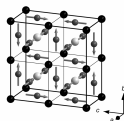


Figure 20.2: Magnetic structure of (Ce₃N)In at T = 1.8 K (without application of an external field). N: small gray spheres, In: black spheres, Ce: gray spheres with arrows, which represent the directions of the magnetic moments. All magnetic vectors are orientated parallel to the crystallographic axes.

T-64 Silkworm silk under tensile stress as a function of humidity investigated by neutron spectroscopy

Wiebke Knoll¹, Tilo Seydel², Imke Diddens³, Cedric Dicko³, Martin Müller¹, Michael M. Koza²

¹IEAP Universität Kiel

²Institut Laue-Langevin

³Dep. of Zoology, Oxford, UK

Natural silks exhibit extraordinary mechanical properties, combining high tensile strength with a high elongation at failure. The mesoscopic structure with crystalline regions embedded in a softer disordered matrix is the key to these properties [1]. We measure the molecular vibrational response of *Bombyx mori* silkworm silk fibres in situ upon externally applied tensile stress using cold neutron time-of-flight spectroscopy. Adding to a previous study on dry silk fibers [2] we presently investigate humid silk fibers. The aligned silk fibres are therefore exposed to a tensile force along the fibre axis generated by a stretching machine in a humidity chamber adapted to neutron scattering. The stress-strain curves are measured in situ and the applied force is sufficient to reach the yield point of plastic deformation. Different regions within the hierarchical silk structure can be masked by selective deuteration. It is already known from X-ray studies that most of the deformation upon extension of the fibres is due to the amorphous regions of the silk [2]. The neutron results on dry fibers indicate that the externally applied force is not reflected by any noticeable effect on the molecular vibrational or diffusional/reorientational properties of the amorphous silk protein [2]. This observation is in agreement with a model of entropy elasticity. We presently study whether similar observations can be made on humid silk fibers and how the adsorbed water enhances the polymer chain mobility.

[1] D. T. Grubb, L. W. Jelinski, *Macromolecules* 30, 2860 (1997)

[2] T. Seydel et al., *Macromolecules* 40, 1035 (2007)

T-65 Exploring Li-Na-bearing Minerals as Prototypes for Li-ionic Conductors

Sohyun Park¹, Markus Hoelzel², Anatoliy Senyshyn²

¹LMU/ Kristallographie

²FRMII/ SPODI

The milarite-family ($A_2B_2C[T(II)3T(I)12O_3]_9$): $A = Sn^{4+}, Ti^{4+}, Zr, Al, Fe^{3+}, \text{vacancy}$; $B = Na, H_2O, \text{vacancy}$; $C = Na, K, \text{vacancy}$; $T(I) = Si, Al$; $T(II) = Li, Be, Mg, \text{vacancy}$ [2, 3] is a new interesting candidate as prototype for Li-Na-ionic conductors due to: 1) the presence of short pathways available for conducting Li; 2) the presence of a crystal-chemical basis for the formation of solid-solutions and defect-engineering; 3) a high thermal stability up to 1200 K. In fact, our recent studies showed ionic conductivity in Li-Na-bearing milarite-type minerals, sogdianite and sugilite for the first time [4, 5]. The ionic conductivity in sogdianite could be assigned to site exchange processes of Li between T(II) and A sites parallel to the (001)-plane at elevated temperatures. Interestingly, the ionic conductivity in this topology is proportional to the amount of Na cations at B sites [5]. These Na cations may play relevant multiple roles, as carrying and transferring charges for the negative-charged framework $[Li_3Si_{12}O_{30}]^{9-}$. Here, the state of the art development of Li-Na-bearing milarite-type battery materials will be presented.

1. J.-M. Tarascon, M. Armand (2001), *Nature*, 414, 359-367.

2. F.C. Hawthorne, et al. (1991), *Am. Mineral.*, 76, 1836-1856.

3. F.C. Hawthorne (2002), *Can. Mineral.*, 40, 699-710.

4. S.-H. Park, et al. (2007), *J. Solid St. Chem.*, 180, 1306-1317.

5. S.-H. Park, Abstract, 16. Jahrestagung der DGK, 03-06.03.2008, Erlangen.

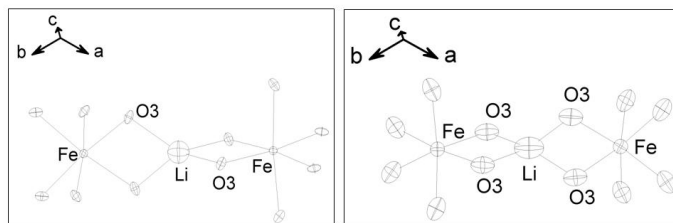


Figure 20.3: ADP ellipsoids of LiO_4^- and FeO_6 at 295K (a: left) and at 973K (b: right) in sugilite.

T-66 Magnetische Struktur der inkommensurablen Spin-Ketten-Verbindung $\text{Ca}_2\text{Y}_2\text{Cu}_5\text{O}_{10}$

Jörg Thar¹, Karine Sparta¹, Georg Roth¹, Bjørn Pedersen², Martin Meven²

¹Institut für Kristallographie

²TUM, ZWE FRM-II, Lichtenbergstr. 1, 85747 Garching

Die Spinkettenverbindungen der Mischkristallreihe $\text{Ca}_{2+x}\text{Y}_{2-x}\text{Cu}_5\text{O}_{10}$ gehören zu den NaCuO_2 -verwandten Strukturen [1], mit einer variablen Oxidationsstufe für Cu. $\text{Ca}_2\text{Y}_2\text{Cu}_5\text{O}_{10}$ stellt dabei das Cu(II)-Endglied mit Spin 1/2 Ionen dar.

Die Raumtemperaturstruktur von $\text{Ca}_2\text{Y}_2\text{Cu}_5\text{O}_{10}$ besteht aus verzerrten CuO_4 -Gruppen, die durch Kantenverknüpfung aplanare Ketten bilden. Diese Ketten werden durch $(\text{Ca},\text{Y})\text{O}_n$ -Polyeder getrennt, wobei Ca und Y statistisch verteilt sind. Die starke Verzerrung der CuO_2 -Ketten (Abb. 1) resultiert aus der Fehlanpassung zwischen ihrer 5-fachen Periodizität und der 4-fachen Periodizität der $(\text{Ca},\text{Y})\text{O}_n$ -Substruktur, und führt zu einer inkommensurablen Composit-Struktur mit dem Modulationsvektor $q = (-0,018, 0, 0,8)$ bezogen auf die CuO_2 Substruktur [2].

Abhängig von der Löcherkonzentration ändert sich der magnetische Grundzustand in $\text{Ca}_{2+x}\text{Y}_{2-x}\text{Cu}_5\text{O}_{10}$: antiferromagnetische Ordnung für $0 < x < 0,14$, Spin-Glass-Phase um $x = 1,5$, Spin-Gap-Zustand ab $x = 1,67$ [3].

Wir präsentieren unsere Ergebnisse über die Temperaturabhängigkeit der strukturellen und magnetischen Eigenschaften von $\text{Ca}_2\text{Y}_2\text{Cu}_5\text{O}_{10}$ aus Einkristall-Röntgen- und Neutronen-Beugung.

[1] P.K. Davies, J. Sol. Stat. Chem. 95, 365-387 (1991).

[2] J. Thar, Diplomarbeit, Aachen (2005).

[3] K.Kudo et al., PRB 71, 104413 (2005).

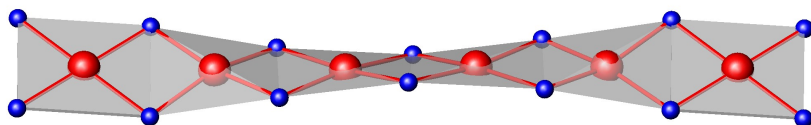


Figure 20.4: Abb. 1: Modulierte Struktur von $\text{Ca}_2\text{Y}_2\text{Cu}_5\text{O}_{10}$

T-67 GISAXS- and GISANS-Measurements on Ni- and Gd-Nanowires

Wolfgang Kreuzpaintner¹, Reinhard Kampmann¹, Jean-Francois Moulin¹, Martin Haese-Seiller¹, Dieter Lott¹, Andreas Schreyer¹

¹GKSS Forschungszentrum GmbH

Recent GISAXS and GISANS measurements on Ni- and Gd-nanowire arrays arranged on a faceted α -Al₂O₃ wafer with a periodicity of approx. 200 nm will be presented.

The investigated samples were prepared by UHV electron beam evaporation. Here, the faceted surface was arranged to the Ni- or Gd-source under a 5° angle causing self shading of neighboring facets with only the upper edges of the facets exposed to the evaporate beam [1]. By this method polycrystalline Ni- and Gd-wires with a cross section of approx. 25 nm x 50 nm and 50 nm x 50 nm at a spacing of 200 nm were grown on the substrate. In the case of Gd a 25 nm thick Al-layer was deposited onto the sample to avoid oxidation.

The GISAXS experiments were performed at ID10b at the ESRF synchrotron source and GISANS was carried out at REFSANS at the FRM II neutron source combining both reflectometer and SANS setup. The time of flight chopper and detector system of REFSANS enables one to take advantage of a continuous neutron wavelength spectrum of 6 to 18 Å. For each wavelength slice, intensities are obtainable at the intersections of the grating truncation rods with the Ewald sphere [2]. Since multiple wavelengths are measured, an integral image over all wavelengths of the GISANS measurement can be obtained, giving a more complete reconstruction of the grating truncation rods in reciprocal space as is possible with single wavelength setups. Additionally, reflectivity curves can be directly obtained from the GISANS measurement.

Both GISAXS and GISANS measurements were carried out for various rotational states around the sample normal. Apart from very detailed information on the lateral structure of the sample, that is obtainable from both x-ray and neutron measurements, the neutron measurements also give scattered intensities that lie below the sample horizon, which is usually not accessed by x-ray measurements. The complementary nature of synchrotron and neutron results will be demonstrated in more detail.

[1.] M. Huth, K.A. Ritley, J. Oster, H. Dosch and H. Adrian, *Adv. Funct. Mater.*, D-69469 Weinheim: WILEY-VCH Verlag GmbH, 2002, pp. 333-338.

[2.] M. Yan and A. Gibaud, *J. Appl. Cryst.*, Int. Union of Cryst, 2007 (40), pp. 1050-1055.

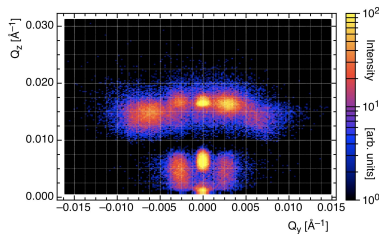


Figure 20.5: Intensity map in reciprocal space of the GISANS measurement on Ni nanowires for a wavelength of 8.31 Angstrom.

T-68 Characterization of core-shell nanoparticles by neutron scattering

Giancarlo Pigozzi¹, Debashis Mukherji², Pavel Strunz³, Ralph Gilles⁴, Markus Hölzel⁵, Ralph Spolenak¹

¹Laboratorium für Nanometallurgie, ETH Zurich

²Institut für Werkstoffe, TU Braunschweig

³Research Centre Rez

⁴ZWE FRM-II, TU München

⁵TU Darmstadt

Core-shell nanoparticles are finding potential applications in medical therapy, in fields like targeted drug delivery and magnetic hyperthermia. For these, a nanoparticle with a magnetic core and inert biocompatible shell is desirable. A variety of methods are available to produce core-shell nanoparticles, most of which require reactions in two-step. Recently, we demonstrated a single-step method to produce core-shell nanoparticles with a core of intermetallic phase and a silica shell. The process extracts precipitates from two-phase alloys through electrochemical selective dissolution of the matrix phase [1,2]. It is possible to select the system, such that the core is ferromagnetic, e.g. Ni₃Fe. In order to optimise the extraction process and to understand the shell formation mechanism, the morphology of the extracted nanoparticles was studied by neutron scattering. Here, results will be presented for Ni₃Si nanoparticles capped by an amorphous Si oxide shell. SANS results [3] confirm that the size distribution of Ni₃Si precipitates in the bulk alloy remain unchanged after the extraction, indicating that the shell forms on top of the nanoparticle core. Further, wide angle neutron scattering (powder diffraction) with in-situ heating and TEM were used to analyze the stability of the extracted core-shell particles during thermal exposure up to 1000°C in vacuum. Estimation of size and strain parameters from the broadening of Bragg peaks show that the as-extracted nanoparticles are strain free and that heating induces internal strain in the crystalline core of the particles (up to 0.15%). This is a consequence of the thermo-mechanical stress developed due to different thermal expansion coefficient of the core and the shell material. Further, the disordering of the core phase was observed, which involves local lattice distortions and promote the formation of new crystal domains inside the amorphous shell. Neutron scattering measurements is a powerful tool for characterising nanoparticles and compliment electron microscopy studies. The present study was successful in describing how the electrochemical selective phase dissolution method leads to the shell formation around the nanoparticles. Effective synthesis of core-shell nanoparticles with magnetic core and specific particle size suitable for diverse medical applications is being pursued.

[1] D. Mukherji, G. Pigozzi, F. Schmitz, O. Näth, J. Rösler and G. Kosterz. *Nanotechnology* 2005, 16, 2176-2187 (2005) [2] G. Pigozzi, D. Mukherji, R. Gilles, B. Barbier, and G. Kosterz *Nanotechnology*, 17 (2006) [3] P. Strunz, D. Mukherji, G. Pigozzi, R. Gilles, T. Geue, and K. Panzas *Applied Physics A*, 88, 277-284 (2007)

T-69 Unraveling the magnetic structure of $\text{CeCu}_2(\text{Si}_{0.55}\text{Ge}_{0.45})_2$ by using the complementarity of neutron and x-ray scattering

Enrico Faulhaber¹, Oliver Stockert²

¹Institut für Festkörperphysik

²Max-Planck-Institut für Chemische Physik fester Stoffe; Dresden; Germany

CeCu_2Si_2 is the first discovered heavy-fermion superconductor and consequently the system was studied with great intense over the past years. Especially the occurrence of magnetic order near the superconducting phase stimulated further investigation of both phenomena. To understand the superconductivity and its interplay with the magnetism one clearly needs to unravel the properties of the magnetic order. The direct magnetic structure determination in pure CeCu_2Si_2 is severely hampered by the low magnetic ordering temperature ($T_N < 1$ K) and the small ordered moment. However, the system can be tuned towards a non-superconducting antiferromagnet with enhanced ordering temperature and increased ordered magnetic moment by substituting germanium for silicon. In $\text{CeCu}_2(\text{Si}_{1-x}\text{Ge}_x)_2$ the alloy with $x = 0.45$ proved to be a good choice with a $T_N = 3$ K. An initial neutron diffraction study [1] was not sufficient for satisfactory determination of the magnetic structure due to a relaxed resolution. In contrast, a combination of high-resolution resonant magnetic x-ray (RMXS) and neutron scattering allowed a separation of overlapping magnetic peaks. As a consequence, the magnetic structure at low temperatures could be solved. It consists of two magnetic sublattices with reduced symmetry [2]. The peculiarities of the resulting magnetic structure as well as the advantages of combining the complementary methods of RMXS and neutron diffraction will be discussed in detail.

[1] E. Faulhaber et. al., *JMMM* **272-276** (2004) 44.

[2] E. Faulhaber, *PhDthesis*, Technische Universität Dresden (2008).

T-70 Magnetic structure of GdCu₆

Anton Devishvili¹, **Martin Rotter**², **Mathias Dörr**³, **Brigitte Beuneu**⁴, **Behr Gunter**⁵

¹Institut Laue-Langevin, Grenoble, France

²Institut für Physikalische Chemie, Universität Wien, Austria

³Institut für Festkörperphysik, TU Dresden, Germany

⁴Labaratoire Leon Brillouin, CEA-CNRS, Saclay, France

⁵Institut für Festkörper und Werkstofforschung, Dresden, Germany

Hot neutron diffraction has been used to study the magnetic structure of GdCu₆. Long range antiferromagnetic order is being established below the Néel temperature $T_N = 16$ K. A propagation vector of (h 0 0) was determined from the neutron powder refinement. The magnetic moments are oriented normal to the *a* direction, which agrees with previously reported bulk experiments (susceptibility, magnetization etc). McPhase has been used to simulate the magnetic properties of this compound on the basis of the standard model of rare earth magnetism. Exchange interactions have been modeled by an RKKY type expression with different Friedel wavelengths along the orthorhombic *a*-, *b*- and *c* axis. The suggested helical magnetic structure with propagation vector of (0.167 0 0) is consistent with neutron data and previously reported bulk measurements.

T-71 Texture evolution of the Mg/Al composite processed by the accumulative roll bonding (ARB)

Weimin Gan¹, Hai Chang², Mingyi Zheng², Heinz-Günter Brokmeier¹

¹TU-Clausthal

²Harbin Institute of Technology

Accumulative Roll-bonding (ARB) is a relatively simple method of generating ultra-fined grained bulk materials in which two metal sheets are bonded during rolling at a relatively high reduction. Structural formation of dissimilar metal systems during ARB may be much more complicated than that of single metal systems, due to the co-deformation of the two dissimilar metals with different flow properties. Accordingly, the texture of the constitute metals in the ARB processed multilayered composite may be quite different from that of ARB processed monolithic metals. Neutron diffraction is quite suitable for the texture analysis of this bi-phase system because of its high penetration depth one can get global textures neglecting local details on the boundaries. The Mg/Al composite was fabricated successfully by accumulative roll bonding (ARB) at 400°C using pure magnesium and Al5052 sheets. The global texture of the two constitute metals were measured by the texture diffractometer TEX-2 at GKSS. The Orientation Distribution Function (ODF) of both metals was calculated using the iterative series expansion method. The texture type of Mg doesn't change obviously during ARB processing; only the texture sharpness is changed from pass to pass. In the case of Al5052, a more complicated texture evolution was detected. The initial texture, mainly a cube component, has a medium texture sharpness which decreases from pass to passes. In addition, new texture components develop.

T-72 Neutron Powder Investigation of Structure and Diffusion in variously doped Mayenites

Hans Boysen¹, Ines Kaiser-Bischoff¹, Martin Lerch², Markus Hölzel³, Anatoliy Senyshyn³

¹Kristallographie, LMU München

²Institut für Chemie, TU Berlin

³TU Darmstadt/FRM II

Mayenite, Ca₁₂Al₁₄O₃₃, has recently attracted much attention for technological applications, e.g. as an oxygen ionic conductor. This can be related to its crystal structure, consisting of a calcium-aluminate framework, in which 32 of the 33 oxygen anions are bound. The remaining "free" oxygen is distributed over 1/6 of large cages in the framework and may diffuse through large openings between adjacent cages. The structure is heavily disordered involving displacements of Ca cations, and the presence of extra anions like O₂⁻, O₂₂⁻, O⁻ and OH⁻. The "free" oxygen can be substituted by nitrogen, therewith opening up possibilities for a first pure nitrogen ionic conductor.

Four samples with nitrogen contents of 0, 0.55, 1.0 and 1.27 wt% N and two iron doped samples with 0.1 and 2.5 wt% Fe were investigated at the neutron powder diffractometer SPODI (FRM2/Garching) using a wavelength of 1.548 Å and an Nb vacuum furnace up to 1050 °C. Additional synchrotron X-ray measurements were carried out at instrument B2 (Hasylab/Hamburg) with a wavelength of 0.49324 Å up to 900 °C using a graphite furnace. Data were analysed by the Rietveld method including anharmonic Debye-Waller factors using the program package JANA2000 and by difference Fourier methods. At ambient temperature the pure and N-doped samples contained extra anion species like peroxide, superoxide, hydroxide, imide and amide, which could partly be disentangled through the complementarities of the X-ray and neutron data. They disappear above ca. 700 °C. In contrast, the Fe doped samples are stoichiometric. The hydrogen content was estimated from the incoherent background. At high temperatures the diffusion of oxygen proceeds via a jump-like process involving exchange of "free" oxygen with framework oxygen, coupled to relaxations of the Ca ions [1]. In contrast, nitrogen diffuses as NH₂- via an interstitial process [2].

This work was supported by the DFG within the priority program SPP 1136 under BO 1199/2 and LE 781/10.

[1] Boysen, H., Lerch, M., Stys, A., Senyshyn, A.: *Acta Crystallographica* (2007) B 63, 675.

[2] Boysen, H., Kaiser-Bischoff, I., Lerch, M.: *Diffusion Fundamentals* (2008) 8, 2.1-2.8.

T-73 The Solvation of Nanocarbons in Ammonia and Organic Solvents

Emily Milner¹, Neal Skipper¹

¹UCL

In order to separate, purify, process and manipulate nanocarbons it is necessary to be able to put them in solution. We have demonstrated that metal-ammonia based liquids can be used as generic solvents with which to charge and solubilise carbon nanostructures such as nanographites.

Small angle neutron scattering experiments conducted on the LOQ instrument at the ISIS pulsed neutron source confirm that fractal aggregates of these nanocarbons are formed in toluene. In contrast to this, well-dispersed solutions can be formed by first charging in metal-ammonia and then by solvation in ammonia, acetone or THF.

THF seems to be the best solvent for charged nanocarbons: further SANS experiments, performed on the D11 instrument at the Institut Laue-Langevin, focussed on confirming the results from our previous experiments and discovering the optimum charge for solvating nanocarbons in THF. We conclude that, for nanographites, charging followed by solvation in THF provides a means with which to controllably disperse and deposit platelets, and also the possibility of dissolving individual graphene sheets.

In situ wide angle neutron scattering experiments, also conducted at the ILL, on the D20 instrument, have shown that entirely new staged graphitic compounds can be made via the metal-ammonia route. These novel pillared materials have numerous potential applications. All our neutron scattering work is complemented by X-ray diffraction and SEM characterisation studies of the structure, morphology, composition and properties of the samples.

T-74 $\text{Al}_4(\text{Cr,Fe})$: Single Crystal Growth by the Czochralski Method and Structural Investigation with Neutrons at FRM II

Birgitta Bauer¹, Bjørn Pedersen², Peter Gille³

¹Department für Geo- und Umweltwissenschaften, Sektion Kristallographie, Ludwig-Maximilians-Universität, Theresienstraße 41, 80333 München, Germany

²Forschungsneutronenquelle Heinz Maier-Leibnitz, TU München, Garching

³Department für Geo- und Umweltwissenschaften, Sektion Kristallographie, Ludwig-Maximilians-Universität, Theresienstraße 41, 80333 München, Germany

The complex metallic alloy $\text{Al}_4(\text{Cr,Fe})$, Pearson symbol *o*/366-59.56, is regarded an approximant to the decagonal AlCrFe phase.

For growing complex metallic phases from off-stoichiometric melts the Czochralski method has been proven to be a very powerful tool. There are several advantages like easy seeding control, good mixing of the melt and the possibility to observe the growing crystal during the whole experiment. To prevent the Al-rich melts from any traces of oxygen the growth chamber used is fully metal-sealed. The growth direction is given by the orientation of a native seed. Due to kinetic reasons pulling rates as low as 0.05 mm/h are necessary. Caused by the incongruent solidification the melt changes its composition proportional to the crystallized amount of material. This results in a decreasing liquidus temperature that has to be compensated by a progressive temperature ramp between 0.1 and 0.4 K/h in order to keep the diameter constant.

Large $\text{Al}_4(\text{Cr,Fe})$ single crystals have been grown in all two-fold directions of the orthorhombic phase. The composition of the investigated crystal was measured by electron probe microanalysis to be $\text{Al}_{78}\text{Cr}_{19}\text{Fe}_3$. Axial as well as radial composition profiles were found to be almost uniform within the error of measurement.

The formula $\text{Al}_4(\text{Cr,Fe})$ suggests that Fe alloyed to Al_4Cr enters Cr sites. On the other hand, phase diagram studies and X-ray powder diffraction measurements by Palm [1] have given an existence region of the $\text{Al}_4(\text{Cr,Fe})$ phase that suggests an isoconcentration behaviour with respect to the Cr content of the solid phase. This could only be explained if Fe would substitute for Al instead of Cr. The question whether Fe substitutes for Cr or also occupies Al sites can not be decided by X-ray diffraction experiments, because Cr and Fe are almost isoelectronic. Therefore a single crystal neutron diffraction experiment (sample size: $3 \times 3 \times 3 \text{ mm}^3$, wave length: 1.5 Å) was performed at FRM-II. Deng et al. [2] determined the space group from X-ray single crystal data to be *Immm*. As a result in the neutron experiment additional reflections *hkl* at $k = 0.5$ were found, lowering the symmetry to a primitive cell and causing a doubling of the *b*-axis, so the space group is now *Pmmm* with $a = 12.516 \text{ Å}$, $b = 25.135 \text{ Å}$ and $c = 30.692 \text{ Å}$. This is most likely due to the ordering of Cr and Fe. These reflections also show diffuse scattering. The full width at half maximum is about doubled compared to reflections without diffuse parts. From this a relatively long-range order can be concluded. A possible explanation for the diffuse scattering might be the occurrence of stacking faults. This and the original question whether Fe enters Cr or/and Al sites could not be answered in the first neutron experiment, but are subject of ongoing investigations.

[1] Palm M., J. Alloys & Compounds **252** (1997) 192-200.

[2] Deng D.W., Mo Z.M., Kuo K.H., Phys. Condens. Matter **16** (2004) 2283-2296.

T-75 Martensitic Transformation of Ni-Mn-X Magnetic Shape Memory Alloys upon Cooling Under Magnetic Field

Mahmoud Rabie¹, Mehmet Acet², Seda Aksoy³, Jürgen Neuhaus⁴, Winfried Petry⁴, Anatoliy Senyshyn⁵

¹Department für Geo- und Umweltwissenschaften, Ludwig-Maximilians Universität München

²Experimental Physik, Universität Duisburg-Essen

³Duisburg-Essen Universitaet

⁴Forschung-Neutronenquelle Heinz Maier-Leibnitz (FRM II), Technische Universität München

⁵FB Material- und Geowissenschaften, Technische Universität Darmstadt

Magnetic shape memory alloys promise innovative applications working at frequencies not achievable by conventional shape memory alloys. The observation of large magnetic-field-induced strains up to 10% [1], large magnetocaloric effect [2] and large magnetoresistance [3] has strengthened the interest on these alloys system.

Neutron diffraction studies were performed on cooling Ni-Mn-Ga, Ni-Mn-Sn and Ni-Mn-Ga alloys under applied magnetic field, in order to understand the martensitic transformation of these alloys and to account for the different properties observed [4,5]. Furthermore, our investigations reveal the structures of the phases involved and study its dependence on an applied magnetic field.

In this work, neutron diffraction measurements of three alloys, Ni(50)Mn(30)Ga(20), Ni(50)Mn(35)Sn(15) and Ni(50)Mn(34)In(16) where taken at the Structure Powder Diffractometer, SPODI at the FRM II facility. Diffraction patterns where obtained at 300K and 5K via cooling under zero magnetic field and 5 Tesla field, subsequently. In Ni-Mn-Ga, a transformation from cubic austenite (Fm-3m) to orthorhombic martensite (Pnm) structure was observed with a 5M martensitic modulation, while in Ni-Mn-Sn the same cubic phase transforms to orthorhombic (Pmma). In Ni-Mn-In, the low temperature phase could not yet be determined. However, close inspection of diffraction patterns of the later alloy shows that the phase transformation was not completed during field cooling by showing retained peaks of the austenite phase at 5K and 5T, which indicate a probable kinetic arrest [6].

This Project is funded by DFG, SPP 1239, „Aenderung von Mikrostruktur und Form fester Werkstoffe durch aeußere Magnetfelder,

[1] K. Ullakko, J.K. Huang, C. Kanter, V.V. Kokorin, R.C. O’Handley, Appl. Phys. Lett. 69 (1996) 1966-1968. [2] J. Marcos, L.I. Manosa, A. Planes, F. Casanova, X. Batlle, A. Labarta, Phys. Rev. B 68 (2003) 094401. [3] S. Y. Yu, Z. H. Liu, G. D. Liu, J. L. Chen, Z. X. Cao, and G. H. Wu, B. Zhang and X. X. Zhang, Appl. Phys. Lett. 89, (2006) 162503. [4] Seda Aksoy, Thorsten Krenke, Mehmet Acet, Eberhard F. Wassermann, Xavier Moya, Lluís Manosa, and Antoni Planes, Appl. Phys. Lett. 91, 251915 (2007). [5] Thorsten Krenke, Eyüp Duman, Mehmet Acet, Eberhard F. Wassermann, Xavier Moya, Lluís Manosa, Antoni Planes, Emmanuelle Suard, Bachir Ouladdiaf; Phys. Rev. B 75, 104414 (2007). [6] V. K. Sharma, M. K. Chattopadhyay, and S. B. Roy, Phys. Rev. B 76, 140401 (R) (2007).

T-76 Columnar magnetic structure coupled with orthorhombic distortion in SrFe₂As₂; one of the parent compounds of new FeAs superconductors

Koji Kaneko¹, Andreas Hoser², Nubia Caroca-Canales³, Anton Jesche³, Cornelius Krellner³, Oliver Stockert³, Christoph Geibel³

¹MPI-CPfS, Japan Atomic Energy Agency

²Helmholtz-Zentrum Berlin für Materialien und Energie

³MPI-CPfS

The recent discovery of superconductivity in doped LaFeAsO[1] attracts considerable interest in layered FeAs system. In addition, superconductivity was also found in another FeAs-system, AFe₂As₂ with the well known ThCr₂Si₂-type structure[2]. Both parent compounds show the structural distortion from tetragonal to orthorhombic symmetry followed by the spin density wave formation(SDW). Electron or hole doping leads to the suppression of the Structural distortion and SDW and to the onset of superconductivity. This is reminiscent of the behavior in the high-T_c cuprates, indicating an importance of magnetic fluctuation for an emergence of superconductivity. The magnetic structure is one of the fundamental questions on the magnetic properties of the materials and is indispensable for understanding the interplay between magnetism and superconductivity. Neutron powder diffraction experiments on SrFe₂As₂ were carried out in order to determine the unique magnetic structure and its relationship with the crystallographic one. With decreasing temperature, an appearance of apparent magnetic reflections concomitant with the orthorhombic distortion were detected at T₀=205 K[3]. From the detailed Rietveld analysis, the magnetic propagation vector of SrFe₂As₂ is determined to be $q=(1\ 0\ 1)$; the antiferromagnetic coupling of Fe moment sets in the longer a direction in the Fe-As layer, and interlayer coupling is antiferromagnetic as well. The size of the Fe magnetic moment is determined to be 1.01(3) μ B which is oriented parallel to the a-axis. The determined magnetic structure is shown in the figure. The temperature dependence of the magnetic moment shows an excellent agreement with those of the structural distortion and the muon precession frequency, revealing the strong coupling of the columnar magnetic order and structural distortion in SrFe₂As₂.

[1] Y. Kamihara et al., J. Am. Chem. Soc. 130, 3296 (2008).

[2] G. F. Chen et al., arXiv:0806.1209 (2008),

[3] C. Krellner et al., arXiv:0805.1043 (2008).

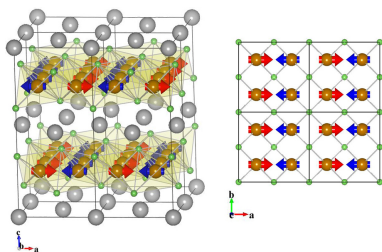


Figure 20.6: Magnetic structure of SrFe₂As₂ with the propagation vector $q=(1\ 0\ 1)$.

T-77 SANS Investigation of Martensite Nuclei in Potassium

Wolfgang Pichl¹, Maciej Krystian¹, Manfred Prem¹, Gerhard Krexner¹

¹Fakultät für Physik, Universität Wien

In potassium, in contrast to the light alkali metals lithium and sodium, no low-temperature phase transformation has been observed down to the lowest temperatures investigated (slightly below 5K). However, evidence for a lattice instability has been reported from inelastic and elastic diffuse neutron scattering measurements [1] on cooling. In the present work SANS experiments under uniaxial compression were performed in situ in the temperature range from 70 to 5 K. The compression direction was along the [001] bcc direction which is known to favor a phase transformation from bcc to close-packed structures.

Cooling to 5K without applied load produced only very slight changes in the SANS patterns. However, after uniaxial compression of 3 % along [001] anisotropic scattering patterns developed indicating the formation of particles with sizes from about 10 up to 100 nm. It seems obvious to interpret these particles as nuclei of a martensitic phase whose formation is supported by the uniaxial pressure helping to overcome the nucleation barrier. Upon releasing the pressure at 5K no change in the SANS pattern was observed indicating that the martensite nuclei, once formed, remain stable. However, after heating to 70 K the signature of the particles completely disappeared. Ab initio density functional calculations confirm that the equilibrium phase of potassium might be fcc though the differences between the ground state energies of the bcc and several alternative close-packed structures are very small.

[1] O.Blaschko, M.de Podesta, and L.Pintschovius, PRB 37 (1988) 4258

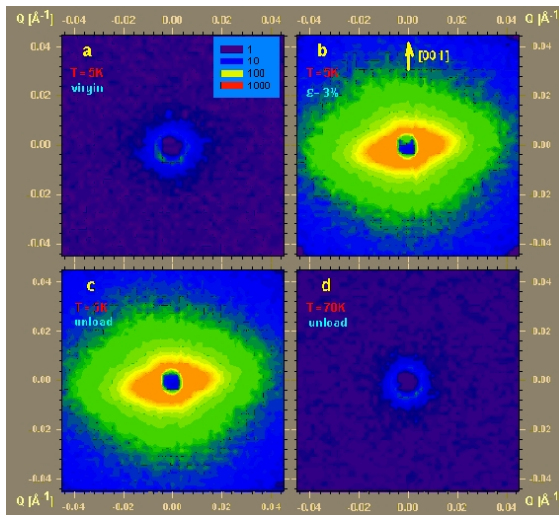


Figure 20.7: SANS patterns in potassium (a) virgin single crystal at 5 K, (b) under uniaxial compression along [001] at 5K, (c) after unloading at 5K, (d) after reheating to 70K.

T-78 Magnetic structure and orbital ordering in KCrF3

Yinguo Xiao¹, Naveen Kumar Chogondahalli M.¹, Yixi Su², Jörg Perßon¹, Anatoliy Senyshyn³, Thomas Brückel⁴

¹1. Institut für Festkörperforschung, Forschungszentrum Jülich, 52425 Jülich, Germany

²2. Jülich Centre for Neutron Science, IFF, Forschungszentrum Jülich, Outstation at FRM-II, 85747 Garching, Germany

³3. Forschungsneutronenquelle Heinz Maier-Leibnitz (FRM II), 85747 Garching, Germany

⁴4. Institut für Festkörperforschung, Forschungszentrum Jülich, 52425 Jülich, Germany;

2. Jülich Centre for Neutron Science, IFF, Forschungszentrum Jülich, Outstation at FRM-II, 85747 Garching, Germany

KCrF3 represents another prototypical orbital-ordered perovskite, where Cr²⁺ possesses the same electronic configuration of 3d⁴ as that of strongly Jahn-Teller distorted Mn³⁺ in many CMR manganites. The crystal and magnetic structure of KCrF3 compound is investigated by using the neutron powder diffraction method. The results show that the KCrF3 compound crystallizes in tetragonal structure at room temperature and undergoes monoclinic distortion with the decrease in temperature. The distortion of the crystal structure indicates the presence of cooperative Jahn-Teller distortion which is driven by orbital ordering. A clear picture of magnetic ordering is obtained below the magnetic ordering temperature (TN = 47 K): the moments of Cr²⁺ ordered antiferromagnetically with the propagation vector (1/2 1/2 0). The interplay between orbital and spin degrees of freedom in this compound will be discussed.

[1] S. Margadonna et. al., Cooperative Jahn-teller distortion, phase transitions and weak ferromagnetism in the KCrF3 perovskite, J. Am. Chem. Soc. 128, 16436-16437 (2006).

[2] G. Giovannetti et. al., KCrF3: Electronic structure and magnetic and orbital ordering from first principles, Phys. Rev. B 77,07511(2008).

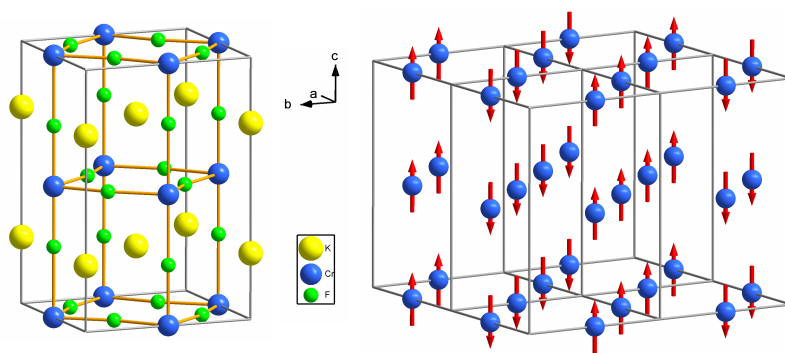


Figure 20.8: Illustration of the crystal and magnetic structures of KCrF3 at 4 K.

T-79 Structural Behaviour of Co₂SiO₄ below Room Temperature

Andrew Sazonov¹, Martin Meven², Vladimir Hutanu¹, Heger Gernot³, Thomas C. Hansen⁴

¹RWTH / FRM II

²FRM II

³Institut fuer Kristallographie, RWTH

⁴ILL

Synthetic Co₂SiO₄ has an olivine structure with isolated SiO₄ groups (space group Pnma) and shows magnetic ordering below 50K. Detailed structure analyses on Co₂SiO₄ were performed by single crystal neutron diffraction using a short wave length of 0.552 Angstrom in the temperature range from 300K down to 2.5K. Measurements up to $\sin(\Theta)/\lambda < 1.1$ inverse Angstrom yielded precise structure parameters for all atoms including the oxygens. The data at room temperature are in good agreement with former X-ray results. There is no indication of any structural phase transition below room temperature down to 2.5K. The interatomic distances and angles as well as the atomic displacement parameters behave quite normally. The lattice parameters of Co₂SiO₄ were determined by powder neutron diffraction studies in the temperature range from 5K to 500K. There is a clear indication of an anomaly in the anisotropic lattice expansion at the temperature of the magnetic phase transition at 50K. Below this temperature the lattice parameter b is shortened abruptly whereas c increases and a keeps constant. The resulting volume of the unit cell also reflects this anomaly. We assume this anomaly as being caused by magnetostriction.

T-80 Deswelling kinetics of micellar solutions and hydrogels from temperature-sensitive amphiphilic block copolymers

A. Meier-Koll¹, A. Golosova¹, A. Jain¹, A.M. Bivigou Koumba², A. Laschewsky², P. Busch³, V. Pipich³, J. Wiedersich¹, P. Müller-Buschbaum¹, C.M. Papadakis¹

¹Physik Department/ E13

²Institut für Chemie, Universität Potsdam

³JCNS-FRM II

Temperature-responsive polymeric hydrogels show a swelling-deswelling transition at the lower critical solution temperature (LCST). A number of applications, such as sensors, or drug delivery systems are associated with the kinetics of this process. So far, chemically connected polymer networks have been used, which, however, have the disadvantage of slow kinetics. Physically connected (micellar) gels based on amphiphilic triblock copolymers with a responsive hydrophilic block and two hydrophobic end blocks constitute an alternative approach. The building blocks of these networks are self-assembled micelles having a size in the 20 nm range [1], thus significantly smaller than the microgels used so far. We expect that these new micellar gels have fast switching times.

We have investigated the structural changes of a concentrated aqueous solution (17 wt.-%) of polystyrene-*b*-poly(*N*-isopropyl acryl amide)-*b*-polystyrene (dPS-*b*-PNIPAM-*b*-dPS) triblock copolymers having short deuterated polystyrene blocks during deswelling upon a temperature jump across the LCST of PNIPAM (32 °C). To determine the contribution of the physical cross-linking to the deswelling kinetics, we have carried out temperature jumps from the swollen state (20 °C) to the collapsed state (45 °C) on the triblock copolymer and on solutions of PNIPAM homopolymers. At this, the sample was annealed at the start temperature and was quickly mounted in the sample cell which was preheated to the end temperature. D₂O was chosen as a solvent to contrast match the dPS blocks. Time-resolved SANS experiments were carried out at KWS2 at FRM II with measuring times of 30 sec.

Below the LCST, the SANS curves show a weakly correlated swollen micelles. Whereas the size of the micelles changes immediately and stays then nearly unchanged, the micellar distance only decreases to half its value 2 min after the temperature change. At this time, the forward scattering shows a significant increase. A subsequent decrease is attributed to the growth of the clusters. SANS is thus an ideal tool to investigate the size changes of the micelles, their distance and their aggregation upon a temperature quench.

1.K. Troll, A. Kulkarni, W. Wang, C. Darko, A.M. Bivigou Koumba, A. Laschewsky, P. Müller-Buschbaum, C.M. Papadakis, *Colloid Polym. Sci.* 286, 1079 (2008).

T-81 Pyroxenes from Mars: Neutron powder investigation up to 900°C

Bastian Fritsch¹, Friedrich Frey¹, Hans Boysen¹, Markus Hölzel², Anatoliy Senyshyn³

¹Sektion Kristallographie, Geo-Department, LMU München

²TU Darmstadt; FRM II

³Materialwissenschaft, TU Darmstadt; FRMII, TU München

Neutron powder data of a meteoritic sample from planet Mars were collected at instrument SPODI/FRMII up to high temperatures. Structural refinements were carried out to learn about the prior history of the sample. The experiment was beyond routine work with respect to a low amount of material available (150 mg), a mixture of low-symmetric and rather similar (extensive peak overlap) pyroxene phases, pigeonite and augite, an additional contaminating glassy phase, and several phases from the sample containment. Refinements could be carried out successfully down to R-values of typically $R_{wp} \approx 2.5\%$. Peaks of both, pigeonite and augite, were considerably broadened, probably due to the impact experienced on Mars, and analysed in terms of particle sizes and strains. Although some uncertainties still remain, reasonable results were obtained for the temperature evolution of the structural parameters, sizes, strains and relative phase amounts. The main interest was devoted to a determination of the cation Mg/Fe²⁺ distribution at the so-called M1 site in the structure of pigeonite as function of the temperature: it allows some conclusions about the (tentative) cooling rate of rocks on planet Mars and is therefore of geoscientific interest.

T-82 Structural evolution of CoFeB/MgO multilayers upon annealing

K. Zhernenkov¹, M. Wolff¹, B.P. Toperverg¹, H. Zabel¹

¹Department of Physics and Astronomy, Ruhr-Universität Bochum, 44780 Bochum, Germany

CoFeB/MgO/CoFeB tunnel junctions display one of the highest TMR values at room temperature [1,2], only surpassed by Fe/MgO/Fe(001) MTJs. In the latter case it is argued that the giant TMR effect is due to the textured epitaxial growth properties which leads to a coherent tunneling process instead of a diffuse tunneling in case of AlO_x barriers [3]. However, CoFeB films are amorphous and the MgO layer is microcrystalline. Nevertheless, very high TMR values of more than 350% have been achieved after proper thermo-magnetic treatment. In order to reveal the structural and magnetic evolution under this treatment in more detail, we have investigated multilayers of CoFeB/MgO with 10 periods fabricated by the standard MTJ procedure and annealed at temperatures between 240 - 360°C. We have carried out polarized neutron reflectometry (PNR) measurements with the ADAM reflectometers at the ILL. Quantitative analysis of PNR profiles has shown that the inner part of the MgO layers has the scattering length density (SLD) close to that of bulk material, while there exist narrow (magnetically dead) interfacial regions with thicknesses and SLDs that experience appreciable changes upon annealing. At temperatures up to 300°C the SLD of those regions tends to reach the SLD of MgO providing the profile of the potential barrier necessary for highest TMR effect. Annealing at higher temperatures reduces the SLD of these regions indicating a possible intermixing between MgO and CoFeB layers and/or re-crystallization of the interfacial areas.

1.S. Yuasa and D. D. Djayaprawira, *J. Phys. D: Appl. Phys.* 40 (2007) R337 2.Y.M. Lee, J. Hayakawa, S. Ikeda, F. Matsukura, and H. Ohno, *Appl. Phys. Lett.* 89 (2006) 042506; 90 (2007) 212507 3.G. Reiss, J. Schmalhorst, A. Thomas, A. Hütten, and S. Yuasa, "Magnetic Tunnel Junctions", in *Springer Tracts in Modern Physics* 227 (2007) 291-333, ed. H. Zabel and S.D. Bader.

21 Dynamics

T-83 Proton dynamics in solid HF

Tyno Abdul-Redah¹, Sylvia McLain²

¹institut für Chemie, Sekr. C2

²Oak Ridge National Laboratory

Hydrogen halides constitute a very interesting class of solid compounds exhibiting strong long-range dipole interactions which are responsible for the existence of different crystal structures and for quite high melting and boiling temperatures. Among the hydrogen halides, hydrogen fluoride (HF) is the one with the strongest hydrogen bond [1] due to the strong electronegative character of fluorine. Compared with the other hydrogen halides, HF has not been the subject of a great number of experimental studies given the toxic and corrosive nature of this compound. For the first time direct measurement of the mean kinetic energy of H in solid HF at $T=180$ K has been conducted using neutron Compton scattering (NCS) on VESUVIO at ISIS/Rutherford Appleton Laboratory (UK). NCS operates at sufficiently high transfers of energy and momentum so that the dynamic structure factor is determined by movement, i.e. the zero point energy, of the atom in the potential. The main panel shows the measured mean kinetic energy of the proton in solid HF calculated from the width of the neutron Compton profile of H. Here, the shape of the momentum distribution is assumed to be of Gaussian shape [2]. The inset shows a representative time of flight spectrum of HF in the monel cell. As one can easily see the H recoil peak is neatly separated from the heavy atom peak being contributed to by F of the sample and by Cu, Ni and Fe of the can. Further data analysis on the exact shape of the H momentum distribution and on possible proton tunnelling processes in this system, using recently available routines [3], as well as further experiments on DF are in progress.

[1] S. E. McLain et al., *Angew. Chem.* 2004, 43, 1952.

[2] V. F. Sears, *Can. J. Phys.* 1985, 63, 68.

[3] G. F. Reiter, et al., *Physical Review Letters* 2002, 89, 135505.

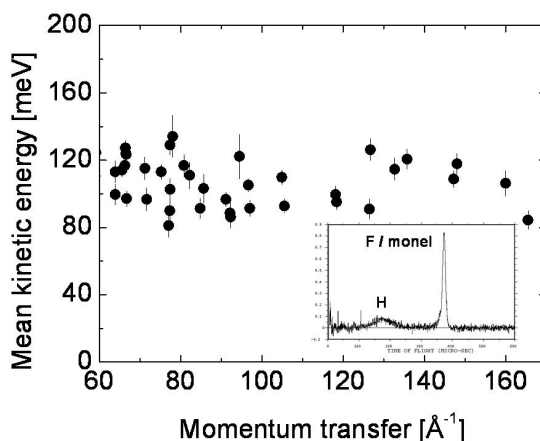


Figure 21.1: Main panel: The measured mean kinetic energy of H in solid HF. Inset: Representative time of flight spectrum of HF in the monel cell.

T-84 Dynamics in hydrous silicates studied by high temperature high pressure quasielastic neutron scattering

Fan Yang¹, Andreas Meyer², Tobias Unruh³

¹Physik Department E13, TUM

²Institut für Materialphysik im Weltraum, DLR

³Forschungsneutronenquelle Heinz Maier-Leibnitz (FRM II), TUM

A high temperature high pressure cell with a relative large opening angle was successfully constructed for the applications on the time-of-flight spectrometer TOFTOF at FRM II. The cell provides temperatures up to 1250 K and pressures up to 200 MPa at the sample position with a sample volume of about 1 cm³, achieved by an internally heated NbZr autoclave. We applied this cell to study hydrogen dynamics in water bearing silicate melts by quasielastic neutron scattering. Experiments on sodium trisilicate (Na₂O₃SiO₂), sodium aluminosilicate (Al₂O₃Na₂O₆SiO₂, Albite: haplogranitic rock composition) and pure silica (SiO₂) samples with 10 mol% water content have been performed in the temperature range from 850 K to 1250 K. Water is chemically dissolved in the melt with a constant pressure of about 150 to 200 MPa applied during the experiments to prevent it from degassing. A contrast variation via H₂O / D₂O substitution gives access to the pure proton dynamics. The q and T dependence of the measured density correlation functions in hydrous sodium trisilicates can not be interpreted by the hydrodynamics of incoherent scatterers in simple liquids. Currently the results are under discussion within the framework of an anomalous diffusion of highly mobile hydrogen atoms embedded in a relative immobile Si-O matrix, described in terms of a glass-glass transition. In the hydrous albite and silica system, no resolvable quasielastic signal has been observed with the instrument resolution available on TOFTOF. This indicates that the addition of water into these systems does not lead to a speeding up of the diffusive dynamics of the species to the order of 10⁻¹⁰ m²s⁻¹ in the temperature range which we have investigated.

T-85 Structure-Property Relationships in the Crystals of the Smallest Amino Acid: An Inelastic Neutron Scattering Study of the Glycine Polymorphs as a Function of Temperature and Pressure

Heloisa Bordallo¹, Elena Boldyreva², Alexandra Buchsteiner³, Michael Marek Koza⁴, Sven Landsgesell³

¹Helmholtz-Zentrum Berlin für Materialien und Energie, SF6

²REC-008 NoVosibirsk State UniVersity

³Helmholtz-Zentrum Berlin für Materialien und Energie, SF2

⁴ILL

Inelastic neutron scattering spectra for the three crystalline polymorphs of glycine (C₂H₅NO₂) at temperatures between 5 and 300 K and at pressures from ambient up to 1 GPa were measured. Significant differences in the band positions and their relative intensities in the density of states (DoS) were observed for the three polymorphs, which can be related to the different intermolecular interactions. The mean-squared displacement dependences reveal a change in dynamic properties at about the same temperature (150 K) for all the three forms, which can be related to the reorientation of the NH₃-group. Besides, a dynamic transition in beta-glycine at about 230-250 K on cooling was also observed, supporting previously obtained adiabatic calorimetry data. This behavior is similar to that already observed in amorphous solids on approaching the glass transition temperatures, as well as in biological systems. It suggests the onset of degrees of freedom most likely related to transitions between slightly different conformational orientations. The DoS obtained as a function of pressure have confirmed the stability of the alpha-form with respect to pressure, and also depicted sign of the previously reported reversible phase transition in beta-glycine between 0.6 and 0.8 GPa. Moreover, a remarkable kinetic effect in the pressure-induced phase transition in gamma-glycine was revealed. After the sample was kept at 0.8 GPa for an hour in the neutron beam, an irreversible transition into a high-pressure form occurred, although previously in X-Ray diffraction and Raman spectroscopy experiments such a phase transition was observed above 3.5 GPa only.

Bordallo, Heloisa N., Boldyreva, Elena V., Buchsteiner, Alexandra, Koza, Michael Marek, and Landsgesell, Sven J. Phys. Chem. B, 2008, DOI:10.1021/jp8014723

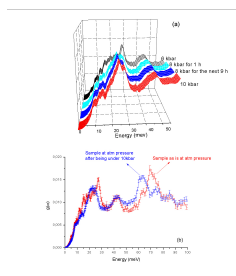


Figure 21.2: Density of states of the lattice phonons for gamma-glycine at 300 K as a function of pressure. (a) A phase transition was observed after the sample was kept at 0.8 GPa in the neutron beam for more than 1 h. For clarity, only the spectra between 0 and 50 meV are shown. (b) Comparison of $g(\omega)$ measured at ambient pressure and after release of the applied 1.0 GPa pressure indicating that the phase transformation was irreversible.

T-86 Water - clay interaction. Quasielastic neutron scattering study

Fabienne Favre Buivin¹, Oleg Sobolev², Laurent Charlet², Ewout Kemner³, Margarita Russina³

¹HES-SO Fribourg, Switzerland

²LGIT, UJF& CNRS, Grenoble, France

³Helmholtz-Zentrum Berlin für Materialien und Energie, Berlin, Germany

Smectites clay minerals are layer-type aluminosilicates consisting of negatively charged silicate layers held together by cations to give a stacked (crystalline) structure. Under humid conditions the interlayer cations and the internal clay surfaces are hydrated. Due to their hydration ability and charged layer, smectites possess some important properties like swelling ability, low hydraulic conductivity, good plasticity, high cation-exchange and adsorption properties that make them very useful for several applications. Clay minerals are widely used in the industry: as a viscous gelling agent or clarifying agent. Clay minerals have been selected as the most suitable buffer material for the high level radioactive waste repository.

The aim of this study is to investigate water diffusion in nontronite interlayer by means quasielastic neutron scattering. A hydrophobic cation, TMA⁺ (NC₄H₁₂), was used to saturate the interlayer space of nontronite clay in order to reduce cation-water interactions that could complicate the observations of the effects related to the clay - water interactions. The water content was low in order to reduce the hydrogen bonding between water molecules. The quasielastic scattering was measured with the instrumental resolution $\approx 30 \mu\text{eV}$ at the temperatures -20 oC, -10 oC, 0 oC, 20 oC using the time-of-flight spectrometer NEAT (BENCS, Berlin).

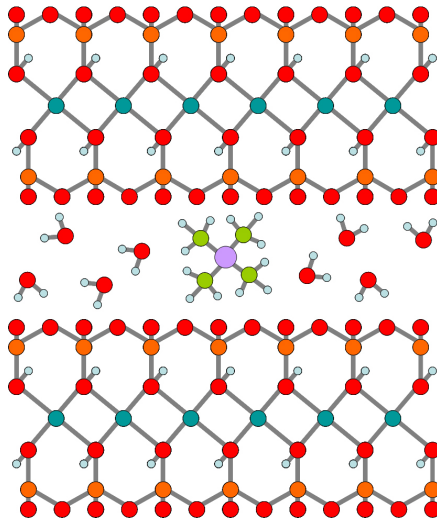


Figure 21.3: Schematic view of two nontronite layers consisting of Fe (dark green), Si (orange), oxygen (reed) and hydrogen (gray) atoms. Isomorphous substitution Fe \rightarrow Mg and Si \rightarrow Al creates a negative net charge of the clay layers. The interlayer region consists of the charge balancing cation TMA⁺ and water molecules.

T-87 Measurement of the phonon dispersion relation in YVO₄

R. Mittal¹, S. L. Chaplot², L. Pintschovius³, S. Kutovoi⁴, A. Zagumennyi⁴, Yu. Zavarstev⁴

¹Institut für Festkörperforschung, Forschungszentrum

²Solid State Physics Division, Bhabha Atomic Research Centre, Mumbai 400085, India

³Forschungszentrum Karlsruhe, Institut für Festkörperphysik, P.O.B. 3640, D-76021 Karlsruhe, Germany; Laboratoire Leon Brillouin, CEA-Saclay, F-91191 Gif sur Yvette Cedex, France

⁴General Physics Institute of RAS, Vavilova 38, Moscow 119991, Russia

The high melting temperature, structural and chemical stability along with long term corrosion resistance of zircon structured (body centered tetragonal, I41/amd) compounds has prompted the suggestion of their use as nuclear waste storage media. Therefore, it is of interest to understand their thermodynamic properties and their phase diagram as a function of pressure and temperature. Earlier, we have shown that transferable interatomic potential models developed for MSiO₄ (M=Zr, Hf, Th, U) allow us to calculate [3-6] the phonon spectra, high pressure and temperature phase diagram as well as thermodynamic properties of these compounds with good accuracy. In particular, we could reproduce the structural phase transformation from the zircon phase to the scheelite phase (body centered tetragonal, I41/a) occurring at high pressure and temperature [1-3].

We now embarked on a similar study of the compounds RVO₄ (R=Rare earth atom). They crystallize in the zircon structure as well and likewise show a zircon to scheelite type phase transition at high pressure. We developed a transferable interatomic potential model for RVO₄ compounds using our experience with MSiO₄ compounds. The most detailed check of such a model can be done by calculate the phonon dispersion relation and to compare it with experimental data. To this end, we have recently measured the phonon dispersion relation for YVO₄ using the 1T1 neutron spectrometer at LLB, Saclay. Data were collected in the (100)-(010) and (100)-(001) scattering planes at 10 K. We could measure all the phonon branches along the (100) and (001) directions up to 65 meV. Our model was successfully used for prediction of one-phonon structure factors in order to select most appropriate Bragg points for the measurement of particular phonon branches. The experimental dispersion relation is in general in good agreement with the predictions of the model. Refinement of the model is in progress.

[1] S. Ono, Y. Tange, I. Katayama and T. Kikegawa, *American Mineralogist* 89, 185 (2004).

[2] X. Wang et al, *Phys. Rev. B* 70, 64109 (2004).

[3] R. Mittal, Alka B. Garg, V.Vijayakumar, S. N. Achary, A. K. Tyagi, B. K. Godwal, E. Busetto, A. Lausi and S. L. Chaplot, *J. Phys.: Condens. Matter* 20, 075223 (2008).

[4] S. L. Chaplot, L. Pintschovius, N. Choudhury and R. Mittal, *Phys. Rev. B* 73, 94308 (2006).

[5] R. Mittal, S. L. Chaplot, N. Choudhury and C. K Loong, *J. Phys.: Condens. Matter* 19, 446202 (2007).

[6] R. Mittal, S. L. Chaplot, Preyoshi P. Bose and N. Choudhury, *Journal of Physics: Conference Series* 92, 012143 (2007).

T-88 Benzene confinement in single-walled carbon nanotubes: inelastic and quasielastic neutron scattering

Nicolas R. de Souza¹, Alexander I. Kolesnikov², Nina Verdal³, Alexander P. Moravsky⁴

¹Forschungszentrum Jülich, Jülich Center for Neutron Science at FRM II, Garching, Germany

²Oak Ridge National Laboratory, Spallation Neutron Source, Oak Ridge, Tennessee, USA

³National Institute of Standards and Technology, NIST Center for Neutron Research, Gaithersburg, Maryland, USA

⁴MER Corporation, Tucson, Arizona, USA

We characterize experimentally the dynamical properties of benzene confined in single-walled carbon nanotubes (SWNT) of diameter 14 Å. The presence of benzene inside the nanotubes is demonstrated by measuring the small-angle neutron scattering intensities from a properly prepared C₆D₆ benzene - SWNT sample. The incoherent inelastic neutron scattering spectra from C₆H₆ benzene in the nanotubes and in the bulk crystal are measured at 4 K, up to an energy transfer of 130 meV. The effective vibrational density of states reveals a significant redistribution of all intermolecular modes for the confined benzene, whereas the intramolecular modes are nearly unaffected. Incoherent quasielastic neutron scattering spectra from C₆H₆ benzene in the nanotubes were also collected from 9 K to room temperature, at an energy-transfer resolution of approx. 80 μeV. The orientational and translational diffusive dynamics of confined benzene are discussed on the basis of these data.

T-89 Behavior of molecular hydrogen in the confinement.

Margarita Russina¹, Ewout Kemner¹

¹Helmholtz Zentrum Berlin

Neutron scattering is a unique experimental tool to study the behaviour of nanostructured materials both in space and time on the most relevant range from atomic dimensions to a few nanometers and from picoseconds to nanoseconds in time. The confinement of hydrogen in nanostructured porous materials is of particular interest not only for superior hydrogen storage but also from fundamental point of view.

We have applied neutron scattering spectroscopy to study the behaviour of the molecular hydrogen confined into highly porous materials such as ice-clathrate and metallic organic framework Cu₃(BTC)₂ and used rotational molecular transitions to probe the interactions of hydrogen with the host. Our results show that the dynamics of confined hydrogen depends on bonding types and on the confinement dimensions. We have observed novel quantum-dynamics phenomena which have a strong impact on the macroscopic properties.

T-90 Molecular Hydrogen – A New Spectroscopic Property in the Attosecond Timescale Revealed with Neutron and Electron Compton Scattering

C. Aris Dreismann¹

¹Institut für Chemie, Sekr. C2, TU Berlin

Several neutron Compton scattering (NCS) experiments [1,2] on liquid and solid samples containing protons or deuterons show a striking anomaly, which is a shortfall in the intensity of epithermal neutrons scattered by the protons and deuterons. E.g., neutrons colliding with water for just 100-500 attoseconds will see a ratio of hydrogen to oxygen of roughly 1.5 to 1, instead of 2 to 1 corresponding to the chemical formula H₂O. Due to the large energy (ca. 5-50 eV, which lead to bond breaking) and momentum transfers applied, the duration of a neutron-proton scattering event is a fraction of a femtosecond, which is extremely short compared to condensed-matter (and intra-molecular) relaxation times.

Recently this effect has been confirmed [2] using an independent method, i.e. electron-proton Compton scattering (ECS). The similarity of the results is striking because the two projectiles interact with protons via fundamentally different forces – electromagnetic and strong.

The above findings have no conventional interpretation. Theoretical considerations [4] suggest the presence of attosecond quantum entanglement of the scattering protons and the surrounding electrons, so that the usual Born-Oppenheimer (BO) approximation and the associated concept of "effective BO potentials" fail to apply. The relevant physical frame for the theoretical treatment of the considered effect may be given by the quantum dynamics of open quantum systems, in which the phenomena of quantum entanglement and decoherence play a pivotal role.

Most recent electron scattering experiments on H₂, D₂ and HD in the gas phase [3] with lower energy transfers (less than 4 eV) demonstrate that the considered effect (i.e. an "anomalous" decrease of scattering intensity by ca. 30%) is present even in H₂ molecules which remain intact after the electron-proton collision. Therefore, this novel finding reveals a thus far unknown spectroscopic property of single H₂ molecules. Associated NCS experiments on the same systems in the liquid phase [5] are compared with the electron scattering results. A qualitative analysis shows that even in the case of single molecules the phenomena of short-lived entanglement and decoherence play a pivotal role. A theoretical outline based on the quantum Zeno effect is presented.

[1] C. A. Chatzidimitriou-Dreismann et al., Phys. Rev. Lett. 79, 2839 (1997)

[2] C. A. Chatzidimitriou-Dreismann et al., Phys. Rev. Lett. 91, 057403 (2003)

[3] G. Cooper, A. P. Hitchcock, C. A. Chatzidimitriou-Dreismann, Phys. Rev. Lett. 100, 043204 (2008).

[4] C. A. Chatzidimitriou-Dreismann and S. Stenholm, arXiv.org/abs/quant-ph/0702038. See also: Laser Physics 15(6), 780 (2005)

[5] C. A. Chatzidimitriou-Dreismann, T. Abdul-Redah, M. Krzystyniak, Phys. Rev. B 72,054123 (2005).

T-91 Renormalization of the longitudinal bond-stretching phonon branch in $\text{La}_{1.95}\text{Sr}_{0.05}\text{CuO}_4$ probed by inelastic neutron scattering technique

A. Hamann¹, D. Reznik¹, D. Lamago¹, L. Pintschovius¹

¹KIT

$\text{La}_{2-x}\text{Sr}_x\text{CuO}_4$ becomes superconducting (sc) in a doping range of $0.06 \leq x < 0.3$, where optimal doping of $x = 0.15$ results in T_c up to 38 K. Neutron scattering experiments focusing on phonon dispersion relations revealed an anomalous renormalization of the longitudinal Cu-O bond-stretching branch in (100)-direction that is only present in the superconducting regime [1] - there also at temperatures above T_c . Thus, this effect might be correlated to superconductivity (SC) via enhanced electron-phonon coupling. On the other hand, non-superconducting samples at low doping show antiferromagnetic or stripe order that vanishes close to the onset of SC [2]. The impact of remaining dynamic (fluctuating) stripes on the lattice possibly competing with SC is still puzzling.

We report on our latest neutron scattering measurements on $\text{La}_{1.95}\text{Sr}_{0.05}\text{CuO}_4$ that fit into the picture of that compound: In comparison to the sc-samples the softening of the bond-stretching branch towards the zone boundary becomes less pronounced. Particularly, the anomalous broadening of the phonon lineshape previously reported around $q = 0.3$ weakens significantly.

In addition to the bond-stretching peak, we observe a second subtle maximum that could easily be misinterpreted either as an intrinsic effect due to exotic physics or as originating from some misoriented domain or even pure statistics and thus corrupt the extraction of the width. We fitted the data using shell model predictions including resolution effects to be convoluted with Lorentzians to extract the intrinsic width. By this means we clearly revealed the role of resolution-based contributions from low-symmetry directions that contaminated our scans, most prominently as the small high-energy peak mentioned above. For a reliable quantitative analysis, such effects turn out to be very crucial - especially since the width is extremely sensitive to the fitting procedure. We compare our data in detail with previous work.

[1] L. Pintschovius, D. Reznik et al., Phys. Rev. B **74**, 174514 (2006)

[2] L. Pintschovius, Phys. stat. sol. (b) **242**, No. 1, 30- 50 (2005)

T-92 Dynamics of Argon in reduced dimensionality

Karin Schmalzl¹, Dirk Wallacher², Michael M. Koza³, Dieter Strauch⁴

¹FZ Jülich

²HMI, Berlin

³ILL, Grenoble

⁴Universität Regensburg

It is well established that geometrical confinement modifies the properties of a material. This can be, e.g., a free surface, an interface, an adsorbate layer, a free standing film (in 2d) or thin tubes (in 1d). In this study we have investigated the role of spatial restrictions on the dynamics of Argon. The study of the influence of reduced dimensionality on the dynamics can give valuable information on general trends for measurable parameters like, e.g., specific heat.

Ab initio calculations of plane sheets of Argon, piles with different distances and thus interaction, rods, and of bulk Argon have been performed. The change in interaction as well as the transition from 2d to 3d states can be seen in the dynamics (e.g. density of states) of the system.

We compare the calculations with experiments performed with ³⁶-Ar adsorbed in nanoporous Gelsil Glass by inelastic neutron scattering. By fractional filling the 'dimensionality' of the system is tuned from a two-dimensional towards the bulk state. At low filling fractions the atoms form an amorphous adsorbate film on the pore walls. At higher fillings, a capillary condensate forms in the pore centre. The preparation of single or of several monolayers were possible what permitted the study of, e.g., the dynamical interaction between the third and second layer.

A shift of various phonon modes to lower energies with decreasing dimensionality is observed in the results of both methods. A general reproducibility of features of the experimental data points out that their origin is found in the reduced dimensionality.

T-93 Attosecond dynamics of protons in crystals: Momentum distribution and “anomalous” neutron scattering intensity

C. Aris Dreismann¹, M. Lerch¹

¹TU Berlin, Institut für Chemie, Sekr. C2

Neutron Compton scattering (NCS) has been widely applied to investigation of proton momentum distributions (MD) and “effective” Born-Oppenheimer (BO) potentials of protons. Moreover, a new striking phenomenon [1(a)] discovered, thanks to NCS, is the “anomalous” shortfall of the scattering intensity from protons. Recently it has been confirmed with an independent experimental method, i.e. electron Compton scattering (ECS); see [1(b,c)].

Being in contrast to any conventional theoretical interpretation, this new effect has been claimed to have no influence on the MD results reported thus far, see e.g. [2]. Ref. [2] provided results of protonic MD's in a single crystal of the super proton conductor $\text{Rb}_3\text{H}(\text{SO}_4)_2$ (at 10 and 70 K), and the 3D effective BO-potential of H has been extracted. Presently we are analysing these data also with respect to the “anomalous” intensity effect [1] and the above claims. The Figure shows preliminary scattering results in the lattice plane spanned by the axes (i) along the bonds O-H-O and (ii) the two adjacent Rb atoms in the a-b-plane of the monoclinic cell. The protonic MD-widths (ca. 3.7 inverse Angstroms) at larger angles correspond to momentum transfers roughly along the H-Rb direction; see [2].

Our preliminary results demonstrate, for the first time, a strong connection between the two physical quantities (i.e., MD and scattering intensity) and, therefore, they contradict the above claims. The very strong variation of H-intensity (by a factor of 2) over the whole angular range should be stressed, thus demonstrating that the attosecond quantum effect of [1] is strongly dependent on details of the microscopic environment of a struck proton.

We thank Prof. G. Reiter and Dr. J. Mayers for making available to us data of their original NCS investigations published in [2].

[1] C. A. Chatzidimitriou-Dreismann et al., (a) Phys. Rev. Lett. 79, 2839 (1997); (b) Phys. Rev. Lett. 91, 057403 (2003); (c) G. Cooper et al. Phys. Rev. Lett. 100, 043204 (2008).

[2] D. Homouz, G. Reiter, J. Eckert, J. Mayers, R. Blinc, Phys. Rev. Lett. 2007, 98, 115502

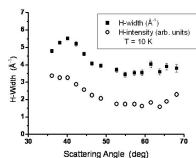


Figure 21.4: Widths of H-momentum distributions (full squares, in inverse Angstroms) and H-intensities (open circles, arbitrary units) measured at different scattering angles.

T-94 In-situ characterisation of the amorphisation of zeolites through average mean-square-displacements.

Florian Kargl¹, G. Neville Greaves¹, Gopinathan Sankar², Felix Fernandez-Alonso³

¹IMAPS, Aberystwyth University, Aberystwyth, SY23 3BZ, UK

²Royal Institution of Great Britain, Davy Faraday Research Laboratory, London, W1S 4BS, UK

³ISIS Facility, The Rutherford Appleton Laboratory, Chilton, OX 11 0QX, UK

Measuring the Debye-Waller factor through the melting transition has been followed by computer simulation in Lennard-Jones systems[1]. Measuring this in a real system conventionally from static powder diffraction is complicated[2]. This can be overcome by measuring the elastic neutron structure factor. Amorphisation, which is a solid state process, allows conventional handling and therefore overcomes difficulties of handling a material at the solid/liquid interface[3]. The rheology of the collapse of zeolites during amorphisation was studied recently through in-situ X-ray diffraction experiments[3]. Employing inelastic neutron scattering low-energy excitations were discovered and reasoned to be the origin of destabilization of the microporous crystal leading to amorphisation and finally characterising the glassy state[4]. Moreover, it has been argued that zeolites exhibit polyamorphism during amorphisation[2-5]. The first transition from the crystalline phase to the LDA phase was reasoned to be of displacive type and thus might be similar to pre-melting in conventional crystals, whereas the second transition from LDA to HDA appeared to be an order-disorder transition[2]. Both of these transitions confirmed to be of first order by ab-initio calculations[6]. Mean-square-displacements are expected to be lower in the more ordered (stronger) glass compared to the more disordered (fragile) one. Moreover, Debye-Waller factors should show a small step-like change for the displacive transition (zeolite-LDA) and a larger discontinuity for the disordering transition (LDA-HDA). In this way amorphisation might mimic classical melting, but on a much longer time scale.

To this end we performed in-situ inelastic neutron scattering characterising the amorphisation of zeolite Y through average mean-square displacements. The data which we present here were obtained by ratioing of high temperature to low temperature data measured on the OSIRIS spectrometer and are discussed in the previously outlined context.

[1] F. H. Stillinger, *Science* **267** (1995) 1935.

[2] G. N. Greaves, and S. Sen, *Advances in Physics* **56** (2007) 1.

[3] G. N. Greaves, F. Meneau, A. Sapelkin, L. M. Colyer, I. A. Gwynn, S. Wade, and G. Sankar, *Nature Materials* **2** (2003) 622.

[4] G. N. Greaves, F. Meneau, O. Majerus, D. G. Jones, and J. Taylor, *Science* **308** (2005) 1299.

[5] G. N. Greaves, F. Meneau, F. Kargl, D. Ward, P. Holliman, and F. Albergamo, *J. Phys.: Condens. Matter* **19** (2007) 415102.

[6] I. Peral and J. Iniguez, *Phys. Rev. Lett.* **97** (2006) 225502.

Index

- Abdul-Redah, Tyno, **300**
 Abele, Hartmut, 145, 153
 Acet, Mehmet, 238, 291
 Ackermann, Ralf, **216**
 Afandi, Ahmed, 258
 Aksenov, Victor, 199, 260
 Aksoy, Seda, **238**, 291
 Alba-Simionesco, Christiane, 180
 Aldridge, Laurence, 71
 Alekseev, Pavel, 169
 Alexander, Frischbutter, 228
 Alexej P., Bulkin, 228
 Alexiou, Christoph, 112
 Aliouane, Nadir, 81, 164
 Allenspach, Peter, 45
 Almgren, Mats, 177
 Altmann, Hans-Jürgen, 184
 Andersen, K.H., 117
 Andersen, Ken, 223, 226
 Antretter, Thomas, 273
 Appavou, Marie-Sousai, **108**, 204
 Arend, Nikolas, 134
 Argyriou, Dimitri, 81, 82, 84, **162**, 164
 Arndt, Julia, **237**, 242
 Arruebarrena, Gurutze, 265, 270
 Asenbaum, Augustinus, 49
 Avdeev, Mikhail, 199, **260**
- Böni, Peter, 61, 136, 139, 158, 207
 Büchner, Brend, 162
 Babcock, Earl, **223**
 Badurek, Gerald, **29**, 147, 213, 215
 Bakr, M., **278**
 Baranchikov, Alexandr, 202
 Bartmann, Roland, 125, **225**
 Bauer, Birgitta, **290**
 Baum, Max, 81, 164
 Bayraktar, Funda S., 96
 Bazzoli, David, 221
 Becker, Petra, 81, 164
 Beckmann, Felix, 72, **100**
 Behr, Günter, 162
 Behr, Nicolas, 225
 Behrmann, Jan H., 119
 Belgya, Tamas, 143
 Bentley, Phillip, 47, 226
 Bergner, Frank, 267
- Bernlochner, Florian, 158
 Berret, Jean-Francois, 88
 Beuneu, Brigitte, 286
 Bica, Doina, 199
 Biehl, Ralf, **27**
 Binz, Benedikt, 61
 Birringer, Rainer, 59
 Bivigou Koumba, A.M., 296
 Bivigou Koumba, Achille M., 33
 Boag, Stephen, 223
 Boehm, Martin, **146**
 Bohatý, Ladislav, 81, 164
 Bohlen, Jan, 259
 Boin, Mirko, 269
 Boldyreva, Elena, 302
 Bonné, Tune B., 198
 Bonnet, Fabien, 179
 Borchert, Gunther, 138
 Bordallo, Heloisa, **71**, **302**
 Bormann, Rüdiger, 72
 Borth, Robert, 237
 Boué, Francois, 179
 Boysen, Hans, 131, **288**, 297
 Brückel, Th., 58, 217, 243
 Brückel, Thomas, 48, 123, 148, 165,
 189, 191, 294
 Brüssing, Frank A., 52
 Braden, Markus, **81**, **164**, 167
 Brandt, Astrid, 114, 183
 Brokmeier, H.-G., 129
 Brokmeier, Heinz-Günter, **101**, 102,
 258, **259**, 268, 287
 Buchsteiner, Alexandra, 132, 302
 Buhler, Eric, 179
 Bulavin, Leonid, 199
 Busch, P., 296
 Busch, Peter, 33, **189**, 191
 Busch, Sebastian, 41, 188, **195**
 Bussmann, K., 217
 Bussmann, Klaus, 48
- Caciuffo, Roberto, 55
 Canella, Lea, 46, 143, 152, **219**
 Canfield, Paul, 162
 Caroca-Canales, Nubia, 292
 Catherine, Pappas, 153
 Chang, Hai, 287

- Chaplot, S. L., 304
 Charlet, Laurent, 303
 Charlton, Tim, 223
 Chass, Gregory A., 187
 Chatterji, T., 58
 Chen, Jiangshun, 34
 Chen, Wangchun, 223
 Chetverikov, Yuri O., 53
 Chogondahalli M., Naveen Kumar, **165**,
 294
 Churchman, G. Jock, 71
 Clemens, Helmut, 272
 Colineau, Eric, 55
 Conrad, Harald, 148
 Cser, Laszlo, 140
 Cubitt, Robert, 172, 204, 263
 Cussen, Leo, 126
 Czeslik, Claus, **87**

 Döbrich, Frank, 59
 Dönch, Ingo, 196
 Dörr, Mathias, 286
 Dadakova, Tetiana, **247**
 Dahint, Reiner, 200
 Dalgliesh, Rob, 223
 Danilyan, Gevorg, **153**
 Das, A., **243**
 Davydov, Vadim, 98
 de Souza, Nicolas R., 134, **305**
 Decker, Heinz, 112
 Deen, Pascal, 238
 del Genovese, Dominique, 98
 Denks, Ingwer, 269
 Devishvili, Anton, **286**
 Dewhurst, Charles D., 239
 Di, Zhenyu, **197**
 Dicko, Cedric, 192, 280
 Diddens, Imke, 192, 280
 Donner, Wolfgang, **257**
 Dornheim, Martin, 72
 dos Santos, Jorge, 253
 Dosch, Helmut, 50
 Doster, Wolfgang, 108, 204
 Dreismann, C. Aris, **307, 310**
 Drevensek-Olenik, Irena, 49
 Drochner, M., 217
 Dronskowski, Richard, 148, 250
 Duine, Rembert, 61
 Dunsinger, Sarah, 158

 Eckerlebe, Helmut, 49, 59, 169, 267
 Efrem D'Sa, J. B. C., 243
 Ehrenberg, H., 278
 Ehrenberg, Helmut, 131

 Eibl, Stefan, **180**
 Eidenberger, Elisabeth, **272**
 Ellabban, Mostafa, 49
 Elmas, Mihdi, 59
 Embs, Jan Peter, **186**, 216
 Ennen, Inga, 239
 Epp, Jeremy, **99**
 Erné, B., 89
 Erné, Ben, 156

 Füzi, János, 225
 Falk, Ann, **185**
 Fallus, Peter, 27
 Fally, Martin, 49
 Falus, Peter, 47
 Fang, De-Cai, 187
 Farago, Bela, 47, 184, 226
 Faulhaber, Enrico, 237, **285**
 Favre Buivin, Fabienne, **303**
 Fenske, Jochen, **157**, 248
 Feoktystov, Artem, **199**, 260
 Ferdinand, Adrian, 59
 Fernandez-Alonso, Felix, 311
 Fery, Andreas, 196
 Feyerabend, Frank, 32
 Feyerherm, Ralf, **83**
 Filges, Uwe, 216
 Findenegg, Gerhard G., 205
 Finger, Thomas, 81, 164
 Fischer, Torben, **253**
 Fleischmann, Claudia, 246
 Flemming, Stefan, 269
 Forgan, E.M., 207
 Fouquet, Peter, 71, **226**
 Frank, Alexander, 68, 151
 Frank, Schilling, 228
 Frei, Andreas, 44, 150
 Frenzel, Jan, 258
 Frey, Friedrich, 277, 297
 Frick, Bernhard, 40, 194, **221**
 Frielinghaus, Henrich, 92, **175**, 182
 Fritsch, Bastian, **297**
 Froitzheim, Nikolaus, **28**
 Frontzek, Matthias, **161**, 240, 244
 Frost, Chris, 223
 Fueß, H., 278
 Fueß, Hartmut, 76, 131

 Gäbler, Frank, **279**
 Gähler, Roland, 89
 Görigk, Günter, 179
 Günther, Jens-Uwe, 205
 Gahl, Thomas, **118**
 Gan, Weimin, **102**, 268, **287**

- Gao, Yan, 70
 Garamus, Vasil, 199, 260
 Garbe, Ulf, 101, 129, 259
 Gebhardt, Ronald, 204
 Geibel, Christoph, 237, 242, 292
 Geltenbort, Peter, 45, 68, 151
 Gemmecker, Gerd, 41
 Gentile, Thomas, 223
 Genzel, Christoph, 269
 Georgii, Robert, 61, 173, 176, **227**
 Gernot, Heger, 295
 Gerth, Stefan, 35
 Gibmeier, Jens, 124
 Gille, Peter, 290
 Gilles, Ralph, **70**, 98, **122**, 264, 284
 Glube, Natalie, 112
 Goll, Gernot, **163**
 Golosova, A., 296
 Gossen, F., 217
 Gröhn, Franziska, **93**
 Grünwald, Alexander, **236**
 Grabmayr, Peter, 152
 Gradzielski, Michael, 271
 Greaves, G. Neville, 311
 Griesche, Axel, **97**
 Grigoriev, Sergey, 169, 201, 202
 Grigoriev, Sergey V., 47, 53
 Grillo, Isabelle, **90**
 Gunter, Behr, 286
 Gutberlet, Thomas, 34, 110, 111
 Gutfreund, Philipp, 35
 Gutsmiedl, Erwin, 44, 150

 Häussler, Wolfgang, **136**
 Hölzel, Markus, **131**, 258, 284, 288, 297
 Hütten, Andreas, 239
 Habicht, Klaus, 89, **126**, 249
 Haese-Seiller, Martin, 32, 135, 197, 212, 214, 283
 Hamann, A., **308**
 Hansen, Bent T., 148
 Hansen, Thomas C., 76, 78, 295
 Haramus, Vasil, 32, **177**, 201
 Harbott, P., 217
 Heger, Gernot, 224
 Heil, W., 117
 Heimbürg, Thomas, 110
 Heintze, Cornelia, 267
 Hellweg, Thomas, **39**, 183, 184
 Helm, Christiane A., 205
 Hempelmann, Rolf, 118, 216
 Henry, Paul, 241
 Hermann, Raphael, 77
 Herwig, Ken, **65**

 Hesse, Christian, 150
 Heunemann, Peggy, **271**
 Heynen, Achim, 48
 Hiess, Arno, **55**, 81, 146, 164
 Hildebrandt, A., 38
 Hilger, André, 215
 Hirsch, Thomas, 99
 Hjörvarsson, Björgvin, 222
 Hoelzel, Markus, 70, 76, 98, 281
 Hoffmann, Bernd, 27
 Hoffmann, Jan, 125
 Hoffmann, Jan-Ekkehard, 225
 Hoffmann, Jens-Uwe, **121**, 161, 240
 Hofmann, Michael, 70, 98, 101, 124, 252, 254, **256**, 273
 Holderer, Olaf, 39, **134**
 Holland-Moritz, Dirk, 69
 Hornauer, Werner, 122
 Hoser, Andreas, **249**, 292
 Houben, Andreas, **148**, 250
 Hradil, Klaudia, 81, 164, 247
 Huber, Klaus, 179
 Hughes, Darren, 220
 Hurtado, Iñaki, 265, 270
 Hutanu, Vladimir, **224**, 295

 Ianeselli, L., 38
 Iannucci, Robert, 138
 Iffoe, A., 217
 Ihringer, Jörg, 121
 Ioffe, Alexander, 123
 Iorio, Luana, 70
 Ivanov, Vladimir, 201, 202
 Ivanova, Ruzha, 198
 Izaola, Zunbeltz, **127**, 142

 Jörg, Perßon, 165
 Jünke, Norbert, 131
 Jacobs, R. M. J., 38
 Jain, A., 296
 Jain, Abhinav, 33
 Janoschek, Marc, **158**
 Jean-François, Barthelemy, 221
 Jeevan, Hirale, 237
 Jeevan, Hirale S., 242
 Jentschel, Michael, 112, 151
 Jericha, Erwin, 147, **213**, **215**
 Jesche, Anton, 292
 Jetschel, Michael, 68
 Jeworrek, Christoph, 109
 Jiang, Xiuli, **182**
 Jochum, Josef, 152
 Johnson, Frank, 70
 Jöhrendt, D., 58

- Jolie, Jan, 46, 143, 152, 219
 Jonietz, Florian, **61**
 Jordan, Rainer, 198
 Jullien, D., 117
 Jurbnyi, Fanni, 118
 Juranyi, Fanni, 111
- Kämmerling, Hans, 48
 Köbler, Ulrich, 249
 Köhler, Ralf, **196**
 Köper, Ingo, 185
 Körstgens, Volker, 173, 204
 Küssel, E., 217
 Kaiser-Bischoff, Ines, 288
 Kaltofen, Rainer, 248
 Kaltofen, Thomas, 200
 Kamel, Simon, **266**
 Kampmann, Reinhard, 32, 135, 197,
 212, 214, 283
 Kaneko, Koji, **292**
 Kardjilov, Nikolay, 215
 Karg, Matthias, 39, **183, 184**
 Kargl, Florian, **187, 311**
 Kats, Efim, 90
 Kaune, Gunar, 176, 262, **276**
 Keiderling, U., **117**
 Keiderling, Ulrich, 89
 Keiderling, Uwe, 156
 Keimer, Bernhard, 74, 159, 160
 Keller, Thomas, 54, 252
 Kemner, Ewout, 303, 306
 Kentzinger, Emmanuel, 189, 191
 Keppens, Veerle, 77
 Kerscher, Michael, **92**
 Kiefer, Klaus, 71, **120**
 Kimber, Simon, 71, 162
 Kirstein, Oliver, 75
 Kis, Zoltan, 143
 Klein, Helmut, 148
 Kleines, H., 217
 Klemke, Bastian, 120
 Klenke, J., 117
 Klenke, Jens, **145, 153**
 Klockenburg, M., 89
 Klockenburg, Mark, 156
 Klose, Frank, 157
 Knite, Maris, 255
 Knoll, Wiebke, 192, **280**
 Kocak, Mustafa, 96
 Kohlbacher, O., 38
 Kohlbrecher, J., 89
 Kohlbrecher, Joachim, 156
 Kohlbrecher, Joachim, 59
 Kolasinska, Marta, 34
- Kolesnikov, Alexander I., 305
 Komarek, Alexander C., 81, 164
 Komenda, Thomas, 198
 Kopitsa, Gennady, **169, 201, 202**
 Korolkov, Denis, 123, 189, **191**
 Koza, Marek, 240
 Koza, Michael M., 78, 192, 280, 309
 Koza, Michael Marek, 302
 Kraan, Wicher, **116**
 Krakhotin, Viacheslav, 153
 Krastev, Rumen, **34, 196**
 Kraus, Hans, 76
 Krellner, Cornelius, 292
 Krempaszky, Christian, 252
 Kreuzer, Martin, **200**
 Kreuzpaintner, Wolfgang, **283**
 Krexner, Gerhard, 140, 255, 293
 Krien, Cornelia, 248
 Krimmel, Alexander, 84
 Krimmer, Bernhard, 122
 Krist, Thomas, **125, 225, 245**
 Krott, Manuel, **250**
 Krystian, Maciej, 293
 Kudejova, Petra, **46, 143, 152, 219**
 Kudryashov, Valeri, 212
 Kuhs, Werner F., **78**
 Kulda, Jiri, 146
 Kulin, German, **68, 151**
 Kulkarni, Amit, 33
 Kulozik, Ulrich, 204
 Kurt, Walther, 228
 Kusche, Tjard, 100
 Kustov, Dmytro, 68, **151**
 Kutovoi, S., 304
- Löser, Wolfgang, 240
 Lüdtke, Karin, 198
 Lages, Sebastian, 179
 Lai, Chih-Huang, 248
 Lamago, D., 308
 Lander, Gerry, 55
 Landsgesell, Sven, **82, 302**
 Langguth, Peter, 112
 Langridge, Shawn, 223
 Lapp, Alain, 183, 184
 Laschewsky, A., 296
 Laschewsky, André, 33, 196
 Lauss, Bernhard, 112
 Lazukov, Vladimir, 169
 Legl, Stefan, 61
 Leiss, Bernd, 148
 Leitner, Harald, 261, 272
 Lelièvre-Berna, Eddy, 47
 Lelièvre-Berna, E., 117

- Lemmel,Hartmut, **147**
 Len,Adél, 255
 Lerch,M., 310
 Lerch,Martin, 288
 Lindner,Peter, **86, 218**
 Link,Peter, 81, 158, 161, 163, 164, 167,
 236, 240, 244, 247
 Linser,Sebastian, 32
 Liz-Marzán,Luis M., 183
 Loewenhaupt,Michael, 161, 237, 240,
 242, 244
 Loidl,Alois, **80, 84**
 Lopez-Anton,Ricardo, 223
 Lott,Dieter, 32, **53**, 157, 248, 283
 Lychagina,Tatiana, **268**
- Möller,R., 217
 Mühlbauer,Sebastian, 61, **207**
 Müller,Axel Reimer, **44, 150**
 Müller,Martin, 192, 280
 Müller,Paul, 148, 250
 Müller-Buschbaum,P., 296
 Müller-Buschbaum,Peter, 33, **172**, 173,
 174, 176, 204, 262, 263,
 276
 Münzer,Wolfgang, 61
 Ma,Yu-E, 253
 Maccarini,Marco, 226
 Machold,Winulf, 96
 Magerl,Andreas, 35, 190, 193
 Magnani,Nicola, 55
 Major,Janos, 50
 Major,Marton, 50
 Mani,Prakash, 157
 Manke,Ingo, 215
 Mankey,Gary J., 157
 Manosa,Lluis, 238
 Markó,Marton, 140
 Markmann,Jürgen, 59
 Martin,C. M., 38
 Martin,R. A., 38
 Masalovich,Sergey, **137**
 Mattauch,Stefan, **123**
 May,Roland P., 49, 89, 112
 Maye,Felix, 50
 Mayer,Simon, **45**
 Mazilu,Irina, 244
 McGreevy,Robert, **64**
 McLain,Sylvia, 300
 Mehaddene,Tarik, 247
 Meier,Leopold, 256
 Meier,Robert, 174, **176**
 Meier-Koll,A., **296**
 Meierhofer,Georg, **152**
- Meissner,Michael, 156
 Menachem,Bamberger, 256
 Merkel,Casjen, **258**
 Merkel,Rudolf, 27
 Mesot,Joel, 118
 Metwalli,Ezzeldin, 172–174, **204, 262**,
 263, 276
 Metz,Oliver, 72
 Meven,Martin, **128**, 224, 282, 295
 Meyer,Andreas, 69, 97, 301
 Mezei,Ferenc, **66**, 142, 153
 Michels,Andreas, **59**
 Mignot,Jean-Michel, 161
 Mikhailik,Vitalii, 76
 Milkereit,Götz, 177
 Milner,Emily, **289**
 Mittal,R., 58, 217, 243, **304**
 Mole,Richard, 76, **241**
 Monkenbusch,Michael, 27, 134, 141
 Moravsky,Alexander P., 305
 Mortensen,Kell, 198
 Moskvin,Evgeny, 47, 226
 Moulin,Jean-Francois, 32, **135**, 172,
 174, 204, 214, 262, 276,
 283
 Mukherji,Debashis, 98, **264**, 284
 Mukhin,A. A., 80
 Mydosh,John, 54, 168
- Nülle,Max, 50
 Nakatsuji,Satoru, 167
 Nawroth,Thomas, **112**
 Neubauer,Andreas, 61
 Neuhaus,Jürgen, 247, 291
 Nickel,Bert, **91**, 214
 Nicklas,Michael, 232
 Niewa,Rainer, 279
 Nikbin,Kamran, 266
 Niklowitz,Philipp, **54**
 Nikolayev,Dimmitry, 268
 Nosov,Vadim, 68, 151
 Novitsky,Vadim, 153
 Nunes Bordalo,Heloisa, 84
 Nusser,Klaus, 181
- O'Brian,Christopher J., 187
 O'Dowd,Noel, 266
 Oberdisse,Julian, **88**
 Oesterreicher,Thomas, 229
 Organ,Michael G., 187
 Ortner,Balder, **273**
 Ostermann,Andreas, 122, 136, **141**
 Ott,Patrick, 196

- P. Gates, Will, 71
 Pérez-Juste, Jorge, 183
 Pairet, Bruno, 112
 Papadakis, C.M., 296
 Papadakis, Christine, **33**, 197, **198**, 263
 Papaefthimiou, Vasiliki, 205
 Pappas, Catherine, **47**, 226
 Pardo Soto, Luis Carlos, 115
 Park, Sohyun, **281**
 Parnell, Steve, 223
 Pastoriza-Santos, Isabel, 183
 Pastrello, Gilles, 226
 Paul, Amitesh, **233–235**
 Paul, Stephan, 44, 150
 Pavel, Shatalov, 153
 Pedersen, Bjørn, **277**, 282, 290
 Perßon, Jörg, 77, 294
 Perillo-Marcone, Antonio, 218
 Perlich, Jan, **173**, 176, 263
 Peters, Judith, 111
 Peters, Tanja, 112
 Petoukhov, A.K., 117
 Petoukhov, Alexandre, 223
 Petry, Winfried, 122, 141, 247, 252, 291
 Pfeleiderer, Christian, **26**, 54, 61, 158, 207
 Pichl, Wolfgang, **293**
 Pigozzi, Giancarlo, **284**
 Pilgrim, Wolf-Christian, 118
 Pimenov, Andrei, 80
 Pintschovius, L., 304, 308
 Pipich, V., 296
 Pipich, Vitaly, 33
 Pirling, Thilo, **220**
 Planes, Antoni, 238
 Plazanet, Marie, 180
 Pleuger, Jan, 28
 Poeste, Tobias, 99, 269
 Pomm, Matthias, 214
 Pommrich, Anja Ines, **69**
 Prévost, S., 89
 Prager, Michael, 48, **75**, 77, 115
 Pranzas, P. Klaus, **49**, **72**, 122, 130, 198, 201, 202
 Pranzas, P.K., 100
 Prem, Manfred, **140**, 255, 293
 Preu, Julia, **110**
 Prevost, S., 38
 Prevost, Sylvain, **156**
 Priolkar, K. R., 243
 Prokes, Karel, **168**
 Pruner, Christian, **49**
 Pyckhout-Hintzen, Wim, 181, 182
 Rösler, Joachim, 264
 Rucker, Ulrich, 123
 Rühm, Adrian, **50**
 Rabie, Mahmoud, **291**
 Radulescu, Aurel, **178**
 Raichle, Markus, **74**, **159**, **160**
 Randau, Christian, 101, **129**, 259, 265, 270
 Rauch, Helmut, 45, **229**
 Reagnault, Louis-Pierre, 81, 164
 Rebelo Kornmeier, Joana, **124**
 Rebizant, Jean, 55
 Reehuis, Manfred, 159, 160
 Reithmeier, Günther, 256
 Rekveldt, Theo, 116
 Rennhofer, Harald, 255
 Rennie, Andrian, 222
 Repper, Julia, **252**
 Reznik, D., 308
 Reznik, Dmitry, 74
 Rich †, Denis, 150
 Richardt, Andre, 39, 184
 Richter, Dieter, 27, 92, 115, 134, 141, 178, 181, 182
 Riekehr, Stefan, 96
 Riekel, Christian, 192
 Ritz, Robert, 61
 Roesler, Joachim, 98
 Roessli, Bertrand, 158
 Rosch, Achim, 61
 Roth, Georg, 282
 Rotter, M., 58
 Rotter, Martin, 286
 Roux, Stephane, 146
 Ruderer, Matthias, **174**, 176, 262
 Rupp, A., 117
 Rupp, Romano, 49
 Russina, M., 89
 Russina, Margarita, 127, **142**, 303, **306**
 Sandhofer, Mathias, 136
 Sankar, Gopinathan, 311
 Sapede, Daniel, 192
 Sazonov, Andrew, **295**
 Schaaf, Peter, 256
 Schedler, Roland, 232
 Scheffzük, Christian, **228**
 Schmölzer, Thomas, 272
 Schmahl, Wolfgang, 131, 144, 258
 Schmalz, Karin, 81, 133, 157, 164, 237, 242, **309**
 Schmidberger, Heinz, 112
 Schmidt, Harald, **203**
 Schmidt, Wolfgang, **133**, 157, 236, 248

- Schmidt-Wellenburg, Philipp, 45
 Schmitz, B., 217
 Schmitz, H.-W., 100
 Schmitz, Heinz-Werner, 72
 Schneider, Gerald, 75
 Schneider, Gerald Johannes, 115, **181**
 Schneider, Julius, **144**
 Schneider, Michael, 216
 Schneider, Rainer, 99, 101, 269
 Schneider, Reiner, 247
 Schneidewind, Astrid, 161, 237, 244
 Schnitzer, Ronald, 261
 Schober, Helmut, 44, 180
 Schreiber, F., 38
 Schreiber, Frank, 121
 Schreyer, A., 100
 Schreyer, Andreas, 32, 53, 72, 96, 101, 122, 157, 212, 214, 236, 248, 253, 283
 Schulz, Leander, 172, 173
 Schulze, Ralf, 46, **143**, 219
 Schwahn, Dietmar, **206**
 Schweika, W., 217, 243
 Schweika, Werner, **77**, 148, 250
 Schweins, Ralf, **179**, 218, 261
 Senff, Daniel, 81, 164
 Senyshyn, A., 58, 278
 Senyshyn, Anatoliy, **76**, 131, 165, 279, 281, 288, 291, 294, 297
 Seydel, Tilo, 71, **192**, 221, 280
 Sharkov, Ivan, 140
 Sharp, Melissa, 33, 59, **130**
 Shigetoh, K., 163
 Sidis, Yvan, 167
 Skipper, Neal, 289
 Skoda, M. W. A., 38
 Skoda, Maximilian, 223
 Skoulatos, Markos, 126
 Skrobucha, M., 217
 Smuda, Christoph, **41**, **188**, 195
 Sobolev, Oleg, 303
 Solina, Danica, **248**
 Sowa, Heidrun, 148
 Spalthoff, Peter, 101, 259, 265, 270
 Sparta, Karine, 282
 Spehr, Tinka, **40**, **194**
 Spieckermann, Florian, **255**
 Spolenak, Ralph, 284
 Stöpler, Rainer, 44, 150
 Stüßer, Norbert, **132**
 Stühn, Bernd, 40, 194
 Starke, Ulrike, 248
 Staron, Peter, **96**, 253, 272
 Steffens, Paul, 81, 164, **167**
 Steglich, Frank, 237, 242
 Stein, Wolf-Dieter, **240**
 Steitz, Roland, 200, **205**, 245, 246
 Stergar, Erich, 272
 Stock, Chris, **166**
 Stockert, Oliver, 163, 232, 237, **242**, 285, 292
 Straessle, Thierry, 118
 Strauch, Dieter, 309
 Strepetov, Alexander, 68, 151
 Stride, John, 241
 Strobl, Markus, 215
 Strunz, Pavel, **98**, 264, 284
 Stunault, Anne, 55
 Su, Y., **58**, **217**, 243
 Su, Yixi, 165, 250, 294
 Sutton, Iain, 226
 Szentmiklosi, Laszlo, 143
 Török, Gyula, 140
 Türlér, Andreas, 46, 143, 219
 Takabatake, T., 163
 Tang, Fei, 161, **244**
 Tartakovskaya, Elena, 236
 Tassini, Leonardo, 150
 Tatakowskaya, Elena, 157
 Tegel, M., 58
 Tehei, Moeva, 111
 Teichert, Anke, 125, **245**, **246**
 Tekouo, William, 101
 Telling, Mark, 71
 Temst, Kristiaan, 246
 Thar, Jörg, **282**
 Thaveron, Eric, 226
 Theis-Bröhl, Katharina, **52**, 236, **239**
 Thilly, Ludovic, 103
 Thomas, Frederic, 226
 Tiden, Nikolay, 169
 Tolkach, Alexander, 204
 Tomita, Yasuo, 49
 Toperverg, B.P., 298
 Toperverg, Boris P., 52, 222, 239
 Tortorella, Daniele, 150
 Trapp, Marcus, **111**
 Troll, Kordelia, 33, 263
 Tsapatsaris, Nikolaous, 142
 Tsurkan, Vladimir, 84
 Ulacia, Ibai, **265**, **270**
 Ulbricht, Andreas, **267**
 Ullemeyer, Klaus, **119**
 Unruh, Tobias, 41, 44, 69, 163, 188, 195, 241, 301

- Urban, Markus, 44
 Uwe, Wasmuth, 256
- Valery, Kuznetsov, 153
 Valicu, Roxana, **138, 139**
 van Bürck, Uwe, 262, 276
 van Eijck, Lambert, 221
 Van Petegem, Steven, **103**
 Van Swygenhoven, Helena, 103
 Vasylechko, Leonid, 76
 Vekas, Ladislau, 199, 260
 Verdal, Nina, 305
 Vogel, Britta, 239
 Vogl, Wolfgang, 101
 Vogt, Karsten, **109**
 Voigt, Jörg, **48**
 Vollbrandt, J., 100
 Vollbrandt, Jürgen, 49
 Vollrath, Fritz, 192
 Voss, Nicole, 35, 190, **193**
- Wagener, M., 217
 Wagner, Bernd, 188
 Waldmann, Oliver, **60**
 Wallacher, Dirk, **114**, 156, 183, 309
 Walter, Jens, 148, 250
 Walz, Marco, 35, **190**, 193
 Wang, Weinan, 33, **263**
 Ward, Roger, 236
 Warr, Nigel, 46, 152, 219
 Wasmuth, Uwe, **254**
 Wastin, Franck, 55
 Weber, Thomas, 277
 Weggler, S., 38
 Weldon, Gerald, 241
 Wellert, Stefan, 39, 183, **184**
 Werner, Ewald, 252, 273
 Wiedenmann, A., 117
 Wiedenmann, Albrecht, **89**, 156, 207
 Wiedersich, J., 296
 Wildes, Andrew, 222, 236
 Willner, Lutz, 181, 191, 197
 Willumeit, Regine, **32**, 199, 260
 Wilpert, Thomas, 153
 Wimpory, Robert, 266, **269**
 Wirth, Hans-Friedrich, 145, 150, 153
 Wischnewski, Andreas, 181
 Witte, Ulrike, **232**
 Wizent, Nadja, 240
 Wolff, M., 298
 Wolff, Max, **35**, 193
 Wolff, Maximilian, 52, 190, **222**, 239
 Wood, Paul, 241
 Wu, Yu- Chang, 248
- Wuttke, Joachim, 75, **115**
- Xiao, Yinguo, 165, **294**
- Yang, Fan, **301**
 Yokaichiya, Fabiano, **84**, 162
- Zabel, H., 298
 Zabel, Hartmut, 35, 52, 190, 193, 222
 Zagumennyi, A., 304
 Zavartsev, Yu., 304
 Zhang, Bo, 97
 Zhang, Fajun, **38**
 Zheng, Mingyi, 287
 Zhernenkov, K., **298**
 Zhernenkov, Kyrill, 222
 Zhokhov, Anatoly, 153
 Zickler, Gerald Andreas, **261**
 Zsigmond, Geza, 45